ANNUAL REPORT 2001

GISAXS: QUANTUM DOTS

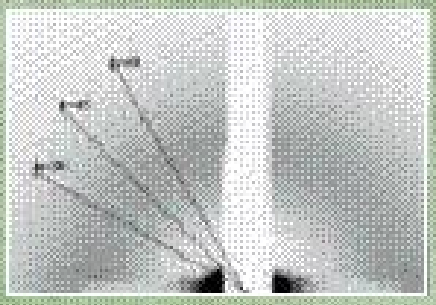

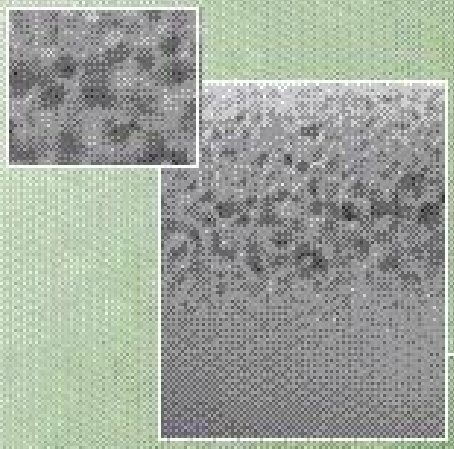

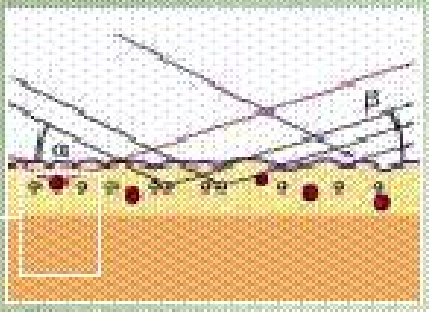

AUSTRIAN SAX BEAMLINE AT elettra

Taken from the user contribution U.V. Desnica et al. *Morphological characterization of CdS quantum dots in SiO_2 substrate by GISAXS, (p. 44*), and with permission from A. Meldrum et al., Nucl. Instr. & Methods B 148, (1999) 957 – 963.

Austrian Small Angle X-ray Scattering (SAXS) Beamline at ELETTRA

Annual Report 2001

Compiled by the SAXS-Group:

- for IBR: M. Rappolt & H. Amenitsch
- for ELETTRA: S. Bernstorff

Table of Contents

Preface

It is a pleasure to introduce this fifth annual report of the Austrian SAX-beamline at Elettra. Again, this is a record of a very successful operation not only for the communities of Italy and Austria, but also as an infrastructure element for the European Research Area. We can see a significant increase in the number of users, and the fraction of “new” users, i.e. groups that had never before been at the beamline, is still sizeable, in spite of the strong competition for beam-time.

The European role for our beamline will doubtlessly increase further with the 6th Framework Programme of the European Commission, when the accessing states will be fully integrated. But Europe does not end there, and we see it as a good sign for the future that the countries Bulgaria, Croatia, Russia and the Ukraine are also represented by their groups.

SAX is arguably the most versatile method among those existing at synchrotron radiation sources. The wide diversity of systems requires a perceptual adaptation of the techniques to the actual needs of the users. No two experiments are the same, and this is a strong challenge to the beamline operators. I want to thank them for their lasting enthusiasm and ingenuity and our partners, the users, for the challenging projects.

Peter Laggner
Director
Institute of Biophysics and X-Ray Structure Research
Austrian Academy of Sciences

It is a pleasure for me to see this new edition of the SAXS beamline Annual Report, summarizing the achievements of the last year. The beamline users statistics speak for themselves about the popularity of this scientific instrument among a wide international community, that extends well beyond the borders of Austria and Italy. The publication record, on the other hand, shows a consistently high quality level.

The credit must go of course to the people that work together with enthusiasm on the beamline, with no distinction of nationality or employing institution. I am very grateful to the Austrian Academy of Science for their continuing support of this project and for their constructive, informal and effective approach to collaboration.

Synchrotron sources are developing at an impressive pace all over the world and in particular in Europe, where new machines are being built in many countries. It is necessary to face this stimulating competition by continuing the upgrade of our installations. I am confident that the Austrian-Italian partnership at the SAXS beamline will be able to meet this challenge and continue to attract excellent users.

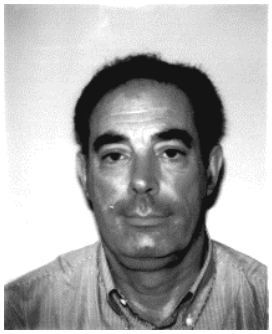

Massimo Altarelli

Director

Elettra Synchrotron Light Laboratory

The SAXS-Group

HEAD OF PROJECT: Peter Laggner[1)]

e-mail: Peter.Laggner@oeaw.ac.at

SCIENTISTS: Heinz Amenitsch[1), 3)]

e-mail: Heinz.Amenitsch@elettra.trieste.it

Sigrid Bernstorff [2)]

e-mail: Sigrid.Bernstorff@elettra.trieste.it

POSTDOCS: Pavo Dubcek (until 31.12.2001)[2)]

e-mail: Pavo.Dubcek@elettra.trieste.it

Michael Rappolt[1), 3)]

e-mail: Michael.Rappolt@elettra.trieste.it

CHEMICAL ASSISTANT: Marlene Strobl (until 31.12.2001)[1, 3)]

e-mail: Marlene.Strobl@elettra.trieste.it

TECHNICIAN: Christian Morello[2)]

e-mail: Christian.Morello@elettra.trieste.it

1) Institute for Biophysics and X-ray Structure Research, Austrian Academy of Sciences, Schmiedlstraße 6, 8042 Graz, Austria.
Tel 0043-316-4120 302
Fax 0043-316-4120 390

2) Sincrotrone Trieste, Strada Statale 14, km 163.5, 34012 Basovizza (TS), Italy.
Tel 0039-040-375 81
Fax 0039-040-938 0902

3) Institute for Biophysics and X-ray Structure Research, Austrian Academy of Sciences c/o Sincrotrone Trieste

The SAXS-Beamline in General

Small Angle X-ray Scattering has become a well known standard method to study the structure of various objects in the spatial range from 1 to 1000 nm, and therefore instruments capable to perform such experiments are installed at most of the synchrotron research centers. The high-flux SAXS beamline at ELETTRA is mainly intended for time-resolved studies on fast structural transitions in the sub-millisecond time region in solutions and partly ordered systems with a SAXS-resolution of 1 to 140 nm in real-space.
The photon source is the 57-pole wiggler whose beam is shared and used simultaneously with a Macromolecular Crystallography beamline. The wiggler delivers a very intense radiation between 4 and 25 keV of which the SAXS-Beamline accepts 3 discrete energies, namely 5.4, 8 and 16 keV. The beamline optics consists of a flat double crystal monochromator and a double focusing toroidal mirror.
A versatile SAXS experimental station has been set-up, and an additional wide-angle X-ray scattering (WAXS) detector monitors simultaneously diffraction patterns in the range from 0.1 to 0.9 nm. The sample station is mounted move-able onto an optical table for optimising the sample detector distance with respect to SAXS resolution and sample size.
Besides the foreseen sample surrounding the users have the possibility to install their own specialised sample equipment. In the design phase, besides technical boundary conditions, user friendliness and reliability have been considered as important criteria.
The optimisation of the beamline with respect to high-flux and consequently high flux density, allows to perform the following experiments:

- Low Contrast Solution Scattering
- Grazing Incidence Surface Diffraction
- Micro-Spot Scanning
- X-ray Fluorescence Analysis
- Time-Resolved Studies ≥ 11 μs
- Simultaneously Performed Small- and Wide-Angle Measurements (SWAXS) on:
    - Gels
    - Liquid Crystals
    - (Bio) Polymers
    - Amorphous Materials
    - Muscles

Furthermore, using 5.4 and 16 keV energies, the beamline is widely applicable also to very thin, e.g. single muscle fibers, and optically thick (high Z) specimen, as often used in e.g., material science and solid state physics.

THE INSERTION DEVICE

The wiggler for the SAXS beamline consists of three 1.5 m long segments, each having 19 poles. The device can work with a minimum gap of 20 mm, which corresponds to K=20 at 2 GeV. The main parameters of the wiggler are:

- Critical Energy 4.1 keV
- Radiation Power 8.6 kW
- Flux 3.5×10^{14} ph/s/mrad/0.1%BW (at 400 mA)

The wiggler radiation cone has a horizontal width of 9 mrad. From this the SAXS-beamline accepts vertically 0.3 mrad, and horizontally +/-0.5 mrad at a 1.25 mrad off-axis position. The resulting source size for 8 keV photons is 3.9 x 0.26 mm^2 (horiz. x vert.).

THE OPTICS

The optics common with the diffraction beamline consists of:

- C-Filter and Beryllium window assembly to reduce the power load on the first optical elements by a factor of 2 and to separate the beamline vacuum from the storage ring.
- Beam defining slit chamber which allows to define the SAXS beam on three sides before the monochromator in order to reduce the straylight in the downstream beamline sections.

The SAXS beamline optics consists of:

- A double-crystal monochromator consisting of four individual chambers, in which three interchangeable asymmetric Si(111) crystal pairs are used to select one of three fixed energies. Each of the crystal pairs is optimised for the corresponding energy to accomplish a grazing angle of 2°. The energy resolution $\Delta E/E$ of the monochromator is in the range of 0.7 - 2.5 10^{-3}.
- A baffle chamber after the monochromator is used as an adjustable straylight fenditure.
- A segmented toroidal mirror focuses the light in horizontal and vertical direction with a 1/2.5 magnification onto the SAXS-detector.
- An aperture slit reduces the straylight after the monochromator and the toroidal mirror.
- A guard slit defines the illuminated region around the focal spot. The spot size on the detector is 1.6 mm horizontally and 0.6 mm vertically. The calculated flux at the sample is in the order of 10^{13} ph/s at 400 mA. For a maximum sample size of 5.4 x 1.8 mm^2 correspondingly a flux density of 10^{12} ph/s/mm^2 has been calculated.

SAMPLE STAGE

The multipurpose sample stage allows to perform fast time-resolved relaxation studies based on temperature- or pressure-jumps as well as stopped flow experiments. Shear jump relaxation experiments are planned. Specifically, T-jumps can be induced by an infra-red light pulse (2 ms) from an Erbium-Glass laser, raising the temperature about 20 °C in an aqueous sample volume of 10 µl. A hydrostatic pressure cell with a maximal accessible angular range of 30° for simultaneous SAXS and WAXS measurements is available. P-jumps are realised by switching fast valves between a low and a high pressure reservoir, increasing or decreasing the hydrostatic pressure in the range from 1 bar to 2.5 kbar within a few ms. A Differential Scanning Calorimeter (DSC) allows for DSC-scans simultaneously to SWAXS measurements. Also a 1.5 T magnet is available. In an overview, the following sample manipulations are possible (further details, see page 25-34):

- Temperature Manipulations: Ramps, Jumps and Gradient Scans
- Pressure Manipulation: Scan and Jumps
- Stopped Flow Experiments
- SWAXS Measurements Applying Mechanical Stress
- SWAXS Measurements Applying Magnetic Fields
- Calorimetric measurements

Scientific applications	Low Contrast Solution Scattering, Grazing Incidence Surface Diffraction, Micro-Spot Scanning, X-ray Fluorescence Analysis, Time-Resolved Studies ≥ 11 μs and Simultaneously Performed Small- and Wide-Angle Measurements (SWAXS) on: Gels Liquid Crystals (Bio) Polymers Amorphous Materials Muscles
Source characteristics	Wiggler (NdFeB Hybrid): Period: 140 mm No. full poles: 57 Gap: 20 mm B_{max}: 1.607 T Critical Energy ε_c: 4.27 keV Power (9 mrad): 8.6 kW Effective source size FWHM: 3.9 x 0.26 mm^2(HxV)
Optics	Optical elements: Double crystal monochromator: Si (111) asym. cut, water cooled. / Mirror: two–segment,toroidal, Pt coated. Distance from source: 18.4 m / 26.5 m Acceptance: 1 mrad/0.3 mrad (HxV) Energy (3 selectable): 5.4, 8, 16 keV (0.077, 0.154, 0.23 nm) Energy resolution ΔE/E: 0.7-2.5 x 10^{-3} Focal spot size FWHM: 1.2 x 0.6 mm^2 (HxV) Spot at Sample FWHM: 5.4 x 1.8 mm^2(HxV) Flux at sample: 5 x 10^{12} ph s^{-1}(2 GeV, 200 mA, 8 keV)
Experimental apparatus	Resolution in real space: 1-140 nm (small-angle), 0.1- 0.9 nm (wide-angle) Sample stage: temperature manipulations: ramps, jumps and gradient scans, pressure manipulation: scan and jumps, stop flow experiments, SWAXS measurements applying mechanical stress, SWAXS measurements applying magnetic fields. In-line calorimetric measurements simultaneously with SWAXS. Detectors: 1D gas-filled detectors for simultaneous small- and wide-angle (Gabriel type), 2D CCD-detector for small-angle.
Experiment control	Beamline control: Program-units written in LabView for Windows 1 D detector control: PC-card and software from Hecus & Braun, Graz. 2 D detector control: Software from Photonic Science, Oxford.

CURRENT STATUS

The beamline has been built by the Institute for Biophysics and X-ray structure Research (IBR), Austrian Academy of Science in collaboration with staff members from Sincrotrone Trieste, and is in user operation since September 1996. The set-up of the beamline started at the beginning of January 1995 with the installation of the support structure. Until the end of 1995, the 8 keV single energy system had been realised. The upgrade to the full three energy system was finished in spring 1998. Time resolved experiments require fast X-ray detectors and data acquisition hard- and software. Depending on the desired resolution in time and in reciprocal space, on isotropic or anisotropic scattering of the sample, one-dimensional position sensitive (delay-line type) or two-dimensional CCD detectors are employed.
In conclusion, due to wide versatility of the beamline and the highly flexible sample stage, there are nearly no limits for the realisation of an experiment, and you are welcome by our team to propose any interesting and highlighting investigation for the benefit of material and life sciences.

Application for Beamtime at ELETTRA

1. Beamtime Policy at SAXS beamline

According to the agreement from March 2001 regarding the co-operation between the Austrian Academy of Sciences and Sincrotrone Trieste, at the Austrian SAXS-beamline the available beamtime of about 5000 hours/year is distributed as follows:

- 35% for Austrian Users, type: "CRG" (Collaborating Research Group)
- 35% for Users of Sincrotrone Trieste (General Users (GU))
- 30% is reserved for beamline maintenance and in-house research

In both user beamtime contingents also any industrial, proprietary and confidential research can be performed according to the "General User Policy" of Sincrotrone Trieste.

To apply for CRG and GU user beamtime proposals must be submitted according to the rules of Sincrotrone Trieste. The international review committee at ELETTRA will rank the proposals according to their scientific merit assessment. Based on this decision beamtime will be allocated according to the specific quotes for the beamtimes (CRG/GU) either for the following semester ("normal application") or for the next two years ("long term application"). However, at the moment no more than a maximum of 10% of the beamtime will be assigned to "long term" projects.

2. How to apply for beamtime

There are two deadlines each year for proposals, namely August 31st and February 28th. Accepted proposals will receive beamtime either in the then following first or second half year period, respectively. The Application Form must be completed on-line according to the following instructions. In addition, one printed form is also required and must be send to:

ELETTRA USERS OFFICE
Strada Statale 14 - km 163.5
34012 Basovizza (Trieste), ITALY
Tel: +39 040 3758628 - fax: + 39 040 3758565
e-mail: useroffice@elettra.trieste.it

INSTRUCTIONS GIVEN BY THE USERS OFFICE
(see also: www.elettra.trieste.it/experiments/index.html)

1. Read carefully the following Guidelines.

2. Connect to the Virtual Users' Office: http://users.elettra.trieste.it using your favorite browser (Netscape 3.0 or above, Internet Explorer 4.0 or above, etc.) with JavaScript enabled.

3. Select the Virtual Users Office link.

4. When prompted, insert your ID and password. If you are a new user fill in the registration form with your data and choose your institution with the search button; in case your institution does not appear in the list, please contact useroffice@elettra.trieste.it giving all the details about it. When registered, you will receive an acknowledgment with your ID and password. You can change your password, if you wish. In case you forget your password, please don't register again but contact useroffice@elettra.trieste.it. At any moment you can select the help button and view more detailed instructions. By inserting your ID and password you will be able to continue.

5. Select the proposals button in the User functions group.

6. Select add and fill in on-line the proposal form. Please, type your proposal in English. Repeat this procedure for each proposal you intend to submit.

7. In case of continuation proposal: a) attach the experimental report of previous measurements; b) give your previous proposal number.

8. When finished, submit the proposal electronically, selecting the save button.

9. Print the proposal form together with each related safety form.

10. Sign the safety form(s).

11. Mail one complete printed copy to the Users Office.

NOTE

From July 2002 on there exists a new possibility for users from developing countries to apply for financial support for their travel expenses. For all other users everything remains as before. For further information, please have a look into the web-pages

http://www.elettra.trieste.it/experiments/users_handbook/index.html)

or contact the USERS OFFICE.

List of Institutes Participating in Experiments

Austria

Austrian Academy of Science, Erich Schmid Institut für Materialwissenschaft, Leoben, and Institut für Metallphysik, Montanuniversität, Leoben

Fratzl Peter
Gupta Himadri
Kopacz Ireneusz
Misof Klaus
Pippan R.
Paris Oskar
Tian Bha Hui

Austrian Academy of Science, Institute for Biophysics and X-ray Structure Research, Graz

Amenitsch Heinz
Bringzu Frank
Hickel Andrea
Kalisz Ewa
Kriechbaum Manfred
Laggner Peter
Lohner Karl
Majerowicz Monika
Pabst Georg
Pozo Beatriz
Rappolt Michael
Strobl Marlene
Teixeira Cilaine Veronica
Vidal Monika

LKT-TGM, Laboratorium für Kunststofftechnik G.m.b.H, Wien

Wilhelm Harald

Ludwig Boltzmann-Institut for Osteology, 4th Medical Department, Hanusch-Hospital, Vienna

Roschger Paul
Tesch Walter

Technische Universität Graz, Institute for Structural Analysis and Computational Biomechanics, Graz

Schulze-Bauer Christian A. J.
Holzapfel G.A.

Technische Universität Graz, Institut für Festkoerper Physik, Graz

Heimel Georg
Oehzelt Martin

Universität Wien, Institut für Materialphysik, Wien

Paris Alfred
Schafler Erhard
Zehetbauer Michael
Zeipper Leonhard

Bulgaria

Sofia University, Faculty of Physics, Department of General Physics, Sofia

Todorova G.

Canada

National Research Council, Steacie Institute for Molecular Sciences, Chalk River, Ontario

Katsaras J.

Croatia

"Ruder Boskovic" Institute, Zagreb

Buljan M.
Desnica-Frankovic I. Dunja
Desnica Uros V.
Kovacevic Ivana
Pivac Branko

University of Zagreb, Institute for Physics, Zagreb

Borjanovic Vesna
Milat Ognjen
Salomon Kresimir

Czech Republic

Academy of Sciences of the Czech Republic, Institute of Macro- molecular Chemistry, Prague

Baldrian Josef

Czech Technical University, Faculty of Nuclear Science and Physical Engineering, Prague

Horky Martin

Czech Technical University, Faculty of Nuclear Science and Physical Engineering, Prague

Benes L.
Melánová K.
Zima V.

Joint Laboratory of Solid State Chemistry of the Academy of Sciences of the Czech Republic, and University of Pardubice, Department of Physics, Pardubice

Steinhart Milos

Finland

Åbo Akademi University, Dept. of Physical Chemistry, Materials Research Group, Turku

Lindén Mika
Tiemann M.

France

Arilait Recherches, Paris

Lopez Christelle

Equipe Physico-Chimie des Systèmes Polyphasés, Chatenay-Malabry

Artzner Franck
Kalnin Daniel
Keller G.
Ollivon Michel

Nestlé S.A. PTC, Beauvais

Quenneson P.

Lure, Orsay / Paris

Pierre Lesieur

University Paris 6, Chimie de la Matiere Condensee, Paris

Alonso Bruno
Babonneau Florence
Boocnara Anne
Cagnol Florence
Grosso David
Sanchez C.
Soler-Illia Galo

University Paris-Sud, Solid State Physics, Orsay/Paris

Albouy Pierre-Antoine

Germany

Hahn-Meitner-Institut, Berlin

Zizak Ivo

Forschungszentrum Jülich, Institut für Festkörperforschung (IFF)

Paul Amitesh

Forschungszentrum Jülich, Institut für Grenzflächenforschung und Vakuumphysik
Paul Neelima

Hamburger Synchrotronstrahlungslabor (Hasylab), Hamburg
Flege Jan-Ingo

Max-Planck-Institut für Kohlenforschung, Mülheim / Ruhr
Bussian Patrik
Schmidt Wolfgang

Universität Bremen, Institut für Festkörperphysik
Clausen Torben
Falta Jens
Gangodadyhay Subhashis
Schmidt Thomas

Universität Siegen, Institut für Physik, Siegen
Besch Hans-Juergen
Orthen Andre'
Wagner Hendrik
Walenta Albert Heinrich

Hungary

Eötvös Lorand University, Institute for General Physics, Budapest
Hanak Peter
Horvath Gyoezoe
Kenesei Peter
Kovacs Zsolt
Simon Kornel
Ungár Tamas

India

Inter University Consortium for DAE Facilities, Univ. Campus, Khandwa Road, Indore
Dasannacharya B.A.
Gupta Ajay

Raman Research Institute, Bangalore
Raghunathan V.A.

Italy

CNR, direzione progetto finalizzato biotecnologie, Genova
Giovine Marco

CNR, Istituto Processi Chimico-Fisici, Messina
Triolo Alessandro

Sincrotrone Trieste, Trieste
Bernstorff Sigrid
Dubcek Pavo
Menk Ralf
Morello Christian

Università di Ancona, Dipartimento di Scienze e Biotecnologie Agrarie ed Ambientali, and INFM
Carsughi Flavio

Università di Ancona, Istituto di Scienze Fisiche, and INFM
Corsi Federica
Di Gregorio Giordano M.
Federiconi Francesco
Mariani Paolo
Pisani Michaela
Spinozzi Francesco

Università di Firenze, Dip. Scienze Fisiologiche, Firenze
Bagni Maria Angela
Cecchi Giovanni
Colombini Barbara
Geiger Paige

Università di Genova, DIMES, sez. Biochimica, Genova
Benatti Umberto

Università di Modena, Dip. di Fisica, Modena
Corni F.
Ottarini G.
Tonini R.

Università di Padova, Dep. of Mechanical Engineering, Padova
Maddalena Amadeo
Principi Giovanni
Meyer Marcos
Dal Toe' Simone

Università di Palermo, Dipartimento di Chimica Fisica, Palermo
Baiata V.
Lo Celso Fabrizio
Triolo Roberto

Università di Parma, Dip. di Fisica, e INFM, Parma
Favilla Roberto
Goldoni M.

Università di Perugia, Dipartimento di Fisica and INFM, Perugia
Cinelli Stefania
Onori Giuseppe

Università del Piemonte Orientale „A.Avogadro“, Dip. Scienze e Tecnologie Avanzate (DISTA), Alessandria
Causa' M.
Croce Gianluca
Frache Alberto
Marchese L.
Milanesio Marco
Viterbo Davide

Università di Roma-II-„Tor Vergata“, Dip. Scienze e Tecnologie Chimiche
Cavalieri F.
Chiessi E.
Paradossi Gaio
Ponassi Valeria

University of Trieste, Dep. of Biochemistry, Biophysics and Macromolecular Chemistry, Trieste
Cesàro Attilio
Nevyjel Marco
Sussich Fabiana
Tiziani Stefano

Poland

A. Mickiewicz University , Department of Macromolecular Physics, Poznan
Maciej Kozak.

Institute of Coal Chemistry, Polish Academy of Sciences, Gliwice
Wolinska-Grabczyk A.

Institute of Nuclear Chemistry and Technology, Warsaw
Griegoriew Helena
Plusa Malgorzata

Polish Academy of Sciences, Institute of Physics, Warsaw
Domagala Jaroslaw

Polish Academy of Sciences, Institute of Metallurgy and Materials Science, Krakow
Bonarski Jan T.

Russia

Arbuzov Institute of Organic and Physical Chemistry, Kazan Scientific Center, Russian Academy of Sciences, Kazan

Kovalenko Valery

Joint Inst. for Nuclear Research - Lab. of Neutron Physics, Dubna, Moscow

Rajewska Aldona

Slovenia

Josef Stefan Institute, Ljubljana

Zidansek Alexander

Spain

IIQAB-CSIC, Dep. Tecnologia de Tensioactius, Barcelona

Caelles Jaime
Cocera Merce
Carrera I.
Lopez Olga
De la Maza A.
Pons Ramon

Sweden

Mid-Sweden University, NTM (Department for Natural Sciences), Sundsvall

Edlund H.
Persson Gerd

Umeå University, Department of Biophysical Chemistry, Umeå

Lindblom G.

Ukraine

Ukraine Academy of Sciences, Research Center for Radiation Medicine, Kyiv

Plyushch Galyna

United Kingdom

Heriot Watt University, Department of Chemistry, Edinburgh
Holmes Paul

University Laboratory of Physiology, Oxford
Ashley Christopher C.
Griffiths Peter J.

University of Strathclyde, Dept of Pure and Appl. Chem., Glasgow
Gordon C. M.

USA

Mount Sinai School of Medicine, New York, NY
Triolo Fabio G.

List of Performed Experiments

2001 (first half year)

Proposal	Proposer	Institution	Country	Title	Research Area
2000219	Gupta Ajay	Inter University Consortium for DAE Facilities, Indore	India	Small angle x-ray scattering study of amorphous to nanocrystalline transformation in Fe-Cu-Nb-Si-B and Fe-Cu-Zr-B alloys	Materials Science
2000235	Paradossi Gaio	Università di Roma "Tor Vergata" - Dip. di Scienze e Tecnologie Chimiche	Italy	Synergic gels: Interaction between glucomannan and xanthan polysaccharides in aqueous solution and in gel phase.	Life Science
2000237	Resel Roland	Technische Universität Graz - Institut für Festkörperphysik	Austria	Crystallographic studies of molecular crystals under isotropic pressures up to 2kbar	Physics
2000263	Babonneau Florence	Université Paris 6 - Chimie de la Matiere Condensee	France	Time resolved in situ XRAY study of the formation of dip-coated mesostructured films	Chemistry
2000268	Grigoriew Helena	Institute of Nuclear Chemistry and Technology, Warsaw	Poland	Depth-depending structure of permeating polymer membranes.	Physics
2000273	Laggner Peter	Austrian Academy of Sciences (A.A.S.) - Inst. of Biophysics and X-Ray Structure Research, Graz	Austria	Self-Assembly and Structural Dynamics of Membrane-Mimetic Systems": 1. Use of surface diffraction to study phospholipids under influence of salt 2. Pretransitional swelling of phospholipid bilayers above the main transition 3. Interface study in the lamellar/inverse hexagonal phase region of PEs: a major component of bacterial membranes 4. Lipid/Cholesterol mixtures: thermodynamical and structuralparameters obtained by pressure scanning SAXS	Life Science
2000274	Zehetbauer Michael	Universität Wien - Inst. für Materialphysik	Austria	Spatial Distribution of Deformation Induced Lattice Defects in Ultrafine-Grained and Nanostructured Metallic Materials."	Materials Science
2000275	Besch Hans-Jürgen	University of Siegen, Dept. of Physics	Germany	Test measurements on advanced gaseous detectors for time resolved SAXS experiments."	Instrumen-tation

2000276	Mariani Paolo	Università di Ancona - Ist. di Scienze Fisiche	Italy	Phase behaviour, molecular conformation and compressibility of inverse lipid systems."	Life Science
2000277	Paris Oskar	A.A.S. - Erich Schmid Inst. für Materialwissenschaft, and University of Leoben	Austria	Correlation between Degree of Mineralization and Mineral Crystal Size in differently mineralized Connective Tissue"	Life Science
2000279	Triolo Alessandro	Hahn Meitner Institut, Berlin	Germany	Critical Micellisation Density (CMD): a Synchrotron SAXS Structural Study of the Unimer-Aggregate Transition of block-copolymers in near- and super-critical fluids."	Chemistry
2000284	Grigoriew Helena	Institute of Nuclear Chemistry and Technology, Warsaw	Poland	Kinetic of the structural changes in the polymer saturated with a penetrant during a desorption process.	Physics
2000303	Triolo Alessandro	Hahn Meitner Institut, Berlin	Germany	Structural Characterization of monomer-aggregate transition in coblock copolymers dissolved in homopolymer matrices.	Chemistry
2000305	Triolo Alessandro	Hahn Meitner Institut, Berlin	Germany	Microheterogeneities in PEO-salt mixtures.	Chemistry
2000332	Kovalenko Valery	Arbuzov Institute of Organic and Physical Chemistry - Kazan Scientific Center - Russian Academy of Sciences (KSC RAS)	Rusia	SAXS and WAXS study of pressure-induced thermotropic mesomorphism of the elementoorganic starburst dendrimers.	Life Sciences
2000347	Mariani Paolo	Università di Ancona - Ist. di Scienze Fisiche	Italy	Time resolved SAXS analysis of porcine pepsin acid induced aggregation.	Life Science
2000360	Sussich Fabiana	Università di Trieste - Dip. Biochim., Biofisica, Chim. Macromol.	Italy	Cryptobiosis: the role of trehalose in the stabilization of lipid membranes	Life Science
2000368	Rajewska Aldona	Joint Inst. for Nuclear Research - Lab. of Neutron Physics, Dubna	Russia	The critical behavior study of the lamellar-nematic phase transition in the ternary system (DACl)/H2O/ammonium chloride (lyotropic liquid crystal) and the chemical reactions of nucleophilic substitution in phosphorus acid esters (PAE) by the SAXS method.	Materials Science
2000370	Dubcek Pavo	Sincrotrone Trieste S.C.p.A.	Italy	Grazing incidence small angle X-ray scattering investigation of structural changes in annealed H implanted monocrystalline silicon	Materials Science
2000381	Mariani Paolo	Università di Ancona - Ist. di Scienze Fisiche	Italy	Pressure-assisted cold denaturation of proteins: a test analysis by SAXS at Elettra	Life Science

2000392	Viterbo Davide	Università di Torino - Dip. di Chimica I.F.M.	Italy	High Resolution Fiber Diffraction for Structure Elucidation of Silicatein Filaments in Spicules from different Sponges	Materials Science
2000404	Ollivon Michel	C.N.R.S. - Université de Paris Sud	France	Triglyceride crystallisation in milk emulsions at subzero temperatures : Study of liquid-crystalline structures and phase transitions by coupling of Differential Scanning Calorimetry and High Resolution Small Angle X-ray Scattering.	Life Science
Inhouse	Steinhart Milos	Czech Academy of Sciences - Inst. of Macromolecular Chemistry, Prague	Czech Republic	Study of Phase Properties of Intercalates by SWAXS	Physics

2001 (second half year)

Proposal	Proposer	Institution	Country	Title	Research Area
2001019	Griffiths Peter John	University Laboratory of Physiology, Oxford	United Kingdom	Time-resolved structural and mechanical studies of the contractile system of isolated skeletal muscle fibres.	Life Sciences
2001053	Triolo Alessandro	Hahn Meitner Institut, Berlin	Germany	Room Temperature Ionic Liquids: phase diagram characterization with combined SAXS-WAXS.	Materials Science
2001081	Baldrian Josef	Czech Acad. of Sciences, Inst. of Macromol. Chemistry, Prague	Czech Republic	Time-resolved SAXS/WAXS Studies on Macromolecular Materials:Cocrystallization Dynamics in Lamellar Systems of PEO/PEO-PPO Blends	Physics
2001089	Mariani Paolo	Università di Ancona - Ist. di Scienze Fisiche	Italy	Structural and energetic effects of hydrostatic pressure on inverse hexagonal and bicontinuous cubic phases in lipid-water systems	Life Sciences / Biophysics
2001090	Pons Ramon	IIQAB-CSIC, Dep. Tecnologia de Tensioactius, Barcelona	Spain	Dynamics of non-equilibrium processes in surfactants systems	Physical Chemistry
2001115	Besch Hans-Jürgen	University of Siegen, Dept. of Physics	Germany	Test measurements on advanced gaseous detectors for time resolved SAXS experiments	Instrumen-tation
2001140	Babonneau Florence	Université Paris 6 - Chimie de la Matiere Condensee	France	In-situ X ray diffraction study of dip-coated TiO2, Al2O3 and Fe2O3 mesostructured films	Materials Sciences
2001162	Triolo Roberto	University of Palermo, Department of Physical Chemistry	Italy	Critical Micellisation Density (CMD): a Synchrotron SAXS Structural Study of the Monomer-Aggregate Transition of block-copolymers in near- and super-critical fluids.	Materials Science

2001171	Falta Jens	Universität Bremen, Institut für Festkörperphysik, Abteilung Oberflächenphysik, Bremen	Germany	Structural characterization of thin SiNx films on Si(111)	Materials Science
2001177	Gupta Himadri Shikhar	A.A.S. - Erich Schmid Inst. für Materialwissen-schaft, and University of Leoben	Austria	In-situ X-ray scattering studies of mechanical properties of mineralizing collagenous tissues	Life Sciences
2001220	Linden Mika	Åbo Akademi University, Department of Physical Chemistry, Materials Research Group, Turku	Finland	In situ SAXS study of the initial stages of particle nucleation and growth from solution	Chemistry
2001225	Zehetbauer Michael	Universität Wien - Inst. für Materialphysik	Austria	Synchrotron WAXS & SAXS Studies of Microstructural Evolution during Post-Yield Deformation of Isotactic Polypropylen	Materials Science
2001229	Laggner Peter	Austrian Academy of Sciences (A.A.S.) - Inst. of Biophysics and X-Ray Structure Research, Graz	Austria	Self-Assembly and Structural Dynamics of Membrane-Mimetic Systems": 1. Use of surface diffraction to study phospholipids under influence of salt 2. Pretransitional swelling of phospholipid bilayers above the main transition 3. Interface study in the lamellar/inverse hexagonal phase region of PEs: a major component of bacterial membranes 4. Lipid/Cholesterol mixtures: thermodynamical and structuralparameters obtained by pressure scanning SAXS	Life Sciences
2001231	Zehetbauer Michael	Universität Wien - Inst. für Materialphysik	Austria	Time and Space Resolved Scanning Synchrotron X-ray Profile Analyses during Plastic Deformation of BCC and HCP Metals	Materials Science
In-house	Bernstorff, Dubcek, Desnica Uros + Ida Dunja	Sincrotrone Trieste + Ruder Boskovic" Institute, Zagreb	Italy / Croatia	Morphological characterization of CdS Quantum Dots in SiO2 substrate studied by GISAXS	Materials Science

In-house	Dubcek Pavo, Bernstorff Sigrid, Pivac Branko	Sincrotrone Trieste S.C.p.A. + Ruder Boskovic" Institute, Zagreb	Italy / Croatia	Grazing incidence small angle X-ray scattering study of irradiation induced defects in monocrystalline silicon	Materials Science
In-house	Amenitsch Heinz, Linden Mika, Babonneau Florence	A.A.S. / IBR, Åbo Akademi University (Turku); Université Paris	Austria / Finland / France	In-situ XRAY study of the formation of mesoporous organosilicates	Chemistry
In-house	Bernstorff Sigrid, Ungar Tamas	Sincrotrone Trieste + Eötvös University, Institute for General Physics, Budapest	Italy / Hungary	Early stages of the decomposition of the solid solution in an Al-Zn-Mg alloy	Materials Science
In-house	Steinhart Milos	Czech Academy of Sciences - Inst. of Macromolecular Chemistry, Prague	Czech Republic	Study of Phase Properties of Intercalates by SWAXS	Physics
In-house	SAXS-Group + Zidansek Aleksander	Sincrotrone, A.A.S., + Institute Jozef Stefan, Ljubljana	Italy, Austria, Slovenia	Smectic Ordering of confined liquid crystals	Physics
Pilot / Test	Schulze-Bauer Christian	Technische Universität Graz, Dep. Computational Biomechanics, Graz	Austria	SAXS investigation of layer-specific collagen structures in human aortas during tensile testing	Life Science
Pilot /Test	Persson Gerd	Mid-Sweden University, Sundsvall	Sweden	Temperature study of two cubic phases in the ternary monooleoyl glycerol / octyl glucoside 2H2O system	Life Science

User Statistics

1. Number of submitted proposals and assigned shifts from 1995 until December 2002

The Austrian SAXS-beamline at ELETTRA opened to users in September 1996. Since then many experiments have been performed related to the fields of life science, material science, physics, biophysics, chemistry, medical science, technology and instrumentation.

From September 96 on users gained access to the SAXS-beamline on the basis of the proposals received for the periods shown in Fig. 1. The assignment of beamtime at this beamline is done separately for the group of "General Users" (GU) and the "Collaborating Research Group" (CRG), i.e., the Austrian users. Beamtime was assigned to the proposals of each group in the order of the rating received by the Scientific Committee, and up to the maximum number of shifts available to each group according to the contract between "The Austrian Academy of Sciences" and the "Sincrotrone Trieste". Until December 1997 up to 55 % of the beamtime was given to CRG, up to 30 % to GU, and 15% was reserved for maintenance purposes. From January 98 to June 2001 the quota for beamtime was up to 35 % for CRG, up to 50 % for GU, and again 15% reserved for maintenance purposes. From July 2001 on the two contingents for user proposals from CRG and GU receive up to 35% of the beamtime each. The remaining 30 % of beamtime are used for inhouse research projects as well as for maintenance purposes.

Fig. 1 gives an overview of the numbers of received proposals, the numbers of requested and assigned shifts, as well as the percentage between assigned and requested shifts. Included in Fig.1 are also the same data for the period End 1995 - August 1996, during which some beamtime had been given already to users in order to perform first pilot- and test-experiments together with the beamline staff. These first experiments during the commissioning phase were not yet based on proposals, since the goal was mostly to evaluate and improve the performance of the beamline and the equipment of its experimental station. As can be seen in Fig.1, the request for beamtime at the SAXS-beamline increased continuously and strongly until the first half year of 1999 (also during the period Sept.-Dec. 1997, if one takes into account that this period was only 4 instead 6 month long, and that for this reason less proposals were submitted). Then, probably due to the high rejection rates, the number of submitted proposals decreased somewhat, which resulted in a better ratio of accepted / rejected proposals. Therefore, during the last two proposal deadlines, the number of submitted proposals increased again considerably.

In 2001, in total 54 proposals (6 from CRG, and 48 from GU) were submitted. From these 13 proposals (all from GU, corresponding to 27 % of the GU proposals) were submitted by "new" usergroups, i.e. groups which so far had never beamtime at the SAXS beamline. From these 4 proposals were officially accepted, while 2 received some shifts for a first „pilot“ experiment. This corresponds to 13% (or 20 % when including the two „pilot experiments“) of all accepted GU proposals.

Figure 1 (Next page). The statistical information about the beamtime periods since end of 1995 are given for the groups "CRG", and "GU" separately, as well as for both together ("Total"). Shown are, for all beamtime periods:
(a) Number of received proposals, (b) Number of requested shifts,
(c) Number of assigned shifts, and (d) Relation between assigned and requested shifts

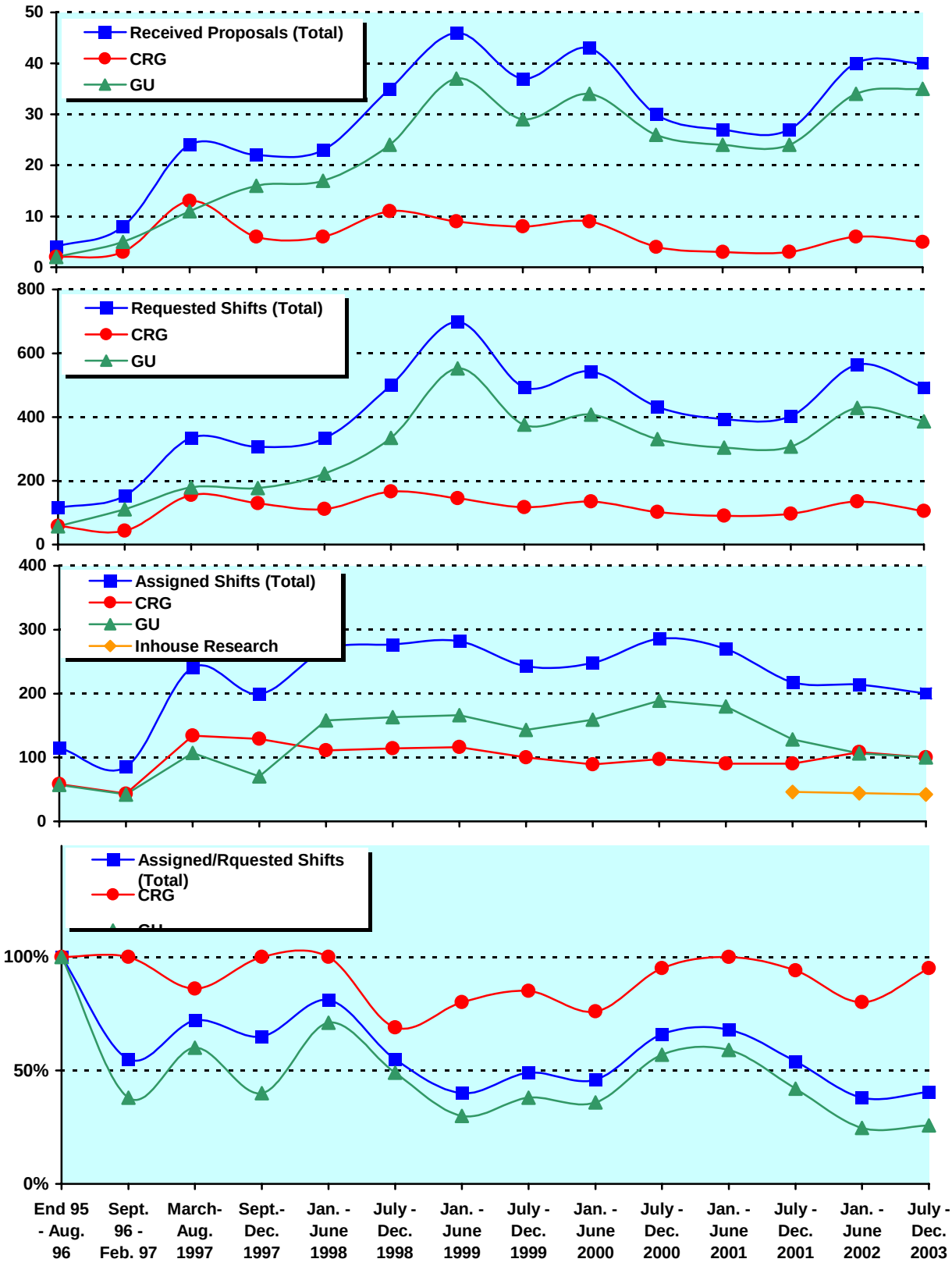
Received Proposals (Total)
CRG
GU
50
40
30
20
10
0
Requested Shifts (Total)
CRG
GU
800
600
400
200
0
Assigned Shifts (Total)
CRG
GU
Inhouse Research
400
300
200
100
0
Assigned/Rquested Shifts (Total)
CRG
100%
50%
0%
End 95 - Aug. 96
Sept. 96 - Feb. 97
March-Aug. 1997
Sept.-Dec. 1997
Jan. - June 1998
July - Dec. 1998
Jan. - June 1999
July - Dec. 1999
Jan. - June 2000
July - Dec. 2000
Jan. - June 2001
July - Dec. 2001
Jan. - June 2002
July - Dec. 2003

2. Quality of proposals

By comparing the „cut-off“-value (i.e. the rating, which a proposals needs at least in order to be eligible for beamtime assignment) and the ratings, which are assigned by the scientific review committee to the proposals of each semester, it becomes clear (see fig. 2), that the quality of the accepted proposals has improved considerably over the years.
This is due to two facts:

- the high over-subscription of the SAXS-beamline allows to choose only the best proposals (of „general users“) for beamtime assignment
- proposals from users, which are „clients“ of our beamline since many years, tend to get better with experience and time

As can be seen in Figure 2, the proposals of „general users“ need nowadays a very good rating for getting accepted. The situation for GdR-users is more relaxed, since the quota of shifts reserved for them corresponds roughly to their request for beamtime.

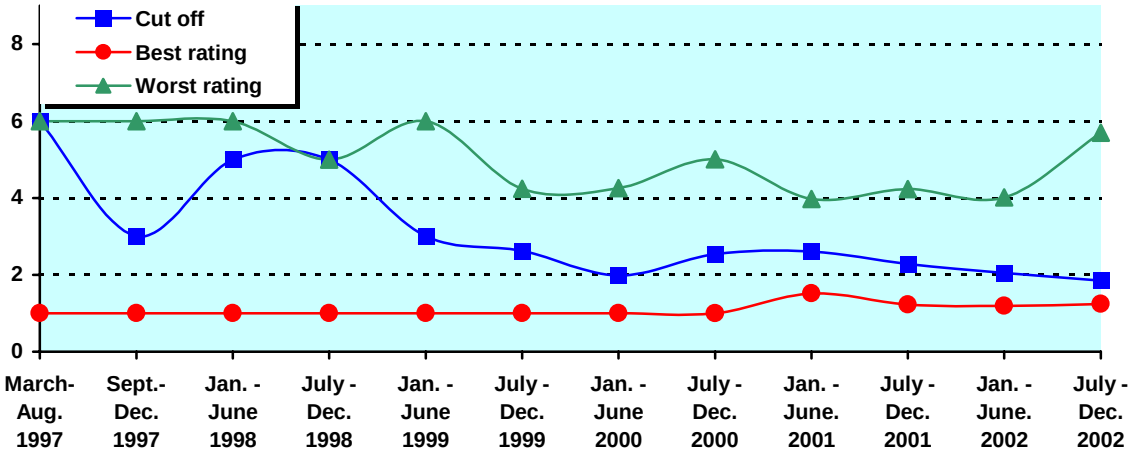

Figure 2. Shown are for the proposals from „General Users“: best rating, worst rating and „cut-off“-value for all beamtime periods since march 1997.

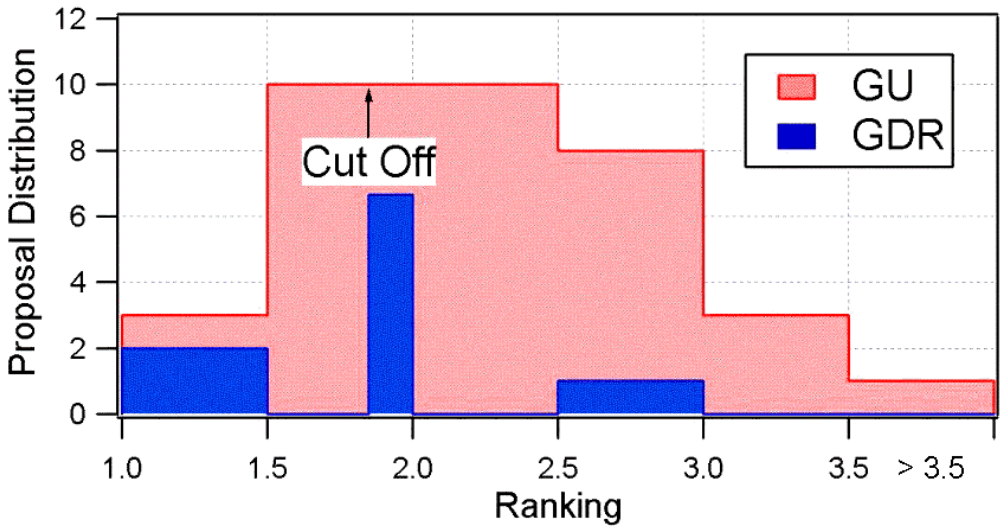

Figure 3. Distribution of the ratings of the proposals submitted for the 2. Semester of 2002. Light gray: referring to general user proposals; dark gray: GDR-user proposals.

3. Provenience of users

During 2001, 158 users from 63 institutes in 19 countries have performed experiments at the SAXS beamline. In Fig. 4 are shown both the provenience of these users, and of their respective institutes. Each user or institute was counted only once, even though many users performed experiments in both beamtime periods of 2001.

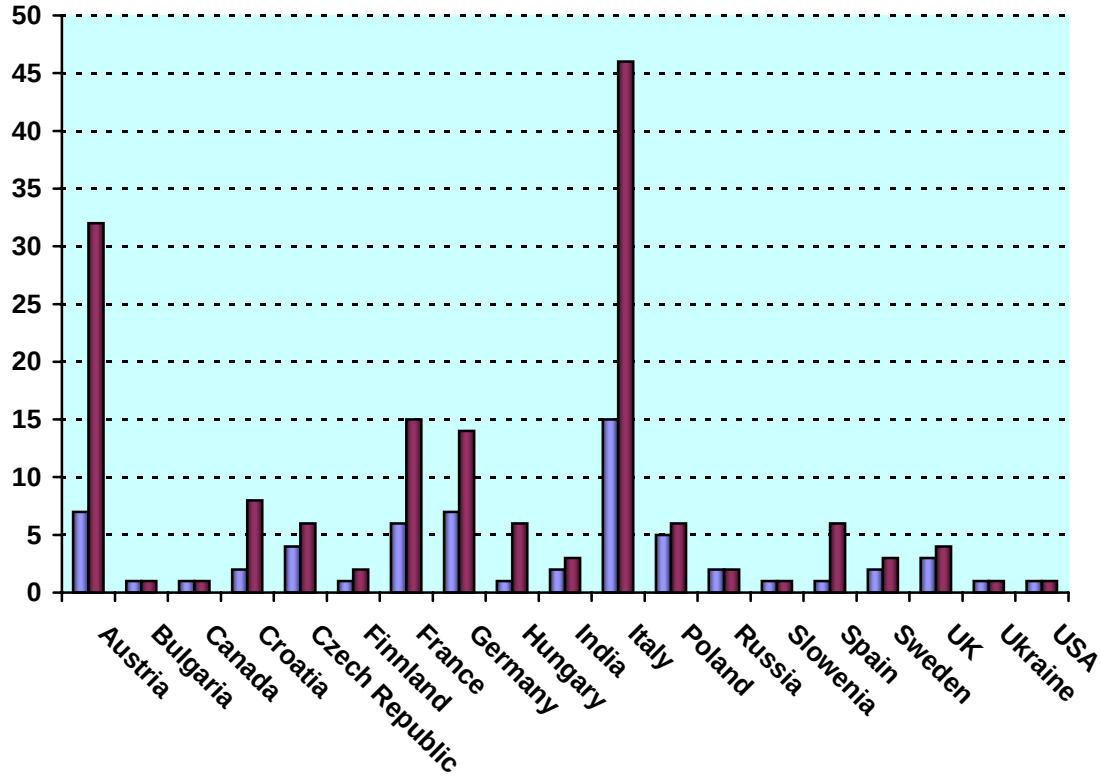

Figure 4. Provenience of users (dark grey) and of their corresponding institutes (light grey).

4. Documentation of experimental results

As could be expected, with the start of user-operation at the SAXS-beamline the number of contributions to conferences started to increase strongly. With a delay of one year - the average time needed for paper publications - also the number of publications increased accordingly, as can be seen in Fig. 5.

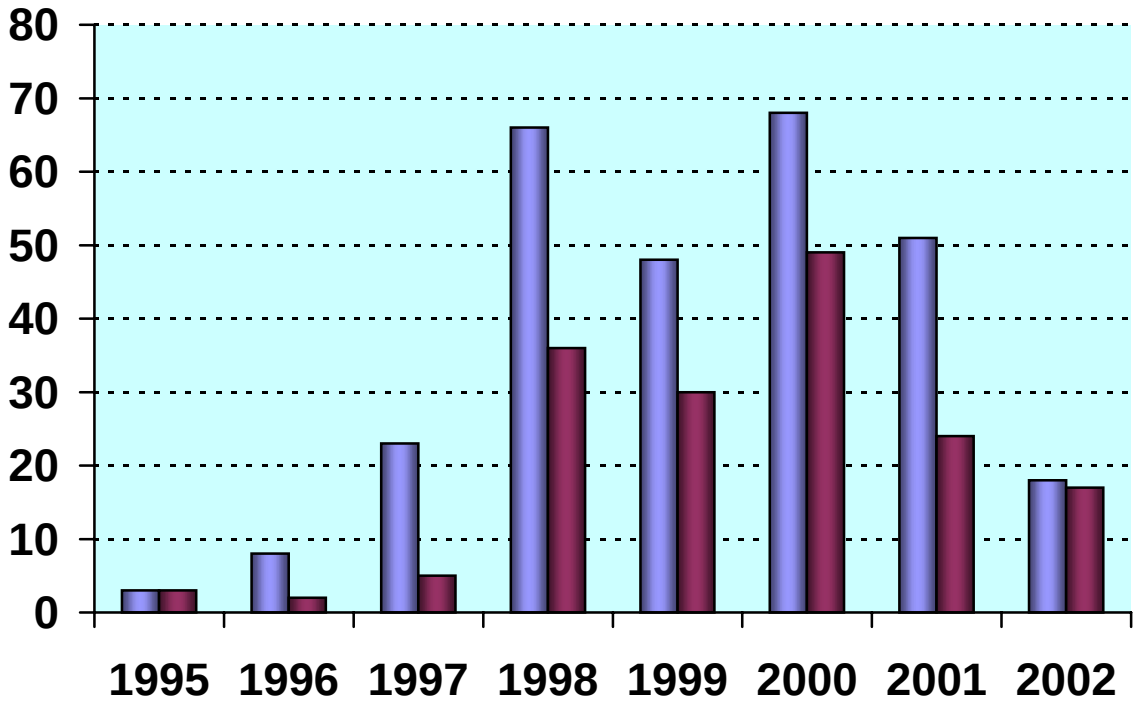

Figure 5. Number of conference contributions (light grey) and of refereed paper publications (dark grey) for the years 1995-2001. Also contributions, which have been published until April 2002 are included.

In addition, from 1995 until March 2002, the following documentations based on instrumentation of the SAXS-beamline, or on data taken with it, have been produced.

Unrefereed publications:

Technical Reports on Instrumentation:	5
Contributions to Elettra Newsletters:	15
Contributions to Elettra Highlights:	13
PhD Thesis:	19
Diploma Thesis :	12

Experimental Possibilities at the SAXS-beamline

1. Accessible SAXS and WAXS ranges

Simultaneous SAXS- and WAXS-measurements can be performed using a linear sensitive gas detector (Gabriel type, windows size 8 x 100 mm, active length 86.1 mm with a resolution of 0.135 mm/channel) for the WAXS-range, and either a second linear Gabriel type detector (windows size 10 x 150 mm, active length 134 mm with a resolution of 0.159 mm/channel), or the 2D CCD-system for the SAXS-range. A specially designed vacuum chamber (SWAXS-nose, see Annual Report of 1996/97, p. 32) allows to use both scattering areas below (for SAXS) and above (for WAXS) the direct beam, respectively.
Depending on the photon energy maximum SAXS resolutions of 2000 Å (5.4 keV), 1400 Å (8 keV) or 630 Å (16 keV) are available. The available possible WAXS-ranges are summarised in Table 1. The overall length of the SWAXS-nose in the horizontal direction, measured from the sample position, is 512 mm and the fixed sample to WAXS-detector distance is 324 mm. At the shortest SAXS camera-length an overlap in the d-spacings covered by the SAXS- and WAXS-detectors, respectively, is possible: then, the common regime lies around 9 Å.

Table 1. Possible d-spacing ranges in the WAXS-regime at the SAXS-beamline at ELETTRA. Since the WAXS-detector can be mounted at four different fixed positions on the SWAXS-nose (range 1-4), with the three possible energy choices (5.4, 8 and 16 keV) this results in 12 different d-spacing regimes. In italic the most common choice (8 keV, range 1) is highlighted. This range is suited for experiments, e.g., on lipid-systems and (bio)polymers.

Range	**2θ [deg]**	**d-spacing (Å)**		
		8 keV	**5.4 keV**	**16 keV**
1	9.4	*9.40*	14.03	4.27
	27.6	*3.23*	4.82	1.47
2	27.4	3.25	4.86	1.48
	45.6	1.99	2.97	0.90
3	45.4	2.00	2.98	0.91
	63.6	1.46	2.18	0.66
4	63.4	1.47	2.19	0.67
	81.6	1.18	1.76	0.54

2. Calibration of the s-axis and flat field correction

At the SAXS beamline various standards are used for the angular (s-scale) calibration of the different detectors:

- rat tail tendon for the SAXS detector - high resolution (rtt*.dat)
- Silver behenate for the SAXS detector – medium and low resolution (agbeh*.dat)
- Para-bromo benzoic acid for the WAXS detector – WAXS range 1 and 2 (pbromo*.dat)
- Combination of Cu, Al foils and Si powder for the WAXS detector – WAXS range 2 and higher

In Fig. 1 a typical diffraction pattern of rat tail tendon is shown, depicting the diffraction orders (from the first to the 14th order) measured with a "high" resolution set-up (2.3 m) and the delay-line gas detector. The d-spacing is assumed to be 650 Å, but this value can vary depending on humidity up to 3%. Thus, the rat tail tendon is often used only to determine the position of the direct beam (zero order), while the absolute calibration is performed using the diffraction pattern of Silver behenate powder. Fig. 2 depicts a diffraction pattern of Silver behenate measured with "medium" resolution set-up (1.0 m) from the first to the 4th order (repeat spacing 58.4 Å) [1].

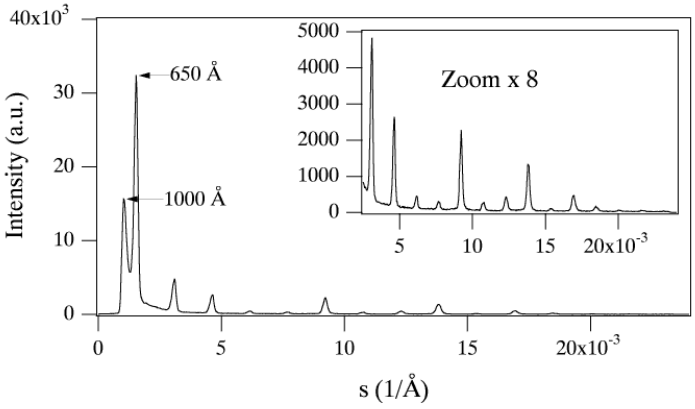

Figure 1. SAXS diffraction pattern of the collagen structure of rat tail tendon fibre at a distance of 2.3 m.

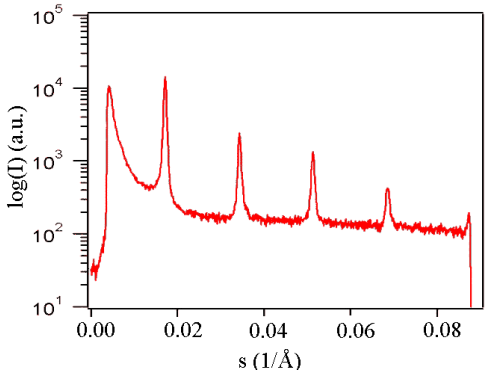

Figure 2. SAXS diffraction pattern of Ag behenate powder at a distance of 1.0 m

In Fig. 3 a typical WAXS pattern of p-bromo benzoic acid is shown. The diffraction peaks are indexed according to the values given in Table 2, taken from [2].

Table 2. d-spacings and relative intensities of p-bromo benzoic acid according to [2].

d-spacing/Å	rel. intensity	d-spacing/Å	rel. intensity
14.72	18000	4.25	490
7.36	1200	3.96	2380
6.02	330	3.84	10300
5.67	980	3.74	26530
5.21	6550	3.68	1740
4.72	26000	3.47	760

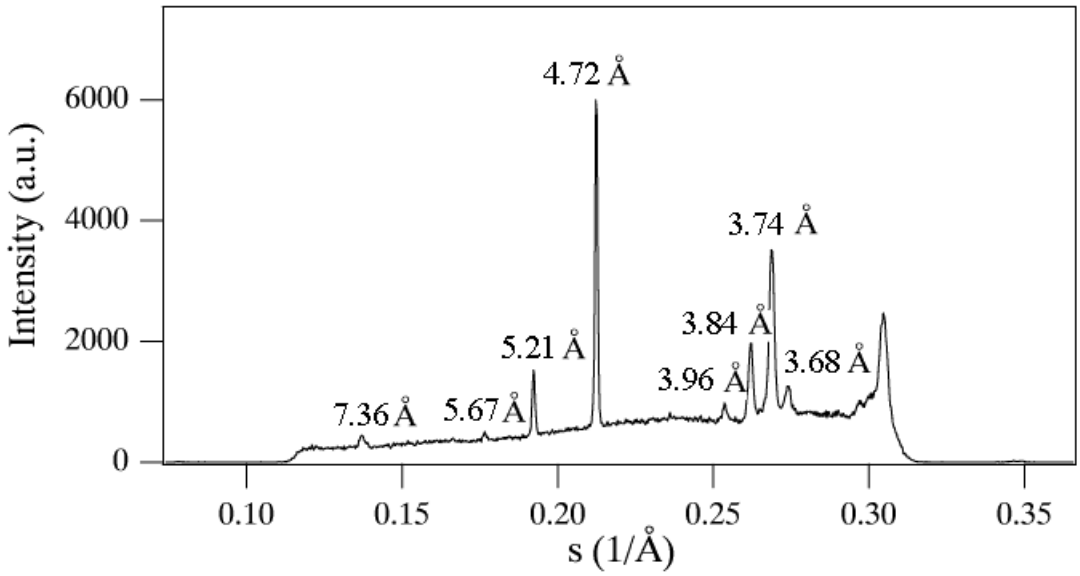

Figure 3. WAXS pattern of p-bromo benzoic acid measured in the WAXS range 1.

The s-scale for both, the SAXS and the WAXS range, can be obtained by linear regression, i.e., the linear relation between the kown s-values of the calibrant versus the measured peak positions has to be found.

A further correction is regarding the flat field response (efficiency) of the detectors. For this correction, the fluorescence light of various foils are used to illuminate the detectors rather homogeneously:

- At 8 keV: iron foil (100 μm thick), fluorescence energy: 6.4 keV K_α, 7.1 keV K_β (effic*.dat)
- At 16 keV: copper foil (> 100 μm thick), fluorescence energy: 8.028 keV $K_{\alpha 2}$, 8.048 keV $K_{\alpha 1}$, 8.905 keV K_β (effic*.dat)

The measured scattering pattern are corrected for the detector efficiency simply by dividing them by the fluorescence pattern. Note: The average of the detector efficiency data should be set to unity and a small threshold should be applied to avoid any division by zero.

[1] T.N. Blanton et. al., Powder Diffraction 10, (1995), 91
[2] K. Ohura, S. Kashino, M. Haisa, J. Bull. Chem. Soc. Jpn. 45, (1972), 2651

3. Available sample manipulations stages

1. General

Usually the sample is mounted onto the sample alignment stage which allows the user to place the sample into the beam with a precision of 5 µm (resolution: 1 µm). In Fig. 4 the ranges for vertical and horizontal alignment as well as the maximum dimensions of the sample holders are given. The maximum weight on the sample stage is limited to 10 kg. In case the envelope dimensions of a sophisticated sample station provided by the users are slightly larger than those given in Fig. 4, the user can ask the beamline responsible for a check up of his space requirements. If it does not fit at all to these specifications, user equipment can also be mounted directly onto the optical table, which allows much larger spatial dimensions.

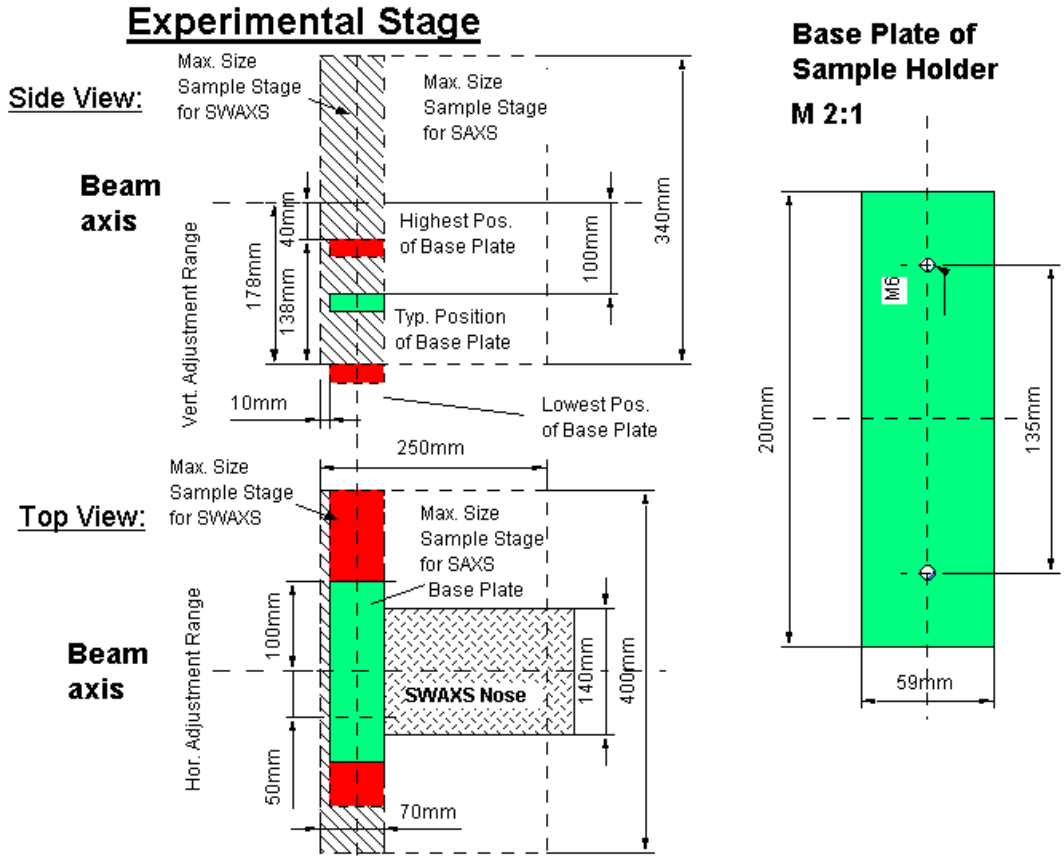

Figure 4. Maximum dimensions and alignment range of the sample holder to be mounted via a base-plate onto the standard alignment stage (left), and dimensions of the base-plate (right).

2. Sample holders

As standard equipment for liquid samples Paar capillaries (diameter: 1 and 2 mm) are used thermostated with the KHR (electrical heating) or KPR (Peltier heating/cooling) sample holders (Anton Paar, Graz, Austria). For use in these sample holders flow through capillaries and Gel holders are standard equipment. Temperature scans can be performed with KHR and/or KPR in the range from 0 to 150 °C, typically the precision and the stability of this systems is < 0.1 °C. Additionally thermostats for temperature control or cooling proposes can

be used at the beamline (0-95 °C, at present). Helium and Nitrogen gas bottles are available at the beamline, for other gases please contact the beamline responsible.
Multiple-sample holders can be mounted onto the standard sample manipulator. At present holders are available for measuring in automatic mode up to 30 solid samples at ambient temperature or up to 4 liquid or gel samples in the temperature range 0 – 95 °C.

3. Online exhaust system

At the experimental station is available a custom-built fume cover and chemical exhaust system for toxic gases. Thus it is possible to e.g. study in-situ chemical reactions, during which toxic gases might develop.

4. Magnet System

For studying magnetic effects in samples, capillaries or sample holders with suitable dimensions can be mounted inside an electromagnet. Up to now a sample holder for standard Paar capillaries (Anton Paar, Graz, Austria) is available for ambient temperature only. The alignment of the magnetic field is horizontal or vertical (transversal to the photon beam). For short times the maximum magnetic field can be up to 1.5 T, and 1.0 T for continues operation, respectively, assuming a pole gab of 10 mm for both.

5. Stopped Flow Apparatus

A commercial stopped flow apparatus (manufactured by Bio-Logic, Paris, France), especially designed for Synchrotron Radiation SAXS investigations of conformation changes of proteins, nucleic acids and macromolecules, is available. The instrument consists of a 4 syringe cell with 3 mixer modules manufactured by Bio-Logic. Each syringe is driven independently from the others by an individual stepping-motor, which allows a high versatility of the mixing sequence (flow-rate, flow duration, sequential mixing). For example, injection sequences using one or up to 4 syringes, unequal filling of syringes, variable mixing ratio, reaction intermediate ageing in three- or four-syringe mode etc.. The solution flow can be entirely software-controlled via stepping motors, and can stop in a fraction of a millisecond.

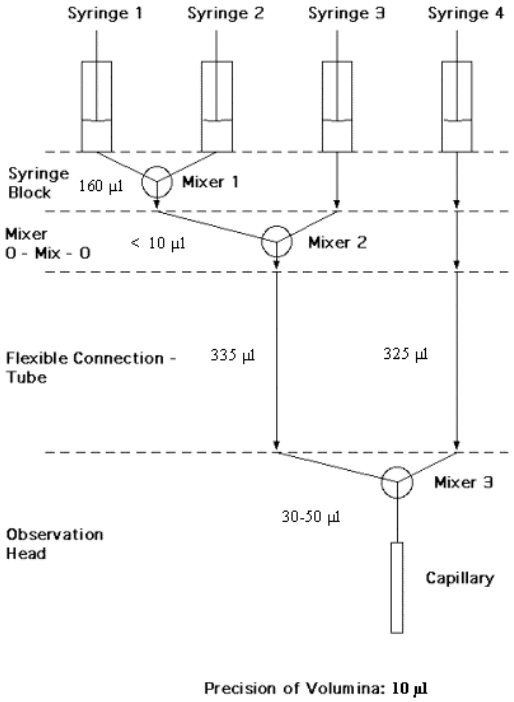

The software allows the set-up of the shot volumes of each of the 4 syringes in a certain time interval. Up to 20 mixing protocols can be programmed. Additionally macros for the repeated execution of individual frames can be defined. Furthermore, the input and output trigger accessible for user operation can be programmed. In the usual operation modus the start of rapid mixing sequence is triggered from our X-ray data-acquisition system (input trigger).

After the liquids have been rapidly mixed, they are filled within few ms into a 1 mm quartz capillary - situated in the X-ray beam- , which is thermostated with a water bath. Depending on the diffraction power of the sample time resolutions of up to 10 ms can be obtained.

Figure 5. Sketch of the stop flow system.

The main parameter of the system are:

- Thermostated quartz capillary (1 mm)
- Temperature stability 0.1 °C
- Total sample used per mixing cycle (shot volume): 100 µl
- Maximum 2θ angle of 45°
- Total Volume 8 ml
- Dead volume 550 µl
- Speed: 0.045 – 6 ml/s
- Duration of flow 1 ms to 9999 ms/Phase
- Dead time: 1 ms
- Reservoir volume: 10 ml each

Further information can be found in the homepage: http://www.bio-logic.fr/

6. Grazing Incidence Small Angle X-ray Scattering

Grazing incidence studies on solid samples, thin film samples or Langmuir-Blodget-films can be performed using a specially designed sample holder, which can be rotated around 2 axes transversal to the beam. Furthermore the sample can be aligned by translating it in both directions transversal to the beam. The precisions are 0.001 deg for the rotations and 5 µm for the translations. Usually the system is set to reflect the beam in the vertical direction. According to the required protocol and the actual assembly of the rotation stages ω, θ, 2θ and φ scans can be performed.

7. Temperature Gradient Cell

A temperature gradient cell for X-ray scattering investigations on the thermal behaviour of soft matter manybody-systems, such as in gels, dispersions and solutions, has been developed. Depending on the adjustment of the temperature gradient in the sample, on the focus size of the X-ray beam and on the translational scanning precision an averaged thermal resolution of a few thousands of a degree can be achieved.

8. IR-Laser T-Jump System for Time-Resolved X-ray Scattering on Aqueous Solutions and Dispersions.

The Erbium-Glass Laser available at the SAXS-beamline (Dr. Rapp Optoelektronik, Hamburg, Germany) delivers a maximum of 4 J per 2ms pulse with a wavelength of 1.54 µm onto the sample. The laser-beam is guided by one prism onto the sample, which is filled in a glass capillary (1 or 2 mm in diameter) and Peltier or electronically thermostated in a metal sample holder (A. Paar, Graz, Austria). With a laser spotsize of maximal 7 mm in diameter a sample-volume of maximal 5.5 µl or 22 µl, respectively, is exposed to the laser-radiation. In a water-solutions/dispersions with an absorption coefficient of A = 6.5 cm^{-1} T-jumps up to 20 °C are possible.

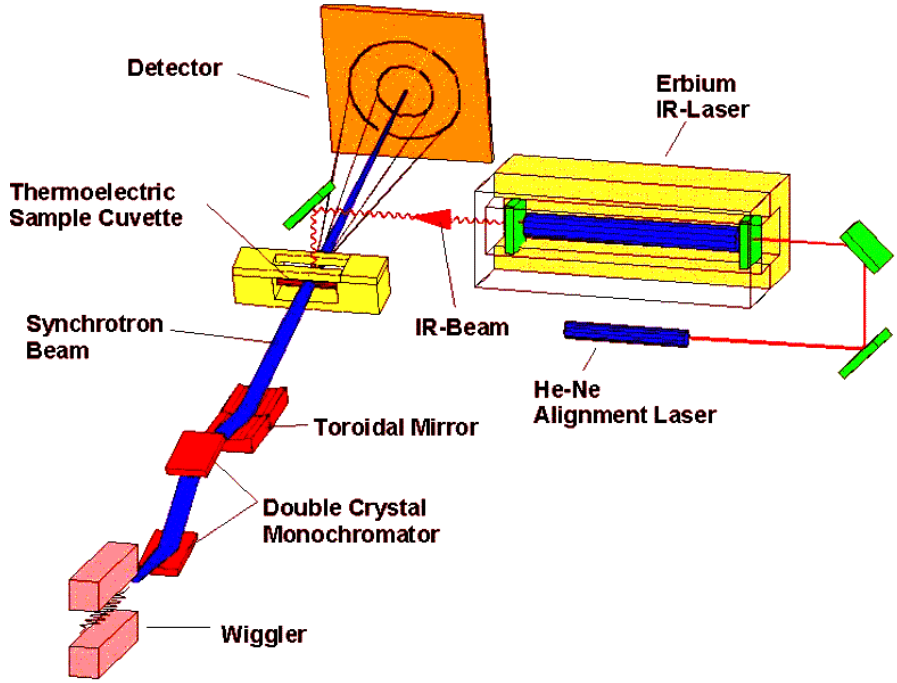

Figure 6. Sketch of the T-jump set-up.

9. High Pressure Cell System

SWAXS measurements of samples under pressure can be performed from 1 to 2500 bar, from 0 to 80 °C in the scattering angle region up to 30 degrees, both in the static or time-resolved mode, e.g. p-jump or p-scan, with a time-resolution down to the ms range. Precise pressure scans of any speed within a broad range (e.g. ca. 1.0 bar/s - 50 bar/s in the case of water as pressurising medium, and a typical sample volume) can be performed. Alternatively, dynamic processes can be studied in pressure-jump relaxation experiments with jump amplitudes up to 2.5 kbar/10ms in both directions (pressurising and depressurising jumps).

In most applications diamond windows of 0.75 mm thickness (each) are used. The transmission of one pair (entrance and exit window) is 0.1 at 8 keV, i.e. lower than 0.3, the value for the originally used 1.5 mm thick Be-windows. However the loss in intensity is more than compensated for by the considerably lower background scattering of diamond thus leading to higher q-resolution in the experiments.
The sample thickness can be 0.6-4.0 mm, with a volume of approximately 0.5-3 mm^3 completely irradiated by pin-hole collimated (< 1.0 mm diameter) X-rays.
The pressure cell system is flexible and can be built according to the needs of the particular experiment. Normally, a liquid (water, ethanol or octanol) is used as pressurising medium. But in principle, also gaseous media can be employed as well. N_2 has been successfully tested, and measurements in supercritical CO_2 became frequent.
Beside bulk measurements on samples in transmission set-up, also grazing incidence experiments using silicon wafer with highly aligned samples on its surface inserted in the high-pressure cell have been carried out successfully.

10. Oxford Cryostream Cooler

The Cryostream cooler creates a cold environment only a few millimeters from the nozzle position. The temperature and the flow of the nitrogen gas stream is controlled and regulated by a Programmable Temperatur Controller based on an 'in stream' heater and a thermo-sensor before it passes out over the sample.

The system has been especially developed for X-ray crystallography to perform diffraction experiments on e.g. shock frozen bio-crystals. However, the programmable temperature controller allows further implication for SAXS-experiments, e.g., rapid temperature drops in solvents. The design of the Cryostream Cooler facilitates:

- nitrogen stream temperatures from -190 to 100 °C,
- a stability of 0.1 °C,
- a system that can be refilled without creating any disturbance of the temperature at the sample,
- temperature ramps can easily be carried out remotely controlled with scan rates up 6 °C/min
- individual temperature protocols can be cycled
- T-jumps in both directions can be performed by rapid transfer of the sample in a pre-cooled or -heated capillary using an fast syringe driver reaching a minimum temperature of -80 °C. Here, typical scan rates are about 15 °C/sec with a total process time in the order of 10 sec.

11. In-line Differential Scanning Calorimeter (DSC)

The in-line micro-calorimeter built by the group of Michel Ollivon (CNRS, Paris, France) allows to take simultaneously time-resolved synchrotron X-ray Diffraction as a function of the Temperature (XRDT) and high sensitivity DSC from the same same sample.
The microcalorimetry and XRDT scans can be performed at any heating rate comprised between 0.1 and 10 °C/min with a 0.01 °C temperature resolution in the range -30/+130 °C. However, maximum cooling rates are T dependent and 10°C/min rates cannot be sustained below 30°C since cooling efficiency is a temperature dependent process. Microcalorimetry

scans can be recorded independently, and also simultaniously, of X-ray patterns. The microcalorimeter head can also be used as a temperature controlled sample-holder for X-ray measurements while not recording a microcalorimetry signal. Isothermal microcalorimetry is also possible when a time dependent thermal event such as meta-stable state relaxation or self-evolving reaction, is expected. The sample capillaries have a diameter of 1.5 mm and are filled over a length of 10 mm.

12. The 2D CCD-camera system

The CCD has a 115 mm diameter input phosphor screen made of a gadolinium oxysulphide polycrystalline layer. The screen is coupled by means of a fiber optic to the image intensifier. The image intensifier is coupled again with an additional taper to the CCD itself. The achieved spatial resolution of a pixel is 79 μm for the whole set-up.
The number of pixels is 1024 x 1024 and they can be pinned down to 2 x 2 and 4 x 4. The dynamic range of the CCD is 12 bit. The dark current of the CCD is in the order of 100 ADU (off-set) and the readout noise (read out speed: 10 MHz) is in the order of 6 ADU. (The CCD is cooled by multistage Peltier element for reducing the dark noise.) The intensifier gain is adjustable between 200 and 20000 photons full dynamic range. Typical readout times and exposure times are 150 ms and 100 ms, respectively. The readout times can be reduced down to 100 ms by using the pinning mode of the CCD. Between the frames additional wait times can be programmed e.g. for reducing the radiation damage in the sample or to extend the time for measuring long time processes.
For the external control a TTL trigger signal is provided (active low, when the CCD is accumulating an image), which is used to control the electromagnetic fast shutter of the beamline on one hand. On the other hand this signal can be used also to trigger processes as requested by the user.
The CCD is controlled by Image Pro+, which also includes non too sophisticated data treatment capabilities. The program is featuring a comprehensive set of functions, including:

- flat fielding/background corrections
- enhanced filters and FFT
- calibration utilities (spatial and intensity)
- segmentation and thresholding
- arithmetic logic operations
- various measurements, like surface, intensity, counts, profiles
- advanced macro management

The data are stored in 12 bit – TIFF format. At the present state up to 300 full images (1024 x 1024) can be recorded by the system, but a strict conservation of the timing sequence is maintained only for the first 15 - 17 frames until the RAM memory is full. Afterwards the images are stored in the virtual memory on the hard disk. At present a software development for the CCD readout system is under way to improve the stability of the readout cycles.
For the complete treatment of the 2D data Fit2D available from the ESRF is used, which is able to perform both interactive and "batch" data processing (homepage: http://www.esrf.fr/computing/expg/subgroups/data_analysis/FIT2D/index.html, programmed by Dr. Andy Hammersley), which supports a complete spatial correction, flat field correction and background correction. Furthermore more elevated data-treatment can be performed within this software package, like circular integration, segment integration and similar.

User Contributions

1. Materials Science

PRELIMINARY SAXS STUDY OF SPICULES FROM MARINE SPONGES40

H. Amenitsch[1], U. Benatti[2], M. Causà[3], G. Croce[3], A. Frache[3], M. Giovine[4], L. Marchese[3], M. Milanesio[3], D. Viterbo[3]

1.) Institute of Biophysics and X-Ray Structure Research, Austrian Academy of Sciences, Graz, Austria
2.) DIMES sez. Biochimica, Universita' di Genova, Via L.B. Alberti 2, I-16132 Genova, Italy
3.) DISTA, Universita' del Piemonte Orientale „A.Avogadro", C.so T.Borsalino 54, I-15100 Alessandria, Italy
4.) CNR, direzione progetto finalizzato biotecnologie, Via L.B. Alberti 4, I-16132 Genova, Italy

The biological formation of amorphous hydrated silica called "biosilification" occurs in a wide variety of organisms [1,2,3]. In particular siliceous sponges deposit hydrated silica in needle-like spicules and other skeletal structures (figure1). Siliceous spicules are produced within specialised cells (sclerocytes) [4] and contain an organic axial filament [5] around which hydrated silica is deposited.

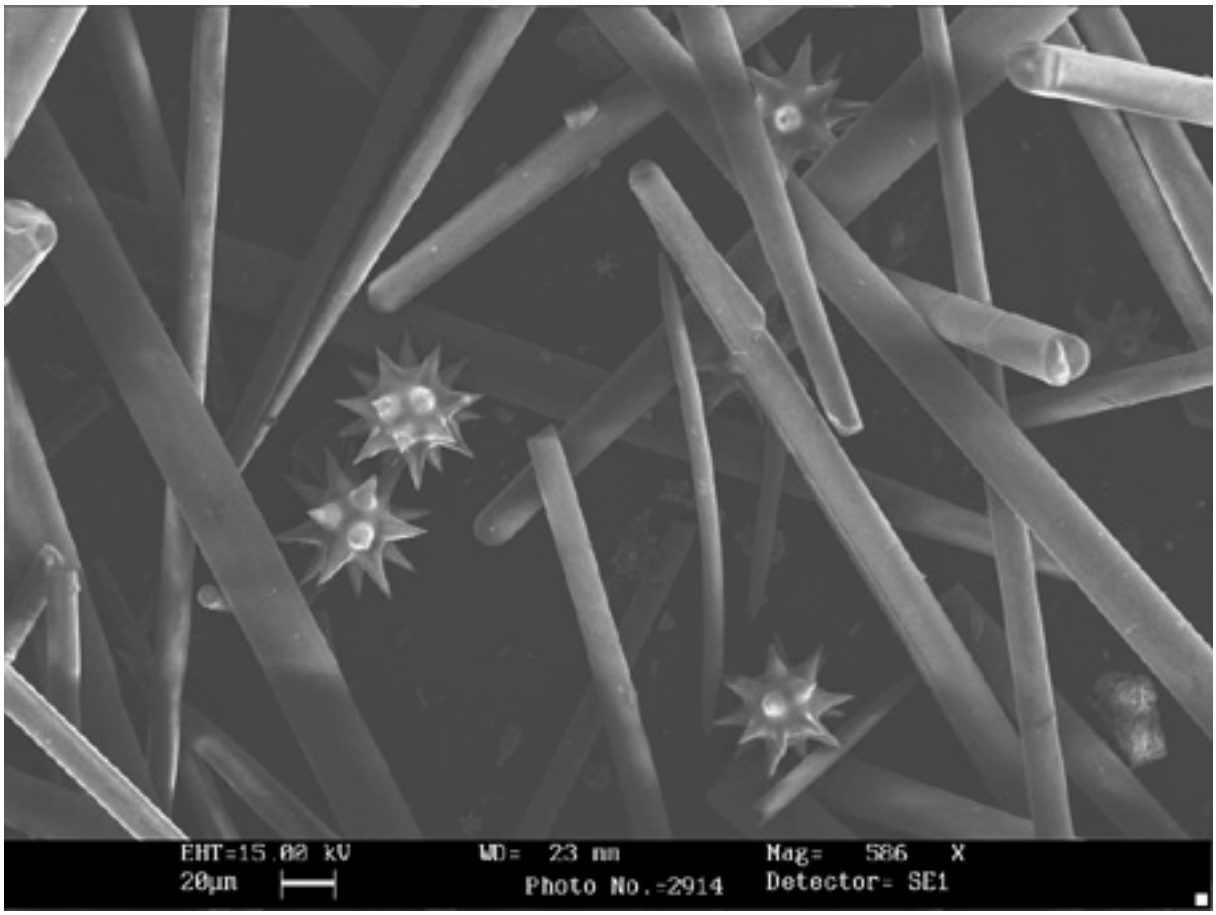

Figure 1. Example of needle-like and spheroidal spicules of Tethya

The concentric arrangement of the silica is the result of a periodic secretion. Siliceous spicules are formed at the intracellular level by the application of hydrated silica to the organic filament. It is generally assumed that spicules growth is a bi-dimensional process: the increase in length is affected by the elongation of the filament while the increase in width is determined by the apposition of the silica.
With our first experiment using synchrotron radiation our aim was to obtain some structural information on the filaments inside the spicules in order to achieve a more realistic picture of

their organisation. We carried out SAXS measurements on a number of Mediterranean species (Petrosia, Geodia, and Tethya,) and on two Antarctic species (Calix and Scolymastra). The samples Scolymastra, Geodia and Tethya present needle-like spicules of sufficient length to be oriented inside a boron-glass capillary. This allowed the collection of fiber diffractograms from a still sample composed by a bundle of almost parallel spicules. Calix and Petrosia only give very thin and short spicules (< 0.02 mm) and can not be oriented by insertion in a capillary. Tethya and Geodia, besides needles, also give almost spherical spicules. The conditions and results of our measurements are summerized in Table 1.

Table 1. Summary of the SAXS measurements on different types of spicules

Sponge species	Spicule shape and size	No. and type of reflections
needle-like Geodia	Oriented needles (2.5÷3.0 × <0.05 mm)	6 sharp spots
spheroidal Geodia	Randomly oriented (Ø ≈ 0.05 mm)	No diffraction
needle-like Tethya	Oriented needles (2.0÷2.4 × <0.02 mm)	more than 15 sharp spots
spheroidal Tethya	Randomly oriented Spheroidal (Ø ≈ 0.06 mm)	No diffraction
Petrosia	Randomly oriented needles (<0.2 × <0.01 mm)	3 sharp rings
Scolymastra	Oriented needles (0.5÷2 × 0.02÷0.1 mm)	4 sharp spots
Calix	Randomly oriented needles (0.2 × <0.02 mm)	No diffraction

The most important result is the different size of the fibres forming the filaments in spicules of different origin: about 50Å for the Mediterranean spicules (figure 2) and about 70Å for the Antarctic one (figure 3). Indeed this is an independent physical confirmation of the hypothesis that the two species belong to different sponge families. Except for Petrosia, giving too small spicules, the SAXS measurements were carried out on still bundles of oriented spicules, and the sharp diffraction spots indicated a high degree of order in the organisation of the filaments. Although these kind of measurements suggested also some degree of order along the fibre axes, its nature could not be clearly established.
The absence of signals in the experiments carried out on Calix and spherical Tethya indicate either that these samples do not contain any protein (as also suggested by independent TGA measurements) or that the protein is not ordered inside these samples.

References:

[1] Simpson, T.L. & Volcani, B.E., Silicon and Siliceous Structures in Biological Systems, Springer, New York eds. (1981)
[2] Voronkov, M.G., Zeichan, G.I. & Lukevits, E.J. Silicon and Life, Zinatne, Riga, 2nd ed. (1977).
[3] Bendz, G. & Lindqvist, I, Biochemistry of Silicon and Related Problems, Plenum Press, New York eds. (1977).
[4] Simpson, T.L. The Cell Biology of Sponges, Springer, New York (1984).
[5] Garrone, E. Phylogenesis of Connective Tissue, Karger, Basel, pp. 176-179 (1978)

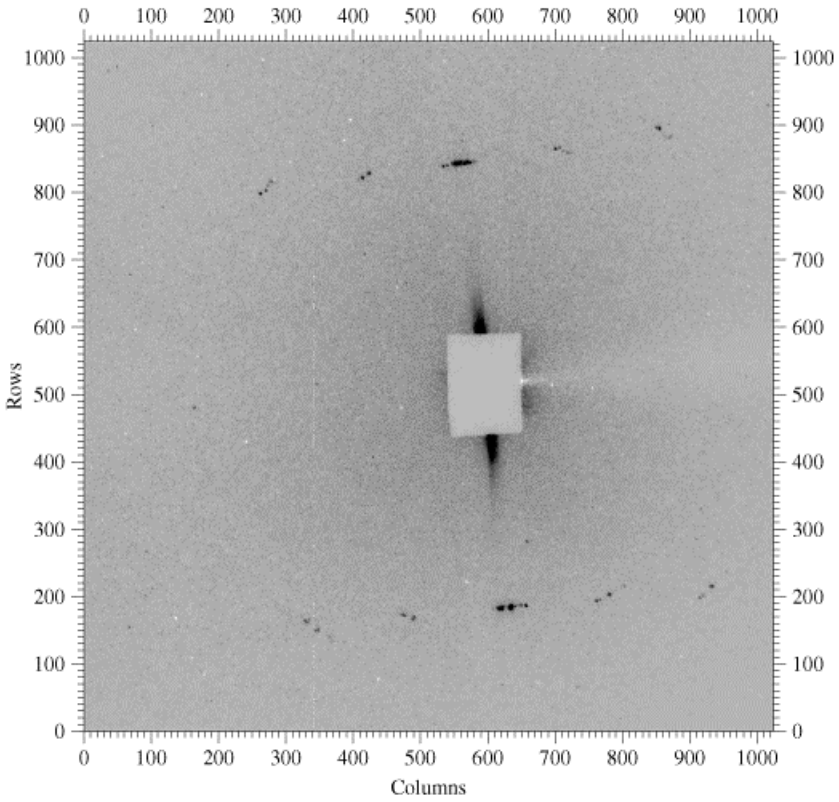

Figure 2. X-ray scattering pattern of Tethya.

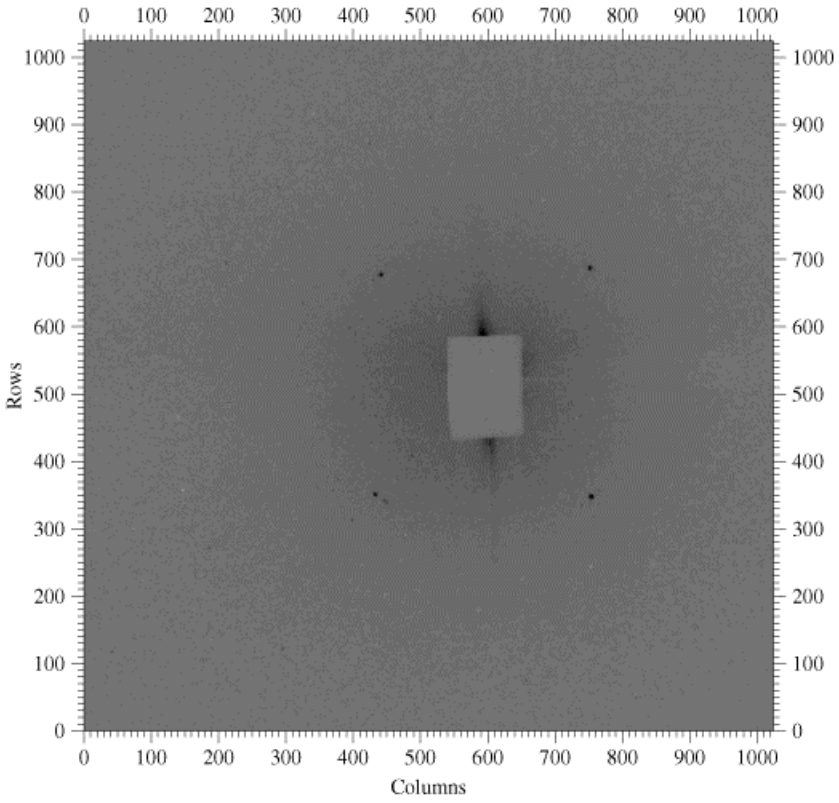

Figure 3. X-ray scattering pattern of Scolymastra.

X-RAY REFLECTIVITY INVESTIGATIONS OF SiN_x-FILMS ON Si(111)

T. Clausen[1], T. Schmidt[1], J. I. Flege[2], S. Gangopadhyay[1], S. Heun[3], S. Bernstorff[3], P. Dubcek[3] and J. Falta[1]

1.) Institute of Solid State Physics, University of Bremen, Postfach 330440, 28334 Bremen, Germany
2.) HASYLAB at DESY, Notkestr. 85, 22603 Hamburg, Germany
3.) ELETTRA synchrotron light source, Strada Statale 14, 34012 Basovizza, Italy

Ultra-thin SiNx-films of thicknesses up to 2 nm, have been investigated by means of x-ray reflectivity (XRR) measurements. Contrast for layered structures in XRR arises from the difference in electron density of the layers under investigation. For the present system this difference is very small. For the SiN_x film the electron density depends on the N content. The largest N concentration in the film is found for the Si_3N_4 phase. Even in this favourable case, the ratio of the electron density of Si and Si_3N_4 is 1.125 only. An additional complication arises from the small thickness of the films under investigation which is less than 2 nm. The inverse film thickness determines the oscillation period of the XRR intensity. Therefore the investigation of very thin films requires measurements of the XRR intensity up to large scattering angles (several degrees). Surface roughness leads to a decay of the observed intensity with increasing scattering angle implying further constraints for the experiments regarding the available photon flux and background intensity. This was the motivation to perform the experiments at the SAXS beamline of ELETTRA.
The samples have been prepared ex-situ in a flux of atomic nitrogen supplied from a rf plasma source (EPI) or an ECR plasma source (Tectra). The ECR plasma source was equipped with a significantly smaller aperture reducing the N flux by an order of magnitude in comparison to the rf plasma source. During N exposure the samples were held at temperatures between 800 and 1070°C. The preparation parameters of the samples which have been studied in two beamtimes are summarized in table 1. An example for the data is given in Fig. 1. A simulation of the XRR intensity of a 1.6 nm thick Si_3N_4 on Si is shown in Fig. 2 for different values of the surface roughness. Good agreement with the data of Fig. 1 is obtained for a surface roughness of approximately 0.2 nm.
At present the analysis is still preliminary and detailed conclusions cannot be drawn yet. However, a first inspection of the data for samples with large N exposures at different temperatures shows that the saturation coverage strongly depends on the deposition rate and the substrate temperature. We find the corresponding film thickness to vary from 1.4 nm to 2.1 nm. The data analysis is ongoing and the results will be presented at the spring meeting of the German Physical Society (DPG) in March 2002 [1] and the European Materials Research Society (E-MRS) spring meeting 2002 in June [2].

Table 1. Variation range of preparation parameters.

Number of samples	**Type of N-Plasma source**	**Exposure time [min]**	**Deposition temperature [°C]**
5	ECR (Tectra)	7 – 150	800 – 1070
3	rf (EPI)	12	900 – 1000

References:

[1] STRUCTURAL CHARACTERIZATION OF ULTRA-THIN SIN FILMS ON SI(111),
J. Falta, T. Schmidt, T. Clausen, O. Brunke, S. Gangopadhyay, J. I. Flege, S. Heun, S. Bernstorff, P. Dubcek, L. Gregoratti, A. Barinov, B. Kaulich, M. Kiskinova, to be presented at the E-MRS 2002 spring meeting, Strassbourg, France, June 2002

[2] STRUKTURELLE UNTERSUCHUNGEN VON ULTRADÜNNEN SI_3N_4-FILMEN,
T. Clausen, T. Schmidt, S. Gangopadhyay, J. Falta, J. I. Flege, S. Heun. S. Bernstorff, P. Dubcek, L. Gregoratti, A. Barinov, B. Kaulich, M. Kiskinova, to be presented at the spring meeting of the German Physical Society (DPG) in March 2002 in Regensburg

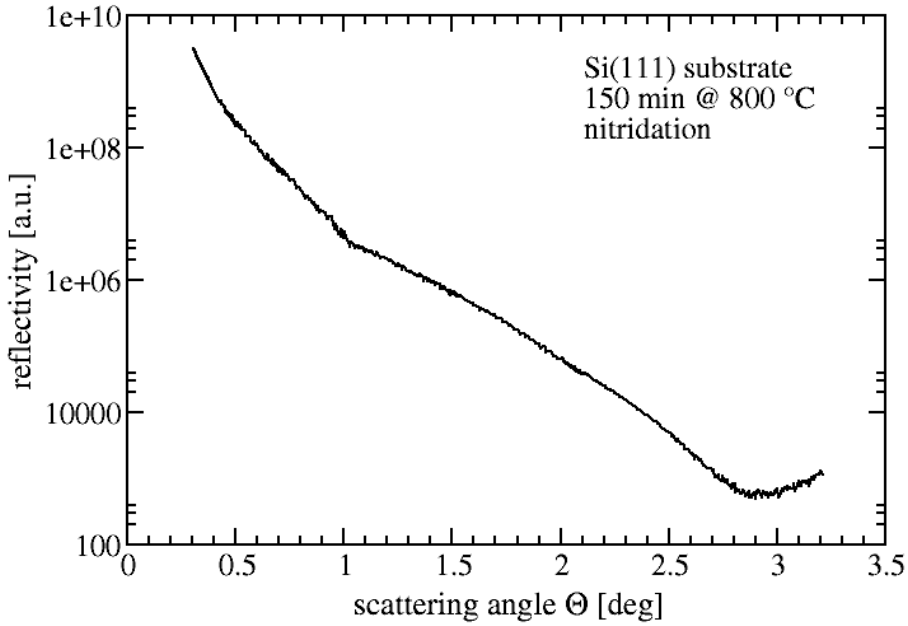

Figure 1. X-ray reflectivity data for a Si(111) sample after exposure to an atomic nitrogen flux from an ECR plasma source for 150 min at a deposition temperature of 800°C.

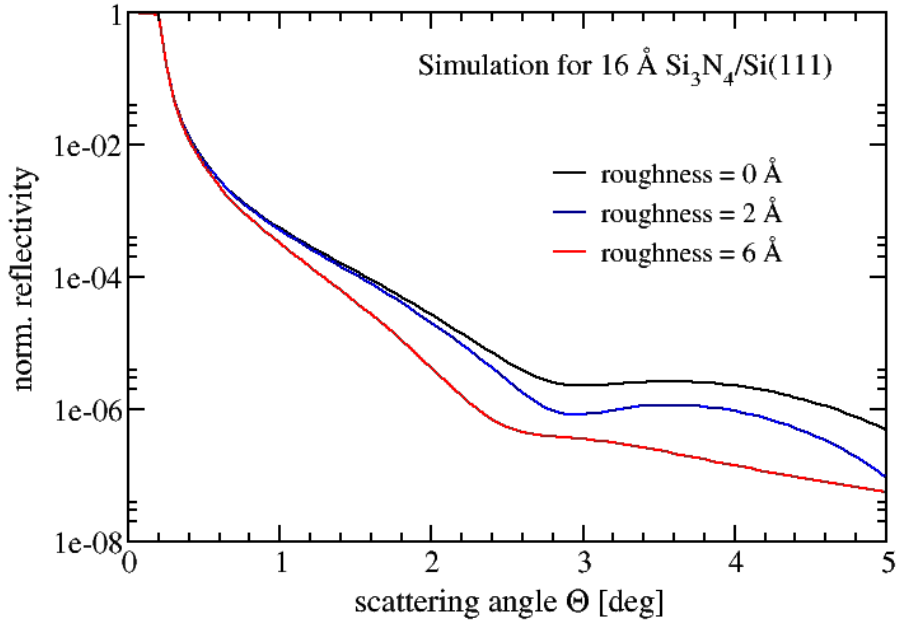

Figure 2. Simulated x-ray reflectivity for Si_3N_4 film on Si. For the calculation, the film thickness was assumed to be 1.6 nm and the surface roughness has been set to 0, 0.2, and 0.6 nm, respectively.

MORPHOLOGICAL CHARACTERIZATION OF CdS QUANTUM DOTS (QDs) IN SiO_2 SUBSTRATE BY GRAZING INCIDENCE SMALL ANGLE X-RAY SCATTERING (GISAXS)

U. V. Desnica[1], P. Dubcek[1,3], I.D. Desnica-Frankovic[1], M. Buljan[1], K. Salamon[2], O. Milat[2] and S. Bernstorff[3]

1.) R. Boskovic Institute, PO Box 180, 10000 Zagreb, Croatia,
2.) Institute of Physics, Bijenicka c. 52, 10000 Zagreb, Croatia
3.) Sincrotrone Trieste, SS 14 km163,5, 34012 Basovizza, Italy

Nanocrystals of CdS have been formed in SiO_2 by sequential multi-energy ion implantation of equal doses of constituent Cd and S ions, and subsequent annealing at 1000° C [1]. Three different concentrations of Cd+S ions: 5.3×10^{21}/cm^3, 2.0×10^{21}/cm^3, and 0.8×10^{21}/cm^3 were implanted in 150 nm surface layer. From the GISAXS analysis, which we based on the local monodisperse approximation (LMA), the shape, size, correlation distance and size distribution of nanoparticles, were determined.

GISAXS signal for the highest concentration (5.3×10^{21}/cm^3) is shown in Figure 1a. It was recorded on 2D detector at critical grazing angle α_c, and was corrected for background intensity and detector response. The circular, 'ring'-like shape of scattered signal indicates the presence of isotropically distributed ensemble of QDs that are spherical in shape.

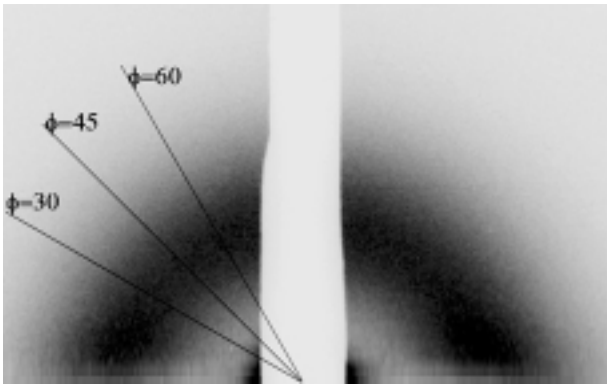

Figure 1. (a) GISAXS spectra of CdS in SiO_2 for concentration of 5.3×10^{21} /cm^3, and $\alpha_i = \alpha_c$.

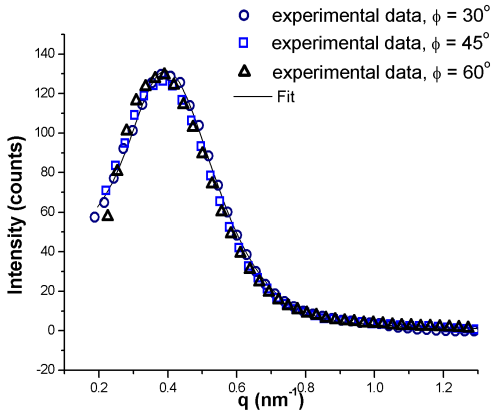

Figure 1. (b) Intensity profiles for polar angles ϕ = 30°, 45° and 60° and $\alpha_i = \alpha_c$

The LMA approximation assumes that the positions and the size of the particles are completely correlated. That is, the system is approximated as a sum of many monodisperse (equal size) subsystems and total scattering is calculated as the sum of the scattering from the subsystems, weighted by the size distribution. DWBA formalism [2] is used to take into account the grazing incidence geometry. Accordingly, the scattered intensity is [3]:

$$I(q) \propto \left|T(\alpha_i)\right|^2 \left|T(\alpha_f)\right|^2 \int_0^\infty P(q,D)\, S(q, D_{hs}, \eta_{hs})\, N(D,w)\, dD$$

where $T(\alpha_I)$ and $T(\alpha_f)$ are the Fresnel transmission coefficients for the angle of incidence α_i and exit α_f respectively. P(q,D) is the form factor of a homogeneous sphere of diameter D_{hs} ($D_{hs} = 2R_{hs}$), and S(q, D_{hs}, η_{hs}) is the structure factor of the assembly within Percus-Yevic approximation, η_{hs} is the volume fraction of the hard sphere, and N(R,w) represents the Gaussian size distribution function specified by its full width at half maximum w.

Figure 1b shows scattered intensities obtained for polar scans at $\phi = 30^{\circ}$, 45°, and 60°, as well as the best fits to LMA. Practically equal intensity profiles for a range of different ϕ indicate isotropical distribution of spherical CdS QDs.
From the fits, the average diameter D of QDs was determined to be 8.8 nm with full width at half maximum ΔD_{FWHM} = 5 nm, in good agreement with TEM results[1]. The average distance between QDs was found to be 10.8 nm, with the range from 7.3 to 13.6 nm. The calculated volume fraction of QDs agrees reasonably well with the expected volume fraction of CdS material in the substrate, assuming that practically all Cd and S atoms were synthesized into CdS. Hence, the result confirms that the annealing parameters were correctly chosen, i.e. that all implanted atoms were indeed fused into the CdS QDs.

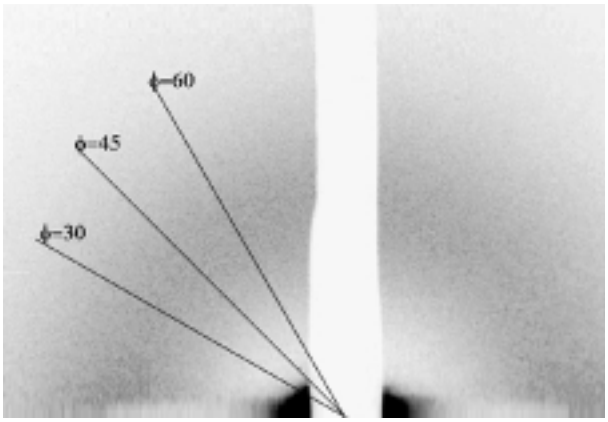

Figure 2. (a). GISAXS spectra of CdS in SiO_2 for concentration of 2.0×10^{21} /cm^3, and $\alpha_i = \alpha_c$.

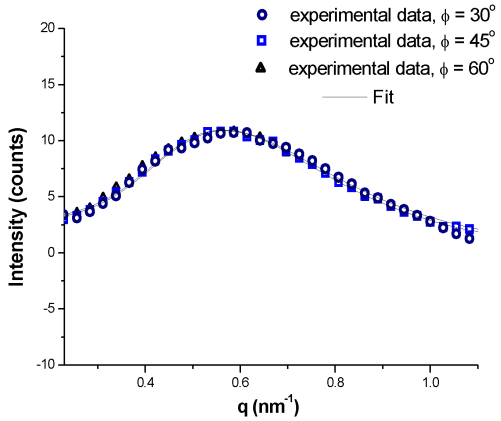

Figure 2. (b). Intensity profiles for polar angles $\phi = 30^{\circ}$, 45° and 60° and $\alpha_i = \alpha_c$.

Figure 2 shows analogous 2D GISAXS spectra and intensity profiles for the same polar angles, for a lower dose. Again, a perfectly circular 'ring' of 2D GISAXS pattern indicates an isotropical establishment of spherical QDs in the surface part of the implanted layer. The analysis has revealed that the QDs are now considerably smaller, and much closer to each other. Again, calculated CdS volume fraction indicates that all implanted Cd and S atoms were synthesized into CdS.
For a larger grazing angle, the beam penetrates deeper into the sample, and the GISAXS spectrum reflects properties of QDs positioned in deeper parts of the layer. Since the measurement and mathematical treatment of GISAXS data, demonstrated above, provides the same type of data (average diameter of QDs, their shape, mean distance between QDs, distribution of diameters and distances, QDs volume fraction), systematic variation of incidence angle enables depth profiling of the whole implanted layer.
In conclusion, we have demonstrated (i) that GISAXS experiment at Elettra - a third generation light source- is sensitive enough to give reasonably strong scattering signal from a very small number of quantum dots, QDs, (i.e. a minute amount of material forming QDs) obtained by implantation, and (ii) developed the analytical methodology and appropriate mathematical apparatus to fully characterize 3D ensemble of QDs formed in implanted layer, from GISAXS spectra recorded on two-dimensional (2D) detector.

References:

[1] C.W. White et al., Nucl. Instr. Meth. Phys. Res. B **148,** 991-996 (1999)
[2] M. Rauscher, T.Saldit and H.Spohn, Phys. Rev. B **52,** 16855-16859 (1995)
[3] J.S. Pedersen, J. Appl. Cryst. **27,** 595-608 (1994)

GRAZING INCIDENCE SMALL ANGLE X-RAY SCATTERING STUDY OF IRRADIATION INDUCED DEFECTS IN MONOCRYSTALLINE SILICON

P. Dubcek[1], B. Pivac[1], S. Bernstorff[2], R.Tonini[3], F. Corni[3] and G. Ottaviani[3]

1.) Ruder Boskovic Institute, Bijenicka 54, 10000 Zagreb, Croatia
2.) Sincrotrone Trieste, SS 14 km 163,5, 34012 Basovizza (TS), Italy
3.) University of Modena, Physics Department, Via Campi 213a, 41100 Modena, Italy

Hydrogen implanted in silicon forms structural defects, including vacancy-like ones, which can, depending on the dose and the implanting energy, amount to complete amorphisation of silicon. Czochralski grown monocrystalline silicon samples have been ion implanted with 31 keV H_2^+ at room temperature and at high doses (beam current density 1mA/cm^2) and in this way a high concentration of defects was introduced. At higher doses and/or temperatures also voids (bubbles) filled with H_2 are produced. The presence of hydrogen bonded to silicon is partly inhibiting the growth of bigger bubbles, and it is controlling the shape of the vacancies too. There are several bonds (and different positions relative to the neighboring Si atoms) that hydrogen can form. To investigate the dynamics of the bubble formation, the samples have been annealed isochronally at discrete temperatures up to 900 °C.

Structural defects were investigated using grazing incidence small angle X-ray scattering, and the scattering intensity was measured using a 2D CCD detector, as displayed in figure 1 for two different annealing tmepratures.

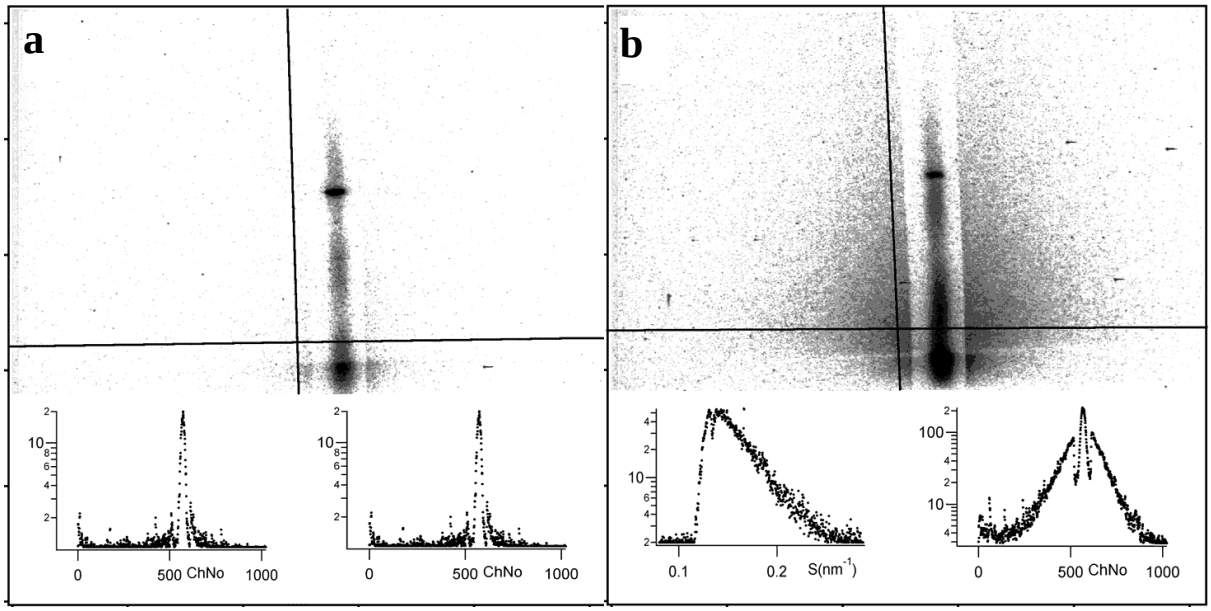

Figure 1. 2D GISAXS pattern from H implanted a) not annealed and b) 350^{o}C annealed silicon. Displayed below are offset (vertical) and inplane (horizontal) scans, left and right respectively, taken along the lines indicated in the scattering pattern.

For as implanted sample (Fig. 1a) mostly surface scattering has been detected. Although the hydrogen depth distribution is expected to be smooth initially, a sharply defined layer (about 28 nm thick) has been observed (intensity oscillations in the specular plane scattering intensity). This thickness is attributed to the top, mostly implantation unaffected layer, while below is the region rich in defects. These defects are mostly too small in size to be detected by SAXS.

For the annealing temperatures lower than 300 °C the signal remains similar to the one shown in fig1a. The vacancies are not able to move far, and only structural relaxation is taking place. At 300 °C vacancies begin to form agglomerates that are up to 10 nm in size, as can be clearly seen from Fig. 1b) where, in addition to the surface scattering in the specular plane, a strong contribution of particle like scattering is present.

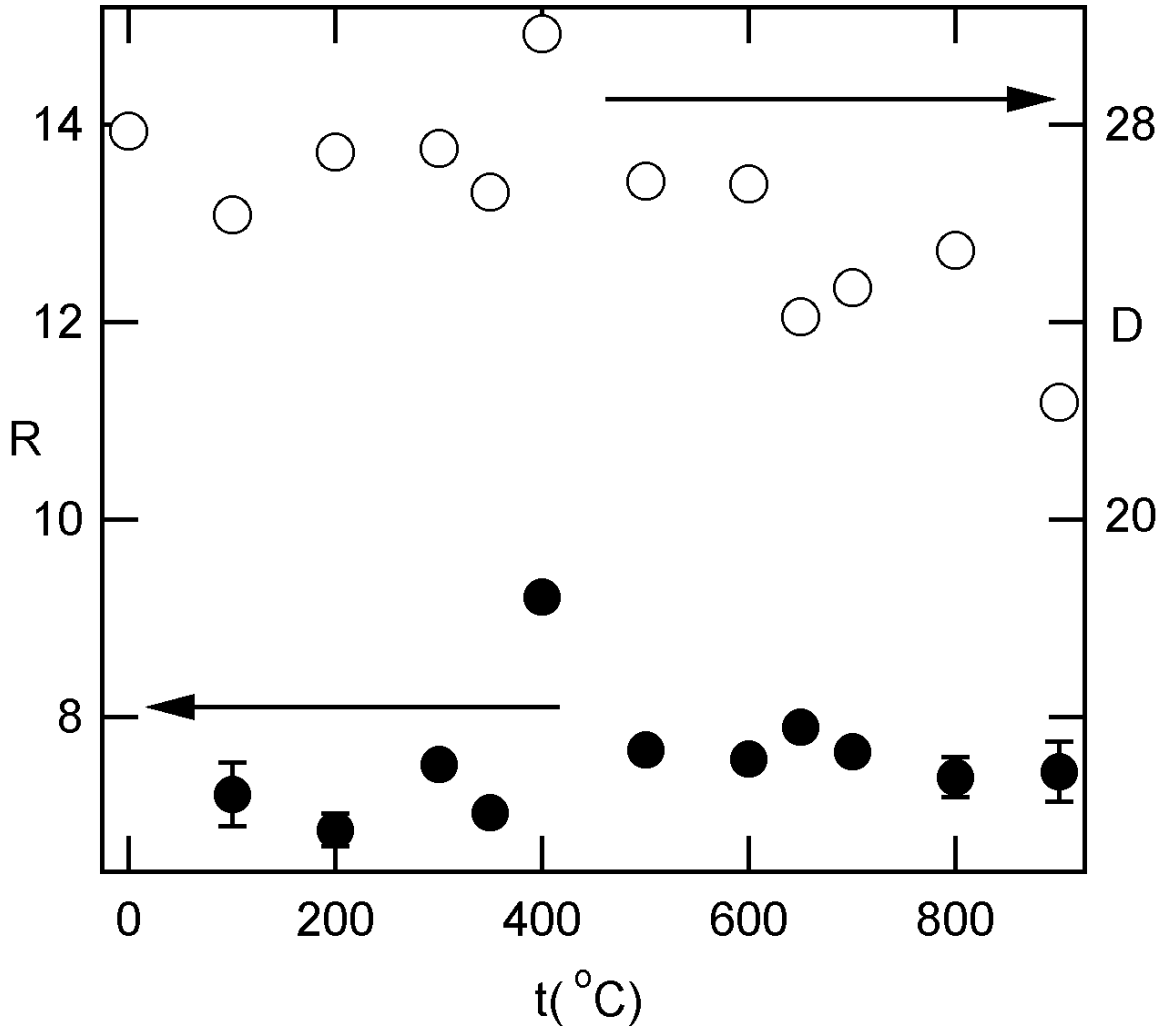

Figure 2. Film thickness D (o) and particle sizes R (•) vs. the annealing temperature for hydrogen implanted silicon.

Between 350 and 400 °C hydrogen is starting to leave the sample (first the excess, then hydrogen distributed in the voids). Here, rather large agglomerates are formed (see maximum value for particle size at 400 °C in fig. 2, although they are reduced by subsequent annealing at higher temperatures due to structural relaxation. However, generally we can observe a steadily increasing agglomerates size vs. annealing temperature, up to about 700 °C, were they start to get smaller since at this temperature all the hydrogen is out. This is again evident in SAXS where the particle signal is diminished above 700 °C, and the scattering pattern again resembles the one in Fig. 1a. At 900 °C the unaffected top layer thickness is decreased because of the diffusion of the defects towards the sample surface. Since the sample has not been completely amorphysized by implantation, the structural defects are being concentrated along the crystal plains.

IN-SITU SAXS AND WAXS STUDY OF NANOCRYSTALLIZATION IN AMORPHOUS FeCuNbSiB AND FeZrCuB ALLOYS

A. Gupta[1], B.A. Dasannacharya[1], G. Principi[2], A. Maddalena[2], M. Meyer[2], S. Dal Toe'[2], N. Paul[3], S. Bernstorff[4], H. Amenitsch[5]

1.) Inter-University Consortium for DAEF University Campus, Khandwa Road, Indore-452 017, India
2.) Settore Materiali, DIM and INFM, Università di Padova, via Marzolo 9, I-35131 Padova, Italy
3.) Institut für Schichten und Grenzflächen, Forschungszentrum Jülich GmbH, D-52425 Jülich, Germany
4.) Sincrotrone Trieste, SS 14, Km 163.5, I-34012 Basovizza, Trieste, Italy
5.) Institute for Biophysics and X-ray Structure Research, Austrian Academy of Sciences, Schmiedlstrasse 6, A-8042 Graz, Austria

Nanocrystalline alloys produced by a controlled partial crystallisation of some amorphous transition metal-metalloid metallic glasses, containing small amounts of Cu, Nb, Ta and Zr, are excellent soft magnetic materials, having high permeability and saturation magnetisation [1,2]. FeZrB and FeZrCuB systems are also important because they exhibit giant magnetoimpedance effects [3], and thus have potential as sensors in magnetic read heads. These systems exhibit a rather peculiar variation in their magnetic properties with annealing time and temperature: with progressive stages of crystallisation during the first crystallisation step itself, the uniaxial anisotropy goes through a minimum [4]. Mössbauer spectroscopy and NMR [4-6] provide evidence for the existence of an intermediate phase, the amount of which varies with annealing temperature and time. In the present experiment, detailed WAXS and SAXS studies of nanocrystallisation of FeCuNbSiB, FeZrB and FeZrCuB systems have been done with an aim to elucidate some structural aspects of the nanocrystalline transformation, and to correlate it with the results of Mössbauer measurements.

In-situ SAXS and WAXS study of nanocrystallisation of FeCuNbSiB system was done using a miniature boron nitride furnace. The sample was heated isochronally at various temperatures up to 600°C. WAXS results were analysed in terms of structural changes occurring in both amorphous as well as nanocrystalline phases. In agreement with the results in literature, the crystallite size increased with increase in annealing time and reached a saturation value at around 550°C, while the lattice constant exhibited a minimum around 220 ^{o}C. The in-situ measurements also give accurate information about the structural changes in the remaining amorphous grain-boundary phase. Fig.1 gives the variation in the position of the broad amorphous peak, which is a measure of the average transition metal-transition metal near neighbour distance. Decrease in the position of the amorphous peak indicates a decrease in the density of the amorphous phase with increasing annealing temperature, which may be attributed to the enrichment of the amorphous phase in metalloid. Width of the amorphous peak, which is a measure of a degree of disorder in the amorphous phase, exhibits an interesting behaviour with annealing temperature, as shown in fig. 2. Initially, for annealing up to 300°C disorder in the system seems to increase a little bit. However, further annealing up to about 480°C causes the disorder to decrease. This may be connected with the structural relaxation in the amorphous phase which results in homogenisation of the system. Annealing at higher temperatures results in a sharp increase in the disorder, concurrent with the on-set of crystallisation. For still higher annealing temperature the disorder goes through a maximum and then shows a rapid decrease. Small angle scattering measurements very well corroborate these results, as reported in fig.3. Up to the annealing temperature at 300°C, Porod constant shows a small increase and then decreases up to the 480 °C. Since in the amorphous phase small angle scattering is expected to occur because of some compositional inhomogeneity, the observed variation in both the width of amorphous phase as well as Porod constant up to an

annealing temperature of 480°C is related to some variation in the compositional inhomogeneity in the system. Beyond 480°C, when the nanocrsytallisation sets-in, the small angle scattering increases rapidly and will have contributions both from the scattering from nanocrystaline grain as well as from the inhomogeneity in the amorphous phase. Similar studies have also been done on FeZrB and FeCuZrB systems.

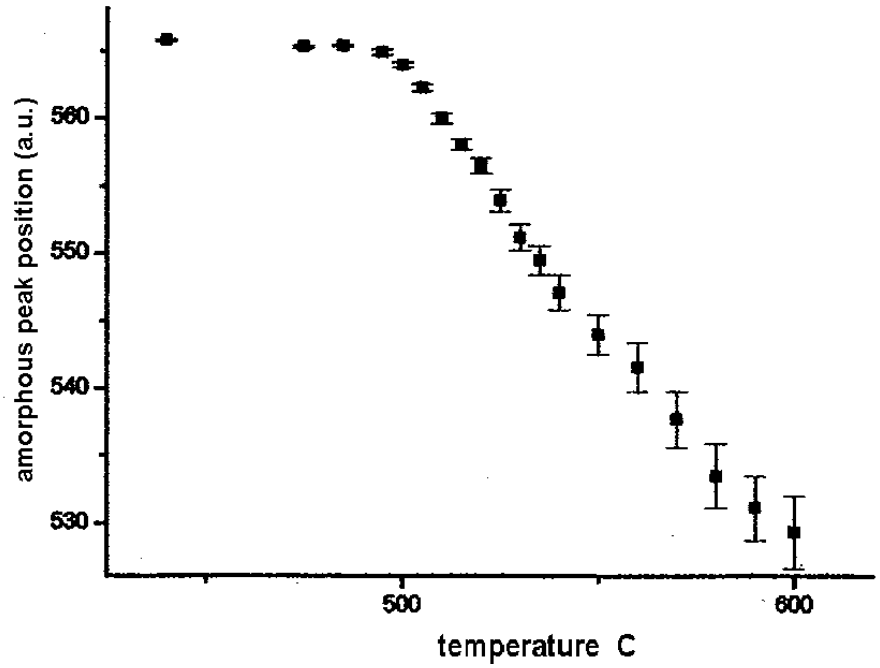

Figure 1. Variation in the position of the broad amorphous peak with annealing temperature.

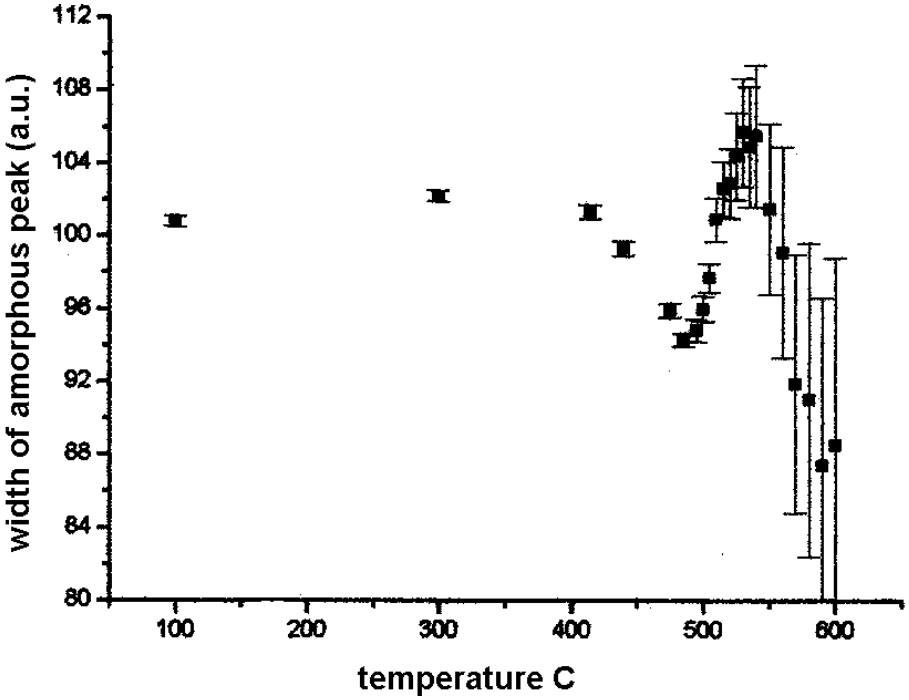

Figure 2. Width of the amorphous peak as a function of annealing temperature.

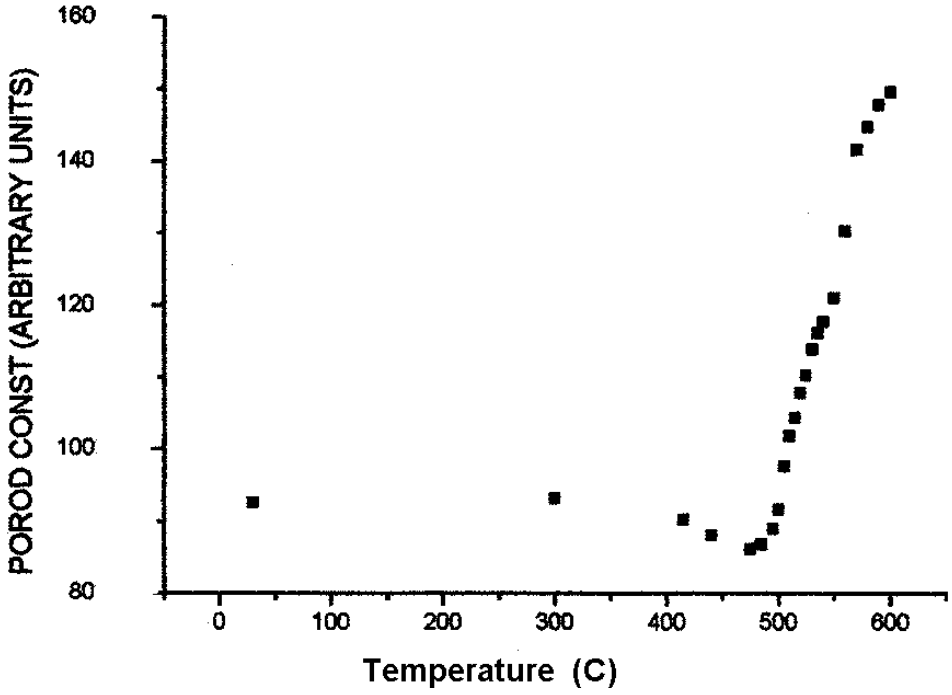

Figure 3. Variation of Porod constant with annealing temperature.

References:

[1] Y. Yoshizawa, S. Oguma and K. Yamauchi, J. Appl. Phys. 64 (1988) 6044
[2] G. Herzer, IEEE Trans. Magn. 25 (1989) 3327
[3] S.S. Yoon et al., J. Appl. Phys. 85 (1999) 5432
[4] D.S. Schmool et al., Phys. Rev. B58 (1998)12159
[5] J.S. Garitaonandia et al., Phys. Rev. B58 (1998) 12147
[6] M. Miglierini et al., J. Phys. Condens. Matter 9 (1997) 2321

ROOM TEMPERATURE IONIC LIQUIDS: PHASE DIAGRAM CHARACTERIZATION WITH COMBINED SAXS-WAXS

A. Triolo[1], F. Lo Celso[2], R. Triolo[2] and C. M. Gordon[3]

1.) Istituto Processi Chimico-Fisici, Sezione di Messina – CNR, Via La Farina 237, 98123 MESSINA, Italy.
2.) Dipartimento di Chimica Fisica, Univ. di Palermo, V.le delle Scienze, I-90128 Palermo (Italy)
3.) University of Strathclyde, Dept of Pure and Appl. Chem., T. Graham Building, 295 Cathedral Street, Glasgow G1 1XL, UK

A structural investigation by means of SAXS and WAXS has been performed on a series of long chain 1-alkyl-3-methylimidazolium (mim) salts, with particular care paid to the [C_{16}-mim][PF_6] salt in a range of temperatures going from 0° C to 150° C.
In the latter range of temperatures the [C_{16}-mim][PF_6] salt displays two different transitions going from a crystalline to a liquid crystal phase and then to a isotropic phase; this behaviour has been already characterized using techniques such as DSC and POM [1].
In the small angle region, a single peak, which corresponds to the crystalline phase of the salt, has been found in the temperature range 0°<T<75° C. This peak indicates the presence of a layered structure of cations that previous XRD studies on a analogous salt[1] (C_{12}-mim) have interpreted in terms of the interdigitation of the alkyl chains in this layered structure. At higher temperatures the development of a smectic phase was characterized. The corresponding d-spacing of the layers can be obtained from the position of the peak by using Bragg's law.

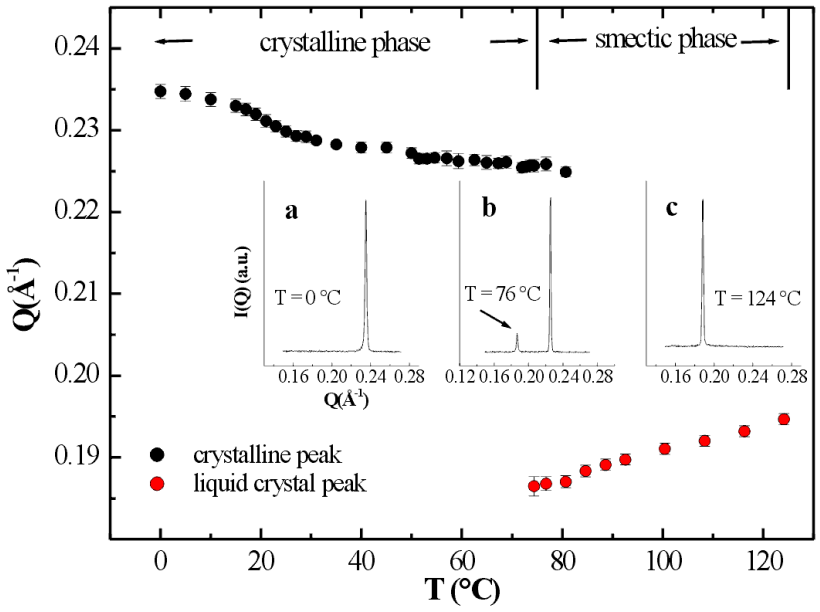

Figure 1. Temperature dependence of the crystalline and smectic peak positions in the SAXS region for [C_{16}-mim][PF_6]. The transition at ca. 10-30 °C corresponds to analogous transitions in the WAXS regime as well as in thermal and dynamical quantities.

Figure 1 reports the position of the interference peaks associated to both the crystalline and smectic phases as function of the temperature; vertical bars were used to show the FWHM of the corresponding fitting function.
It is possible to see that there is a temperature region between 10 and ca. 30 °C, where a smooth variation of the crystalline peak position is observed. This original finding is of interest, as in this

temperature range substantial thermal (DSC), structural (SAXS-WAXS), dynamical (QENS) and conductivity changes are found. We are now in the progress of rationalising this amount of data.
Going towards the melting temperature (75 °C) a second peak appears at lower Q values indicating that the liquid crystal phase is forming and the crystalline phase is disappearing. Inset **b** of figure 1 shows the upcoming liquid crystal phase peak together with crystalline phase peak; the two peaks coexistence is located in a temperature window around 75-85 °C, in this temperature range the transition from the crystalline to liquid crystal phase takes place. For a temperature higher than 80 °C a single peak, corresponding to the liquid crystal phase, remains in the SAXS region (inset **c** of figure 1) up to nearly 125 °C. Experimental data were also collected beyond 125 °C and the transition from the liquid crystal to the isotropic phase (low intensity broad peak) has been found.

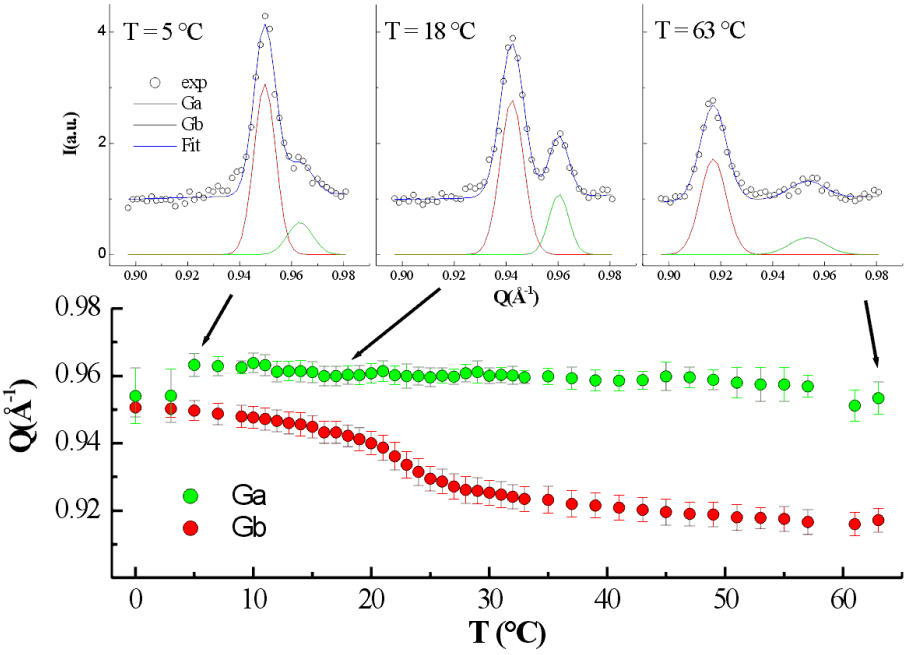

Figure 2. Temperature dependence of the crystalline peak positions in the WAXS regime (in the region 0.9-0.98 $Å^{-1}$) for [C_{16}-mim][PF_6].

Experimental data were also collected in the wide angle region in order to investigate the behaviour of the crystalline phase in a quite wide range of temperatures. Analogously to the small angle region every single WAXS peak has been fitted by a gaussian function. Figures 2, 3 and 4 report the most important features of the WAXS time resolved spectrum; temperature dependence of peak position as the main part of the graph, and single temperature snapshots (intensity vs. momentum transfer) in the insets. Furthermore the insets reports also the fit result as well as the gaussian lines that identify every single peak (a constant offset has been considered for the entire Q accessible range). It is clear that major variation in the peak positions is again observed for 10<T<30 °C, as already seen for the crystalline peak in the small angle region. It is noteworthy that, in the latter temperature range, while some peaks show a shift towards lower Q values by increasing the temperature (Gb in fig. 2, Gc in fig. 3 and Gf in fig. 4) other peaks show, at the same time, an opposite trend (Gd in fig. 3 and Ge, Gh in fig. 4). In other words there is a crossover region (10<T<30 °C) that could be an indication of a significant structural rearrangement.
These preliminary results on [C_{16}-mim][PF_6] indicate the interest of this class of materials. We are currently very active aiming to rationalize similar findings obtained also for other similar materials.

Reference:

[1] C.M. Gordon et al., J. Mater. Chem., **8**, 2627-2636 (1998)

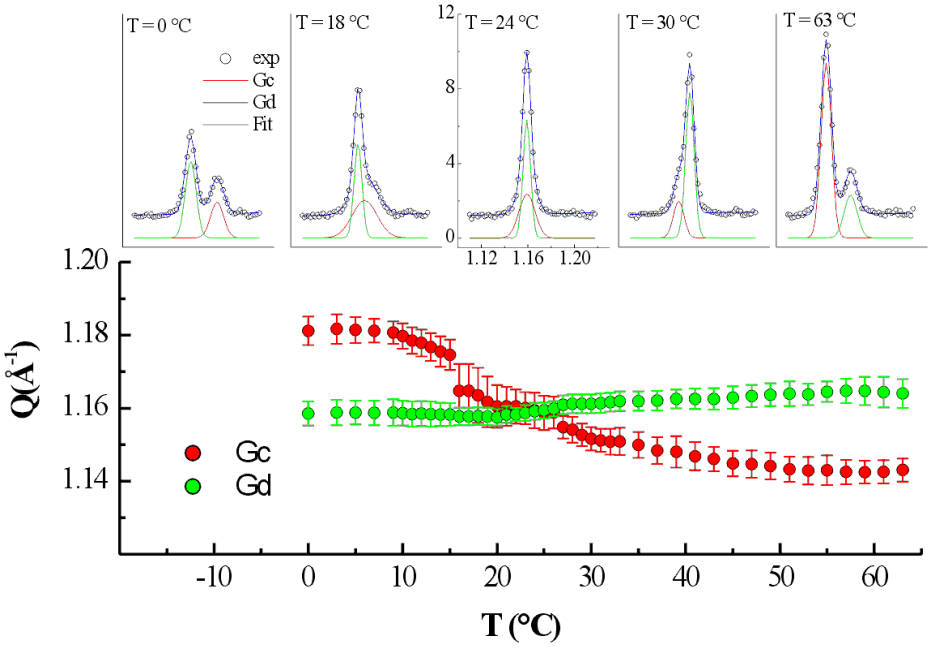

Figure 3. Temperature dependence of the crystalline peak positions in the WAXS regime (in the region 1.12-1.20 $Å^{-1}$) for [C_{16}-mim][PF_6].

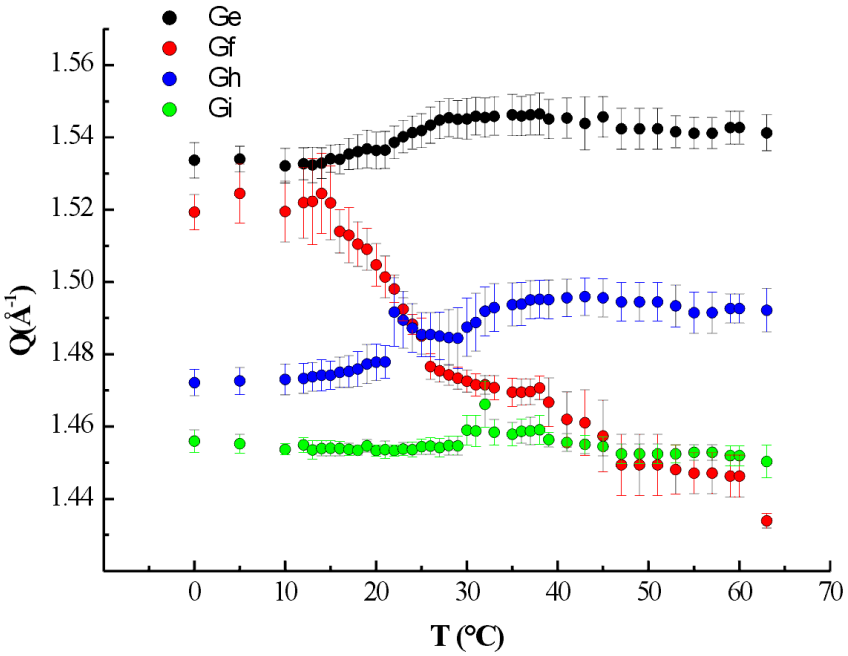

Figure 4. Temperature dependence of the crystalline peak positions in the WAXS regime (in the region 1.42-1.56 $Å^{-1}$) for [C_{16}-mim][PF_6].

CRITICAL MICELLISATION DENSITY (CMD): A SYNCHROTRON SAXS STRUCTURAL STUDY OF THE UNIMER-AGGREGATE TRANSITION OF BLOCK-COPOLYMERS IN NEAR- AND SUPER- CRITICAL FLUIDS

R. Triolo[1], F. Lo Celso[1], A. Triolo[2], F. Triolo[3], M. Steinhart[4], M. Kriechbaum[5], S. Bernstorff[6] and H. Amenitsch[5]

1.) Department of Physical Chemistry, University of Palermo, 90128 Palermo (Italy)
2.) Istituto Processi Chimico-Fisici, Sezione di Messina – CNR, Italy
3.) Mount Sinai School of Medicine, New York, NY (USA)
4.) Institute of Macromolecular Chemistry, Academy of Science of the Czech Republic, Prague, Czech Republic
5.) Institute of Biophysics and X-ray Structure Research, Austrian Academy of Sciences, Graz, Austria
6.) Sincrotrone Trieste Elettra, Italy

This report deals with the time-resolved small angle X-ray scattering (TR-SAXS) investigation of aggregate formation by fluorocarbon-hydrocarbon block copolymers in supercritical CO_2 ($scCO_2$) as a function of pressure and temperature. In these systems, by profiling the pressure at constant temperature, a sharp monomer-micelle transition is obtained due to the tuning of the solvating ability of $scCO_2$ [1-7]. Furthermore the transition can be obtained, changing the solvent density by profiling the temperature at constant pressure. Preliminary SANS experiments on a block copolymer with 4 kDa (PS, polystyrene) and 40 kDa fluorinated (PFOA, perfluoroctylacrilate) moieties have shown that at high pressure the copolymer is in a monomer state with a random coil structure, while at low pressure core-shell aggregates are formed with the *hydrocarbon* segments forming the core and the *fluorocarbon* segments forming the corona of the aggregate.

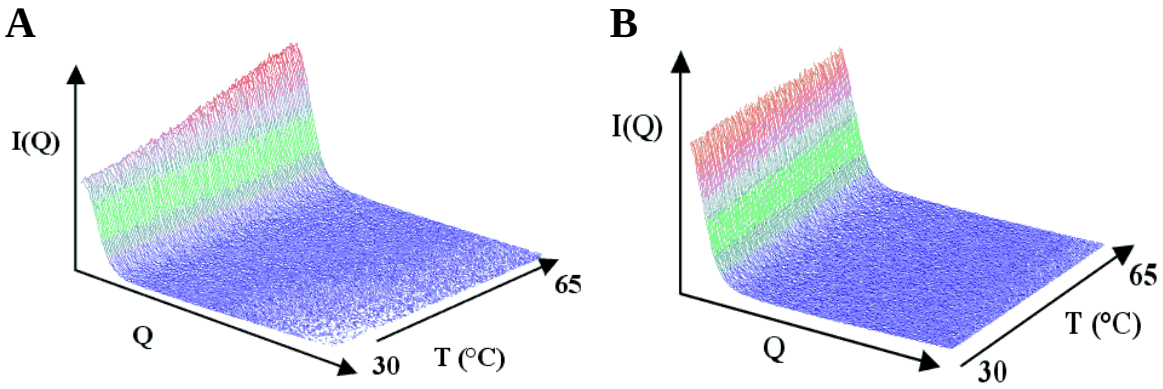

Figure 1. X-ray scattering pattern of PS-b-PFOA as function of temperature at A.) P = 340 bar, and B.) at P = 500 bar.

We have studied this block copolymer by means of TR-SAXS. In one set of experiments data were collected at constant pressure (340 bar and 500 bar) while the temperature was changed between 30 and 65 °C. In figure 1A it is shown the TR-SAXS pattern obtained at constant pressure (P = 340 bar) changing the temperature between 30°C and 65°C. It is clear that the scattering intensity at lowest Q accessible, going from 30°C to 65°C, shows a constant increase due to the formation of aggregates. In fact in this temperature range the CO_2 density changes considerably going from 0.84 g/cm^3 (P=340 bar, T=65°C) to 0.97 g/cm^3 (P=250 bar, T=30°C). Changing the solvent density, by profiling the temperature, depends strongly, as it should be, upon the constant pressure value chosen. We have performed similar experiments at 500 bar. In figure 1B it is reported the TR-SAXS pattern recorded in the same temperature range above mentioned at 500 bar. It clearly appears that the intensity profile, over this temperature range, does not show significant variations; small intensity values are comparable with the initial part of the scattering surface seen in figure 1A (T=30°C P=340 bar). Evidently at this pressure the system does not aggregate in the temperature range examined. Experiments have been performed also by changing the pressure at constant temperature for other block copolymers where the CO_2 phobic block was Poly tertialbutylmethilacrylate (PtBMA) and the

CO_2 philic block was perfluoroctylmethilacrylate (PFOMA). In figure 2A it is reported the SAXS pattern obtained at constant temperature (T=35ºC) for 18kDa PtBMA -b- 65 kDa PFOMA sample, going from P = 840 to P = 420 bar and vice versa, in a series of several alternate up and down pressure ramps.

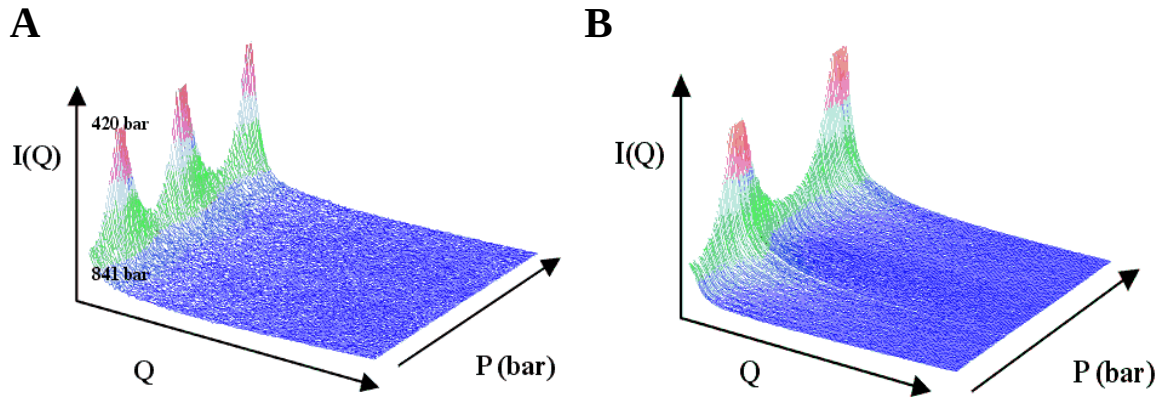

Figure 2. A.) X-ray scattering pattern of 18 kDa. PtBMA -b- 65 kDa. PFOMA as function of pressure at T = 35 °C, and B.) same for 16 kDa. PtBMA -b- 52 kDa. PFOMA.

At low momentum transfer values, the intensity initially (high pressure) does not show considerable changes in its values until the transition zone is approached. Suddenly it starts increasing as the pressure decreases giving a clear indication the system is evolving towards the formation of micelles (high intensity values and low pressure) from a collection of random coils (low intensity and higher pressure). The pressure is kept constant at 420 bar and then increased again up to 840 bar; the reversed transition, from micelles to random coil chains, is observed, getting again the low intensity value when the pressure is higher than 400 bar. Similar P ramps have been obtained in the temperature range 35-55 °C in steps of 5 °C as well as for other block copolymers such as 16K PtBMA-b- 52 K PFOMA. In Figure 2B it is reported an analogous pressure ramp for the latter block copolymer system at 35 °C. It is very interesting to note that the formation-destruction of the aggregates is a highly reproducible process as it has been shown in the alternate up and down pressure ramps. From these experiments it is also possible to estimate the critical micellization density (CMD), the solvent density at which a sharp transition from random coils to aggregates occurs. Table 1 reports preliminary results for CMDs found for PtBMA-b-PFOMA block copolymers characterized by different molecular weights.

Table 1. Critical Micellization density (CMD) for different molecular weights of copolimer's blocks .

Mn PtBMA (KDa.)	Mn PFOMA (KDa.)	CMD (g/cm^3)
7	48	0.86
13	20	0.98
16	52	0.96
18	65	1.03

Since two configurations of the polymer can essentially be observed in solution, the random coil one at high pressure (low intensity) and the aggregate at low pressures (high scattering intensity values), in principle one may think to design an experiment in which the pressure can jump almost instantaneously and observe the relaxation process. Pressure jumps were performed, at different temperatures, for a series of PtBMA-b-PFOMA systems characterized by different molecular weights of the two blocks. It is clear that there is a relaxation effect due to the formation of the aggregates and to the solvent itself (figure 3). As first attempt to rationalize this behaviour, we have proposed a model that gives a fit with two exponentials growth function, from which it is possible to derive two characteristic relaxation times. In figure 4 the opposite P-jump experiment has been performed on the same solution at the same temperature (from 341 to 912 bar). In this case the system, at the initial pressure, is constituted mainly of aggregates that can be destroyed with a P-jump to a much higher pressure. The integrated intensity profile shows no relaxation effect after the pressure jump.

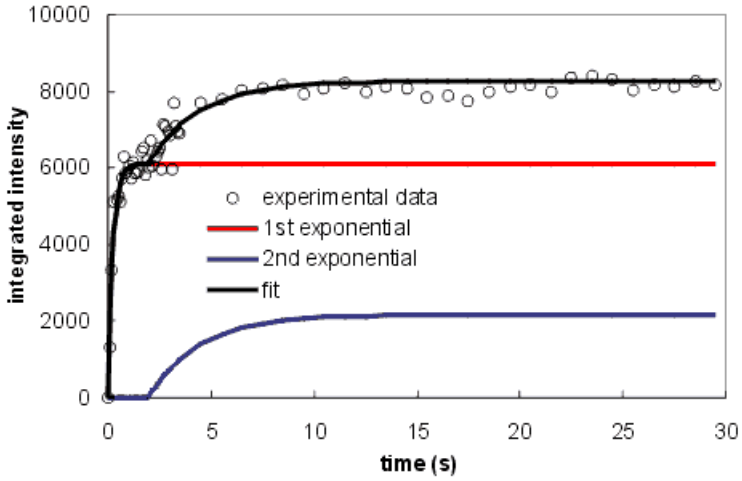

Figure 3. Typical relaxation effect for a pressure jump from 1300 to 350 bar for the 18KDa PtBMA-b-65 KDa PFOMA solution at 40 °C.

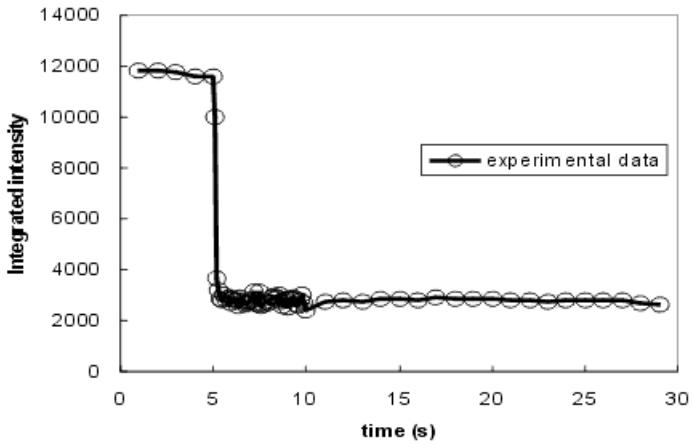

Figure 4. Results from a pressure jump from 341 to 912 bar for the 18KDa PtBMA-b-65 KDa PFOMA solution at 40 °C.

References:

[1] J.B. McClain et.al.; Science; **274**, 2049-2053 (1996)
[2] F. Triolo et al.; Langmuir; **16,** 416-421 (2000)
[3] F. Triolo et al.; J. Appl. Cryst.; **33**, 641- 644 (2000)
[4] A. Triolo et al.; Phys. Rev. E.; **61**, 4640-4643 (2000)
[5] F. Triolo, A. Triolo, F. Lo Celso, D. E. Betts, J. B. McClain, J. M. DeSimone, G. D. Wignall, and R. Triolo; Physical Review E; **62**, 5839-5842 (2000)
[6] F. Triolo, A. Triolo, F. Lo Celso , J. S. Johnson Jr., D.I. Donato and R. Triolo; Nuclear and Condensed Matter Physics, American Physics Institute; (2000) pp. 222-225
[7] F. Triolo, A. Triolo, F. Lo Celso, D.I. Donato, R. Triolo, *Physica A*, 304, 135–144 (2002)

SPATIAL DISTRIBUTION OF DEFORMATION INDUCED LATTICE DEFECTS IN ULTRAFINE- AND NANO-GRAINED METALLIC MATERIALS

M. Zehetbauer[1] , T. Ungar [2] , E. Schafler [1] , R. Pippan [3] and S. Bernstorff [4]

1.) Institute of Material Physics, Vienna University, Boltzmanngasse 5, A-1090 Wien, Austria

2.) Institute of General Physics, Eötvös University, Pazmany Peter Setany 1/A, H-1518 Budapest, Hungary
3.) Erich Schmid Institute for Material Science, Austr.Acad.Sciences, Jahnstrasse 12, A-8700 Leoben, Austria
4.) SAXS Group, Synchrotron ELETTRA, Basovizza, I-34012 Trieste, Italy

Besides a series of extraordinary properties (enhanced soft magnetic properties, lowered thermal and electrical conductivity, enhanced diffusion coefficient [1]) ultrafine- and nanograined materials exhibit both ***high strength*** (because of small grain size, [2]) as well as ***extended ductility*** (because of enhanced grain boundary sliding, "superplasticity" [2, 3]). Up to now, these materials could be only produced in small sample shapes (at most, thin foils) by different methods (inert gas condensation, ball-milling with subsequent consolidation, and electrodeposition [1]) which restricted their use to a few special applications like e.g. as transformator sheets. However, since recently, these materials can be achieved in bulk shape by special methods of severe plastic deformation [2] which markedly extends their application to commercial areas such as tool production, automobile industry as well as for medical purposes (prostheses).

At present, strong efforts are made by the scientific community (our group included) in order to characterize the microstructure of such materials produced by these new deformation methods which all have in common a high hydrostatic pressure component. Among them the most important ones are the Equal Channel Angular Pressing (ECAP, [2]), and the Torsion under high Hydrostatic Pressure (HPT, [2]). Not only the grain size, but also the nature, density and local distribution of lattice defects and of long range internal stresses markedly govern the particular properties of these materials [4, 5]. X-ray Bragg Profile Analysis in combination with Synchrotron radiation (SXPA) proved to be an appropriate method to study these quantities by a high lateral resolution in several large strain cold worked metals [6, 7].

In presently reported experiments lateral static scans of XPA (X-ray Bragg Profile Analysis) on ultrafine-grained bulk samples of polycrystalline Cu have been performed. The ultrafine-grained structure was realized by ECAP which provided an average grain size of about 200 nm. Depending on the route of deformation (route A: without rotation around sample axis between single deformation passes, route B: with rotation by 90° after each pass), the grain shows unequal (A) or equal (B) diameters in at least two different dimensions. Fig. 1a shows that the spatial variations of dislocation density ρ^* occur almost in parallel to those of local internal stress $\Delta|\Delta\sigma|$ and dislocation arrangement parameter M, which indicates a simple accumulation of dislocations in so-called dipolar walls, as has been already observed in conventionally deformed polycrystalline Cu [6] and other metals [7]. The situation strongly changes when approaching states of large deformation (Fig. 1b): Positive spatial variations of ρ^* correspond to negative ones of $\Delta|\Delta\sigma|$ and M which is connected with the increasing occurrence of dislocation tilt walls, representing the growth of new grain boundaries which are responsible for the formation of the ultrafine or even nanocrystalline structures [5, 6]. Comparing the scans done in route B deformed Cu (Fig. 1b) with those done in route A deformed one (Fig. 1c) it is obvious that the spatial frequency of variations in ρ^*, $\Delta|\Delta\sigma|$ and M is much lower: this agrees with the fact that this deformation mode resembles to the conventional large strain deformation modes where the size of developing grains is of order 1000 nm and more.

References:

[1] H.Gleiter**,** Nanocrystalline Materials, Progr.Mater.Sci. 33, 223-315 (1989), and: Materials with Ultrafine Microstructures: Retrospectives and Perspectives, Nanostruct.Mater. 1, 1- 19 (1992)

[2] R.Z.Valiev, R.K.Islamgaliev, I.V.Alexandrov, Bulk Nanostructured Materials from Severe Plastic Deformtion, Progr.Mater.Sci. 45, 103-189 (2000)

[3] S.X.McFadden, R.S.Mishra, R.Z.Valiev, A.P.Zhilyaev, A.K.Mukherjee; Low-temperature Superplasticity in Nanostructured Nickel and Metal Alloys; Nature 398, 684-685 (1999)

[4] Ultrafine-Grained Microstructures Evolving During Severe Plastic Deformation; T. Ungár, I. Alexandrov, M. Zehetbauer, JOM 52, 34-36 (2000)

[5] M.Zehetbauer, Strengthening Processes of Metals at Severe Plastic Deformation: Analyses with Electron and Synchrotron Diffraction, keynote paper in: Investigations & Applications of Severe Plastic Deformation, Proc. NATO Adv.Research Workshop, August 2-6 (Moscow, Russia 1999), ed. T.C.Lowe and R.Z.Valiev, Kluwer Acad. Publ., The Netherlands (2000), p.81-91

[6] M.Zehetbauer, T.Ungar, R.Kral, A.Borbely, E.Schafler, B.Ortner, H.Amenitsch, S.Bernstorff, Scanning X-Ray Diffraction Peak Profile Analysis in Deformed Cu-Polycrystals by Synchrotron Radiation, Acta Mater. 47, 1053-1061 (1999)

[7] M.Zehetbauer, E.Schafler, T.Ungar, I.Kopacz, S.Bernstorff, Investigation of the Microstructural Evolution During Large Strain Cold Working of Metals by Means of Synchrotron Radiation – A Comparative Overview, J.Eng.Mater.Techn. ASME, special issue on "Micromechanics in Crystal Plasticity" 24, 41-47 (2002)

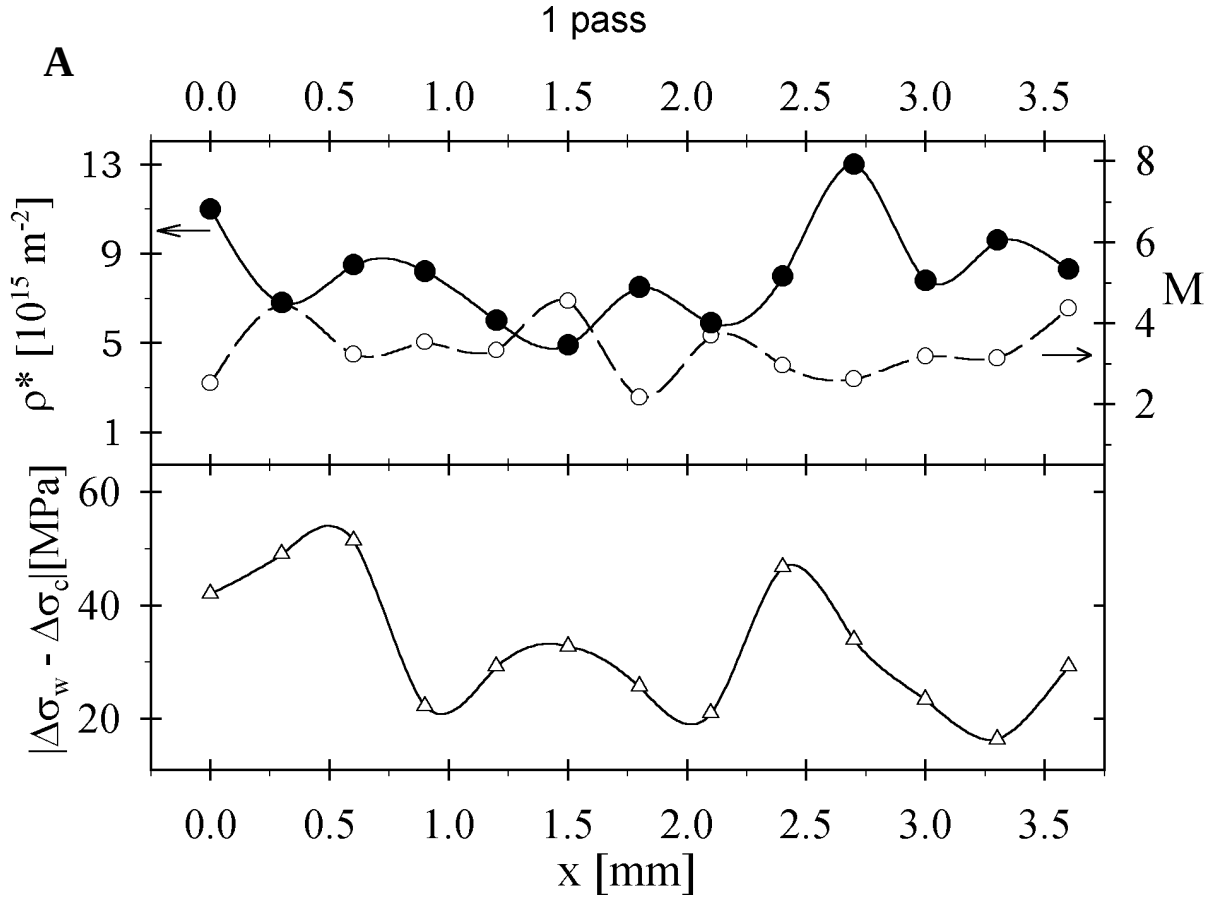

Figure 1. Spatial variations of dislocation density ρ*, local internal stresses Δ|Δσ|, and disloation arrangement parameter M, measured in a Cu polycrystal deformed by ECAP up to different deformation degrees, quantified in terms of true strain ε. The measuring errors Δρ*, ΔM are equal to symbol size while Δ (Δ|Δσ|) is about twice the symbol size.
A.) ε = 1 (routes A and B, 1 pass each);
Next side: B.) ε = 4 (route B, 4 passes); C.) ε = 4 (route A, 4 passes)

B

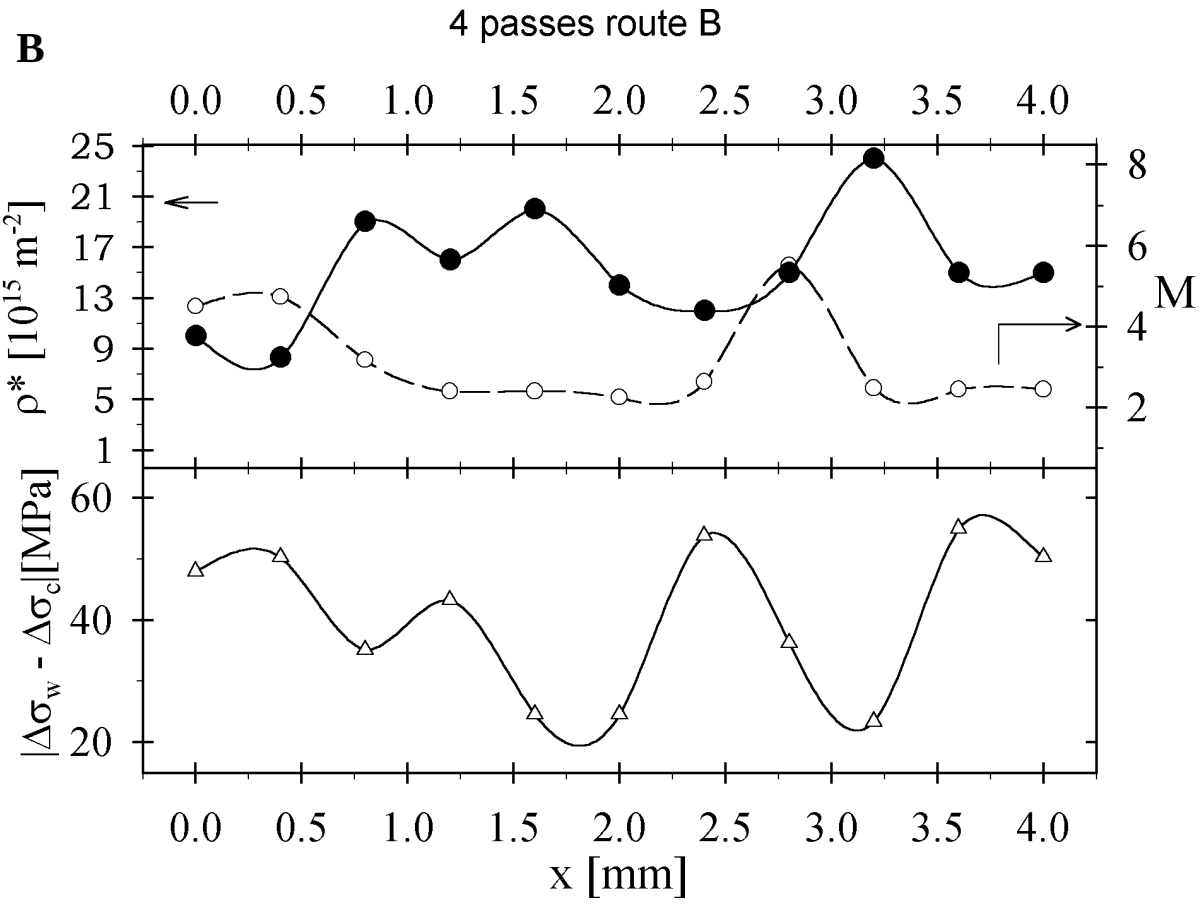
4 passes route B
0.0 0.5 1.0 1.5 2.0 2.5 3.0 3.5 4.0
25 21 17 13 9 5 1
ρ* [10^15 m^-2]
8 6 4 2
M
60 40 20
|Δσw - Δσc|[MPa]
0.0 0.5 1.0 1.5 2.0 2.5 3.0 3.5 4.0
x [mm]

C

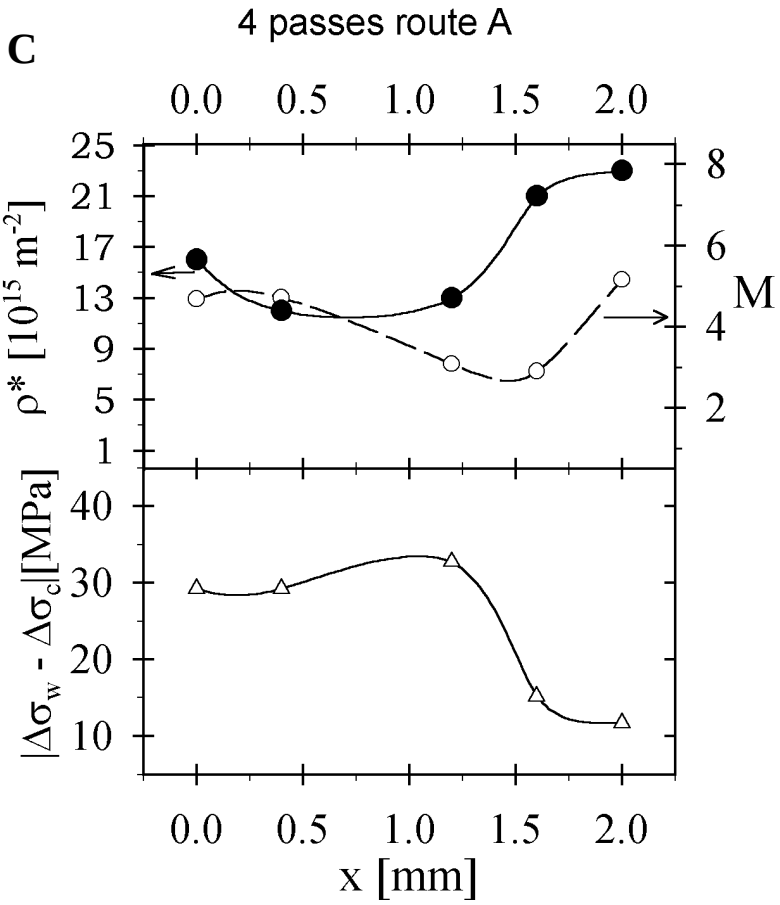
4 passes route A
0.0 0.5 1.0 1.5 2.0
25 21 17 13 9 5 1
ρ* [10^15 m^-2]
8 6 4 2
M
40 30 20 10
|Δσw - Δσc|[MPa]
0.0 0.5 1.0 1.5 2.0
x [mm]

SYNCHROTRON WAXS & SAXS STUDIES OF MICROSTRUCTURAL EVOLUTION DURING POST-YIELD DEFORMATION OF ISOTACTIC POLYPROPYLEN

M. Zehetbauer[1], S. Bernstorff[2], J. Bonarski[3], E. Schafler[1], H. Wilhelm[1], A. Paris[1]

5.) Institute of Material Physics, Vienna University, Boltzmanngasse 5, A-1090 Wien, Austria
6.) SAXS Group, Synchrotron ELETTRA, Basovizza, I-34012 Trieste, Italy
7.) Institute of Metallurgy and Materials Science, Polish Academy of Sciences, Ul.Reymonta 25, PL-30-059 Kraków, Poland

1. Aim and Tasks of Experiment

The presented project is the start of a systematic research program in order to (a) find out which microstructural processes are responsible in controlling the microscopic slip and, thus, the macroscopic mechanical properties observed in plastic deformation of semi-crystalline iPP, and (b) clarify the role of deformation mode for hardening characteristics, in particular that of craze formation in tensile experiment. These goals require the careful measurement of the following parameters, for different plastic strains from compression, rolling and tension tests: (i) of the **volume fraction (f_c) of crystalline and amorphous phases,** (ii) of (δ) being the **long period of lamella,** as well as their size and their orientation distribution ("texture"), and finally (iii) the **density of crystal lattice defects**, their distribution and internal stresses connected.

2. Need for Synchrotron Radiation

While f_c is accessible by careful WAXS measurement, δ can be determined by SAXS measurement. From both f_c and δ the lamella size can be calculated. From literature [1] and pilot studies done in our home laboratory (Fig.1), it is clear that a quantitative determination of f_c requires careful determination and averaging of WAXS spectra for different rocking angle pairs α and β, in order to correct for inhomogeneous orientation distributions of lamella crystals („texture") in the sample. For this reason it is necessary to detect as many diffraction orders as possible – and the amorphous part - in 2-theta range. According to our pilot tests on iPP samples, this is a very time consuming task in a home laboratory because of the weak high order diffraction peaks in this material. For spectra exemplarily shown in Fig.1 the total measuring time was over 1000 min in total but only 3 peaks of α phase (at $\alpha \approx 15$, 21 and 27°) could be detected. Even when using a line detector and a high intensity rotating anode generator, the measuring time necessary for one full 2θ - spectrum exhibiting 5 peaks of α-phase at only one certain rocking angle pair was up to 60 min especially when the sample has been plastically deformed. For the reasons quoted, the use of a high-flux synchrotron SAXS-WAXS beamline is mandatory here.

One of the central aims of this project is the proof of existence of dislocations, particularly those generated from plastic deformation process. This experiment is still missing until today [2], mainly due to lack of experimental methods for such a proof. Recently, such a critical analysis has been developed by T.Ungar et al. [3] who found the dislocation induced broadening ΔK^{DIS} to show a characteristic increase with increasing diffraction vector K, in contrast to size broadening effects ΔK being constant in K. Nevertheless, the proof for dislocations needs the measurement of deformation induced broadening in 5 different reflections at miminum, which can be hardly realized by the limited intensity of a standard X-ray diffraction equipment. Moreover, from our pilot tests it is clear that the deformation induced broadening is much smaller than in metals, i.e. 10% in FWHM as compared to the

undeformed state which needs a higher resolution i.e. a high number of counts in Bragg Peaks. Both arguments strongly confirm the need for highly intensive Synchrotron radiation.

Our first Synchrotron experiment within this project on semicrystalline iPP has been performed in December 2001. Injection moulded samples of α-iso-polypropylene which had been delivered from strongly oriented surface layers, were subjected to plastic deformation to true equivalent strains ε = 0.1 to 0.5. The plastic deformation was achieved by compression in two different directions perpendicular and in parallel to injection direction. WAXS measurements with primary Synchrotron radiation have been performed in transmission and reflection by 0.77 and 1.54 A, and the shape and broadening of Bragg reflections (110), (040), (130), (111), (-131) and (041) have been analyzed, as a function of ε. The results are shown in Fig. 2 (perpendicular compression, with results being similar to those of parallel compression) where the broadening at FWHM $\boldsymbol{\Delta K}$ is plotted as a function of diffraction vector $\boldsymbol{K}$. The fact that $\boldsymbol{\Delta K}$ is distinctly not constant with $\boldsymbol{K}$ clearly indicates the presence of dislocations in the sample, since the limited size of lamellas would cause a ***constant ΔK(K)*** only. The fact that $\boldsymbol{\Delta K}$ increases even ***more*** for ***increasing*** deformation degree ε, the ***higher*** the Bragg reflection considered (Fig. 2) strongly suggests that the number of dislocations multiplies with increasing plastic deformation. For a more careful evaluation, further measurements and/or evaluations particularly from the higher reflections will be necessary.

References:

[1] S. Vleeshouwers, Simultaneous in-situ WAXS/SAXS and d.s.c. Study of the Recrystallization and Melting Behaviour of the α and ß form of iPP, Polymer 38, 3213-3221 (1997)

[2] B.Crist, Plastic Deformation of Polymers, ch. 10 in: Structure and Properties of Polymers, vol.12, ed. E.L.Thomas, Materials Science and Technology, eds. R.W.Cahn et al., Verlag Chemie, Weinheim (Germany, 1993)

[3] T.Ungar, A.Borbely, The Effect of Dislocation Contrast on X-Ray Line Broadening: A New Approach to Line Profile Analysis, Appl.Phys.Letters 69, 3173-3175 (1996)

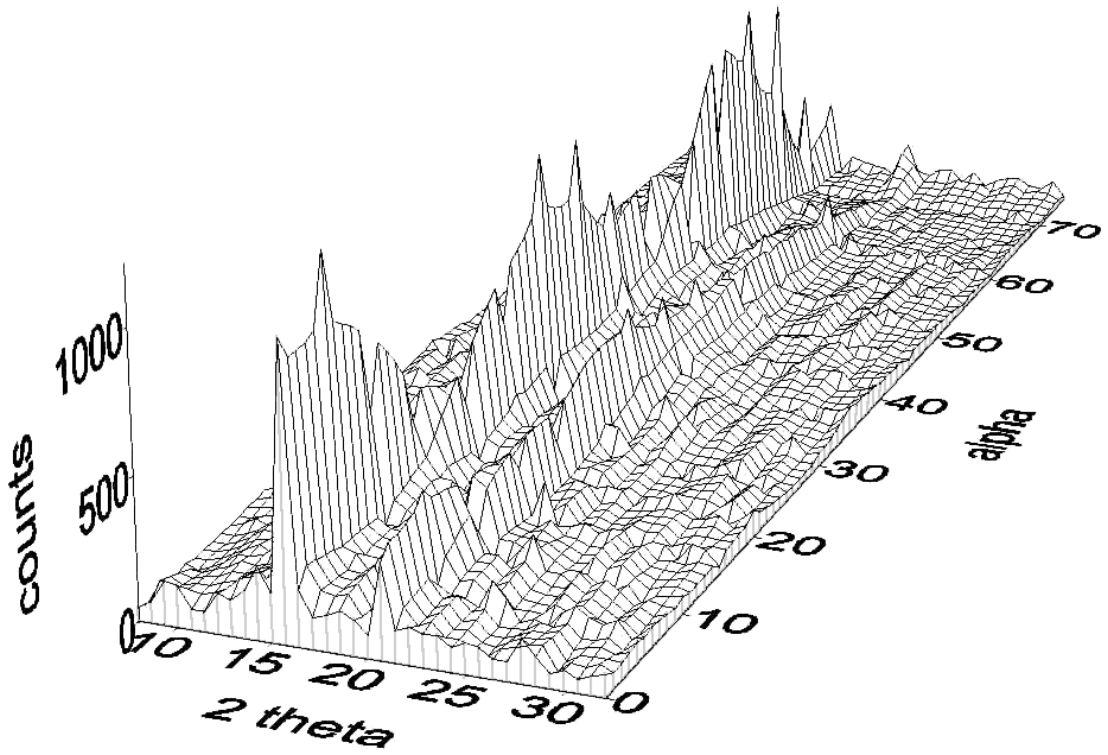

Figure 1. Diffraction patterns from iPP samples, as a function of radial rocking angle α of the sample orientation (horizontal rocking angle β = 0 for all α). Note that the height (i.e., intensity) of peaks representing the α (β) – phase strongly changes with α, due to marked texture in the material. The three largest peaks denote (from left to right) the reflections of phase α: (110), β: (300), α: (111).

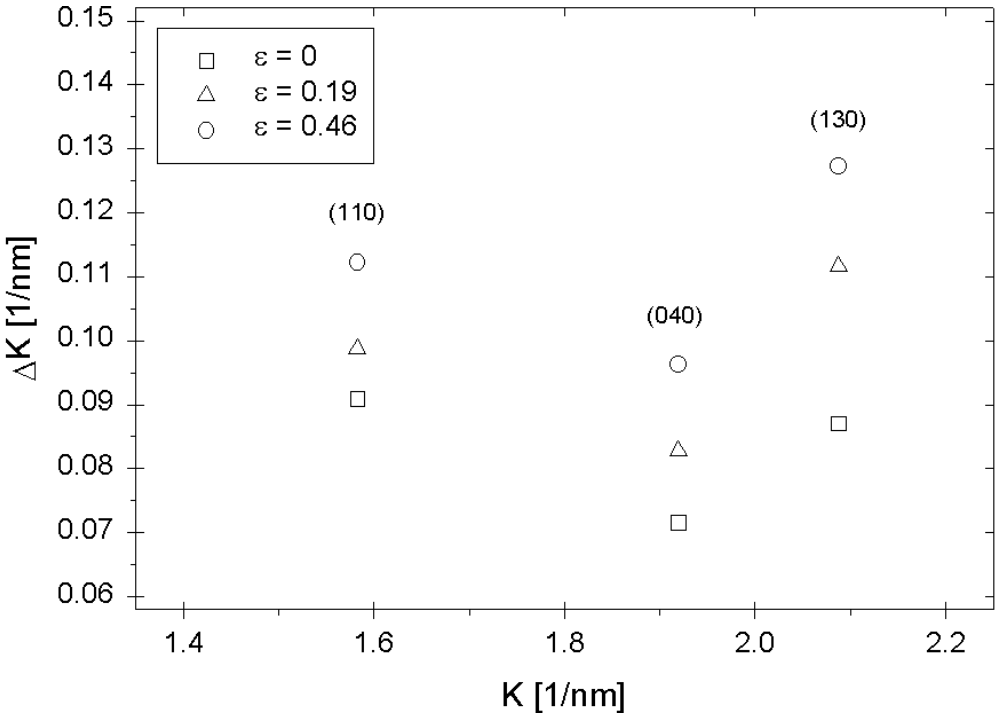

Figure 2. Broadening of profiles of different Bragg reflections in α-iPP, as a function of true equivalent plastic strain, after compression perpendicular to injection direction.

2. Life Sciences

S1 TAIL DOMAIN DISPOSITION DEPENDS ON FORCE EXERTED BY A MYOSIN MOTOR

H. Amenitsch[1], C.C. Ashley[2], M.A. Bagni[3], S. Bernstorff[4], G. Cecchi[3], B. Colombini[3] and P.J. Griffiths[2]

1.) Institute of Biophysics and X-ray Structure Research, Austrian Academy of Sciences, Schmiedlstraße 6, A-8042 Graz, Austria.
2.) University Laboratory of Physiology, Parks Road, Oxford, OX1 3PT, U.K.
3.) Dipartimento di Scienze, Università degli Studi di Firenze, Viale G.B. Morgagni 63, Firenze, I-50134, Italy.
4.) Sincrotrone Trieste, Area Science Park, Basovizza/TS, I-34012, Italy.

Myosin motors perform work during interaction with G-actin filaments. The subfragment 1 (S1) moiety of myosin binds to actin and undergoes a force-producing conformational change associated with ATP hydrolysis (the 'power stroke', [1]). Although 17 classes of myosin motor exist, myosin II (responsible for all muscle contractility) possesses the unique advantage that it is aggregated into highly ordered filaments. In skeletal muscle, these 'thick' filaments overlap 'thin' (actin) filaments in a hexagonal array, giving a quasi-crystalline structure and enabling simultaneous collection of X-ray diffraction and mechanical data from a working population of myosin motors. The X-ray reflections undergo spacing and intensity changes during force development, from which aspects of the underlying structural changes may be inferred. The quick recovery of tension, following the elastic response produced by a step change in fibre length, is accompanied by a fall in intensity of the strong meridional X-ray reflection at the third harmonic of the axial myosin unit cell (I_{M3}). Both this intensity fall and the quick recovery of force are attributed to a synchronised power stroke [2]. I_{M3} therefore provides an important dynamic, non-invasive probe of S1 configuration.

In relaxed muscle, the 14.32nm meridional reflection (M3) originates from the 3-fold helical projection of S1 along the thick filament backbone. I_{M3} changes during force generation are complex, arising from both the effects of disordering of radial alignment of filaments, and also from changes in S1 disposition. S1 is an elongated, pear-shaped structure, divisible into a lever domain (corresponding to the narrow end of the pear and attached to the thick filament backbone via the S2 moiety) and a motor domain (corresponding to the broad end, containing both ATP and actin binding sites [1]). The power stroke is thought to be a rotation of the lever domain about the motor, generating a torque at the S1/S2 junction, resulting in axial tension and filament sliding. Changes in the axial mass projection of the lever arm as a result of the power stroke are sampled by the M3 reflection, leading to an I_{M3} signal [2]. The I_{M3} change associated with a stretch is instantaneous with the length change (ie: elastic), but is delayed for a release. This asymmetry may arise because, in addition to the effect of the power stroke, the angle of disposition of the lever domain varies with load in the manner of an elastic element, and its orientation when I_{M3} is maximal ($I_{M3\ max}$) is reached after a release of ca. 1nm [3]. Summation of elastic and power stroke displacements of the lever domain leads to a delay in I_{M3} response to a release because of the time required for the lever to be displaced to its $I_{M3\ max}$ position. Recently, at Elettra, we studied changes in I_{M3} in tibialis anterior fibres from *Rana temporaria* during sinusoidal perturbation of fibre length. We found that, at high frequencies (>1kHz), the I_{M3} response was sinusoidal. At lower frequencies, IM3 was deformed during the shortening phase of the oscillations [4]. This is consistent with an instantaneous elastic distortion of S1, which dominates the I_{M3} signal at high frequencies, plus a slower power stroke distortion, which proceeds further during low frequency oscillations, causing an additional displacement of the lever domain through $I_{M3\ max}$ during the release phase. We were able to simulate the I_{M3} changes as a function of oscillation frequency by taking the Fourier transform of a rectangular body representing S1 in which the upper portion of the rectangle was bent about the lower in the same manner as the lever domain is thought to bend about the motor. By adjustment of the initial disposition of the upper portion of the rectangle, we were able to match the observed changes in I_{M3} with our simulations, and in this way to determine the orientation of the lever domain in the isometric state. This technique of determination of S1 structure is novel, and provides an alternative method of defining lever disposition to the classical approach of Fourier reconstruction of S1 from static intensities, which is prone to difficulties both because of the weakness of some of the reflections required and because of the presence of other factors influencing intensity.

A rise in temperature from 4°C to 22°C increases tension developed by frog muscle 1.28 fold without significant change in fibre stiffness, i.e. increasing the load per cross-bridge without recruitment of new bridges. We found that I_{M3} deformation during oscillations increased with temperature, consistent with a shift in lever domain orientation towards its $I_{M3\,max}$ position when S1 exerts more force. We used our Fourier transform simulations of S1 to demonstrate that this increased distortion of I_{M3} signals could not arise from power stroke acceleration with temperature. However, it could be argued that the presence of distortion is related to the power stroke event *per se*, and not to an increased lever domain displacement. To resolve this issue, we repeated the observations at high frequency (3kHz), where power stroke effects are minimal. By using short muscle fibres (dorsal interossei), we were able to increase the oscillation amplitude per sarcomere beyond what was possible with tibialis fibres, and we were able to observe I_{M3} distortion in the virtual absence of the power stroke event (fig. 1). This finding supports the proposal that power stroke and elastic distortions of S1 both cause a change in lever disposition, and that these distortions are additive.

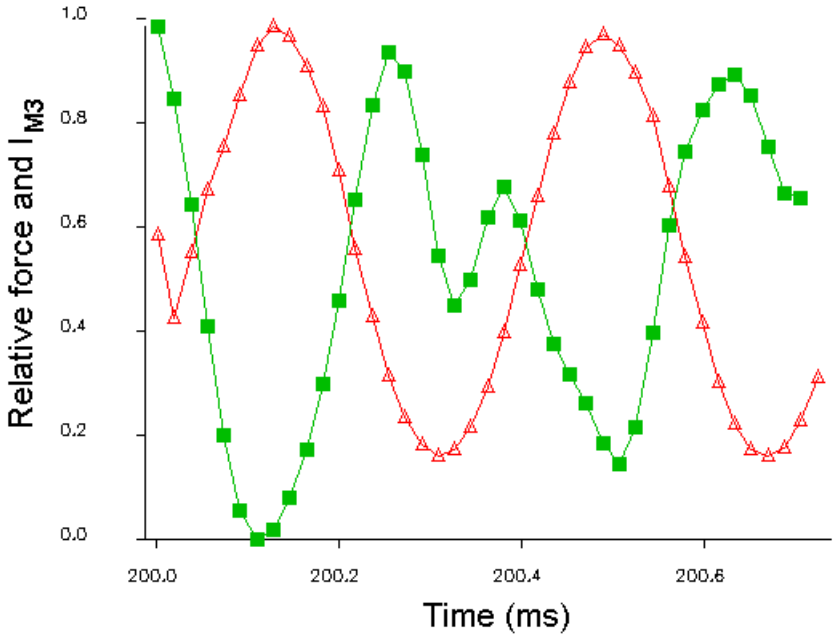

Figure 1. I_{M3} (■) and force (Δ) measured during 3 kHz sinusoidal length oscillations. Force and intensity are normalised to their average maximum and minimum values. Time is measured from the start of data collection (i.e. the onset of the tetanus) to the onset of the oscillations. When length oscillation amplitude is reduced, the double peak in I_{M3} corresponding to minimum force becomes smaller, and I_{M3} approaches an undistorted sinusoidal function [4].

References:

[1] I. Rayment, W.R. Rypniewski, K. Schmidt-Bäse, R. Smith, D.R. Tomchick, M.M. Benning, D.A. Winkelmann, G. Wesenberg and H.M. Holden. Three-dimensional structure of myosin subfragment-1: A molecular motor. *Science*, **261**: 50-58 (1993)

[2] M. Irving, V. Lombardi, G. Piazzesi and M. Ferenczi. Myosin head movements are synchronous with the elementary force generating process in muscle. *Nature*, **357**: 156-158 (1992).

[3] V. Lombardi, G. Piazzesi, M.A. Ferenczi, H. Thirlwell, I. Dobbie and M. Irving. Elastic distortion of myosin heads and repriming of the working stroke in muscle. *Nature*, **374**, 553-555 (1995).

[4] M.A. Bagni, B. Colombini, H. Amenitsch, S. Bernstorff, C.C. Ashley, G. Rapp and P.J. Griffiths. Frequency dependent distortion of meridional Intensity changes during sinusoidal length oscillations of activated skeletal muscle. *Biophys. J.*, **80:** 2809-2822 (2001).

PRESSURE –ASSISTED COLD DENATURATION OF PROTEINS: A TEST ANALYSIS BY SAXS AT ELETTRA

S. Cinelli[1], F. Spinozzi[2], F. Carsughi[3], G. Onori[1] and P. Mariani[2]

1.) Dipartimento di Fisica and INFM, Università di Perugia, Via Pascoli, I-06123 Perugia (Italy)
2.) Istituto di Scienze Fisiche and INFM, Università di Ancona, Via Ranieri 65, I-60131 Ancona (Italy)
3.) Dipartimento di Scienze e Biotecnologie Agrarie ed Ambientali and INFM, Università di Ancona, Via Brecce Bianche, I-60131 Ancona (Italy)

The native conformations of hundreds of proteins are known in great detail from structural determinations by X-ray crystallography and, more recently, NMR spectroscopy. However, detailed knowledge of the conformations of denatured and partially folded states is lacking, which is a serious shortcoming in current studies of protein stability and protein folding pathways [1]. Therefore, increasing attention has been focused on denatured and partially folded states [2], and most studies dealing with protein denaturation have been carried out at atmospheric pressure with various physico-chemical perturbations, such as temperature, pH, or denaturants, as experimental variables [3,4,5,6,7]. The thermal unfolding can often be represented by a two state equilibrium of the type $N \leftrightarrow D$, where N is the fully native and active protein and D an inactive, denatured state. Detailed studies of the reversible denaturation of chymotrypsinogen and ribonuclease enabled to demonstrate that the two-state $N \leftrightarrow D$ model was applicable and that the free energy of denaturation exhibits an unusual temperature dependence [8]. The two-state model thermodynamics predicts that the free energy of denaturation, $\Delta G(T)$, has the form of a distorted parabola. This parabola may have zero at two temperatures corresponding, respectively, to the temperature T_h for heat denaturation and to the one T_c for cold denaturation of the native protein. A significant consequence of Brandts' experimental studies was the prediction that in addition to the much-investigated thermal transition, there should exist a low-temperature transition at some temperature T_c. Although the phenomenon of cold inactivation of enzymes is well known, until recently no thermodynamic information was available about low-temperature-induced $N \leftrightarrow D$ transitions. The main reason is that for all proteins that have been studied in detail, the predicted T_c values lie well below the equilibrium freezing point of water, which makes T_c inaccessible to experimental determination.

Quantitative investigations of the effect of pressure on proteins is the only practical way to acquire information on volume effects associated with conformational transitions of proteins. Proteins are not very sensitive to pressure, and only at extremely large values of pressure do they exhibit the changes which are very similar to those observed in temperature-induced denaturation. This pressure-induced denaturation of proteins takes place in a relatively narrow pressure interval which depends strongly on the temperature of the solution. At the same time, the temperature of denaturation is itself dependent on pressure. Thus, these two parameters are interdependent, and a variation of any of them at fixed value of the other leads to denaturation change in protein. Compared to varying temperature, which produces simultaneous changes in both volume and thermal energy, the use of pressure to study protein solutions perturbs the environment of the protein in a continuous, controlled way by changing only intermolecular distances [9]. In addition, by taking advantage of the phase behavior of water, high pressure can substantially lower the freezing point of an aqueous protein solution. Therefore, by applying high pressure, one can investigate in detail not only pressure-denatured proteins, but also cold- denatured proteins in aqueous solution. Moreover, previous work [10] on pressure and cold denaturation has suggested that these methods can leave appreciable residual structure in proteins, particularly when compared to other methods such as thermal or urea denaturation. Therefore, pressure-assisted, cold-denaturation appears to be a milder method of denaturation than the more conventional.

In the proposed experiment, we tested the possibility to perform at the SAXS beamline of Elettra small-angle X-ray scattering analysis of a protein in dilute solution (about 5 mg/ml) under mechanical pressure (up around 2 kbar) and different temperatures (from 10 to 45°C). The SAXS experiment concerned the pressure-induced denaturation and pressure-assisted, cold-denaturation of metmyoglobin. The folding pathways of the metmyoglobin have been described [11,12] and it has been reported that at pH around 4 the protein undergoes the changes, denatured state – native state –

denatured state, when the protein is heated from 0 to 60°C at pressures below 1500 bar. The Figure 1 shows the contours of the pressure-temperature values at which the folded/unfolded states are in equilibrium.

Experiments were than performed using a scattering vector *Q* range ($Q = 4\pi \sin\theta/\lambda$, being 2θ the scattering angle, and λ the X-ray wavelength) from 0.03 to 0.24 $Å^{-1}$. Metmyoglobin solutions were measured using the pressure cell and the pressure-control system designed and constructed by M. Kriechbaum and M. Steinhart [13]. The pressure cell has two diamond windows (3.0 mm diameter and 1 mm thickness) and allows to measure diffraction patterns at hydrostatic pressures up to 3 kbar. SAXS was performed at four different temperatures (namely 10, 20, 30 and 45°C) for different pressures, from 1 bar to 2 kbar, with steps of about 100 bar. To avoid radiation damage, the exposure time was 300 s/frame and a lead shutter was used to protect the sample from excess radiation within periods where no data were recorded. Particular attention has been devoted to check for radiation damage: in several cases, measurements were repeated several times at the same constant pressure or using new samples. The experimental intensities were corrected for background, buffer contributions, detector inhomogeneities and sample transmission. The results are reported in the form of Kratky plots in Figure 2. The Kratky plot is a useful tool in SAXS analysis for the characterization of globular protein and for the detection of intermediate folded states [14]. For a globular particle, the Kratky plot shows a typical peak, whose position mainly depends on its gyration radius, Rg; on the other hand, when an unfolding process takes place, the peak usually vanishes and the curve tends to show a plateau when the protein assumes a completely unfolded random-coil conformation.

The Figure 3 shows the dependence of the Rg on pressure at the different investigated temperature: considering a two-state equilibrium, the transition pressures reported in Table 1 have been derived. The data are in very good agreement with spectral results obtained by [11]. Two general results have been then obtained: first, the quality of the data indicates that it is possible to start a long-term project on the study of the pressure-induced denaturation and pressure-assisted, cold-denaturation of different proteins to provide critical insights into the mechanisms and pathways of protein folding. Second, the data will be used to extend the work of [11] to derive the molecular mechanism of the pressure-induced unfolding process in the metmyoglobin.

Table 1.
Radii of gyration of the native and the denaturated state and the transition pressure obtained from the fits reported in figure 3.

T (°C)	$R_{g,1}$ (Å)	$R_{g,2}$ (Å)	P_{trans} (bar)
10	18±1	24±2	1200±300
20	17.6±0.4	21.5±0.6	1070±90
30	18.9±0.4	22.1±0.7	1100±90
45	19.0±0.5	29±1	1320±50

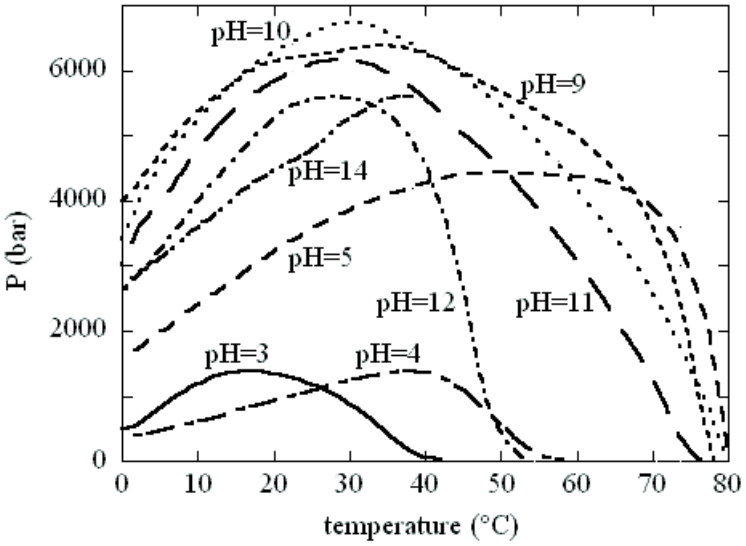

Figure 1. Contours of the pressure-temperature values at which the folded/unfolded states are in equilibrium.

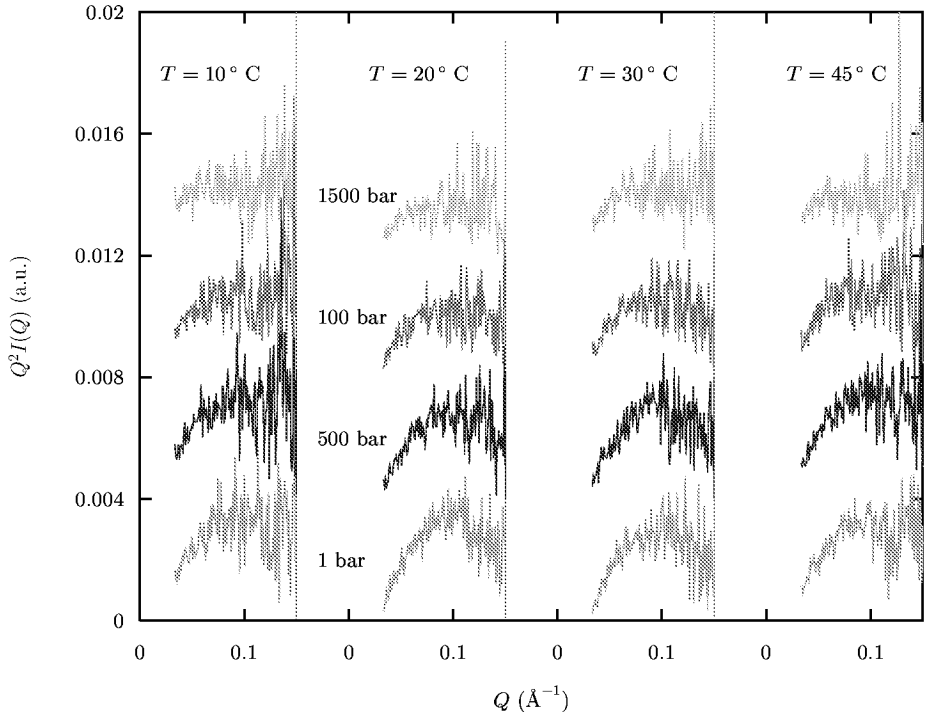

Figure 2. Kratky plots as a function of pressure and at different temperature.

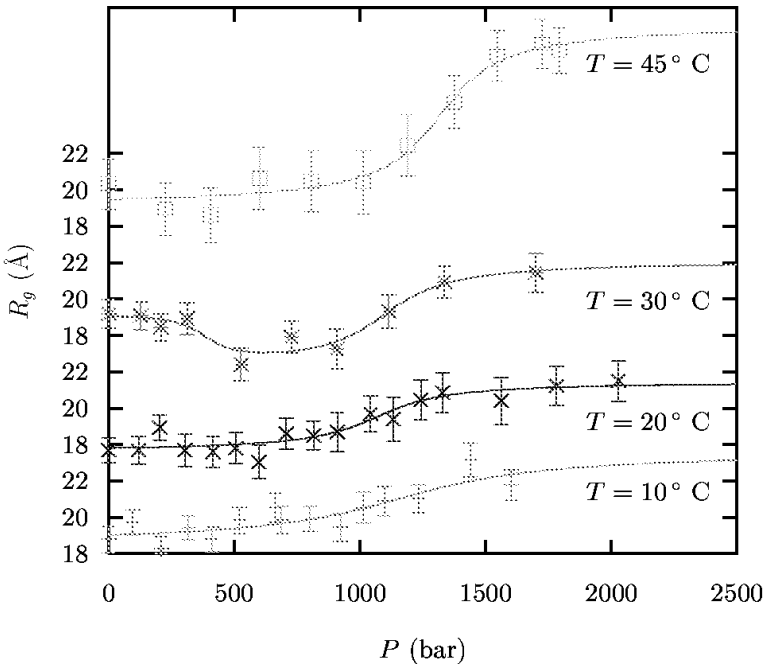

Figure 3. Dependence of the Rg on pressure at the different investigated temperatures.

References:

[1] Robertson, A. D., and R. L. Baldwin; Hydrogen exchange in thermally denatured ribonuclease A.; Biochemistry **30**, 9907–9914 (1991)

[2] Calandrini V., D.Fioretto, G.Onori and A.Santucci; Role of hydrophobic interactions on the stabilisation of native state of globular proteins, Chem. Phys. Letters, in press (2000)

[3] Cinelli S., G.Onori and A.Santucci; The effect of aqueous alcohol solutions on the thermal transition of lysozyme: a calorimetric study, J. Phys. Chem B, **101**(40), 8029-8034 (1997)

[4] Cinelli S., G. Onori and A. Santucci; Effect of 1-alcohols on micelle formation and protein folding, Colloids and Surfaces A, Physicochemical and Engineering Aspects, **160**, 3-8 (1999)
[5] Bonincontro A., A.De Francesco, M.Matzeu, G.Onori and A.Santucci. Conformational changes of lysozyme in water-ethanol mixtures, Colloid & Surfaces, B, **10**, 105-111 (1997)
[6] Bonincontro A., A. De Francesco and G. Onori, Temperature-induced conformational changes of native lysozyme in aqueous solution studied by dielectric spectroscopy Chem. Phys. Letters, **301**,189-192 (1999)
[7] Bonincontro, E.Bultrini, V.Calandrini, S.Cinelli, G.Onori.. Effect of trehalose on alkaline transition of cytochrome C. J. Phys. Chem, in press (2000)
[8] Brandts JF, RJ Oliveira, C. Westort, Thermodynamics of protein denaturation. Effect of pressure on the denaturation of ribonuclease A. 1970
[9] Weber, G., and H. G. Drickamer.. The effect of high pressure upon proteins and other biomolecules. Q. Rev. Biophys., **16**, 89 –112 (1983).
[10] Wong, K.-B., S. M. V. Freund, and A. R. Fersht, Cold denaturation of barstar: 1 H, 15 N, and 13 C NMR assignment and characterisation of residual structure. J. Mol. Biol. **259**, 805-818 (1996)
[11] Zipp A., W. Kauzmann, Pressure denaturation of Metmyoglobin. Biochemistry, **12**, 4217-4227 (1973)
[12] Smeller L., P. Rubens, K. Heremans, Pressure effect on the temperature-induced unfolding and tendency to aggregate of myoglobin. Biochemistry, **38**, 3816-3820 (1999)
[13] M.Steinhart, M.Kriechbaum, K.Pressl, H.Amenitsch, P.Laggner and S.Bernstorff. High-pressure instrument for small- and wide-angle x-ray scattering.II. Time-resolved experimentsRev.Sci.Instrum. **70/2**, 1540-1545 (1999),
[14] Semisotnov, G. V., H. Kihara, N. V. Kotova, K. Kimura, Y. Amemiya, K. Wakabayashi, I. N. Serdyuk, A. A. Timchenko, K. Chiba, K. Nikaido, T. Ikura, and K. Kuwajima, Protein Globularization during Folding. A Study by Synchrotron Small-Angle X-ray Scattering, J. Mol. Biol. **262**, 559-574 (1996).

STRUCTURAL CHANGES AND MECHANICAL PROPERTIES OF MINERALIZING COLLAGENOUS TISSUES

H. S. Gupta[1,2], K. Misof[1], S. Bernstorff[3], H. Amenitsch[4], I. Zizak[5] and P. Fratzl[1]

1.) Erich Schmid Institute for Materials Science, Austrian Academy of Sciences, Jahnstrasse 12, A-8700 Leoben, Austria
2.) Ludwig Boltzmann Institut of Osteology, 4th Medical Department, Hansch Hospital & UKH-Meidling Hospital, Vienna, Austria
3.) Sincrotrone Trieste, Area Science Park, Trieste, Italy
4.) Institute of Biophysics and X-Ray Structure Research, Austrian Academy of Sciences, Graz, Austria
5.) Hahn-Meitner Institue, Glienicker Strasse 100, D-14109 Berlin, Germany

In bone and related mineralized tissues, the architecture at different hierarchical levels: organ (macroscopic bone geometry), tissue (trabecular and cortical bone) and material level (mineralized collagen matrix) are important in determining the mechanical properties such as stiffness, toughness (or crack propagation resistance), and fatigue resistance. While finite element modeling [1], confocal laser scanning microscopy [2] and other techniques can be used to predict and study the changes in architecture at the macroscopic and tissue level, the response of the mineralized collagen fibrils to tensile stress has not been fully understood, Using a setup developed by us previously [3, 4] we carried out in-situ tensile testing combined with small angle X-ray scattering on a parallel fibered model system for bone mineralization – mineralized turkey leg tendon – in order to correlate the changes in fibrillar D-period with macroscopic mechanical properties obtained from tensile testing. Intrafibrillar D-stagger was measured by the positions of the peaks in the meridional small-angle X-ray scattering pattern.

In the current experiment we carried out tensile testing at different strain rates on 200-500 micron thick mineralized tendon slices sectioned with a diamond saw. At low strains ($< 1 – 2$ %) increase in stress leads to fibril extension, indicated by the shift of meridional peaks to smaller q values. As the applied stress is increased, partial failure or fracture is deduced from changes in the slope of, and drops in stress value of, the macroscopic stress-strain curve (Figure 1(b)).

Concurrent with these macroscopic changes, the fibrils at the sub-micron level also undergo a dramatic change in structure - meridional diffraction pattern exhibit a split-peak pattern corresponding to 2 different degrees of fibril elongation in the tendon (Figure 1(c),(d)). If the applied force and D-periods of the two components are plotted parallel to each other (Figure 1(b)) it is seen that with occurrence of macroscopic damage, one set of collagen fibrils continue to elongate, at a faster rate, to much larger D-strains of (> 5 %) up to but less that 70 nm. In contrast, the second component relaxes back to the unstressed value.

If the D periodicities are plotted against the nominal applied stress, this change in behavior can be clearly seen in the initial steep portion of the curve followed by the rapid extension of the second component (Figure 2). Quantitatively, if equivalent elastic moduli are defined for the fibrils from the slopes of the σ-D curve, then the typical values for the initial segment are 2.8 GPa and for the second segment about 440 MPa, which is a reasonable value for unmineralized collagen.

A preliminary model for our results may be obtained by combining results from scanning electron microscopy (SEM) investigations on mineralized turkey leg tendons, macroscopic mineral weight fraction measurements and the current results. Namely, the turkey leg tendons, especially at early ages and low degrees of mineralization, consists of both mineralized and unmineralized fibrils and fibril bundles (fibers).

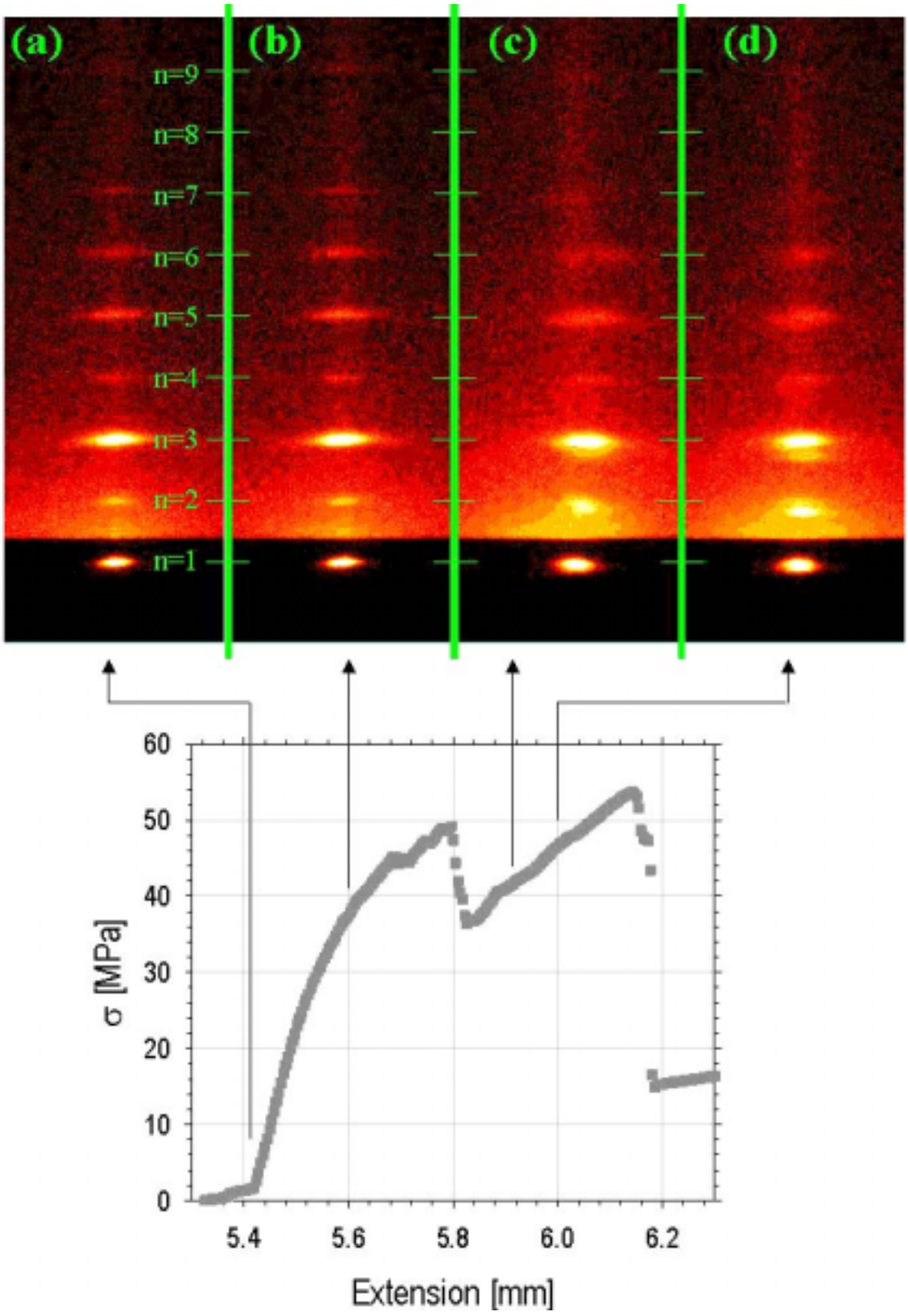

Figure 1. Time development of the meridional reflections of collagen from mineralized turkey leg tendons collected over different parts of the stress-strain curve during constant strain rate tensile testing experiment. Partial failure of tendon is associated with peak splitting into main (M) and secondary (S) peaks.

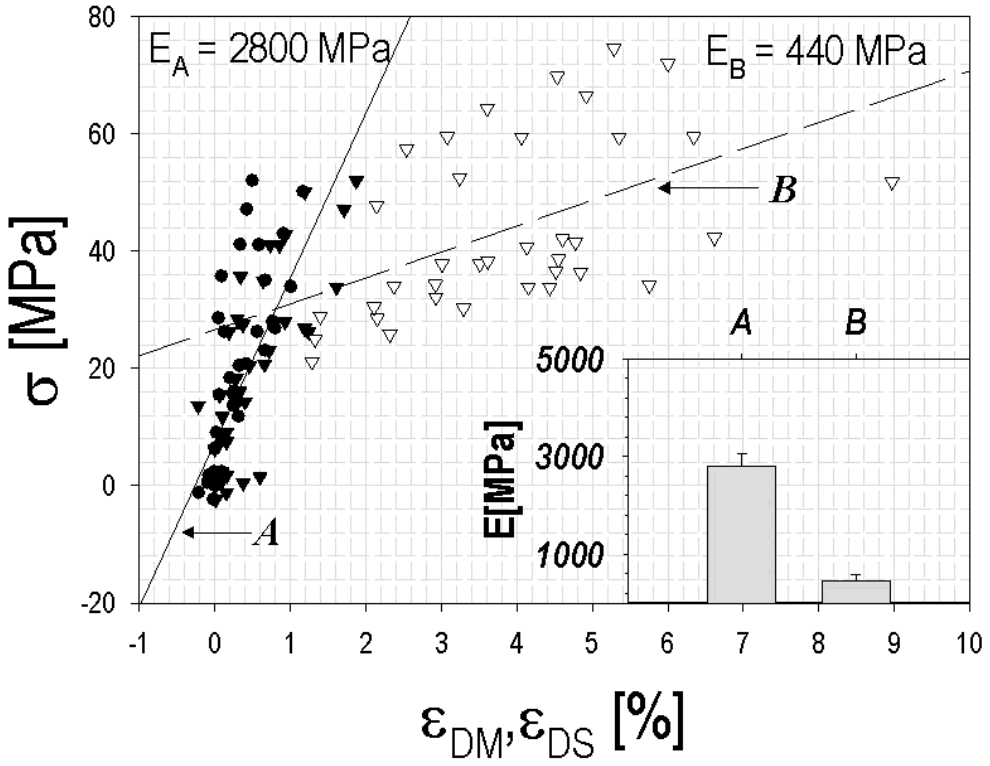

Figure 2. Stress σ versus fibril strain ε_D (either from main (M) or secondary (S) peaks : see Figure 1). For simplicity, the relaxation segments of M and S peaks (following partial or complete failure of the tendon) are not shown. Following division of the strain axis into $\varepsilon_D < 2$ % and $\varepsilon_D \geq 2$ % (corresponding to isostrain and split peak regions respectively), linear regressions in the two regions yield $E_M = 2800 \pm 260$ MPa and $E_S = 440 \pm 130$ MPa.

Transmission electron microscopy results [5] have shown that near the edge of mineralization the fiber bundles consist of both mineralized and unmineralized fibrils. When this heterogenously mineralized arrangement is strained, the two components elongate to the same extent as long as the applied stress is below that of fully mineralized collagen. On exceeding this value (20-60 MPa in our experiments), the mineralized component fractures and relaxes, while the unmineralized component elongates to much larger extensions, resulting in the peak splitting observed.

References:

[1] J Kabel, B van Rietbergen, A Odgaard, R.Huiskes; Constitutive relationships of fabric, density, and elastic properties in cancellous bone architecture; Bone **25,** 481-486 (1999).

[2] P. Zioupos ; Recent developments in the study of failure of solid biomaterials and bone: 'fracture' and 'pre-fracture' toughness; Mater.Science & Engng-C **6**, 33-40(1998).

[3] K. Misof, G. Rapp, P.Fratzl; A new molecular model for collagen elasticity based on synchrotron X-ray scattering evidence.; Biophys. J. **72**, 1367-1381 (1996).

[4] P.Fratzl, Misof K, Zizak I, Rapp G, Amenitsch H, Bernstorff S.; Fibrillar structure and mechanical properties of collagen.; J. Struct. Biol. **122**, 119-122 (1998).

[5] WJ Landis, KJ Hodgens, MJ Song, J Arena, S Kiyonaga, M Marko, C Owen, BF McEwen.; J Struct Biol **117,** 24-35 (1996).

CRYSTALLIZATION IN EMULSION: TRIACYLGLYCEROL POLYMORPHISM

D. Kalnin[1,2], C. Lopez[1,3], P. Quenneson[2], G. Keller[1], F. Artzner[1], H. Amenitsch[4] and M. Ollivon[1]

1.) Equipe Physico-Chimie des Systèmes Polyphasés, 92296 Chatenay-Malabry, France
2.) Nestlé S.A. PTC rue Charles Tellier 60000 Beauvais, France
3.) Arilait Recherches, 75382 Paris, France
4.) Institute of Biophysics and X-Ray Structure Research, Austrian Academy of Sciences, Graz, Austria

Triacylglycerols (TAG) are the main constituents of fats. TAGs exhibit a complex monotropic polymorphism that frequently prevents the study of thermal and structural properties of the fats. Moreover, TAGs are frequently found in food products in an emulsified form that further complexify such studies. Therefore, until recently, the identification of the crystalline varieties formed by TAGs within the emulsion droplets was not addressed (1,2). Lopez et al. have shown the interest of monitoring the evolution of X-ray patterns at small angles for the understanding of the time- and temperature-induced structure changes occurring within the globules of the dairy emulsions (3). Cream which is the oil-in-water emulsion resulting from the concentration of milk, was used as a model for native milk, the fat globule mean diameter of which is about 2-3 µm while globules range from 0.2µm to 20µm. The oil-water interface of milk fat globules is stabilised by membranes composed of phospholipid and protein complexes, and by proteins such as caseins partitioning between the interface and the aqueous phase. Crystallisation and melting of TAGs of different types of food emulsions, including dairy and vegetable fat-based emulsions were examined at SAXS beamline using coupling of Differential Scanning Calorimetry (DSC) with time-resolved X-ray diffraction as a function of temperature (XRDT) at both small and wide angles technique. The complex behavior of dairy emulsions will not be presented here (1-2, data not shown). That of palm based emulsions has been published elsewhere (4). Crystallization, polymorphic transition and melting of the TAGs of an emulsified vegetal fat (VF) is discussed below in order to illustrate the capabilities of the coupled techniques for the investigation of crystallised colloidal dispersions. The emulsion was prepared, in the presence of sodium azide, by homogenization of 40% VF and 5% sodium caseinate to obtain a stable oil in water emulsion, the mean diameter of the droplets measured by laser light scattering analysis (Malvern mastersizer) was centered around about 0.8µm. Analysis of thermal and structural properties was obtained from an emulsion sample of about 25 µl placed in Glass Müller capillary of Ø = 1.6mm. Figure 1 illustrates the monitoring by DSC-XRDT of the crystallisation in emulsion of VF-TAGs resulting of the cooling at a scanning rate of 5K/min. Crystallization which starts below 20°C, develops until 14°C as shown by both the exotherm recorded in DSC and the variation of the integrated SAXS signal. Most of the TAGs of the emulsified fat initially crystallises in an α form characterized by an hexagonal lateral packing of the TAG chains (4.15Å WAXS line) and a 2L stacking of the whole molecule (41.3Å SAXS line). In this longitudinal packing of the molecules the chains are oriented perpendicular to the stacking plane (Figure 2). The sample heating, monitored at 1K/min., is characterised by a progressive $\alpha \rightarrow \beta'$ phase transition spreading at this scanning rate from 0° to 25°C that precedes the melting of the β' phase (orthorhombic perpendicular subcell evidenced by lines at about 4.15 and 3.8Å, with 2L stacking of 37.3Å period) formed during this transition (Figure 3). At the molecular level this $\alpha \rightarrow \beta'$ phase transition is characterised by a tilt of about 25° of the chains over the perpendicular to the stacking plane (Figure 2). On DSC recording, an exotherm with an apparent maximum at about 20°C precedes a β' form endotherm ending at about 45°C. DSC signal is well correlated with the variations of both integrated SAXS signals. It is worth

noting the presence of a TAGs liquid phase during the α → β' phase transition evidenced by a broad bump at q= 1.35Å^{-1}. Further aims of the work are to determine the respective influences of ice crystallization and of the interface constituents (proteins, polar lipids and emulsifiers) onto the TAGs crystallisation.

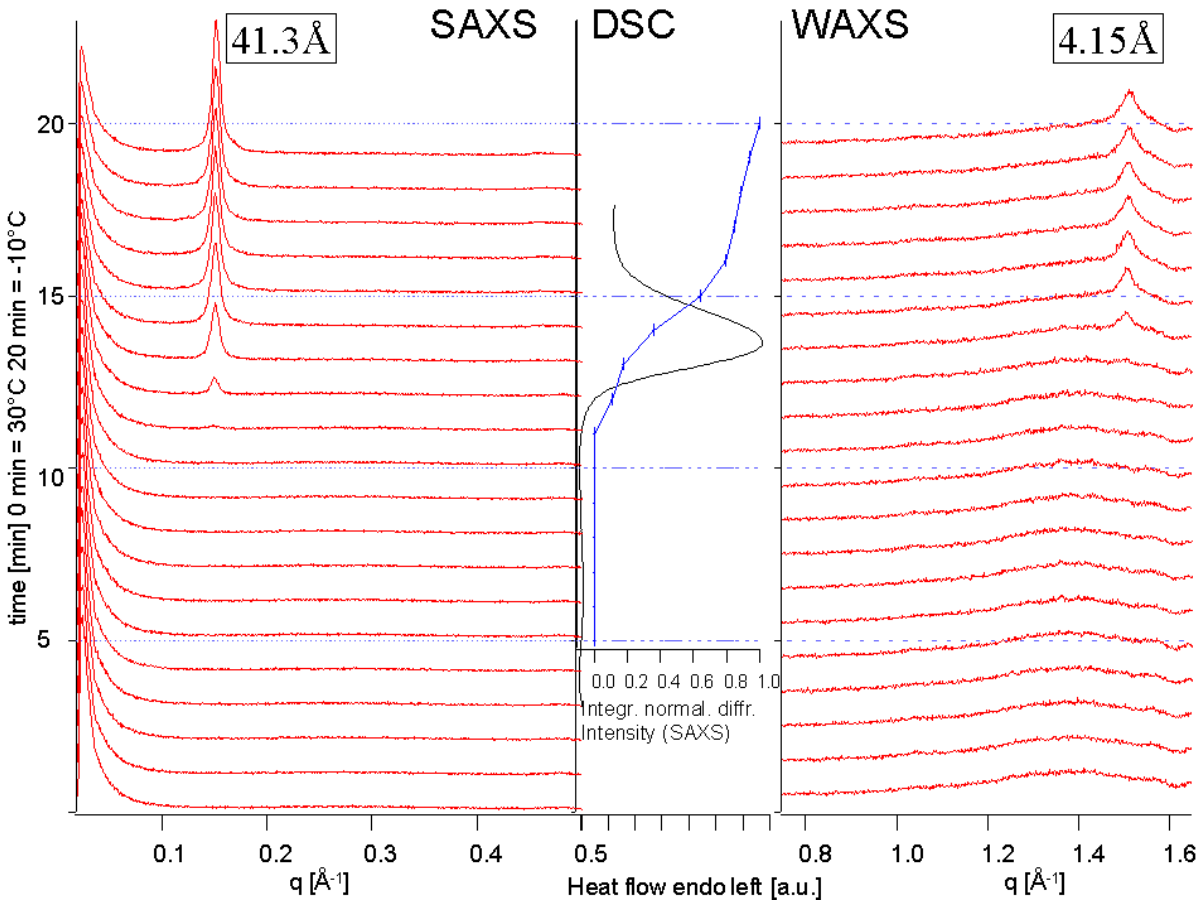

Figure 1. Crystallization of the TAGs of an O/W vegetable fat emulsion as followed by simultaneous SAXS, WAXS and DSC analysis. SAXS (left) and WAXS (right) pattern evolutions as a function of temperature show the crystallisation of an α phase from the melt (liquid crystalline). In the middle DSC recording is compared to integrated SAXS intensity of the peak at 41.3Å.

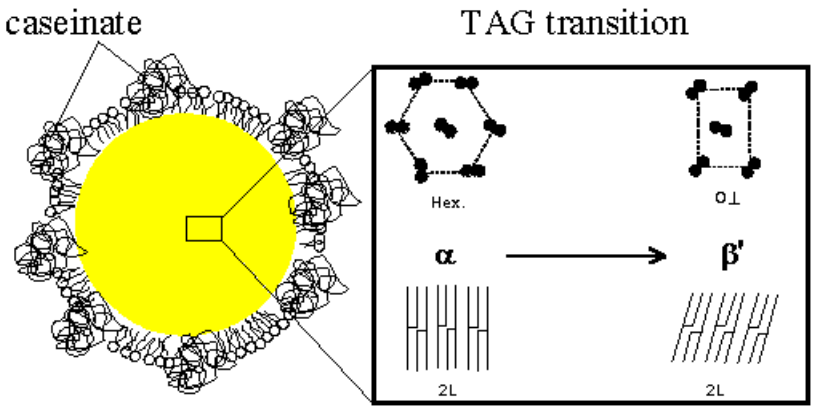

Figure 2. Schematic illustration of the crystallization in emulsion of TAGs. The α → β' phase transition is depicted in the frame.

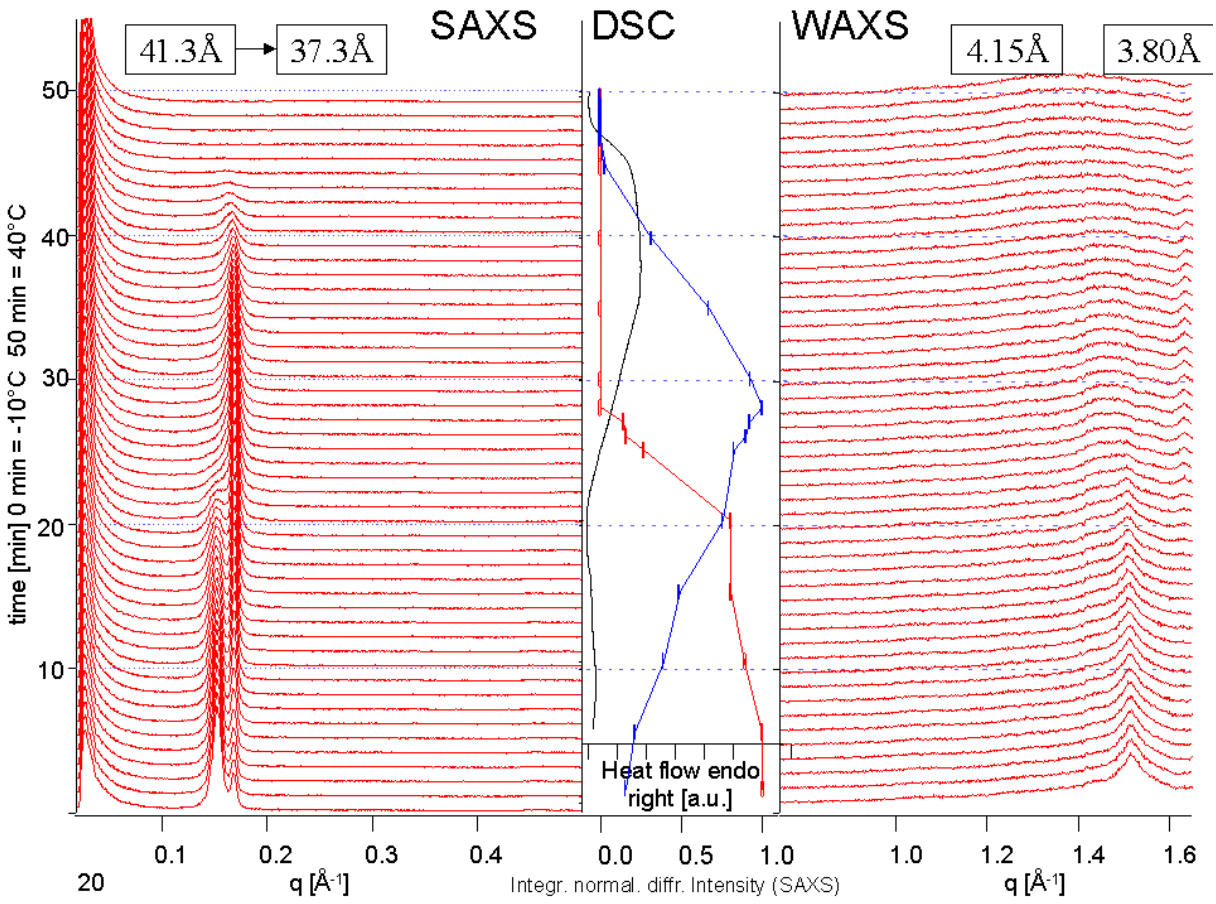

Figure 3. Phase transition and final melting of TAGs of an O/W vegetable fat emulsion as followed by simultaneous SAXS, WAXS and DSC analysis (legend as figure 1).

References:

[1] C. Lopez, P. Lesieur, C. Bourgaux and M. Ollivon, Thermal and Structural behaviour of milk fat : 1 Unstable species of cream., J. Colloid Interf. Sci., **229** 62-71 (2000).

[2] K. Sato, (2001) Crystallization behaviour of fats and lipids, a rev., Chem. Eng. Science, **56** 2255-65- (2001).

[3] C. Lopez, P. Lesieur, C. Bourgaux, G. Keller and M. Ollivon, Thermal and Structural Behavior of Milk Fat: 2. Crystalline Forms Obtained by Slow Cooling of Cream, J. Colloid Interface Sci., **240** 150-161 (2001)

[4] M. Ollivon, D. Kalnin, C. Lopez, P. Lesieur, C. Bourgaux, F. Artzner, H. Amenitsch and G. Keller, Combined DSC and time-resolved synchrotron X-ray diffraction for fat crystallization monitoring with reference to palm oil. International Palm Oil Congress (PIPOC), Kuala-Lumpur. **C25** pp 1-20 (2001).

PRETRANSITIONAL SWELLING OF PHOSPHOLIPID BILAYERS ABOVE THE MAIN TRANSITION

G. Pabst[1,2], J. Katsaras[1], V.A. Raghunathan[3] and M. Rappolt[2]

1.) National Research Council, Steacie Institute for Molecular Sciences, Bldg.459, Stn.18, Chalk River, Ontario, K0J 1J0, Canada
2.) Institute of Biophysics and X –Ray Structure Research, Austrian Academy of Sciences, Schmiedlstrasse6, 8042 Graz, Austria
3.) Raman Research Institute, Bangalore 560 080, India

We have carried out X-ray diffraction studies as a function of temperature on fully hydrated samples of dimyristoyl phosphatidylcholine (DMPC) bilayers. The data were analyzed using the recently developed full q refinement method [1]. In the vicinity of the fluid to gel phase transition we find a sharp increase of the water layer, d_W, whereas the increase in lipid bilayer thickness, d_B, is more or less linear within the range of T_M to T_M + 10°C [2] (Fig. 1).

The latter increase is explained by a gradual stretching of the hydrocarbon chains on approaching the transition temperature. Increased bilayer undulations, determined from an analysis of the fluctuation parameter η_1 (Fig.1), account for the expansion of the water layer. Additional osmotic pressure experiments on aligned samples using neutron diffraction support this notion. By combining results from X-ray and neutron experiments we have estimated the temperature dependence of the bilayer bending rigidity and the interbilayer compressional parameter. Both parameters exhibit a drop as the system approaches the transition temperature revealing that the increase in d_W is the consequence of steric repulsion due to an abrupt softening of the bilayers.

These observations give a complete picture of the changes in structure and interactions in the anomalous swelling regime of DMPC and also other phosphatidylcholines [3].

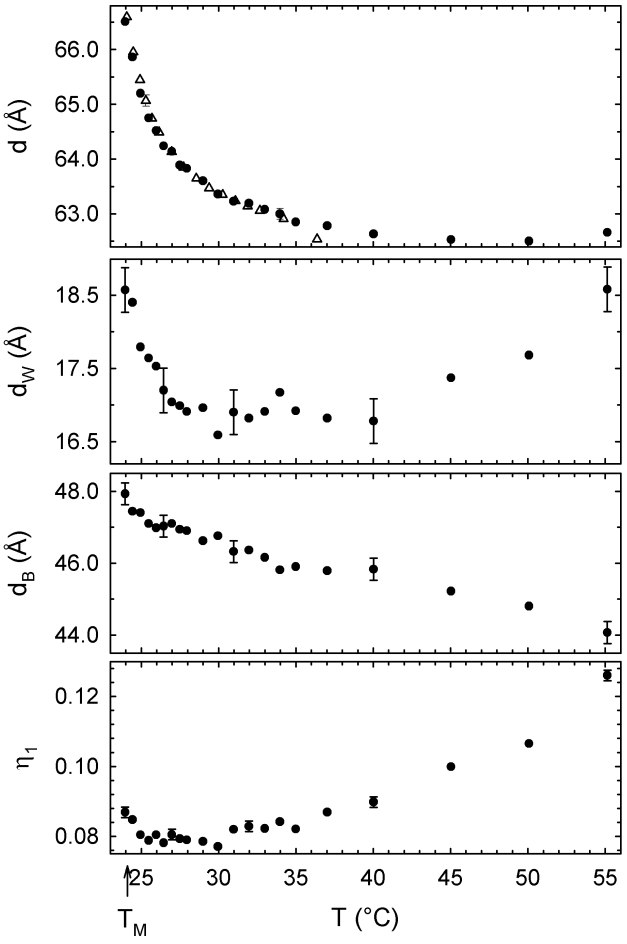

Figure 1: Temperature dependence of the lamellar spacing d ($d = d_B + d_W$), water layer thickness, d_W, bilayer thickness, d_B, and the fluctuation parameter, η_1, in fully hydrated DMPC. The Δ's in the d(T) plot correspond to the neutron diffraction experiments.

References:

[1] G. Pabst et al., Phys. Rev. **E 62**, 4000 (2000).
[2] T_M is the main transition temperature, which is at ~24°C for DMPC bilayers.
[3] This work has been submitted to Langmuir in June 2002

SYNERGIC GELS: INTERACTION BETWEEN GLUCOMANNAN AND XANTHAN POLYSACCHARIDES IN AQEUOUS SOLUTION AND IN GEL PHASE

G. Paradossi, E. Chiessi, F. Cavalieri

Department of Chemistry, University of Rome „Tor Vergata“, Via della Ricerca Scientifica, 00133 Rome, Italy.

Investigation of structural organization of macromolecular assemblies is necessary for the understanding of the factors influencing gel formation.
Synergistic interaction between two structurally different polysaccharides can cause the formation of a physical hydrogel. Many of the works that recently appeared in the field of polysaccharidic hydrogels were addressed to the understanding of the factors governing this interaction. A structurally organized macromolecular complex is often a pre-requisite to the gel formation of a synergic gels. This is the case of a vegetal polysaccharide as glucomannan from *konjac* and a microbial polysaccharide as xanthan from *Pseudomonas Campestris*. The two macromolecular partners mixed together form a complex with a conformational change of xanthan [1]. We monitored the arrangement of xanthan chains by means of circular dichroism spectroscopy, C.D., in the uv region in the presence of glucomannan, observing an increase in the ellipticity of xanthan, both in the sol and gel phases. A cooperative melting with a transition temperature around 55 °C was detected by CD indicating a structuring of xanthan moiety in interaction with glucomannan. Moreover a circular dichroism investigation at different weight fractions revealed a preferential mixing ratio of 0.55 [2]. According to this stoichiometry two possible molecular models where formulated by conformational analysis calculations [2].
Xanthan/Konjac glucomannan were studied at the same conditions using the SAXS beam line at Elettra. In Figure 1 it is reported the scattering excess, i.e. scattering intensity of the xanthan/glucomannan mixture subtracted from the scattering of the separate macromolecular components. An interesting feature of these spectra is the presence of scattering pattern even at temperatures where, according to C.D., the ordered structure of xanthan is melted. This finding can be interpreted with the presence of residual ordered zones in the macromolecular complex similar to those present in the gel phase. An evaluation of the dimensions of these ordered domains in terms of an average radius of gyration, R_g, can be accessed by a Guinier analysis at low scattering vector values (see fig. 2).
In figure 3 it is shown the stability of these domains over the explored temperature range.
A further investigation of this thermal behaviour is needed both by means of SAXS and light scattering. It is noteworthy that this thermal behaviour has analogies with the light scattering behaviour of double stranded xanthan solution in ordered conformation, where to a temperature increase did not follow a molecular weight decrease. This result can be interpreted by considering the formation in the vicinity of the transition temperature of entropy-stabilized clusters made of more the two strands held together only at some points of the chain by non covalent bonding.

References:

[1] F.M. Goycoolea, R.K. Richardson, E.R. Morris, M.J. Gidley, *Macromolecules*, **1995**, 28, 8308-8320.
[2] Paradossi, G.; Chiessi, E.; Barbiroli, A.; Fessas, D. *Biomacromolecules*, in press, 2002

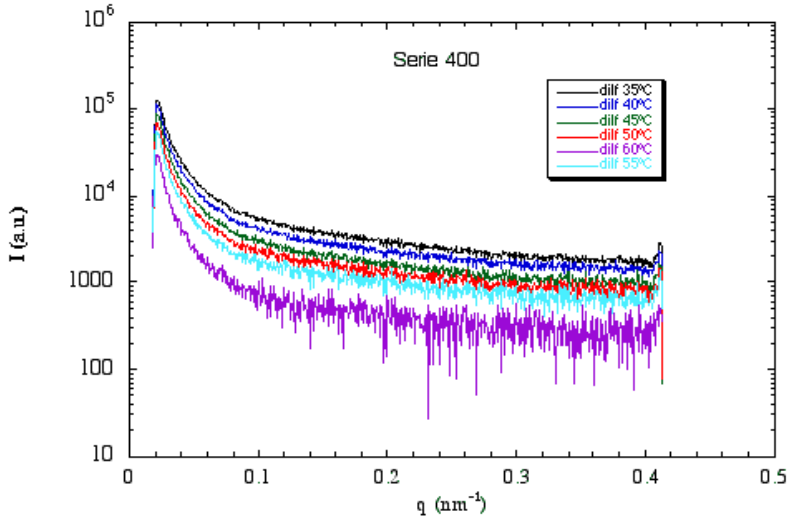

Figure 1. Excess scattering at different temperatures for the mixture xanthan/Konjac gluco-mannan subtracted from the contribution of the two separate polysaccharides. Xanthan weight fraction in the mixture was 0.5. Total polymer concetration 1.5 % (w/w).

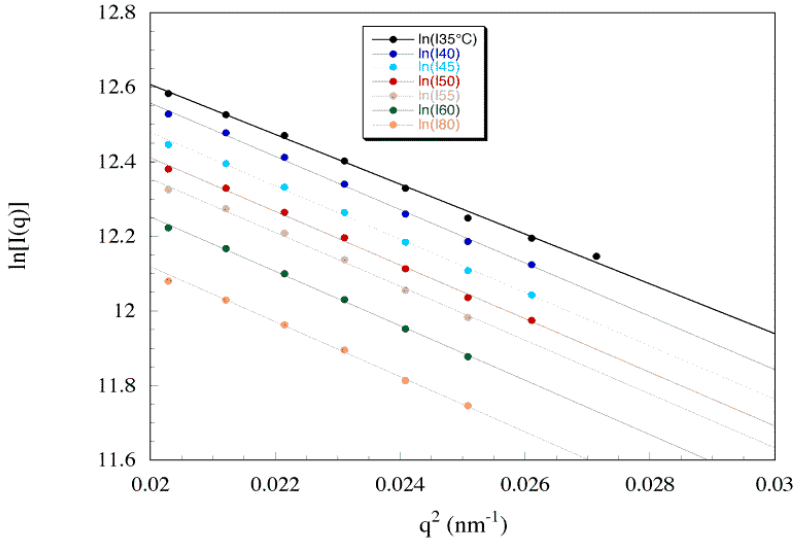

Figure 2. Guinier plot at low q values of the excess scattering for the mixture xanthan/Konjac gluco-mannan. Conditions as in figure 1.

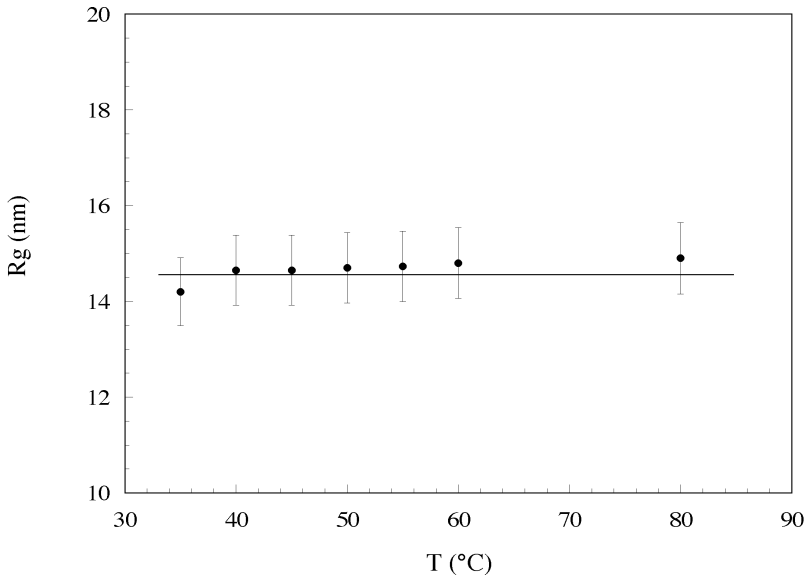

Figure 3. Radius of gyration of the ordered domains present in the xanthan/Konjac gluco-mannan mixture as a function of the temperatures.

TEMPERATURE STUDY OF TWO CUBIC PHASES IN THE TERNARY MONOOLEOYL GLYCEROL / OCTYL GLUCOSIDE ^2H_2O SYSTEM

G. Persson[1], H. Edlund[1] and G. Lindblom[2]

1.) Department of Natural and Environmental Sciences, Mid-Sweden University, S-851 70 Sundsvall, Sweden.
2.) Department of Biophysical Chemistry, Umeå University, S-901 87 Umeå, Sweden

Obtaining high-quality crystals for x-ray diffraction from membrane proteins has proven to be a difficult task. One recently presented method utilizes the cubic phases formed by 1-monooleoyl-*rac*-glycerol (MO) [1]. Removing the proteins from their native environment requires the use of surfactants and one commonly used surfactant is n-octyl-β-D-glucopyranoside (OG). We have determined the ternary phase diagram of MO / OG / ^2H_2O in general [2], and studied the MO-rich cubic phases in particular. The phase diagram consists of an OG-rich isotropic micellar phase, three different cubic phases, one normal hexagonal phase and at low water content a large lamellar phase. Our results show that the MO-rich cubic phases are indeed not very stable in the presence of OG. Only small amounts of OG can be solubilized in either of the two structures. Further, we wanted to study the thermal behavior of these cubic phases, as well. Liquid crystalline phases in general, and those of the cubic type in particular, are notorious for their metastability. There are examples of samples that remain in the metastable cubic structure for years. We used a rather rapid temperature scanning rate (1 deg/min) which most likely is to rapid to allow for true equilibrium to occur. However, for real samples handled in a laboratory a change in temperature with 1 deg/min may not be very unrealistic. All samples were also rotated during acquisition of the diffractograms in order to assure powder patterns. The general temperature behavior upon heating for all samples at low water content was not very surprising. The lattice parameter decreases slightly with temperature, the *Ia3d* structure changes to *Pn3m* at elevated temperatures and the lamellar component in the two-phase samples decrease and disappear (see table 1). But in all the samples consisting of cubic phases only, an additional, unidentified peak first appears and then disappears during heating (fig 1). The additional peaks are also present in samples C2:6, C2:7 and C2:8, which consists of isotropic solids in equilibrium with excess water. Also, sample C2:6 show a different thermal behavior than what one might suspect. At 20 ^oC the sample contains both the *Ia3d* and *Pn3m* structure, while at higher temperatures the *Pn3m* disappears. Upon cooling the *Pn3m* structure reappears. This is similar to the behavior under pressure found by Pisani et.al. [3].

Acknowledgements.

We wish to thank the local contacts H. Amenitsch, M. Rappolt, M. Strobl and S. Bernstorff for their support during the experiments. Professor Laggner is gratefully acknowledged for granting us the beam time.

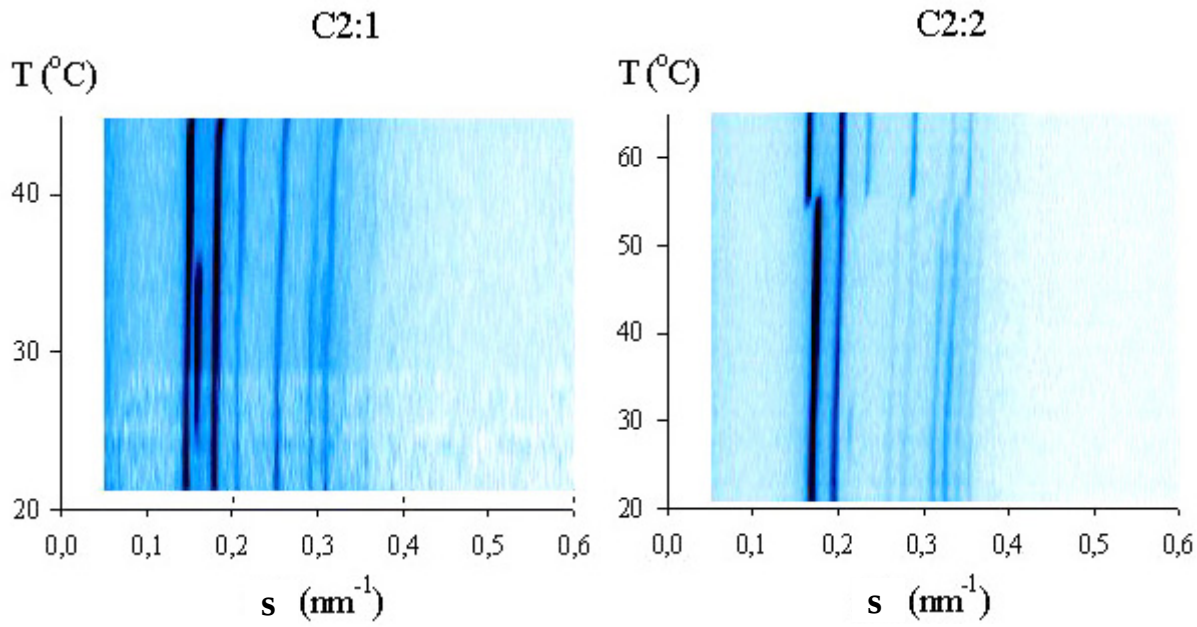

Figure 1. The thermal scans for sample C2:1 and C2:2. The additional peaks can be seen at s ≈ 0,17 nm^{-1} between 24-36 °C (sample C2:1), and at s ≈ 0,21 nm^{-1} between 25-32 °C (sample C2:2).

Table 1. Lattice parameters for the different phases obtained during heating.

Sample	wt % MO / OG / ^2H_2O	T (°C)	*Pn3m* (nm)	*Ia3d* (nm)	L_α (nm)
C2:1	57.81 / 0.34 / 41.85	20	9.66		
		25	9.63		
		35	9.54		
		45	9.20		
C2:2	57.81 / 1.31 / 40.88	21		14.29	
		25		14.22	
		35		14.22	
		45		13.97	
		50		13.91	
		55	8.68	13.81	
		65	8.48		
C2:3	57.44 / 2.54 / 40.02	22		15.55	
		26		15.72	
		36		15.41	
		45		15.15	
C2:4	57.7 / 3.37 / 38.93	21		16.16	4.86
		25		16.23	4.81
		35		16.08	4.79
		45		14.31	4.62
		50		14.90	

C2:5	57.95 / 4.20 / 37.85	21 25 35 45 50 55		18.25 17.92 17.86 15.55 15.55 14.31	4.86 4.88 4.84 4.69 4.64
C2:6	44.54 / 2.29 / 53.17	21 25 35 45	11.12	17.15 17.01 17.04 16.95	
C2:7	44.67 / 1.14 / 54.19	21 25 35 45	10.89 10.78 10.71 10.03		
C2:8	44.77 / 0.30 / 54.93	21 25 35 45	9.78 9.89 9.71 9.38		

References:

[1] E. Landau and J. P. Rosenbusch; Lipid cubic phases: A novel concept for the crystallization of membrane proteins; Proc. Natl. Acad. Sci. **93**, 14532-14535 (1996)

[2] G. Persson, H. Edlund and G. Lindblom; Phase behaviour of the 1-monooleoyl-*rac*-glycerol / n-octyl-β-D-glucoside / water - system; Submitted to Progress in Colloid and Polymer Science (2002)

[3] M. Pisani, S. Bernstorff, C. Ferrero and P. Mariani; Pressure induced cubic-to-cubic transition in monoolein hydrated system; J. Phys. Chem. B **105**, 3109-3119 (2001)

STRUCTURAL AND ENERGETIC EFFECTS OF HYDROSTATIC PRESSURE ON INVERSE HEXAGONAL AND BICONTINUOUS CUBIC PHASES IN LIPID-WATER SYSTEMS

M. Pisani[1], G. M. Di Gregorio[1], H. Amenitsch[2] , S. Bernstorff [3] and P. Mariani[1]

1.) Istituto di Scienze Fisiche, Università di Ancona, Ancona, Italy
2.) Institute of Biophysics and X-Ray Structure Research, Austrian Academy of Sciences, Graz, Austria
3.) Sincrotrone di Trieste S.C.p.A., Basovizza (Trieste), Italy

In this experiment we studied the pressure-dependent phase behaviour of the L-α- dioleoyl phosphatidyl ethanolamine that exhibits stable or metastable nonlamellar structures. The phosphatidylethanolamines are between the most represented phospholipids of biological membranes, and among them one of the most studied is L-α- dioleoyl phosphatidyl ethanolamine (DOPE). This lipid has been investigated because the phase diagram DOPE-water shows a wide range of existence of the inverse H_{II} phase [1]. In fact above 25°C the inverse hexagonal phase H_{II} exists at all water concentrations. In addition, below 25°C, an H_{II} phase occurs at high water concentrations, and the L_α phase is formed at intermediate water concentrations and finally the system switches back to an H_{II} phase at low water concentrations. Whereas the previous studied monoolein-water system [2] formed cubic phases at atmospheric pressure and room temperature, the hexagonal appeared only at high temperature, therefore it was not possible to investigate the inverse hexagonal phase.
The DOPE has been investigated in a range of concentrations from c=0.67 to c=0.87, where c is the weight of lipid per weight of mixture. For each concentration a series of diffraction patterns have been recorded at 25°C for different pressures, from 1 bar to 2 kbar, with steps of 100 bar (see fig.1).
In figure 2, the pressure at which the H_{II} and L_α phase transition occurs is reported as a function of concentration. The error bars indicate the extension of the two-phase region.
Increasing the lipid concentration the H_{II} and L_α phase transition occurs at lower pressure.
At all the investigated concentrations, the unit cell dimensions of both phases increase as a function of pressure. The dependence is rather linear in the range where only one phase exists, while for the H_{II} phase a quadratic dependence is detected in the biphasic region. This effect could indicate that a compositional change occurs in the two phases region, due to changes in the DOPE hydration level: because of the constant sample composition, a large variation of the hexagonal unit cell is detected during compression due to an increased water content in this phase. In dried samples the pressure has induced a cubic structure not well characterized.
Siegel has suggested that formation of these cubic structures may arise from topological defects of the membrane surface generated by cycling through the L_α - H_{II} so that the topology of bicontinuous cubic phases can result in less frustration and hence in a lower free energy than either the lamellar or H_{II} phase[3].
Pressure effect on DOPE molecule can be derived determining the structural parameters in the different phases (e.g., the lipid length, the area-per-molecule, the interface curvature and so on). From this analysis it can be observed that the increase of the unit cells observed during compression at all concentrations involves an increase of the length of the DOPE molecule and a decrease of its molecular area at the lipid-water interface: as a consequence the curvature of the lipid-water interface reduces as a function of pressure (see fig. 3). Data suggest in these phase transitions is involved a very delicate balance of competing energetic contributions such that small changes in overall volume result in large structural transformations.

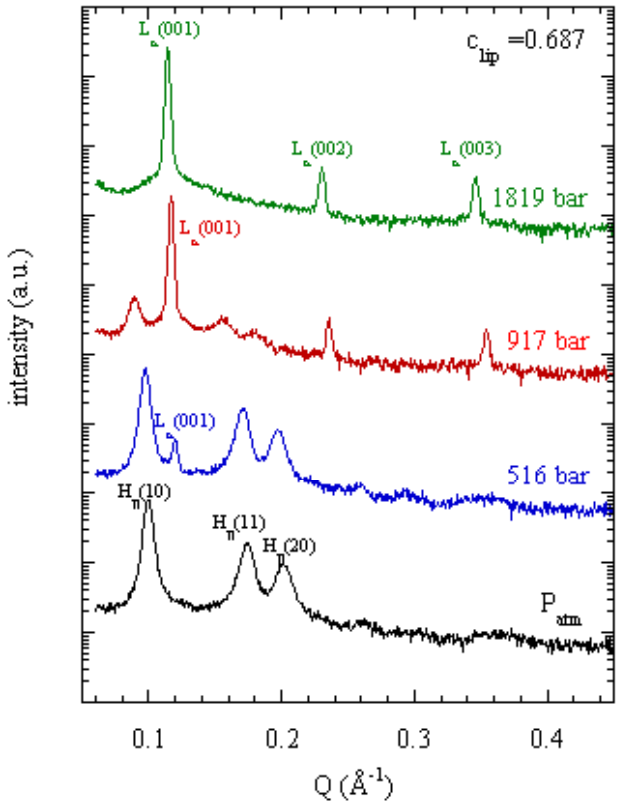

Figure 1. Low-angle X-ray scattering pattern from DOPE sample at concentration c=0.687 at different pressure.

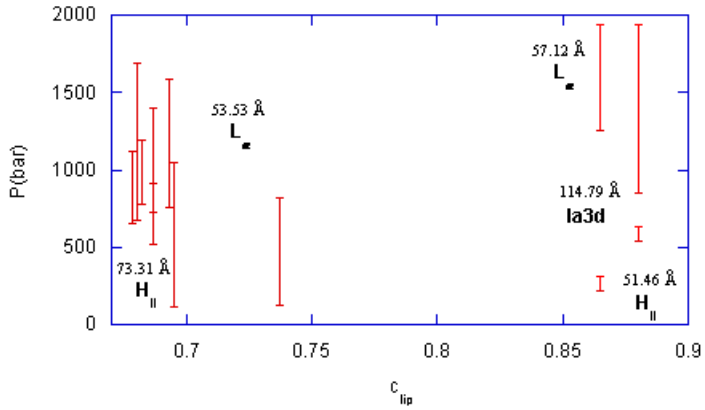

Figure 2. Concentration dependence of the pressure range at which the H_{II} and L_{α} coexist in equilibrium.

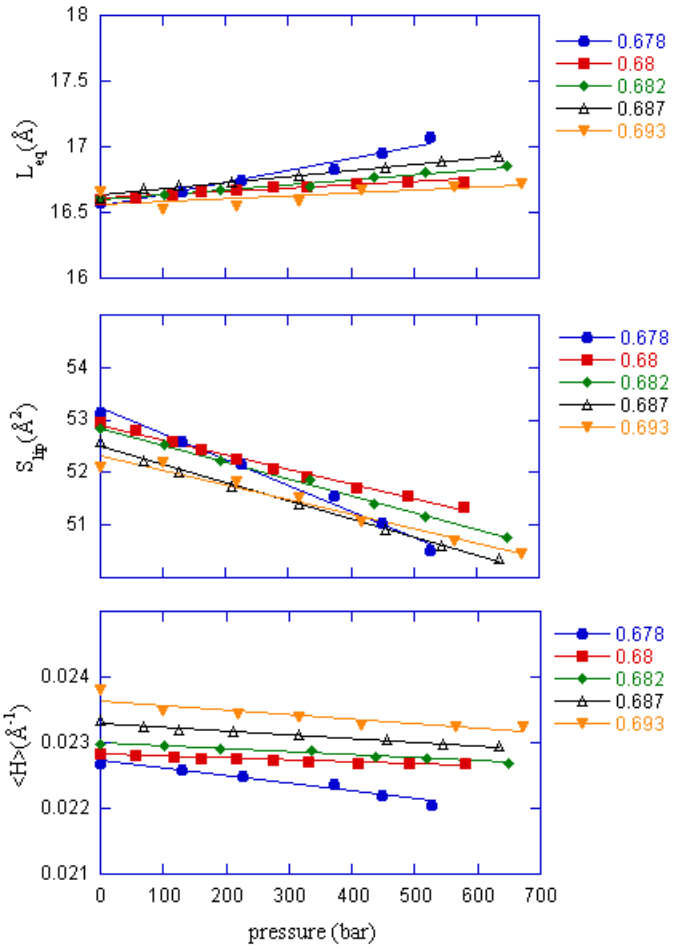

Figure 3. Pressure dependence of the length of the lipid l_{mean}, of the headgroup area at the lipid-water interface $S_{w/l}$ and of the curvature of the lipid-water interface, H, for the H_{II} phase.

References:

[1] R.P. Rand, N. L. Fuller, S. M. Gruner and V.A. Parsegian; Membrane curvature, lipid segregation and structural transitions for phospholipids under dual-solvent stress; Biochemistry **29**, 1, 76-83 (1990)

[2] M. Pisani, S. Bernstorff, C. Ferrero and P. Mariani; Pressure induced cubic to cubic phase transition in monoolein hydrated system; J. Phys. Chem. B**105**, 3109-3119 (2001)

[3] R. Winter; Effects of hydrostatic pressure on lipid and surfactant phases; Colloid and Interface Science **6**, 303-312 (2001)

INTERFACE STUDY IN THE LAMELLAR/INVERSE HEXAGONAL PHASE REGION OF PEs: A MAJOR COMPONENT OF BACTERIAL MEMBRANES

M. Rappolt[1], A. Hickel[2] , F. Bringezu[2] and K. Lohner[2]

1.) Institute of Biophysics and X-ray Structure Research, Austrian Academy of Sciences, c/o Sincrotrone Trieste, SS 14, km 163.5, 34012 Basovizza, Italy.
2.) Institute of Biophysics and X-ray Structure Research, Austrian Academy of Sciences, Schmiedlstrasse 6, A-8042 Graz, Austria

In the broader framework of this project phospholipids will serve as membrane systems mimicking either the cytoplasmic membranes of bacteria or erythrocyte membranes, which differ markedly in their membrane architecture (complexity and lipid composition). These model systems allow us to investigate the mode of action of antimicrobial peptides, which primarily kill bacteria by permeation of their cytoplasmic membrane [1,2]. There exists a wealth of information concerning the phoshopholipid composition of individual genera and species of Gram-negative and Gram-positive bacteria [2 and references therein]. In the latter, we face a rather primitive situation dealing basically with a simple lipid bilayer membrane. The phospholipids constitute up to 80% of the total cellular lipids and consist besides of phosphatidyl-ethanolamine (PE) to a large extent of negatively charged phosphatidylglycerol (PG) and derivatives of it, mostly diphosphatidylglycerol (DPG or cardiolipin). PE represents the major phospholipid class in the outer and inner membrane of Gram-negative bacteria, e.g. 82% in *E. coli*. One remarkable feature is that antimicrobial peptides induce in PEs an accelerated formation of cubic phases [3], which is most pronounced near the lamellar to inverse hexagonal phase transition. Thus, in this work we investigated the structural parameters of both, the lamellar and inverse hexagonal packing of pure palmitoyloleoyl-PE (POPE) in order to understand the interaction of antimicrobial peptides with such lipid matrixes. For the first time we could solve the structure of the two co-existing phases at a fixed temperature.

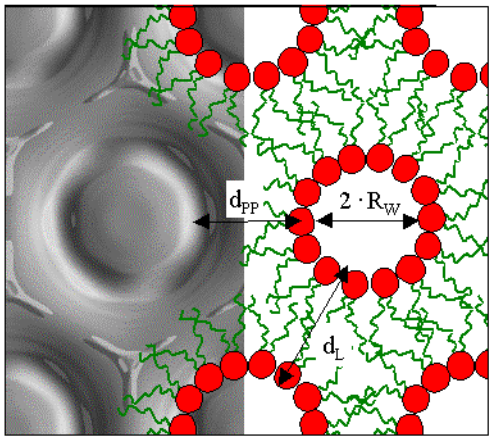

Figure 1: Electron density map of POPE at 84 °C (left). The organisation of the lipid molecules is schematically demonstrated on the right hand side: d_{pp} is the phosphate to phosphate distance, R_W is the radius of the water tube, and d_L defines the lipid layer thickness along the main axis of the hexagonal lattice.

References:

[1] K. Lohner and E.J. Prenner. Biochim. Biophys. Acta 1462 (1999) 141-156.
[2] K. Lohner. The Role of Membrane Lipid Composition in Cell Targeting of Antimicrobial Peptides. in: "Development of Novel Antimicrobial Agents: Emerging Strategies", (Ed. K. Lohner), Horizon Scientific Press, Wymondham, Norfolk, U.K. (2001) pp. 149-165.
[3] A. Hickel and K. Lohner. Biophys. J. 80/1 (2001) 713.

SAXS INVESTIGATION OF LAYER-SPECIFIC COLLAGEN STRUCTURES IN HUMAN AORTAS DURING TENSILE TESTING

C. A. J. Schulze-Bauer[1], H. Amenitsch[2] and G. A. Holzapfel[1]

1.) Institute for Structural Analysis, Computational Biomechanics, Graz University of Technology , 8010 Graz, Austria
2.) Institute of Biophysics and X-ray Structure Research, Austrian Academy of Sciences, 8042 Graz, Austria

The stress-strain behavior of most animal tissues is governed by the mechanical response of collagen fibrils. However, the molecular motions of fibrils in mechanically loaded collageneous tissues are poorly understood. In particular, the relations between the tensile behavior of arterial walls and the conformational changes of their layer-specific collagen structures are largely unknown. Detailed information about the relation between collagen structures and mechanical tissue function will help to improve our understanding of the mechanical behavior of soft biological tissues. Appropriate data provide a basis for constitutive modeling at the nano- and microstructural level, which is a rapidly emerging discipline in the field of biomechanics. The present *in vitro* study is aimed to investigate SAXS diffraction patterns of isolated arterial wall layers (intima, media and adventitia) during tensile testing.

Fresh stripes of intima, media and adventitia were prepared from aortas of human cadavers. Specimens underwent uniaxial extension tests in 0.9 % NaCl solution at 37°C. Simultaneously, diffraction patterns were taken at the small angle x-ray scattering (SAXS) beamline.

Single-layered arterial stripes with circumferential and axial orientations are prepared and tested in a customized tensile testing machine designed for uniaxial extension. A tissue bath provides a physiological environment with 0.9 % NaCl solution at 37° C. Diffraction patterns are recorded by means of a 2D image intensified X-ray CCD camera. Mechanical experiments comprise unit step-relaxation tests, whereas diffraction data and mechanical behavior are recorded simultaneously. In order to check for homogeneity of diffraction patterns, specimens are studied at several positions (size: 500 μm × 500 μm). After the experiments specimens are analyzed histologically.

For unloaded specimens diffraction maxima are ring-shaped, corresponding to an isotropic arrangement of the collagen fibrils. Increasing tensile loads lead to meridional peak intensities indicating fibril alignment along the tensile axis. Highest intensities (up to the 12th order diffraction) were observed for the adventitia, followed by the intima, while medial layers show predominately diffuse scattering. Relations of intensity and degree of the fibril orientation (azimutal peak sigma) to the tensile stresses in the tissue are shown in Fig. 2a and 2b for a representative adventitial specimen. The d-spacing of 67.6 nm corresponding well to pure collagen I and the peak width are relatively independent from the applied axial stresses and stretches, respectively (Fig. 2). This means that even for stresses beyond the physiological range, i.e. stresses >100 kPa, adventitial collagen fibrils exhibit inextensible behavior.

In particular for the adventitia SAXS is a valuable tool for the investigation of collagen structures deforming under extensional loads. Combination of SAXS data and mechanical responses with histological analyses (light microscopy), which are used to determine the crimping of large collagen fibers, will provide an excellent basis for nano- and microstructural constitutive modeling of the material responses of adventitias.

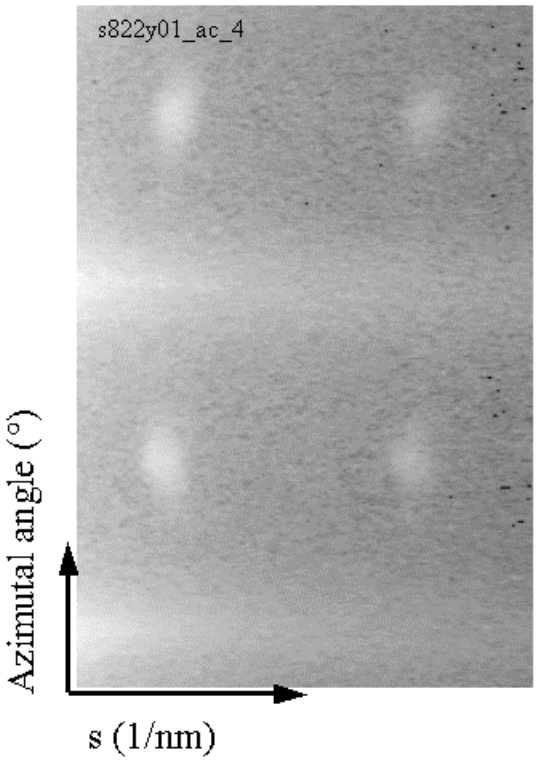

Figure 1. Diffraction pattern after transformation into polar coordinates of the adventitias subjected to tensile stress. The 3 and 5th diffraction order of collagen are visible.

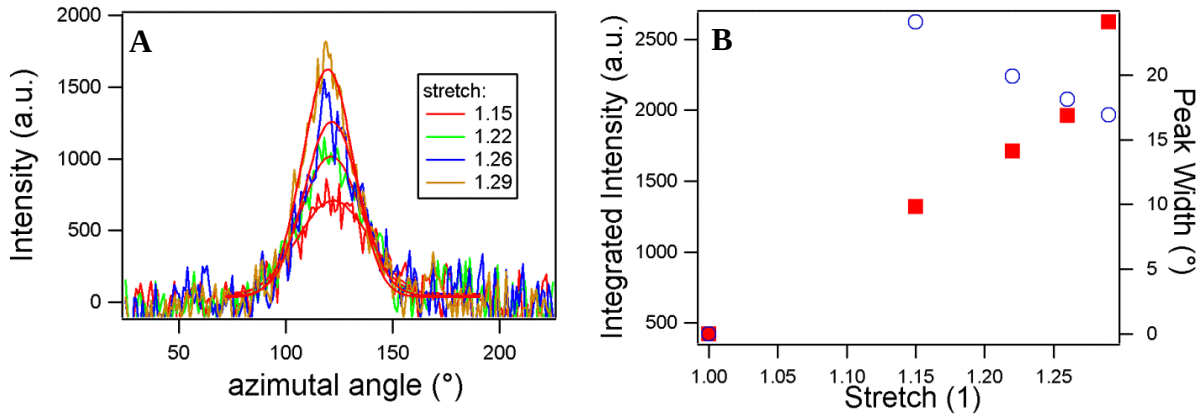

Figure 2. Integrated intensities of the 3rd diffraction order (a), integrated intensity and peak width (b) of adventitial collagen fibrils subject to tensile stresses.

ALKALINE DENATURATION OF PEPSIN STUDIED BY SAXS AND OPTICAL TECHNIQUES

F. Spinozzi[1], F. Corsi[1], H. Amenitsch[2], M. Goldoni[3], R. Favilla[3] and P. Mariani[1]

1.) Istituto di Scienze Fisiche and INFM, Università di Ancona, Via Ranieri 65, I-60131 Ancona (Italy)
2.) Institute of Biophysics and X-ray Structure Research, Schmiedlstr. 6, 8042 Graz (Austria)
3.) Dipartimento di Fisica and INFM, Università di Parma, Viale delle Scienze, Parma (Italy)

Pepsin is the main digestive protein of vertebrates and one of the most studied proteins [1]. Its three-dimensional structure has been solved at high resolution several years ago (PDB code 1PSN) [2]. This notwithstanding, several aspects of its folding dynamics are still obscure, in particular how its native structure is achieved from its zymogen pepsinogen. As a zymogen-derived protein, pepsin undergoes an irreversible denaturation at neutral or slightly alkaline pH (so called alkaline denaturation), as a result of an irreversible unfolding of one of its two lobes [3,4]. Global unfolding occurs only under more drastic conditions (higher pH or chemical denaturant). More recent investigations suggest that the alkaline denatured state of pepsin may be involved in the formation of the active enzyme [5]. Therefore we have investigated how the structural properties of porcine pepsin change with pH (and, by comparison, with GuHCl), following two optical signals (fluorescence and circular dichroism) and the small angle X-ray scattering (SAXS) of the protein.
Samples of pepsin from porcine stomach (crystalline, SIGMA) with concentration 10 g/L have been studied at several pHs (0, 1.9, 5.5, 7.5, 12.5) and at GuHCl concentration from 0 to 5 M. The temperature has been fixed to 20 °C.
Three different optical spectra have been recorded: near UV CD, far UV CD and fluorescence. As a results, the amount of the different secondary structure elements as a function of pH have been obtained (Tab. 1). Results confirm that pepsin remains functionally active below pH 6, but is inactivated above pH 7. This is due to an irreversible conformational transition occurring between pH 6 and 7. In addition, significant differences are also observed among acid as well as basic samples, implying that important conformational changes do also occur within each pH range. At pH 7.5, where the protein is fully and irreversibly inactivated, a rather large spectral change is observed, suggesting a considerable loss of tertiary structure.
SAXS technique has been applied in order to check if the global conformation of pepsin changes according to the results of optical spectra. SAXS measurements have been performed at ELETTRA (SAXS beamline) on the same samples studied by optical techniques. Scattering curve at several pHs in the form of Guinier and Kratky plot are reported in Fig. 1 and 2, respectively. Radii of gyration calculated by applying the Guinier law are reported in Tab. 2. The fitting curves shown in Fig. 2 have been obtained by applying the following methods. At pH 0 and 2 a form factor from the 1PSN coordinates has been calculated by a Monte Carlo approach [6]. A shell of width σ which accounts for the chain mobility on the protein surface has also been fitted. Results are σ=1.6Å at pH=0 and σ =3.2Å at pH=1.9. At pH 5.5 and 7.5 the fits have been calculated by using the worm-like chain model [7]. The parameters describing the chain are the radius of the finite cylindrical cross section, *R*, the contour length, *L*, and the statistical segment length, *b*, which is a measure of the flexibility of the chain. Results are pH=5.5: *R*=15Å, *L*=245Å, *b*=15Å ; pH=7.5, *R*=13Å, *L*=135Å, *b*=54Å. At pH 12.5 the Debye model (random-walk chain) has been applied. It is noticeable that each applied model is able to fit the corresponding curve in the entire *Q* range.
SAXS curves as a function of the GuHCl concentration are reported in Fig. 3 in the form of Kratky plots. The fitting curve have been calculated by using the Debye model. Observing the fitted R_g (Tab. 3) a transition of a more elongated chain at [GuHCl] 2.5 M can be estimated.
Combining fluorescence, near UV and far UV CD with SAXS, the following conclusions can be drawn: i) acidic pH range: the protein is in a compact structure, consistent with its biological activity; the protein in-solution shape can be described by the crystallographic structure by taking into account the mobility of the chains on the surface. ii) basic pH range: the protein is irreversibly inactivated at pH 7.5; its structure is well represented by the semiflexible chain model. This is due to partial unfolding (N-terminal lobe still compact, C-terminal lobe unfolded). iii) In fact at pH 12.5 pepsin results completely denatured and its shape is fully described by a random walk polymer chain. A two-

state unfolding transition (C½ 2.6-2.8 M) can adequately describe the unfolding of pepsin at pH 5.5 by GuHCl (far and near UV CD as well as fluorescence measurements).

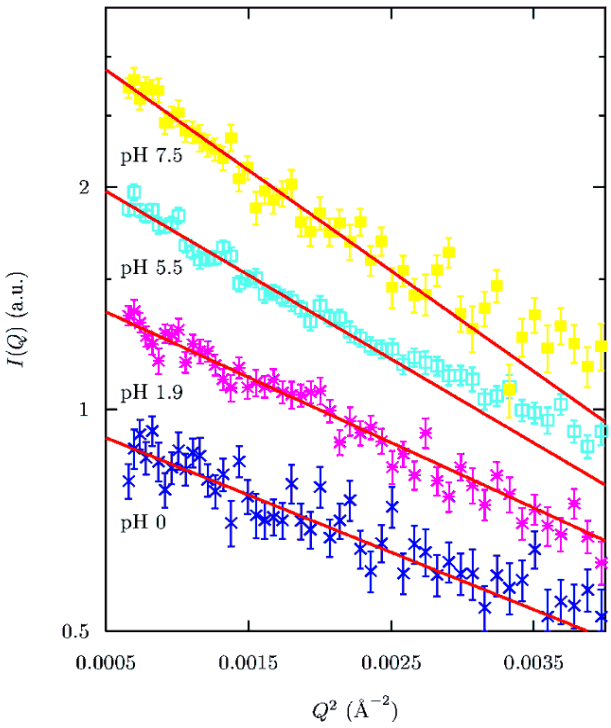

Figure 1. Guinier plots of the SAXS data of pepsin at several pH values.

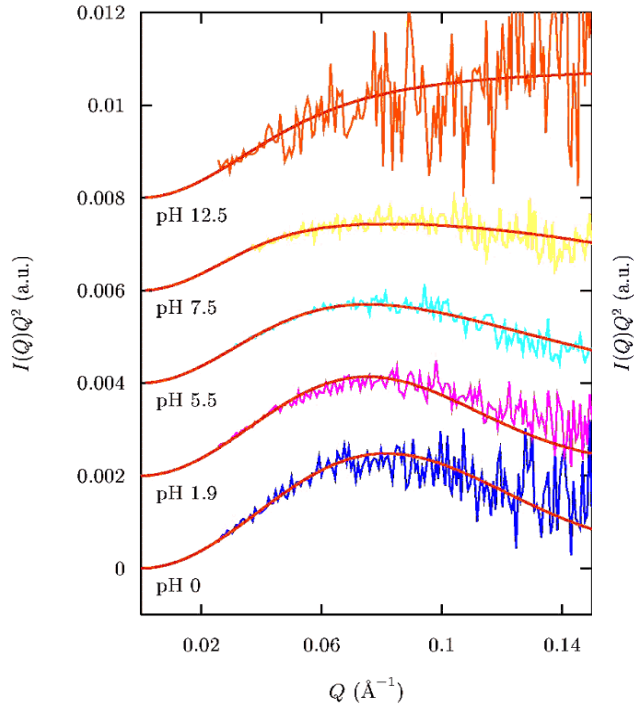

Figure 2. Kratky plots of the SAXS data of pepsin at several pH values. Fitting curves have been calculated by using the Monte Carlo method (pH 0 and 1.9), the worm-like model (pH 5.5, 7.5), the Debye model (pH 12.5).

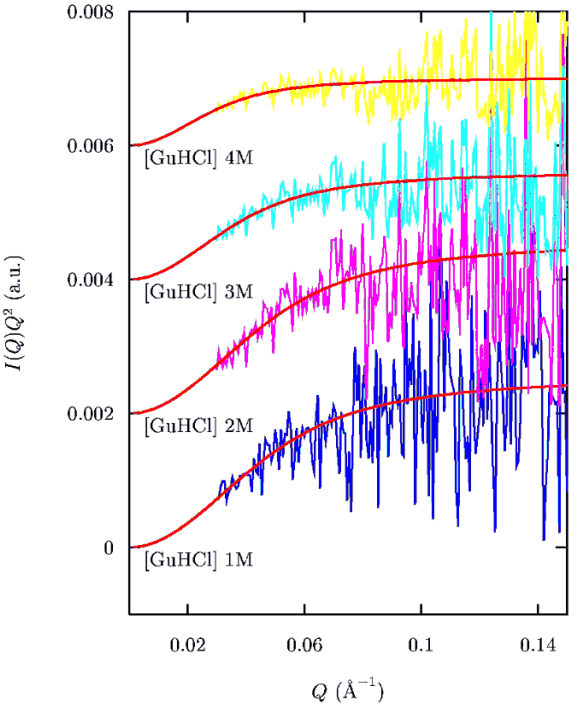

Figure 3. Kratky plots of the SAXS data of pepsin at increasing GuHCl concentrations.

Table 1. Secondary structure content of pepsin. Data evaluated according to two different methods: CCA: Convex Constrained Analysis, CDNN: CD Neural Network.

CCA	**α-helix %**	**β-sheet antip**	**β-sheet p. + turns**	**Random coil**	**Other**
PH 1.9	12.92	33.82	10.96	30.18	12.13
PH 5.5	13.13	34.44	11.7	26.47	14.26
PH 7.5	5.23	22.78	13.34	36.41	22.24
CDNN	α- helix %	β-sheet antip	β-sheet p	Turns	Random coil
PH 1.9	12.8	26.8	5.3	20.8	34.4
PH 5.5	13.6	25.4	5.4	20.5	34.6
PH 7.5	10.7	22.7	4.3	25.1	37.8

Table 2. Fitting parameters calculated by the Guinier analysis of the SAXS curves at several pHs.

pH	R_g **(Å)**	$I(0)$
0	23 ± 1	0.75 ± 0.02
1.9	24.7 ±0.7	1.06 ± 0.02
5.5	28.0 ±0.5	1.78 ± 0.02
7.5	30.7 ± 0.6	1.12 ± 0.02

Table 3. Fitting parameters calculated by the Debye model of the SAXS curves at increasing GuHCl concentrations.

[GuHCl] (M)	R_g **(Å)**	$I(0)$
1	28 ± 1	0.29 ± 0.01
2	28 ±1	0.44 ± 0.02
3	35 ±1	0.64 ± 0.03
4	44 ± 2	0.93 ± 0.05

References:

[1] F.A. Bovey et al., in The Enzymes III (1960), 63-91.
[2] A.R. Sielecki et al., J. Mol. Biol. (1990) **214**, 143-170.
[3] X. Lin et al., Protein Sci. (1993) **2**, 1383-90.
[4] R. Favilla et al., Biophys. Chem. (1997) **67**, 75-83.
[5] T. Konno et al., Biochemistry (2000) **39**, 4182-90.
[6] P. Mariani et al. Biophys. J. (2000) **78**, 3240-51.
[7] J. S. Pedersen et al. Macromolecules (1996) **29**:7602-12.
[8] P. Debye P. J. Physics Coll. Chem.(1947) **51**, 18-32.

CALORIMETRIC AND TIME-RESOLVED SWAXS STUDY OF DPPC TRANSFORMATIONS IN PRESENCE OF TREHALOSE

F. Sussich[1], H. Amenitsch[2] and A. Cesàro[1]

1.) Dept. Of Biochem. Biophysics and Macromolecular Chem., Univ. Trieste, v. L. Giorgieri 1, 34127 Trieste, Italy.
2.) Austrian Academy of Science-Inst. of Biophys. and X-ray Structure, Schmiedlstr. 6, 8042 Graz, Austria

Sugars are the most well known chemicals that nature and man use as stabilizers for complex biostructures and foods preservatives. Mushrooms, drought-adapted organisms, spores, yeasts, and several bacterial cells are able to induce the production of trehalose as they desiccate [1]. The organisms in the dried state are able to survive in a dormant state and then to "resuscitate" when environmental humidity permeates the cell, restoring the original conditions. Even though several hypotheses have been proposed [1-5], none of them can be considered fully satisfactory, the physical basis for the remarkable effect of trehalose being still unknown. In our laboratory a new hypothesis has been formulated [6], on the basis of the existence of various trehalose polymorphs. For this reason we studied the effect of trehalose on the thermal transformations occuring in model membranes (DPPC) under several conditions of hydration with the aim to understand its stabilizing effect on the lipidic transitions and to identify which of trehalose polymorphs is involved.

Measurements were carried out by heating the ternary systems DPPC/water/trehalose with the microcalorimeter MICROCALIX, in-line with the SWAXS set-up, and were acquired with an aquisition time of 12 seconds every 48 seconds. In Figure 1a and 1b are reported the diffraction patterns of DPPC/water/trehalose mixtures at different trehalose content (a. χ_{treh} = 0; b. χ_{tre} = 0.55), as a function of temperature.

It can be clearly seen that the thermal transformations of DPPC are affected by the presence of trehalose: at ambient temperature the system is in the crystal like phase Lc' and, by increasing the temperature, the transition towards the ripple metastable $P_{\beta'}$ phase is observable and furthermore this latter phase transforms at higher temperature into the liquid crystal lamellar phase L_α. While thermograms (data not shown here) show the same features regardless the composition in trehalose, from an accurate analysis of the SWAXS profiles it can be seen that the metastable $P_{\beta'}$ phase and gel $L_{\beta'}$ phase, on cooling are less evident by increasing the amount of trehalose in the sample. This fact points out that these structures do not perfectly form and that the biological relavant liquid crystalline phase is stabilised. Furthermore there is anomalous swelling of the membrane in the L_α phase, with an increase of 10 Å in the repeat distance of the lipid bilayer.

The further step was the study of the system in the dry state, where trehalose shows its protective action. The high curvature phases (P_δ, Q_α and Ha) present in the dry system without trehalose (Figure 2a) become, by adding trehalose, less pronounced and at high trehalose content do not even form (Figure 2b).

A very important result is the formation, in the system at the highest trehalose content (Figure 2b), of crystals of dihydrate trehalose, thus confirming our hypothesis that the mechanism of biopreservation implies the formation of dihydrate trehalose.

`

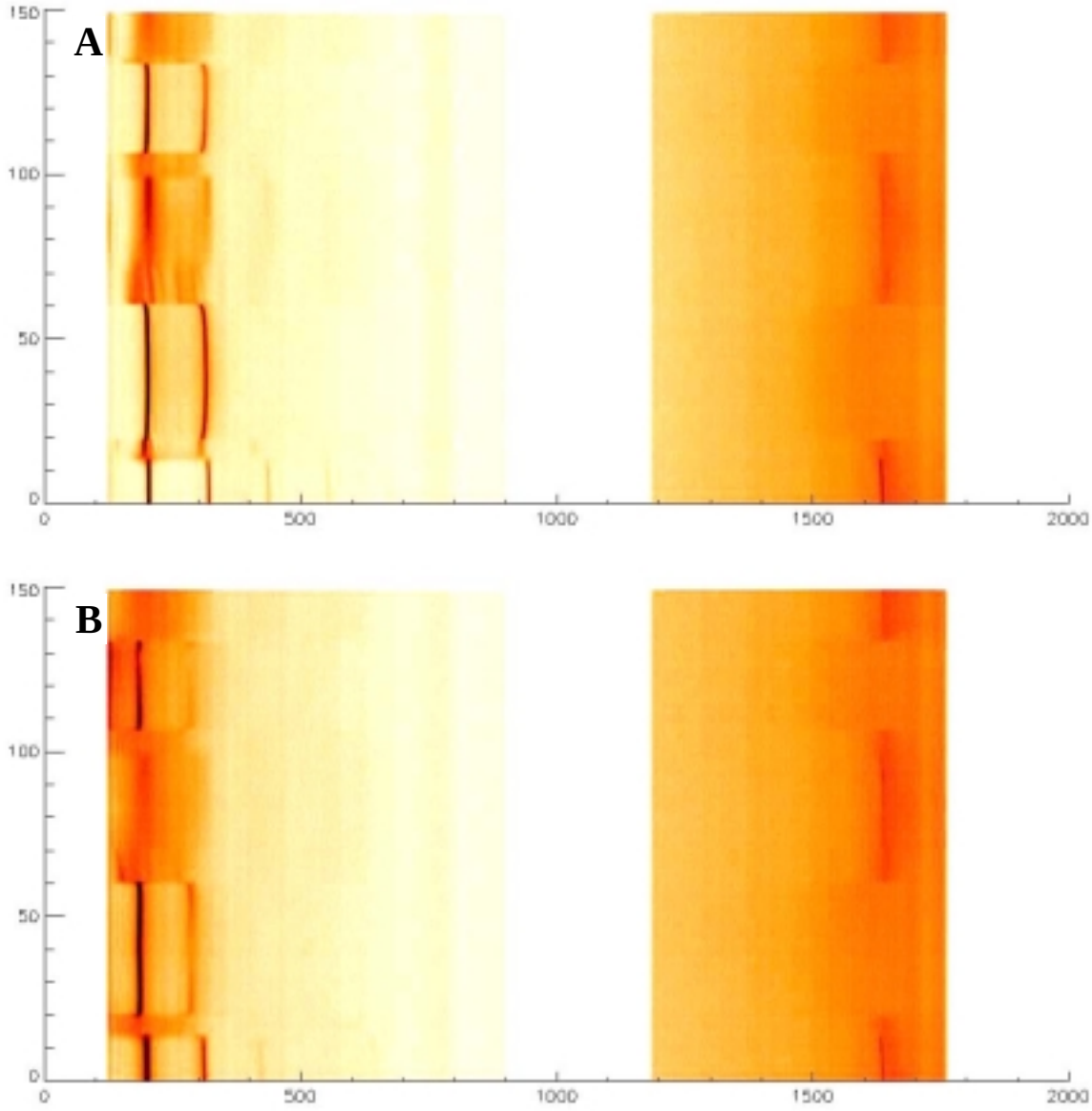

Figure 1. SAXS (left) - and WAXS (right) - diffraction patterns of DPPC/water trehalose mixture (a. $\chi_{treh} = 0$; b. $\chi_{tre} = 0.55$) in the temperature range 25-65-25-65 spanned with a scan rate of 1 K min^{-1}.

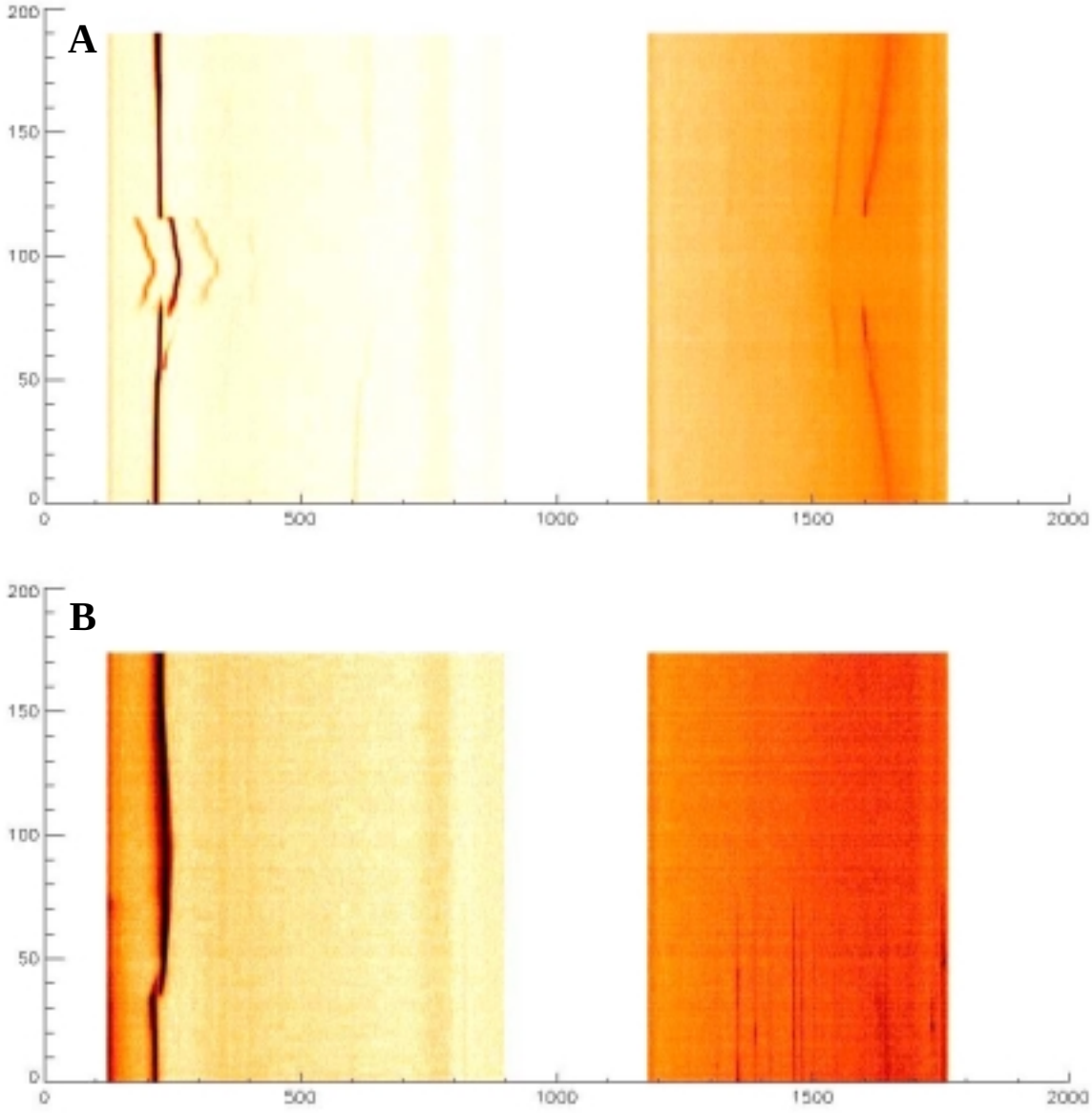

Figure 2. SAXS (left) and WAXS (right) diffraction patterns of DPPC/trehalose mixtures in the dry state (a and b χ_{tre}= 0 and 0.55, respectively) in the temperature range 25-125-25°C (scan rate 1 K min^{-1}).

References:

[1] J.H. Crowe, F.A. Hoekstra and L.M. Crowe; Anhydrobiosis; Ann. Rev. Physiol. **54**, 579-599 (1992)

[2] T. Hanamura; N. Asakawa; Y. Inoue and M. Sakurai; A solid-state ^{31}P NMR study of the interaction between trehalose and DPPC bilayer; Chemistry Letters **8**, 713-714 (1998)

[3] J.L. Green and C.A. Angell; Phase relations and vitrification in saccharide-water solutions and the trehalose anomaly; J. Phys. Chem. **93**, 2880-2882 (1989)

[4] F. Franks, Freeze drying: from empiricism to predictability; Cryoletters **11**, 93-110 (1990)

[5] C.A. Angell; Formation of glasses from liquids and biopolymers; Science **267**, 1924-1935 (1995)

[6] F. Sussich, C. Skopec, J.W. Brady and A. Cesàro; Reversible Dehydration of Trehalose and Anhydrobiosis: from Solution State to an Exotic Crystal? Carbohydrate Research, 334 (2001) 165-176

USE OF SURFACE DIFFRACTION TO STUDY PHOSPHOLIPIDS UNDER INFLUENCE OF SALT

C.V. Teixeira, H. Amenitsch, M. Rappolt , M. Majerovic and P. Laggner

Institute of Biophysics and X-ray Structure Research, Austrian Academy of Sciences, Schmiedlstr. 6, A-8042 Graz, Austria

Surface diffraction on oriented multilamellar membranes is a powerful technique, as it provides higher intensities and allows to derive refined structural information. The aim was to extend the work by Rappolt et.al. [1], who studied the influence of LiCl on liposomes. That work described a splitting of the diffraction peaks into up to three distinct phases, which was linked to osmotic stress [2].
In the present, the effects of water and LiCl on well aligned multilayers were followed by time-resolved surface diffraction using a transmission X-ray surface diffraction cell similar to reference [3]. As multilayer samples we have particularly used POPC films deposited on polished hydrophobic silicon wafers by spin coating. The addition of LiCl causes an immediate broadening of the diffraction peaks, which can be separated into two contributions. The first one is related to the osmotic stressed phase and a second one is related to the equilibrium phase, in which the LiCl has already diffused inside the water layer.

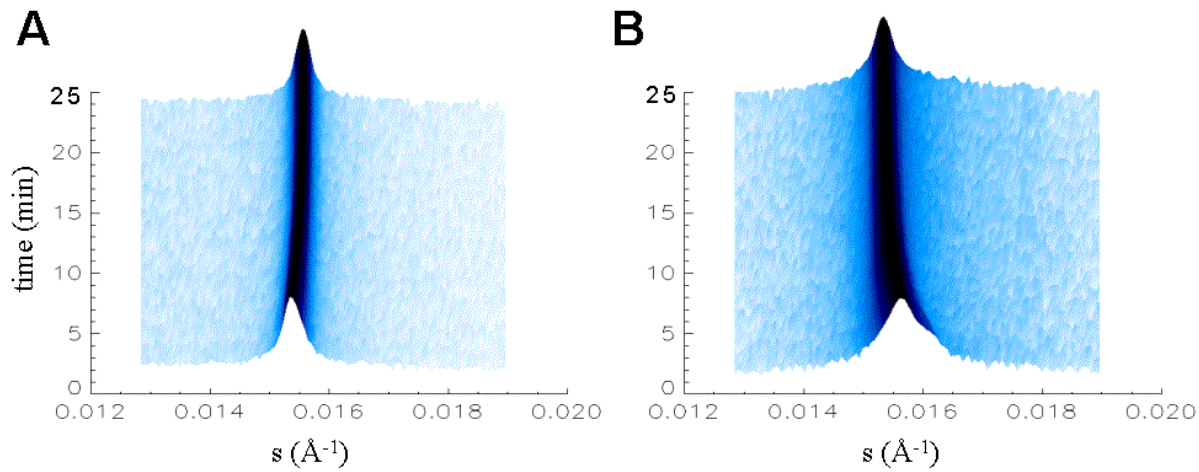

Figure 1. Stack plot of surface X-ray diffraction pattern of POPC (in this example with the addition of 5 mol% cholesterol) during (a) exchange of 0.3 M LiCl by pure water, and (b) after adding of 0.1 M LiCl solution to the fully hydrated aligned sample.

Contrarily to the before mentioned work, the transition into the final equilibrium phase was much shorter than in liposomes (1000 s compared to days) and the splitting was not so strongly pronounced. Additionally, the full splitting was observed due to a very weak liposomal contribution in the multilayer samples. The occurrence of the different phases are explained as a consequence of various bilayer defects depending on the sample preparations, which facilitates either the Li diffusion through the membranes or the establishment of osmotic stress.

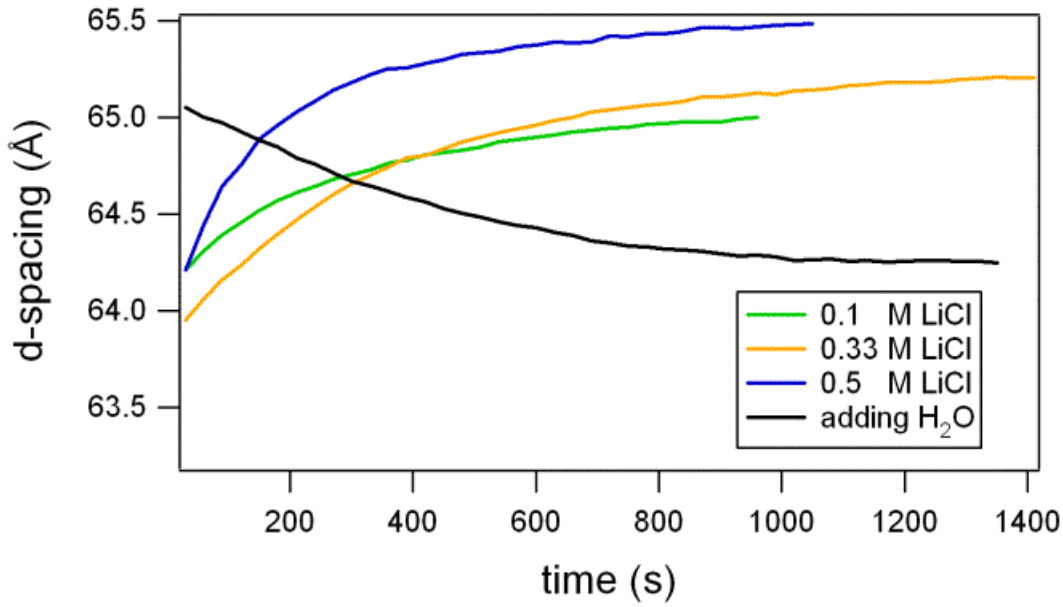

Figure 2. Evolution of the measured d-spacing after adding different LiCl concentrations or pure water after 0.3 M LiCl.

References:

[1] Rappolt M., et.al. (1998), Biochim. Biophys. Acta **1372**, 389.
[2] Rappolt M., et al. (2001), Colloids and Surfaces A **183-185**, 171.
[3] Vogel M., et.al. (2000), Phys. Rev. Lett. **84**, 390.

CHARACTERIZATION OF MINERALIZATION IN BONE DISEASES

W. Tesch [1,2], P. Roschger [2], I. Zizak [3], O. Paris [1], S. Bernstorff [4], H. Amenitsch[5] and P. Fratzl[1]

1.) Erich Schmid Institute of Materials Science, Austrian Academy of Sciences, and Metals Physics Institute, University of Leoben, Leoben, Austria
2.) Ludwig Boltzmann Institute of Osteology & 4th Medical Department, Hanusch Hospital, Vienna, Austria
3.) Hahn Meitner Institut, Berlin, Germany
4.) Sincrotrone Trieste, Area Science Park, Trieste, Italy
5.) Institute of Biophysics and X-Ray Structure Research, Austrian Academy of Sciences, Graz, Austria

Human bone exhibits a foam-like structure (trabecular bone) which is surrounded by a compact outer layer (cortical bone). From the viewpoint of materials science, the trabeculae with a typical thickness of 200 μm can be described as particle reinforced nano-fibercomposite. The degree of mineralization of the collagenous matrix as well as the size, shape and arrangement of the mineral particles are crucial parameters which influence the mechanical and functional properties of the whole structure [1].

The reason for mechanically deficient bone in many bone diseases is a localized disorder of the mineralized collagen matrix during bone modeling or remodeling processes. As an example, the process of Paget's disease is initiated by an abnormal increase in bone resorption, with subsequent compensatory increase in new bone formation, resulting in a disorganized mosaic of woven and lamellar bone. This leads to bone that is expanded in size, less compact, more vascular, and more susceptible to deformity or fracture than normal bone. An other example is coeliac sprue, an inherited disease where one of the symptoms in adults is bone pain and bone weakness.

Therefore, the characterization of bone material in these diseases requires sophisticated methods originating from materials science, such as small-angle X-ray scattering (SAXS), X-ray diffraction (XRD), quantitative backscattered electron imaging (qBEI) or nanoindentation. The aim of such studies is to understand how the integrity of bone is influenced by certain diseases in order to provide sufficient information for medicine to develop efficient diagnoses and therapies.

In order to find out how the basic collagen-mineral structure is altered in the case of bone diseases, several iliac crest bone samples were investigated (normal, pagetic, coeliac sprue). A combination of scanning small angle x-ray scattering (scanning SAXS) and quantitative backscattered electron imaging (qBEI) studies were applied to study normal and pathologically new formed bone areas in a position resolved way. Prior to the SAXS measurements, qBEI images were taken to map the local mineral density of the iliac crest bone samples. From the digital images, areas of interest were chosen for the scanning SAXS measurements. 20μm slices were prepared from theses sections containing the same surface as investigated by qBEI. Using the microbeam-setup at the SAXS beamline at ELLETRA, the first step of the measurement procedure was to aquire a radiography of the sample by detecting the transmitted intensity at each point of the section with a x-ray sensitive diode. This radiography provides an exact mapping of the mineral density distribution in the sample which can be compared with scanning electron micrographs. In the second step, the SAXS-signal was recorded with a 2D-detector, providing line scans or area maps of the area of interest. The 2D-SAXS patterns were evaluated by standard evaluation methods for bone as described in [7].

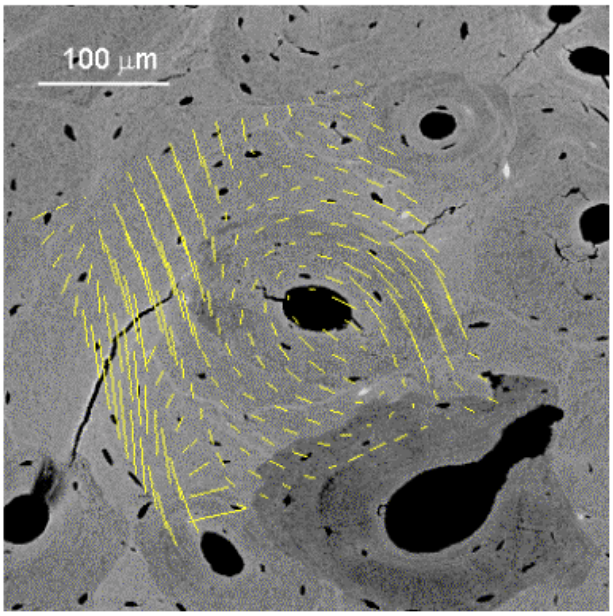

Figure 1. Orientation map of the mineral particles measured by scanning SAXS, overlaid on a qBEI.

In a first approach, we investigated the microstructure of bone tissues in osteons of healthy bone. Osteons are regions of compact bone around blood vessels and are particularly interesting due to the high degree of bone remodeling in this regions. By scanning areas of about 0.3 x 0.3 mm², we were able to map some structural parameters of the mineral crystals in compact (lamellar) bone. Figure 1 shows an example of the orientation mapping in the neighborhood of an osteon. The yellow lines superimposed on an backscattered electron image indicate the orientation of the mineral particles embedded in the organic matrix as measured by scanning SAXS at ELETTRA. For this study a total number of four osteons from healthy patients were examined. As illustrated in Figure 1 the mineral particles are arranged in an onion-skin structure around the hole as the mineral particles follow the direction of the lamellae winding around the hole. - As a continuation of these measurements, we investigated new formed bone areas of healthy and diseased human iliac crest bone samples. In order to understand if and how the nanostructure of the mineralized collagen matrix is affected by these bone diseases, SAXS line-scans perpendicular to the trabeculae were performed.

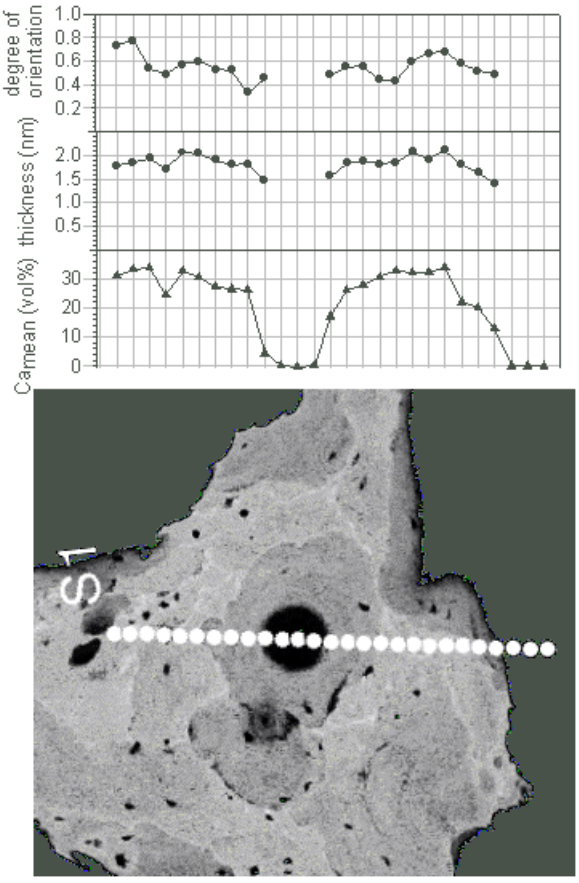

Figure 2. qBEI of pagetic bone with measurement values (thickness from SAXS and calcium content from qBEI)

Figure 2 shows a line-scan across a region of new formed and matured bone from a patient with Paget's disease.In the lower part of the figure (qBEI), high and low gray-levels correspond to high and low mineral content. The white dots indicate positions of SAXS measurements at ELETTRA. The black hole in the middle of the picture is the lacuna of a former blood vessel, comparable to the osteon from Figure 1. As the x-ray beam was approximately 20µm in diameter, the linescan was made with a step-width of 20 µm. The diagrams placed above the qBEI show the mean mineral thickness and the mean calcium content for each measurement point. Therefore, these results can be correlated locally to different stages of tissue maturation or diseases. In

addition, using such combined images as shown in Figure 2, the results from investigation of the mineralization can be combined with previous histological studies revealing more information about the organic matrix embedding the mineralized particles.
The locally combined multimethod approach can provide also new insights into the structure-function relationship of these tissues.

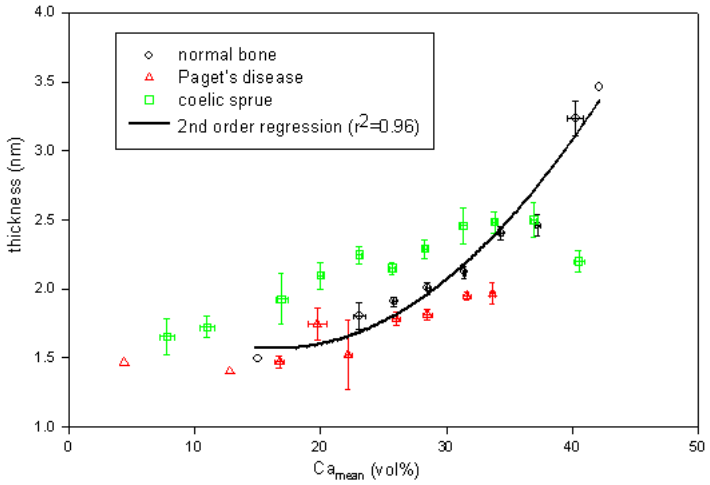

Figure 3. Correlation between mineral particles thickness (nm) and calcium content (vol%)

Figure 3 shows how the thickness d (nm) of the plate-like mineral particles is correlated to the mean calcium content Ca_{mean} (vol%). For healthy bone (circles) a second order law can be found. Interestingly, although pagetic bone (triangles) does not seem to get as highly mineralized as normal bone, the correlation between the thickness and the mineral content is quite similar to the normal case. This might indicate that the basic building block, the mineralized collagen fibril, is not severly affected. In coeliac sprue (squares), however, the correlation behavior is different. It shows somewhat larger crystals at lower mineralization values and a rather linear correlation between the mineral thickness and the mineral content.
These results give important information on changes in bone material due to bone diseases. The defect in the case of the Paget's disease seems to be mostly at the microscopic level as the mineral crystal size and the correlation with the local calcium content are similar to normal bone. In contrast, in the case of coeliac spruce, the basic bone building block seems to be also altered by the disease, in addition to microstructural changes of the trabeculae.
In conclusion, our studies demonstrate that third generation synchrotron radiation sources such as ELETTRA are powerful research handles to investigate bone diseases.

References:

[1] S. Weiner & H.D. Wagner; *Ann. Rev. Mater. Sci.* **28** (1998) 271.
[2] Siris ES, Canfield RE. Paget's disease of bone. In: Becker KL (ed) Principles and practice of endochrinology and metabolism. 2nd ed. Lippcott JB, Philadelphia, 1995
[3] I. Zizak, O. Paris, P. Roschger, S. Bernstorff, H. Amenitsch, K. Klaushofer & P. Fratzl, *ELETTRA NEWS* (1999) **31: (**http://www.elettra.trieste.it/science/news/volume36/EN60.html).
[4] I. ZIZAK, O. PARIS, P. ROSCHGER, S. BERNSTORFF, H. AMENITSCH, K. KLAUSHOFER & P. FRATZL; *J. APPL. CRYST.* **30** (2000) 820-823.
[5] O. Paris, I. Zizak, H. Lichtenegger, P. Roschger, K. Klaushofer and P. Fratzl, *Cell. Mol. Biol.* **46** (2000) 993-1004.
[6] P. Fratzl, et al., *Calcif. Tissue Int.* **48** (1991) 407.
[7] P. Fratzl, S. Scheiber, K. Klaushofer *Conn Tissue Res* **34** (1996) 274

LIPID/CHOLESTEROL MIXTURES: THERMODYNAMICAL AND STRUCTURAL PARAMETERS OBTAINED BY PRESSURE SCANNING SAXS

M. Vidal[1], M. Kriechbaum[1], M. Steinhart[2], P. Laggner[1], C.V. Teixeira[1], M. Rappolt[1], H. Amenitsch[1] and S. Bernstorff[3]

1.) Institute of Biophysics and X-Ray Structure Research, Austrian Academy of Sciences, Graz, Austria
2.) Institute of Macromolecular Chemistry, Czech Academy of Sciences, Prague, Czech Republic
3.) Sincrotrone Trieste, Basovizza, Trieste, Italy

We have studied the structural, dynamical and mechanical properties of binary mixtures of 1-palmitoyl-2-oleoyl-*sn*-glycero-3-phosphatidylcholine (POPC) and cholesterol in slow pressure scanning experiments [1,2] followed by time-resolved small angle X-ray scattering (Fig. 1), giving us a unique possibility to obtain thermodynamical and structural parameters simultaneously from these measurements. Particularly, our investigations were focused on the biological most relevant pressure-temperature-cholesterol regime, i.e., on the liquid crystalline phase and at its phase boundary to the lamellar gel phase within a cholesterol concentration up to 25 mol%, which is of interest for understanding the regulatory function of cholesterol in nature, especially in the presence of unsaturated lipid species.

Directly from pressure scan experiments we derived a value of 19 kJ/mol for the transition enthalpy ΔH_m of POPC in excess water (Clausius Clapeyron relation). With in-creasing cholesterol concentration ΔH_m drops to about 7 kJ/mol at 20 mol% cholesterol (Table 1). These pressure-scan experiments reveal that at very low cholesterol content (< 5-8 mol%) the fluidity and also the bilayer compressibility increase remarkably. In contrast, at concentrations between 5 and 25 mol% cholesterol the bilayer becomes more rigid again and at the same time the lipid bilayer spacing increases about 2 Å. Theses changes are attributed to the onset of phase separation between liquid disordered (*ld*) and liquid ordered (*lo*) phase.

From these results - together with results from complementary temperature-jump experiments on the same system - we can draw the following conclusions: (i) Slow P-scans have demonstrated, that the coexistence region between the gel phase (*so*) and the liquid disordered phase (*ld*) does increase up to a concentration of 5 mol%, (ii) between 5 and 25 mol% *so* and *ld* phase do not mix anymore, which reduces the main transition widths, but the formation of a new fluid ordered phase *lo* - coexisting both with the *ld* and *so* phase - opposes the later effect. This confirms the fact that up to 5-8 mol%, cholesterol causes a fluidisation of the membrane, and above a stiffening is induced, which coincides with the creation of the cholesterol-rich fluid, but chain-ordered phase *lo*. In respect to saturated lecithin species the fluid-fluid miscibility gap seems to be strongly enlarged, stressing once more the important regulatory role of unsaturated lipids in this regime.

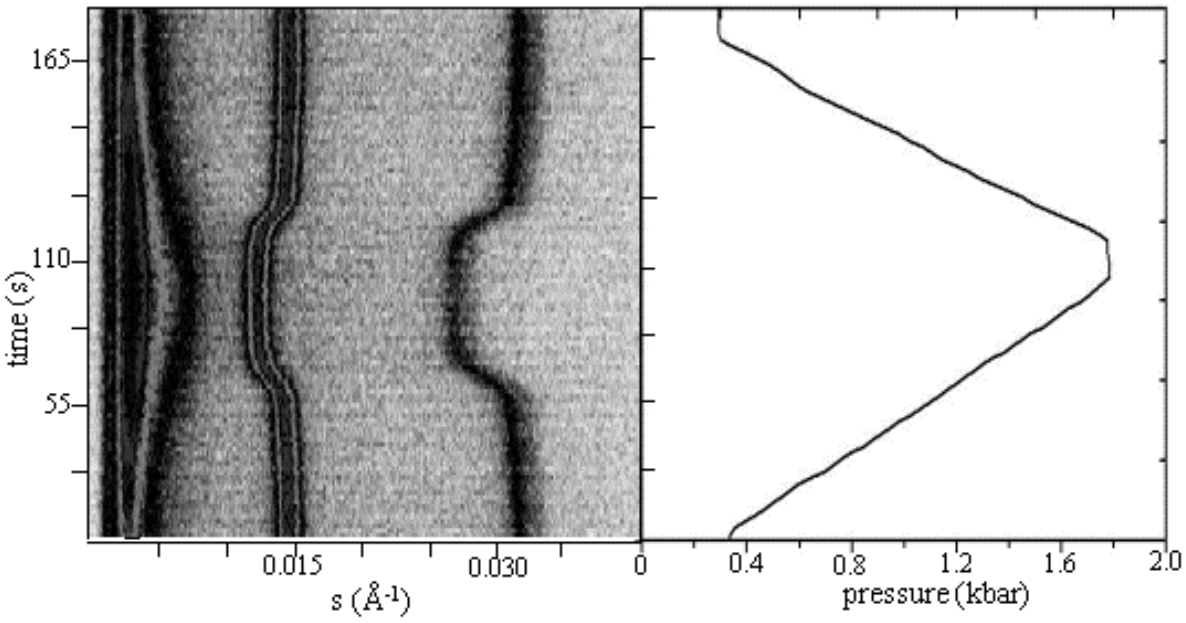

Figure 1. Main transition of POPC (20 wt% plus 1 mol% cholesterol at 20°C) during a pressurizing and depressurizing scan, respectively. Left: the time-resolved SAXS patterns (150 frames, each 2 s exposure time) in a contour plot are shown, for each frame the corresponding pressure value is displayed in a vertical plot to the right.

Table 1. Thermodynamical parameters (change of transition pressure P_m as a function of temperature T, dP_m/dT, and transition enthalpy, ΔH_m) for the phase transitions of POPC with increasing cholesterol concentrations obtained from pressure scanning SAXS experiments.

POPC + cholesterol (mol%)	dP_m/dT (bar/°C)	ΔH_m (kJ/mol)
0	45.4	18.9
1	36.9	14.5
5	46.4	15.8
10	46.5	13.3
20	32.8	6.7

References:

[1] K. Pressl, M. Kriechbaum, M. Steinhart, and P. Laggner; High pressure cell for small- and wide-angle x-ray scattering; Rev. Sci. Instrum. **68**, 4588-4592 (1997)

[2] M. Steinhart, M. Kriechbaum, K. Pressl, H. Amenitsch, S. Bernstorff and P. Laggner; High-pressure instrument for small- and wide-angle x-ray scattering II. Time resolved experiments; Rev. Sci. Instrum. **70**, 1540-1545 (1999)

3. Physics

COCRYSTALLIZATION OF PEO-*b*-PPO-*b*-PEO / PEO BLENDS DURING COOLING AND HEATING

J. Baldrian[1], M. Horky[2], M. Steinhart[1], H. Amenitsch[3], S. Bernstorff[4] and G. Todorova[5]

1.) Institute of Macromolecular Chemistry, Academy of Sciences of the Czech Republic, Heyrovsky Sq. 2, 162 06 Prague, Czech Republic
2.) Faculty of Nuclear Sciences and Physical Engineering, Czech Technical University, V Holešovickách 2,180 00 Prague 8, Czech Republic
3.) Institute of Biophysics and X-ray Structure Research, Austrian Academy of Sciences, Schmiedlstraße 6, 8042 Graz, Austria
4.) Sincrotrone Trieste, Strada Statale 14, km 163.5, 34012 Basovizza (Trieste), Italy
5.) Sofia University, Faculty of Physics, Department of General Physics, James Bourchier Blvd 5, 1164 Sofia, Bulgaria

Intensive research studies in the last years were devoted to the important family of polymer blends, namely block copolymer/homopolymer mixtures, where the homopolymer is identical with one block of the copolymer used. Prevailing part of these studies was devoted to blends with amorphous homopolymer admixture. However, very little is known about the blends with homopolymeric crystalline component**.** The aim of this work was to study real-time development of the structure of such blends during cooling and heating, and to contribute to deeper knowledge of these technologically important systems.

Binary mixtures of a narrow-molecular-weight fraction (Mw ~ 3000) of PEO with a triblock copolymer PEO-PPO-PEO (Pluronic FP68, Fluka, Mw ~ 3340-1760-3340) of 8/2, 6/4, 4/6 and 2/8 compositions were studied by the time-resolved SAXS method. The copolymer was chosen because it has similar Mw of PEO tails as the neat PEO used. The middle PPO block is amorphous. Measurements were performed in the course of cooling of the melt and subsequent heating (30 °C $\rightarrow$ 60 °C$\rightarrow$ 30 °C).

It has been shown that low-molecular-weight fractions of PEO crystallize in stable lamellae with extended (EC) and integrally folded (IF) chains, and in transient unstable lamellae with an intermediate thickness, which corresponds to the lamellae with nonintegrally folded (NIF) chains. During isothermal crystallization, two different lamellar systems LP1 (with thicker lamellae) and LP2 are simultaneously formed in neat copolymer and in the blends with predominant copolymer. In blends with majority of neat PEO, a single lamellar system forms. The lamellar systems are cocrystalline in all studied blends [1].

The molten blends crystallize during cooling in two systems of cocrystalline lamellae in the blends with concentration of neat PEO 3000 lower than 20 % (Fig.1a). A single cocrystalline system is formed in the blend with 20 % of neat PEO (Fig.1b). In both cases the lamellar thickening proceeds during crystallization and heating. Close to the melting point the lamellae in all blends recrystallize and form a single cocrystalline system with the thickness around 25 nm. This value corresponds to the lamellae formed from copolymer molecules with extended PEO tails and PPO folds. The extended molecules of neat PEO 3000 are embedded in these lamellae. The relatively broad SAXS scattering peak, corresponding to this structure, suggests the presence of a not very well developed lamellar system.

The research was supported by the Grant Agency of the Czech Republic (grant No:106/99/0557)

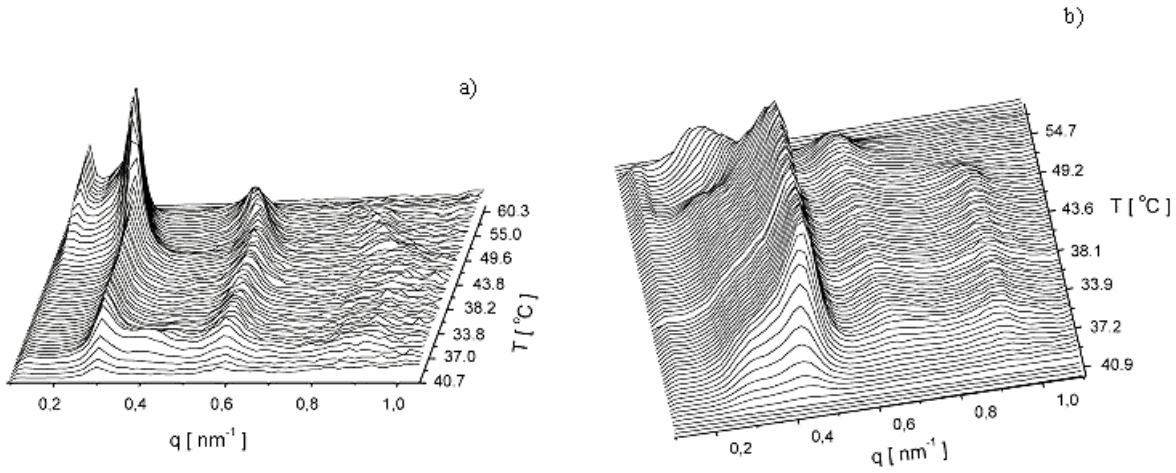

Figure 1. SAXS curves development of PEO-*b*-PPO-*b*-PEO / PEO 3000 8/2 (a) and 2/8 (b) blends during cooling and heating

References:

[1] J.Baldrian, M. Horký, M. Steinhart, H. Amenitsch and S.Bernstorff: Crystallization of PEO-PPO/PEO blends Annual Report 2000, Austrian SAXS Beamline at ELETTRA, pp. 74-75

THE STRUCTURAL ASPECTS OF THE DESORPTION PROCESS POLYURETHANES

H. Grigoriew[1], A. Woliñska-Grabczyk[2], M. Plusa[1] and S. Bernstorff[3]

1) Institute of Nuclear Chemistry and Technology Warsaw, Poland
2) Institute of Coal Chemistry, PAS, Gliwice, Poland
3) Sincrotrone ELETTRA, Trieste, Italy

The segmented polyurethane block copolymers differing in the length of soft and hard segments, and hard segment composition, have been studied. They are denoted here as $((TDI\text{-}ChExt)_x TDI\text{-}PTMO\text{-}M_n)_n$, where PTMO, poly(oxytetramethylene) of M_n= 650, represents a soft segment. Hard segments consist of a 2,4-tolylene diisocyanate (TDI) chain extended with hydroquinone bis(2-hydroxyethyl)ether (HQE) or with 4,4'-bis(2-hydroxyethoxy)biphenyl (BH) with chain extension x=0, 1 or 3. Molar compositions of the materials are:

PU-H: $(TDI\text{-}BH)_1$ -TDI-PTMO, 2/1/1
and PU-Q: $(TDI\text{-}HQE)_3$ -TDI-PTMO, 4/3/1.
As a solvent benzene was used.

The SAXS measurements of these materials were carried out in transmission at room temperature. The samples were taken from the solvent after the equilibrium saturation was reached, immediately blotted and placed vertically in the X-ray beam without any cover. Time-resolved sets of 18 SAXS curves in 5 min. steps were carried out for each sample.
The same conditions were maintained for the SAXS experiments and for the determination of desorption kinetics.
A representative set of the time-resolved SAXS scattering patterns for one of the materials investigated is shown in Fig. 1.

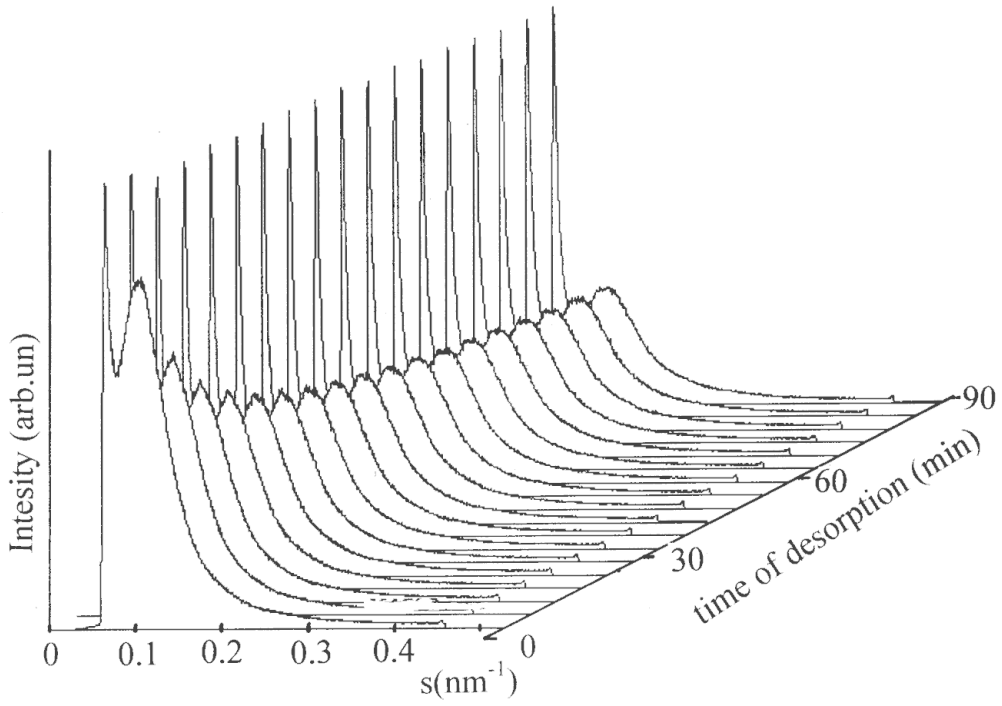

Figure 1. Set of time-resolved SAXS curves for PU-H.

The main differences between the subsequent SAXS curves recorded as a function of time were observed during the initial period of time, after which the curves asymptotically approached their shape registered for the dry material. Therefore, the six first curves from each measured sequence were chosen for further treatment. No phase transition (order-order) takes place in the systems studied, but only the L distance increases slightly with the solvent amount.

The exponential dependence of the mass loss, ΔM related to maximal M, with time was found according to Fick's law of diffusion (Fig. 2a). A similar exponential dependence of the relative change in the interlamellar distance, ΔL, when it is plotted as a function of time, has been found (Fig. 2b).

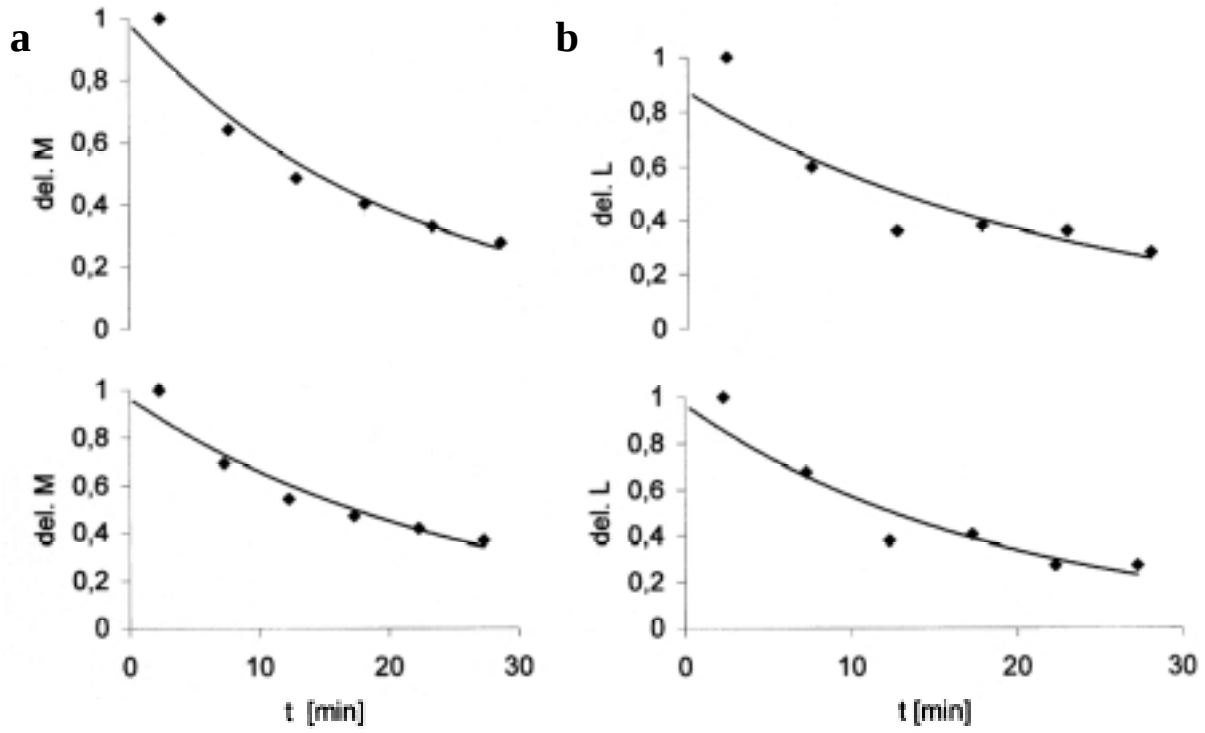

Figure 2a. ΔM and **b.** ΔL vs. time of desorption for first 6 SAXS measurements. From top to bottom: PU-H and PU-Q.

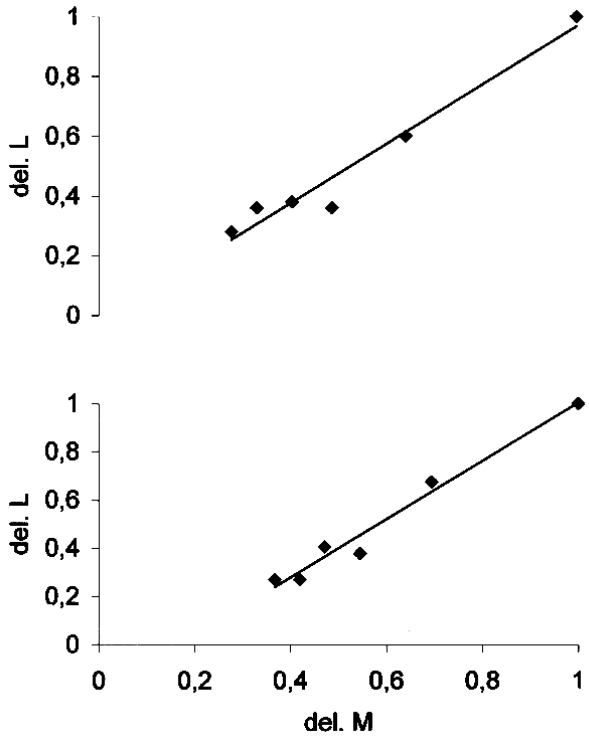

Figure 3. Relation of ΔL to ΔM for the first 6 measurements. From top to bottom: PU-H and PU-Q.

The same behaviour of ΔM and ΔL with time prompted us to check their mutual dependence, i.e. the relative decrease of interlamellar distance vs. relative decrease of solvent mass. (Table 1 and Fig. 3)

Table 1. Relative changes in interlamellar distance and mass after 6 steps of desorption time.

material	ΔM relative mass of solvent M_6/M_{max}	relative ΔL $\Delta L_6/\Delta L_{max}$
PU-H	0.28	0.28
PU-Q	0.38	0.27

Fig. 3 shows that indeed ΔL is a linear function of ΔM. Taking into account that the dense layer in the polyurethane lamellar structure is impenetrable for the solvent [1], one can assume that the decrease in the L value is caused exclusively by the decrease of the loose layer thickness. It means that:

i/ the change of the thickness of the loose layer is proportional to the relative amount of the solvent in the sample independently of the polyurethane composition.
ii/ this change is simultaneous with the solvent mass loss.

Reference:

[1] H.Grigoriew, S.Bernstorff, A.Woliñska-Grabczyk, J.Domagala, A.G.Chmielewski *J.Membr.Sci.* 186 (2001) 1-8.

PHASE BEHAVIOUR OF α-ZrP INTERCALATES WITH HIGHER ALCOHOLS FROM AMBIENT CONDITIONS UP TO 70 °C AND 2000 BAR

M. Steinhart[1], V. Zima[2], L. Beneš[2], K. Melánová[2], H. Amenitsch[3] and S. Bernstorff[4]

1.) Department of Physics, University of Pardubice, 530 09, Pardubice, Czech Republic
2.) Joint Laboratory of Solid State Chemistry of the Academy of Sciences of the Czech Republic and University of Pardubice, 530 09 Pardubice, Czech Republic
3.) Institute of Biophysics and X-ray Structure Research, Austrian Academy of Sciences, Schmiedlstraße 6, 8042 Graz, Austria
4.) Sincrotrone Trieste, Basovizza, 34012 Trieste, Italy

Intercalation represents a reversible insertion of mobile atomic or molecular guest species into a solid layer host lattice [1,2]. By intercalation a variety of new materials with interesting properties can be prepared. This fact is the obvious reason for the fast development in this field.

The intercalation process is accompanied by a change of the basal spacing (i.e., the interlayer distance of the host lattice) that can easily be detected by X-ray diffraction at relatively low angles. For this reason a SWAXS instrument is a highly preferable device for structure studies of intercalates.

Intercalations of zirconium phosphate (α-Zr(HPO4)2H2O, hereafter α-ZrP) and vanadyl phosphate belong among largely studied processes. Still, only a few cases of "in situ" observations have been reported up to now. So far we have thoroughly studied the influence of temperature and composition, particularly the chain length of the intercalating agent, on the structure. The motivation of this work has been to extend our studies by logically adding a new thermodynamic dimension – the pressure.
Our previous studies on $VOPO_4$ – liquid alcohol systems showed that temperature influences the rate of intercalation [3]. Also, the final arrangement of the alcohol molecules in the interlayer region of the host can be influenced by temperature. For instance, in our research on α-ZrP – alcohol systems [4], we have observed a phase transition in which the bimolecular film undergoes a change from an all-trans conformation to a conformation in which the O-C1-C2-C3 torsion angle changes from 180° to 136° during cooling of the samples. These two phases differ in their basal spacing. Since the interlayer distance is connected [5] with the thickness of the whole crystal, a pressure dependence of the phase behaviour (the arrangement of the guest molecules in the interlayer space) had been expected.

We have carried out our recent measurements on α-ZrP – 1-octanol and α-ZrP – 1-nonanol systems. We have tried to trace phase behaviour in the region from room temperature to 55 °C and from ambient atmospheric pressure up to 2000 bar.

Phase diagrams derived from our measurements are shown in the Figures 1A and 1B. They clearly proved the influence of pressure on the phase behaviour. The existence of both (known) phases with different basal spacings is visible. In addition, a new phase with lower basal spacing was observed at very high pressures. In addition, it can be deduced from the comparison of the data for the 1-octanol and 1-nonanol intercalates that the pressure, at which this phase is formed, decreases with increasing length of the alkanol chain.

Research was supported by the Grant agency of the Czech Republic (Grant No. GV202/98/K002).

References

[1] A. J. Jacobson in Encyclopaedia of Inorganic Chemistry, Ed. R. B. King, Vol. 3, Wiley, Chichester 1994, p. 1556.
[2] "Intercalation Chemistry", Ed. M. S. Whittingham and A. J. Jacobson, Academic Press, New York, 1982.
[3] L. Beneš, V. Zima, I. Baudyšová, J. Votinský, J. Incl. Phenom., 1996, 26, 311
[4] U. Costantino, R. Vivani, V . Zima, L. Beneš, K. Melánová, Langmuir 18 (2002) 1211-1217.
[5] V. Zima, L. Beneš, J. Málek, M. Vleek, Matt. Res. Bull., 1994, 29, 687

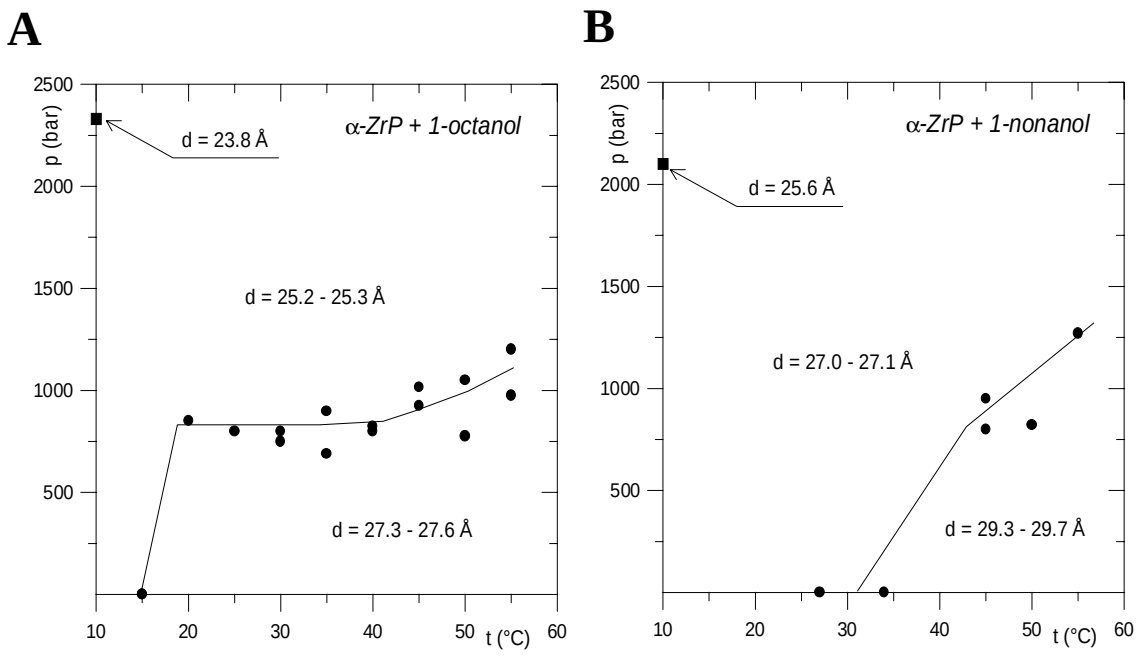

Figure 1.
p-T phase diagrams of α-ZrP intercalated with 1-octanol (A) and 1-nonanol (B). In both figures lines among the measured points represent phase boundaries.

SMECTIC ORDERING OF CONFINED LIQUID CRYSTALS

A. Zidansek

J. Stefan Institute, Jamova 39, 1000 Ljubljana, Slovenia

The influence of the surface treatment on the nematic (N) to smectic A (SmA) phase transition of the 8CB (octylcyanobiphenyl) liquid crystal confined to controlled pore glass (CPG) matrices was studied[1]. The voids' surface was either nontreated or covered with silane enforcing tangential or homeotropic anchoring, respectively. The phase and the structure of the confined liquid crystal in this system reflect the interplay between elastic and surface interactions.

We measured the smectic order parameter and the smectic correlation length as a function of temperature and characteristic diameter of CPG voids between 300 nm and 24 nm with small angle X-ray scattering (SAXS) method. The SAXS patterns were measured between 20 and 50° C showing a first order diffraction peak of the smectic layers in the SmA phase. In silane-treated samples with void diameter between 130 nm and 300 nm the N-SmA phase transition is shifted to a higher temperature, which depends on the void diameter. Non-treated samples with the void diameter above 130 nm do not exhibit a significant shift in the N-SmA transition. In smaller pores the Smectic A phase is weaker and appears at a lower temperature than in the bulk.

A theoretical description based on the Landau-de Gennes type approach was used to explain the experimental data.

References:

[1] A. Zidansek, S. Kralj, G. Lahajnar, S. Sumer, M. Rappolt, H. Amenitsch, S. Bernstorff, *Influence of the CPG Confinement on the Nematic - Smectic A Liquid Crystal Phase Transition*, 19th International Liquid Crystal Conference, Edinburgh, UK, 2002.

[2] A. Zidansek, S. Kralj, R. Repnik, G. Lahajnar, M. Rappolt, H. Amenitsch, S. Bernstorff, *Smectic ordering of octylcyanobiphenyl confined to control porous glasses*, J. Phys., Cond. Matter, 2000.

[3] Repnik, Robert. Vpliv omejenosti na fazni prehod med nematicno in smekticno-A fazo, Diplomarbeit, University of Maribor (1999).

4. Chemistry

IN SITU – SAXS INVESTIGATIONS ON ZINC SULFIDE PRECIPITATION IN A LIQUID JET

P. Bussian[1], W. Schmidt,[1] M. Lindén[2], M. Tiemann,[2] and H. Amenitsch[3]

1.) Max-Planck-Institute für Kohlenforschung, Kaiser-Wilhelm-Platz 1, D-45470 Mülheim/Ruhr, Germany
2.) Department of Physical Chemistry, Åbo Akademi University, Porthansgatan 3-5, FIN-20500 Turku, Finland
3.) Institute of Biophysics and X-ray Structure Research, Austrian Academy of Sciences, Schmieldstr. 6, A8042, Graz, Austria

Introduction

The understanding of the fundamental processes involved in precipitation reactions from solution is one of the most challenging problems in solid-state chemistry. However, only a few techniques are available for analysis of these reactions. In combination with a tubular reactor setup (represented by a liquid jet), SAXS can give new insights in the early stages of precipitation on a microsecond time scale. We have chosen the precipitation of sparingly soluble sulfides from aqueous solution as a model system. A more thorough discussion on the results can be found in our Elettra Highlights 2000-2001 communication [1].

Experimental setup

The precipitation of ZnS is carried out in a flow jet cell as seen in figure 1. A liquid jet (diameter 80 µm) containing an aqueous $ZnCl_2$ solution (1 molar) is injected into a reactive gaseous atmosphere of H_2S. By diffusion H_2S is transported into the jet and dissolved. Precipitation of ZnS occurs by the reaction of Zn^{2+} cations with S^{2-} anions created by the reaction of H_2S with water:

$$H_2S + H_2O \longrightarrow S^{2-} + 2\,H_3O^+$$

$$S^{2-} + Zn^{2+} \longrightarrow ZnS\downarrow$$

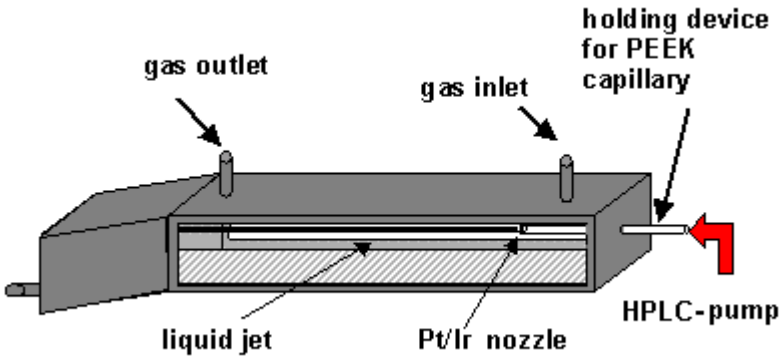

Figure 1: Schematic illustration of a flow jet cell

By measuring at different positions along the liquid jet, the ongoing crystallization reaction can be followed *in situ*. Every position in the jet corresponds to a certain residence time after mixing the liquid jet and the gas. We have now also successfully applied a 50 µm nozzle which has made it possible for us to measure times as short as 20 µm from the nozzle. The body of the cell is made of stainless steel and the nozzle, which is connected to a HPLC pump via a PEEK capillary, is made out of a Pt/Ir alloy. Each point was measured for 300 seconds.

Results and discussion

The new, encouraging, finding of the current measurement session was that the Guinier region now could be successfully studied by applying the new 50 μm nozzle. The obtained, very reproducible, values of the corresponding Guinier radius as a function of time is shown in Figure 2. We have now been able, for the first time, to scan the whole general feature window of particle growth and subsequent aggregation in a liquid jet reactor. As can be seen in Figure 2, we are approaching the first stages of the birth of the ZnS particles, but we are not really there yet, as can be understood from the smallest determined particle Guinier radius of 12 nm. The included fits to the data correspond to diffusion and reaction limited particle growth, respectively. It is evident that more points are needed in the short reaction time regime before a precise conclusion concerning the particle growth mechanism can be made. Furthermore, it is yet not possible to draw conclusions concerning the induction time, if any, for the particle growth. In Figure 3 the old results of the Porod data treatment for the longer reaction times are given for clarity.

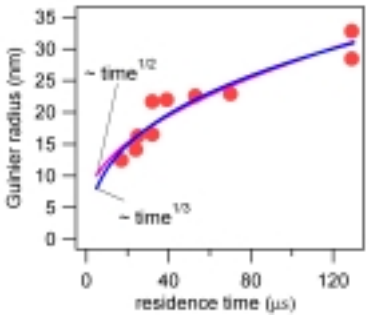

Figure 2: Results of the Guinier radius of ZnS as a function of residence time.

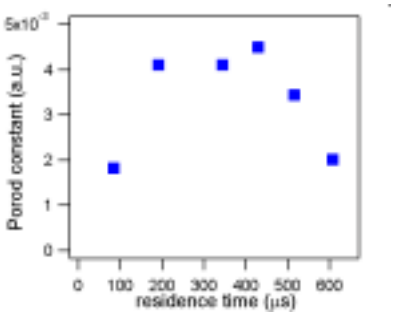

Figure 3: The Porod constants versus distance x. (1mm ≡ 86 μs residence time)

Outlook

To get a better insight into the very early stages of precipitation (< 20 μs) we plan to use a new holder for the successfully applied 50 μm nozzle, which will facilitate an additional reduction of the residence time by more than 10 μs, a 100 % increase in the time resolution! The development is based on the removal of the to date applied external nozzle holder, which has a dead-time in the range of 10-15 μs. This new nozzle holder has been designed, constructed, and tested in-house (MPI/Mülheim) and is working without any problems. We are convinced that this new, novel, design will allow us to reach the time-resolution needed for the final conclusion of our series of studies, the initial stages of inorganic particle nucleation and growth.

Reference:

[1] P. Bussian, W. Schmidt, F. Schüth, P. Ågren, J. Andersson, M. Lindén, H. Amenitsch, Elettra Highlights 2000-2001, p. 30.

PHASE TRANSFORMATION DURING CUBIC MESOSOSTRUCTURED SILICA FILM FORMATION

David Grosso[1], Florence Babonneau[1], Galo J. de A. A. Soler-Illia[1], Pierre-Antoine Albouy[2] and Heinz Amenitsch[3]

1.) Chimie de la Matière Condensée, UPMC - CNRS, 4 place Jussieu, 75005 Paris, France. Fax: 33 (0)1 4427 4769; Tel: 33 (0)1 4427 3365; E-mail: grosso@ccr.jussieu.fr.
2.) Lab. de Physique des Solides, Université Paris-Sud, 91405 Orsay, France.
3.) Institute of Biophysics and X-ray Structure Research, Austrian Academy of Sciences, Schmiedlstraße 6, 8042 Graz, Austria.

The preparation of porous oxide thin films has undergone a major improvement since mesoporous films showing large surface area and narrow pore size distribution can be prepared by surfactant templating methods.[1] One of the most studied system is based on the self-assembly of TEOS derived oligomers and CTAB surfactant micelles during dip-coating. By carefully adjusting the conditions, a discontinuous Pm3n cubic mesoporous thin film can be synthesised by dip-coating.[2] It is of optical quality and is formed of large organised domains that have a preferential orientation with respect to the substrate surface. The self-assembly requires the spontaneous organisation of the material, via electrostatic interactions at CTAB/silica solution interface, induced by the rapid evaporation of solvent associated with dip-coating.[3] The rigid mesoporous film is thereafter obtained by thermal degradation of the surfactant. The very low quantity of mater and the rapid kinetic of organisation make chemical and physical investigations difficult to perform. We recently succeeded to follow the structural evolution of the system by SAXS during the first minutes that followed the deposition.[4] This was made possible by using synchrotron radiation (Austrian high-flux SAXS beamline of the 2GeV electron storage ring ELETTRA, Trieste, Italy). Concerning the CTAB/silica system, it was reported that the mesostructures form close to the drying line and are not only highly dependent on the solution composition but also on the solution age[2] (e.g. silica species condensation). With the aim of completing this study, additional investigations were performed and the results are presented in this report. The experiments were focused on the precise structural transformations that take place during the Pm3n cubic film formation. The initial solution was prepared as detailed previously and contained 1 TEOS: 20 EtOH: 0.004 HCl: 5 H_2O: 0.14 CTAB (molar ratio) and was aged for 5 days prior to be deposited.[2] For such an experiment, the initial solution container was lowered while the substrate remained fixed in order to analyse the same film region during evaporation (Fig. 1). Substrates were placed at an angle of 0.18° with respect to the incident X-ray beam direction. Structures were deduced from the diffracted patterns collected every 1s with a 2D-CCD detector (see Fig. 1).

A selection of in-situ 2D-SAXS patterns recorded at various times after deposition (acquisition time =1s) are shown in Fig 1. The scheme shown on the upper right depicts the geometry used for this experiment. The displayed patterns correspond to the dashed framed area on the CCD detector (the diagrams have been rotated of 90° for clarity). The intensity profiles corresponding to the in-plane diffraction between the two ♦ points represented on the 10s pattern are also given for the other patterns. The in-plane black line labelled *S* on the 13s pattern exists even when no film is deposited and corresponds to the residual specular reflection. One can clearly see that the formation of the cubic Pm3n structure involves the formation of various intermediate phases for which recorded d-spacings enter in the characteristic dimensions of CTAB micelles. 10s after deposition, no diffraction is observed, suggesting that the film is not organised. After 13s, a single well-defined peak starts to appear at q = 0.0183 $Å^{-1}$ (55Å). This peak, labelled L(001) corresponds to planes that are parallel to

the surface and since no other diffraction are present one can assume the phase to be lamellar. A feint diffusion ring is also present, suggesting that randomly located and oriented micelles (average distance ≈ 60Å) start to form at this stage. From 14s, together with the diffusion ring and the lamellar phase peak, characteristic diffraction peaks corresponding to the H(002) (d_{002} = 53Å), H(101) and H(100) reflections of the 3D-hexagonal $P6_3/mmc$[5] are recorded, confirming that spherical micelles are present and organise in the latter compact structure. After 16s, the characteristic diffraction pattern of the Pm3n cubic structure begins to overlay the 3D-hexagonal and the lamellar ones, while the diffusion ring is not visible anylonger. The characteristic C(211) diffraction is located at d_{211} = 50Å and on the in-plane profile line, suggesting that the domains have their (211) planes parallel to the film surface. At this stage one may assume that the whole film is organised in three different mono-oriented mesostructures. At 20s and at 21s the lamellar and the 3D-hexagonal phases respectively disappear, while the cubic structure remains the only phase present in the dry film. A progressive concentration of non-volatile species takes place at the air/film interface that induces a concentration gradient between both interfaces. This evaporation modifies the micelle morphology and organisation. As the air/film interface is always more concentrated it should be the first area to undergo the micellisation. The initial lamellar phase may thus form at this interface. Disorganised micelles are also present in the beginning as revealed by the diffusion ring. A compact 3D-hexagonal mesophase is then progressively formed by self-organisation of micelles, that is subsequently transformed in the final compact cubic structure through rearrangement.

Therefore between 15s and 20s, all the phases coexist in the system and it is likely that a depth profile during this period would be as shown in Fig. 2. The formation by evaporation of a Pm3n CTAB/TEOS based mesostructured film begins with the formation of a lamellar phase at the air interface. Spherical micelles forms then underneath this phase and organised into 3D-hexagonal phase that rearranged afterward into the discontinuous cubic phase. This process progresses then towards the substrate interface. During this process the location of the phases with respect to both interfaces concords with the general behaviour of surfactant in composition phase diagrams : isotropic → arrangement of spherical micelles → arrangement of cylindrical micelles → lamellar, with increasing concentrations.

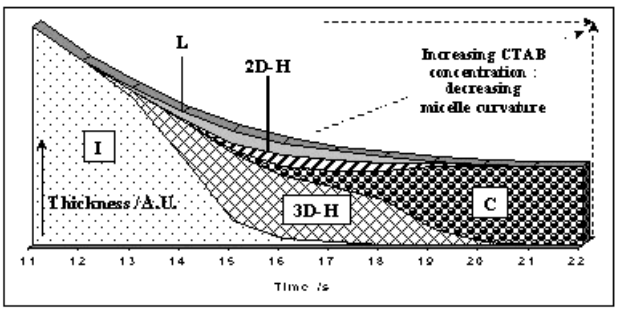

Figure 1 (next page).

Figure 2. Model of phase position during solvent evaporation.

References:

[1] C. J. Brinker, *Current Opinion in Colloid & Interface Science*, 1998, **3**, 166.

[2] D. Grosso, F. Babonneau, H. Amenitsch, A.R. Balkenende, P.A. Albouy, A. Brunet-Bruneau and J. Rivory. *Chem. Mat.*, 2001, in press.

[3] C. J. Brinker, Y. Lu, A. Sellinger, and H. Fan, *Adv. Mater*., 1999, **11**, 579.

[4] D. Grosso, P.A. Albouy, H. Amenitsch, A. R. Balkenende, F. Babonneau, Mat. Res. Soc. Symp. Proc., 2000, **628**, CC6.17.1.

[5] D. Grosso, A. R. Balkenende, P.A. Albouy, M. Lavergne, and F. Babonneau, *J. Mater. Chem*. 2000, **10**, 2085.

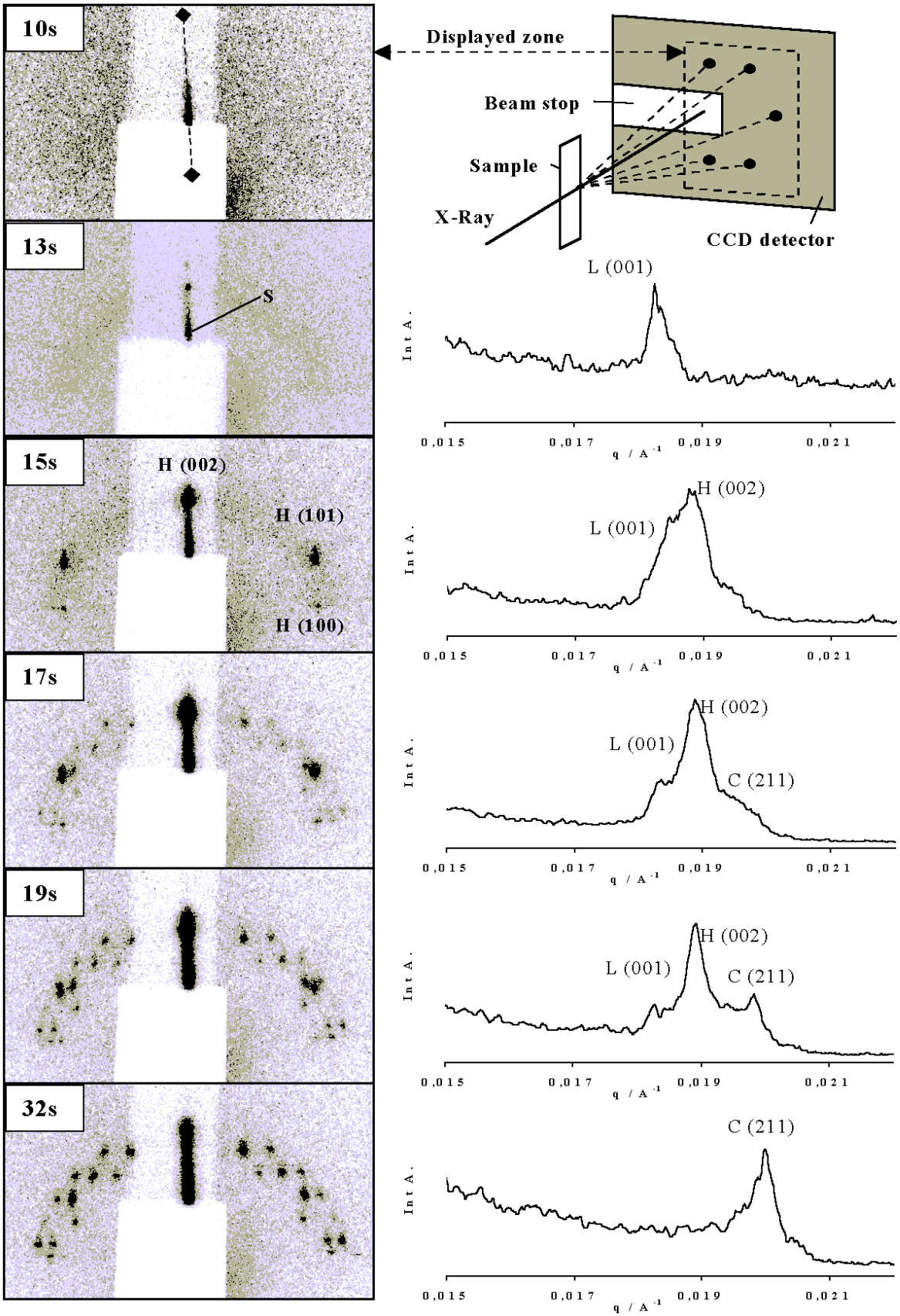

Figure 1. Two-dimensional and one-dimensional SAXS patterns showing the structural evolution of the film during solvent evaporation. Upper right : scheme of the SAXS geometry used.

TIME RESOLVED SAXS STUDY OF THE MECHANISM INDUCING THE SOLUBILIZATION OF ELECTROSTATIC CHARGED LIPOSOMES BY SODIUM DODECYL SULFATE

O. López[1], M.Cócera[1], A. de la Maza[1], H. Amenitsch[2], R. Pons[1]

1.) IIQAB-CSIC, Jordi Girona 18-26 08034 Barcelona, Spain
2.) Institute of Biophysics and X-Ray Structure Research, Austrian Academy of Sciences, Graz, Austria

The interest in the study of the interaction between surfactants and liposomes lies in the similarity of these lipid structures with the bilayer of the biological membranes. Given that these membranes contain ionic lipids, the study of the charge effect on the liposome solubilization is essential for the understanding of the processes in which charges are involved, such as the insertion of proteins, transport of ions and proteins and cell signalling. At a solubilizing level, the electrostatic charge seems not to have a relevant influence [1]. However, the electrostatic effect on the mechanism that led to the initial subsolubilizing steps, in which a very fast adsorption of surfactant is involved, is not still clear due to the lack of techniques with enough time resolution. Thus, the development and application of techniques such as time resolved small angle x-ray scattering (SAXS) using a stopped flow cell is increasingly important.

In previous works we investigated the solubilization of liposomes by surfactants from a structural viewpoint that raised a number of questions about the kinetics. Dynamic light scattering, freeze fracture electron microscopy and spectroscopy techniques have reported interesting data on this topic [2-4]. However, the initial steps of liposome solubilization were too rapid to be detected using these methods. In this work, we describe these initial steps for the liposome solubilization induced by the surfactant sodium dodecyl sulfate (SDS) from mechanistic and kinetic viewpoints. To this end, the technique of time resolved SAXS using a stopped flow cell and Synchrotron radiation was used. In order to study the effect of the electrostatic charges on the kinetic of these initial steps, neutral (non-ionic) and slightly charged (anionic and cationic) liposomes were used. The mechanism that induces the solubilization process consisted in an adsorption of surfactant on the bilayers and a desorption of mixed micelles from the liposomes surface. The different structures (liposomes, mixed micelles and pure SDS micelles) were detected by observation of the different peaks present in the scattering curves that were taken every 1 sec. The peak corresponding with the liposome was detected at a q value about 0.089 $Å^{-1}$, which corresponds with a bilayer thickness of 70 Å. The peak due to the pure SDS micelles was detected at q=0.139 $Å^{-1}$ that corresponds with a micelle diameter of 45 Å. The peak attributed to the mixed micelles appeared at q values around 0.120 $Å^{-1}$ corresponding to diameters of about 52 Å. The x-ray scattering curves of the systems: a) anionic liposome-SDS and b) cationic liposome-SDS are shown in Figs 1A and 1B respectively. Regardless of the lipid charge, the time needed for the desorption of the first mixed micelles was shorter than that needed for the complete adsorption of the surfactant in the liposomes surface. The present work suggests that the adsorption of the SDS molecules on negatively charged liposomes was slower and the release of mixed micelles from the surface of these liposomes was faster than for neutral liposomes. Inversely, in the case of positively charged liposomes the adsorption and the release processes were respectively faster and slower than those for neutral vesicles. Thus, the use of this sensitive methodology offers new possibilities for the control of processes containing surfactants and lipids from both biological and physical-chemical perspectives. Although the kinetic differences are only of few seconds, it is necessary to consider that a lot of biological processes related to membranes are really dependent on short periods of time. This and the fact that the electrostatic charges can either accelerate or slow down

these processes could explain the effects of electric fields generated in membranes when potential differences are established.

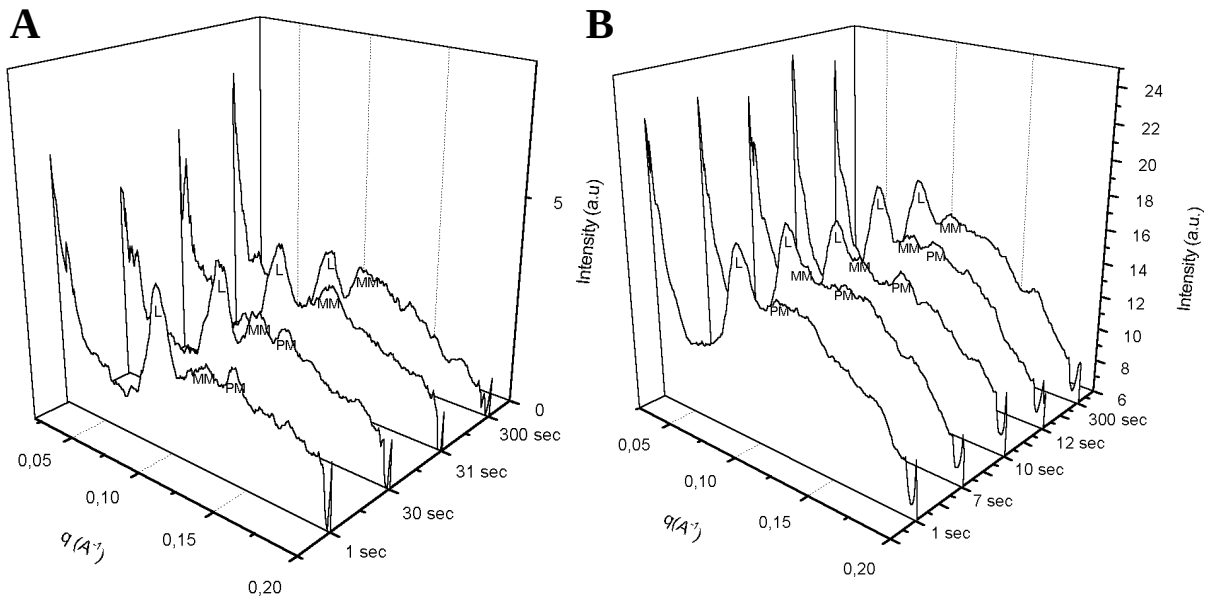

Figure 1. X-ray scattering patterns for the system anionic liposome-SDS (1A) and cationic liposome-SDS (1B) after different times of mixing. These times represent the most relevant stages at which changes in the number and position of the diffraction peaks were detected. L: liposome; MM: mixed micelles; PM: pure SDS micelles.

References:

[1] O. López, M. Cócera, A. de la Maza, H. Amenitsch and R. Pons, Effect of electrosatic charges on the kinetic of solubilization and reconstitution of liposomes induced by surfactants: A study using time resolved SAXS, Annual Report 1999 Austrian SAXS Beamline at ELETTRA, 101-102 (2000).

[2] O. López O, A. de la Maza , L. Coderch, C. López-Iglesias, E. Wehrli and J.L. Parra, Direct formation of mixed micelles in the solubilization of phospholipid liposomes by Triton x-100, 426, FEBS Lett., 314-318 (1998).

[3] O. López, M. Cócera, L. Coderch, J.L. Parra, L. Barsukov and A. de la Maza, Octyl glucoside-mediated solubilization and reconstitution of liposomes: Structural and kinetic aspects, 105, J. Phys. Chem. B, 9879-9886, (2001).

[4] M. Cócera, O. López, J. Estelrich, J.L. Parra and A. de la Maza, Use of a fluorescence spectroscopy technique to study the adsorption of dodecylsulfonate on liposomes, 109, Chem. Phys. Lipids, 29-36, (2001).

DYNAMICS OF OIL-IN-WATER EMULSIONS PREPARED BY MICROEMULSION DILUTION FOLLOWED BY TIME RESOLVED SAXS

R. Pons[1], I. Carrera[1], J. Caelles[1], H. Amenitsch[2]

1.) IIQAB, CSIC, Jordi Girona 18-26, Barcelona 08034, Spain
2.) Institute of Biophysics and X-Ray Structure Research, Austrian Academy of Sciences, Graz, Austria

Emulsions are important from a practical point of view because of widespread applications, e.g. pharmaceuticals, papermaking, cosmetics, paints, etc (1). Understanding the processes of emulsification can allow for a better control of their properties. Low energy emulsification methods have attracted increasing interest, not only because of energy savings, but also as a way to control their properties (e.g. particle size and stability). Two promising methods of emulsification have been proposed. a) Phase transition by temperature change (2) and b) phase transition by mixing two different phases (3). We centered our study in the latter.
Our interest is in the process of emulsion formation by mixing a microemulsion with excess water. The system comprises a classical microemulsion formed by sodium dodecyl sulphate, hexanol, water and decane or mixtures of decane with other oils. The compositions are identical except for the mixture of oils. In the present experiment we used a home made mixing and measuring cell to assure the mixing of very different viscosity fluids and mixture. Our time resolution was 1s. We investigated the effect of oil mixture on the emulsification process. It is well known that Ostwald Ripening can be slowed down by using mixtures of oils one of which is much more insoluble than the other (4). We choose two different systems. On the one hand we mixed our standard oil (decane) with hexadecane with a ratio of water solubilities that corresponds to about 1000 times. On the other hand we added a much more insoluble oil, tetracosane, which is solid at room temperature but soluble in decane and which solubility in water can be estimated as eight orders of magnitude lower than that of decane. As expected, the system without additive evolves much faster than the other samples. This is shown in figure 1. Figure 1a shows the scattering curves taken every second after mixing. A shoulder at $q=0.02Å^{-1}$ moves first to higher q values converting to a peak and afterwards continuously moves to lower q values, finally merges with the peak at low q, figure 1b. The peak at low q continuously increases intensity after the first few seconds.
In figure 2 the initial scattering curves for the mixing of a system containing hexadecane as additive are shown. The scattering curves remain constant afterwards for the maximum experimental time of 1000s. In fact there are not significant changes after the first 25 seconds in the position and form of the peaks are apparent. The form of those constant curves are similar to the curves obtained after about 3 seconds of mixing in absence of hexadecane, see figure 1a. This shows that this additive effectively freezes the system on these timescales without greatly affecting the materials distribution in the system. In case of using tetracosane as additive, no strong differences are observed compared to hexadecane. The main difference is the time to reach a constant pattern, which in this case is of only about 10 s.

References:

[1] P. Becher (Ed.) "Encyclopedia of Emulsion Technology", Vol 1.Marcel Dekker Inc., N.Y.1983
[2] Shinoda, K., Saito, H. (1969): *J. Colloid Interface Sci*., 30: 258
[3] C. A. Miller, "Spontaneous Emulsification Produced by Diffusion- A Review", *Colloids Surfaces*, 89: 29 (1988)
[4] Buscall R., Davis S.S. and Potts D.C., "The effect of long-chain alkanes on the stability of oil-in-water emulsions. The significance of Ostwald ripening.", Colloid and Polymer Science 257: 636 (1979)

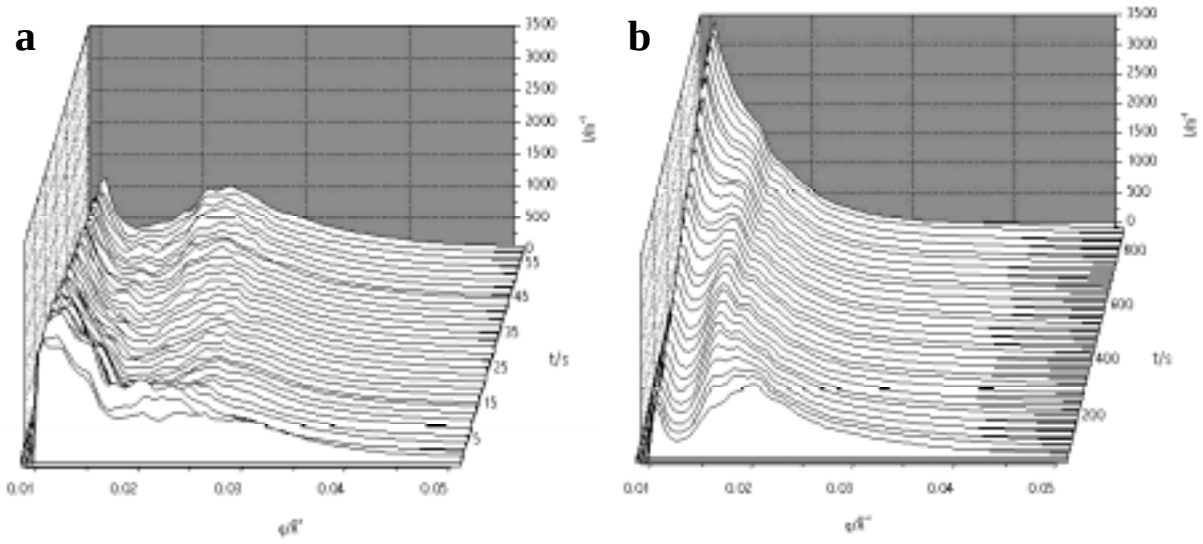

Figures 1a and 1b. Scattering curves for a system without additive at short times, first 50s, and long times, up to 900s.

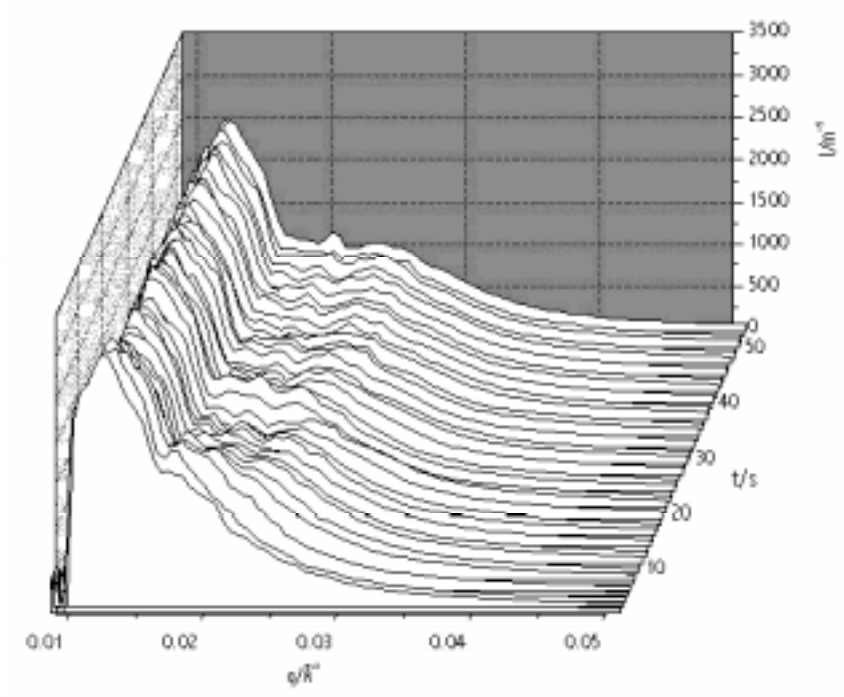

Figure 2. Scattering curves for a system with hexadecane added taken every second after mixing.

MICROHETEROGENEITIES IN PEO-SALT MIXTURES

A. Triolo[1], F. Lo Celso[2], V. Baiata[2], S. Bernstorff[3] and R. Triolo[2]

1.) Istituto Processi Chimico-Fisici, Sezione di Messina – CNR, Italy
2.) Department of Physical Chemistry, University of Palermo, 90128 Palermo (Italy)
3.) Sincrotrone Trieste, Italy

This report deals with a structural investigation on PEO-based polymer electrolytes and in particular with mixtures of lithium bis(perfluorethylenesulfonyl)imide (LiBETI) and poly(ethylene oxide). In the recent years a lot experimental effort has been addressed to solid polymer electrolytes thanks to their large application in consumer electronics products. The typical example is represented by rechargeable lithium salt batteries where a lithium salt is dispersed in a PEO matrix to form a solid electrolyte. It is known that the lithium ion form crystalline complexes thanks to the coulombic interaction with the ethereal oxygen of the PEO chains; moreover the salt is dispersed as well in the amorphous region of the PEO matrix that separate the lamellar crystalline regions. Indeed ionic conductivity is mainly due to high mobility of the ions in the amorphous region of the PEO-Li salt mixtures rather than the ion transport in the crystalline domain. WAXS data were collected for several $P(EO)_nLiBETI$ mixtures in a series of thermal ramps in order to investigate the phase behaviour.

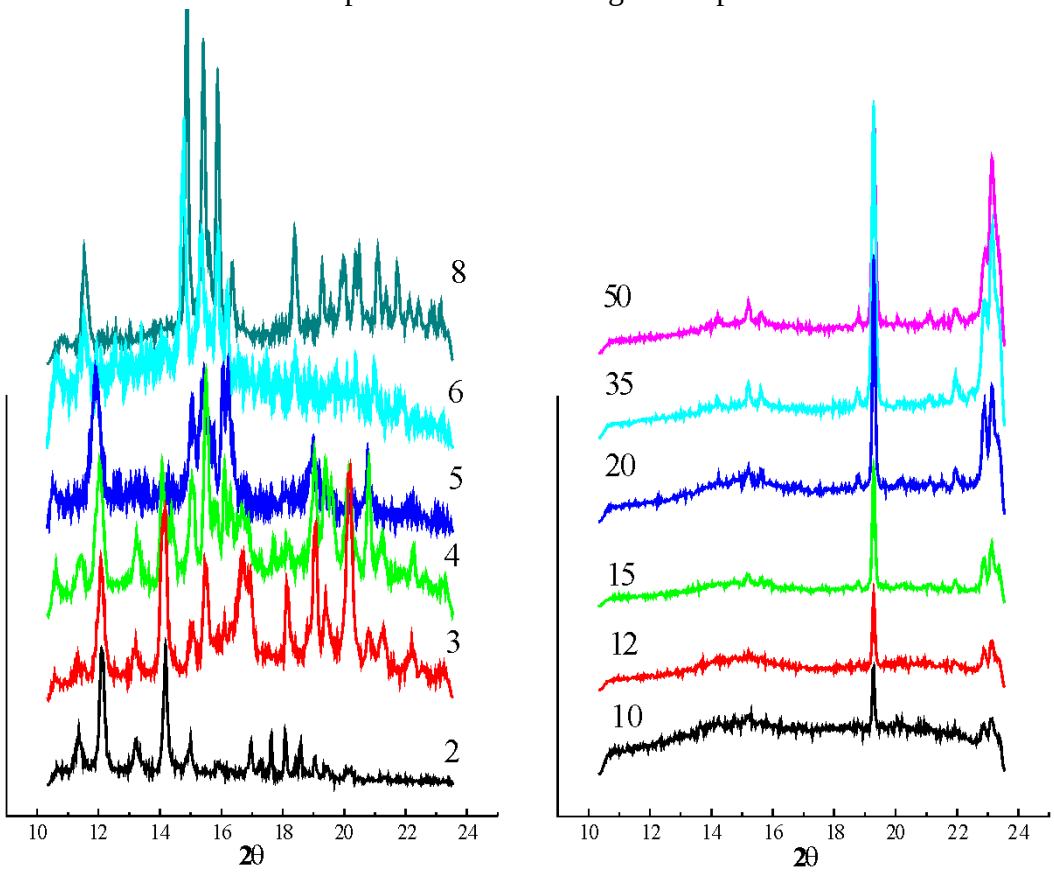

Figure 1. X-ray diffraction patterns for different $P(EO)_nLiBETI$ mixtures at T = 5 °C (values of *n* , which indicates the EO/LiBETI molar fraction ratio, are reported in the plot).

Figure 1 reports the WAXS spectra for different *n* values at 5° C (where *n* refers to the stoichiometry in the $P(EO)_nLiBETI$ mixtures). Starting from low salt concentration mixtures (n = 50) it is possible to see that there are few additional peaks with respect to the classical PEO pattern (characteristic features of crystalline PEO are essentially located in the spectrum portion above 18°). This is an indication of the coexistence between a PEO-BETI crystalline complex and the pure PEO crystalline phase. As the salt concentration increases (for n < 10) it is clear that the spectra present additional features with respect to the low concentration samples. This fact is probably due to the formation and, at the same time, the coexistence of crystalline complexes characterized by different composition; meanwhile peaks belonging to the pure PEO crystalline phase have almost disappeared. Starting in fact from the n = 8, going towards higher salt concentrations (n = 2 is the highest LiBETI concentration) it is possible to see that new peaks appear in the lower part of the spectra ($10°<2\theta<15°$) while others disappear in the higher angle region ($15°<2\theta<25°$). Time resolved WAXS data were collected by varying the temperature applied in order to investigate the phase diagram of the PEO-BETI system.

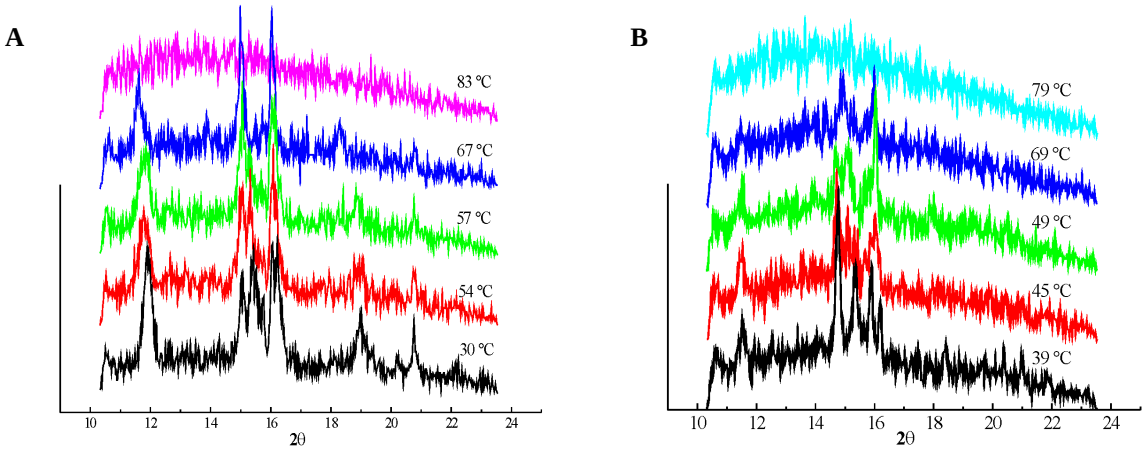

Figure 2. X-ray diffraction patterns at different temperatures for **A.** the $P(EO)_5LiBETI$ mixture, and **B.** the $P(EO)_6LiBETI$ mixture.

Figure 2 reports several WAXS snapshots taken out from temperature ramps for two selected compositions (n = 5 and 6). As shown in figure 2A, it is very likely that there are WAXS peaks belonging to different crystalline phases (30 °C); as temperature increases, one of these crystalline phases disappears (around 57 °C) leaving only WAXS signals coming from the remaining crystalline phase. Indeed the region where $14° < 2\theta < 17°$ (for T = 30 °C) presents a complex pattern that, as temperature increases (around 57 °C) resolves in a much simpler one characterized essentially by two strong peaks; at higher temperature this crystalline phase will melt giving the usual broad isotropic peak (around 80 °C). Figure 2B reports WAXS spectra for a different composition (n = 6); a similar transition in the same range of 2θ as in figure 2A is observed as well for this sample, although it occurs in a different temperature range (45-49 °C). These phase transitions and therefore the presence of different crystalline phases were investigated by a Differential Scanning Calorimetry analysis. Figure 3 reports DSC thermograms for a series of different $P(EO)_nLiBETI$ mixtures. For the samples of figures 2A and 2B (n = 5 and 6, respectively) melting peaks were observed in the same range of temperatures where the WAXS investigation has shown structural variation (57 and 45 °C for n = 5 and n = 6 mixtures respectively).

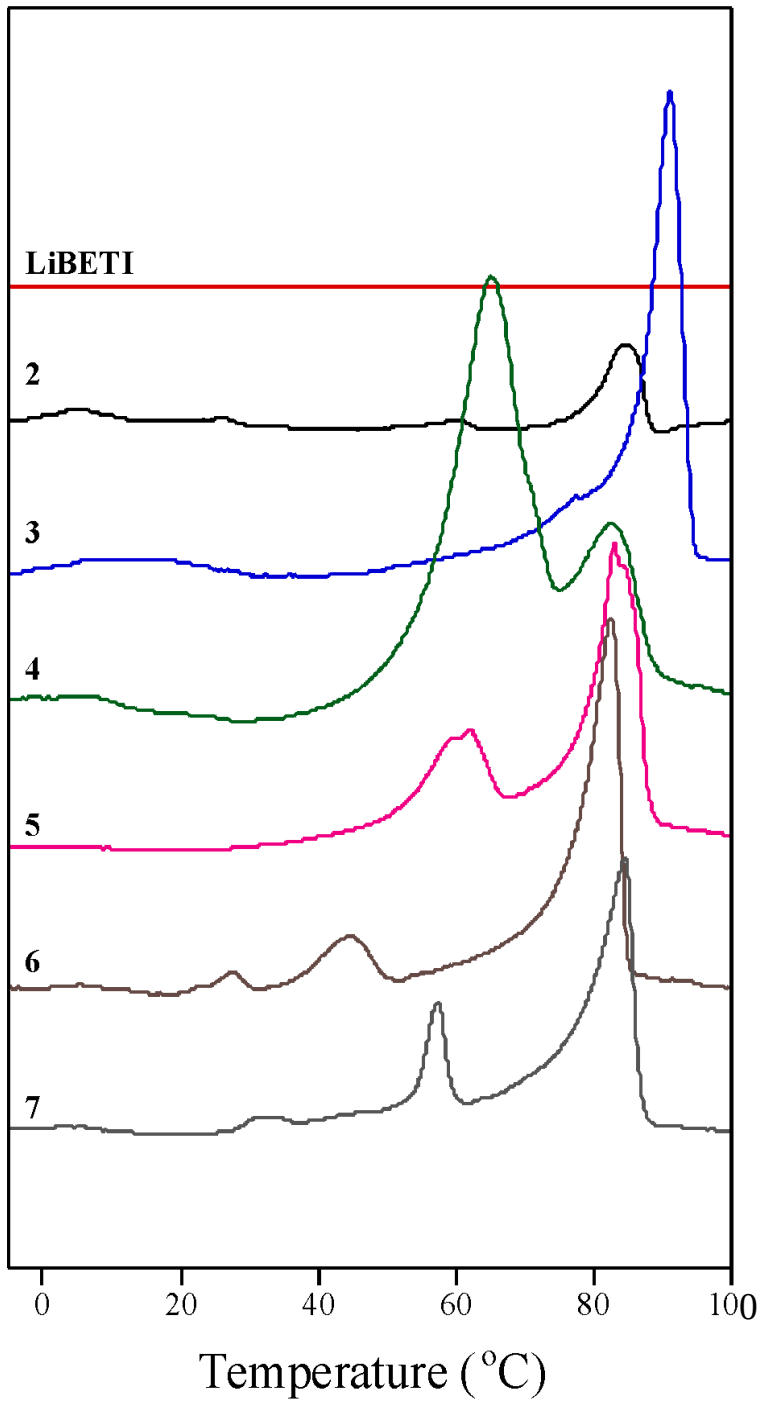

Figure 3. DSC traces for the $P(EO)_nLiBETI$ mixtures. (values of *n*, which indicates the EO/LiBETI molar fraction ratio, are reported in the plot).

5. Instrumentation

DEVELOPMENT OF A 2D X-RAY DETECTOR FOR TIME-RESOLVED STUDIES IN THE MICROSECOND RANGE

A. Orthen[1], H. Wagner[1], S. Bernstorff[2], H.J. Besch[1], R.H. Menk[2], M. Rappolt[3], A.H. Walenta[1]

1.) Department of Physics, University of Siegen, Walter-Flex-Str. 3, D-57068 Siegen, Germany
2.) ELETTRA, Sincrotrone Trieste, S.S.14 km 163.5, 34012 Basovizza/Trieste, Italy
3.) IBR, Schmiedlstrasse 6, Graz, Austria

Since a lot of physical, chemical or biological processes take place in sub-second or even sub-millisecond time range detectors with sensible spatial resolution and surpassing high rate capabilitiy have to be combined with a time-resolution sufficient for these applications, especially at high flux synchrotron facilities. At the department of physics at the University of Siegen a two-dimensional gaseous single-photon counter with an interpolating readout structure is currently developed [1,2,3] with respect to an optimised time-resolution.
The current sensitive detection area amounts to 56 x 56 mm^2 at a spatial resolution in the range of 200-500 μm depending on the particular Signal-to-Noise ratio. As a further step it is planned to implement a GEM gas gain structure (CERN development) as a preamplification stage in combination with an optimised MicroCAT gas gain structure [4]. With this constellation the operation stability is hoped to be further improved. The detector itself is able to provide a physical time-resolution in the μs-range but currently the time-resolution is limited by the electronic FADC system to about 20 μs and to a much larger extent by the data readout cycle to the processing PC. This limits the readout rate to less than 3 kHz. For that reason only periodical processes can be observed at the moment, but further investigations in this field will overcome this restriction.

In lab experiments the prototype device has already proven its suitability for repetitive mechanical processes [5]. During the data collection process each photon is stored together with a time stamp (here: the arrival time). When the experiment is finished, single time slices can be applied to the recorded image, sorting the photons with respect to their timing information.

The attempt to record a periodically stretched chicken tendon collagen at the SAXS beamline with this method is shown in Fig 1: the meridional reflections of the collagen are displayed in three different spectra taken at a constant strain rate at different moments during the extension of a fiber. At large mechanical load the fibrils in the tendon elongate with the increase in external stress, which results in strong changes in the relative intensities of the meridional diffraction orders. While at low mechanical loads the tendon remains elastic, partial failure occurs in the tissue after streching it heavily.

In a second experiment the main transition of palmitoyl-oleoyl-phosphatitylethanolamine (POPE) was studied. At about room temperature the lamellar liquid crystalline phase L_α forms from the lamellar gel phase L_β. Therefore, a heating/cooling unit was programmed to transverse the main transition temperature at about 25°C several times. The temperature information was stored together with the diffraction pattern in a digital fashion. Two examples of the applied temperature slices after the experiment are shown in Fig. 2. The fraction of the gel phase $h = A_\beta/(A_\beta+A_\alpha)$, where A is the area under each reflection, displays clearly the hysteresis of this transition (Fig. 3).

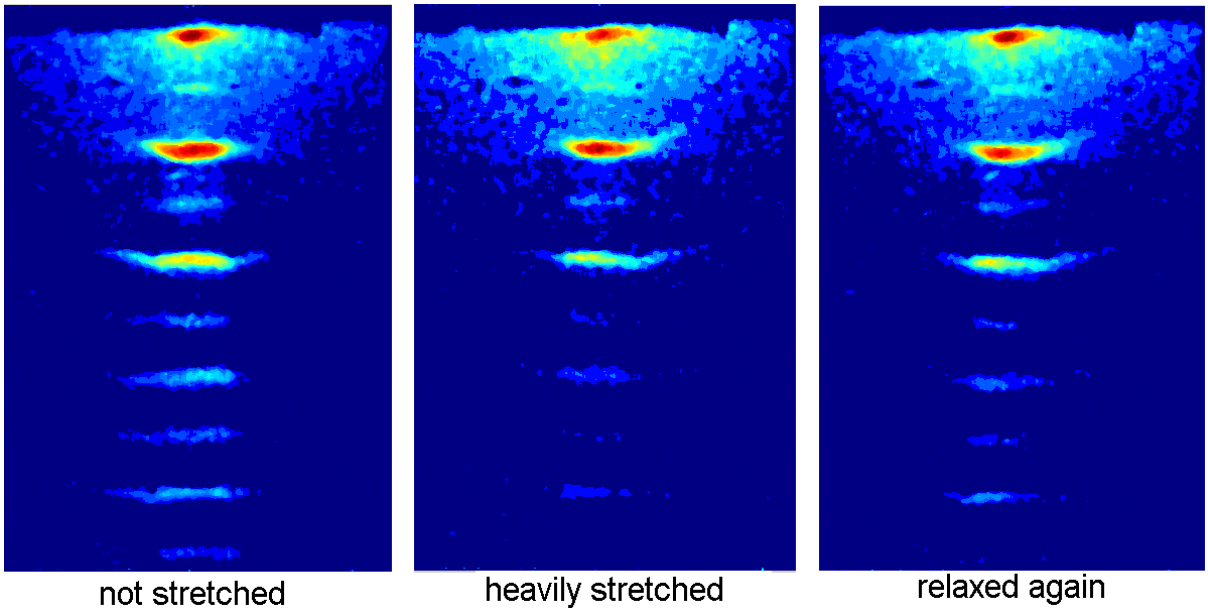

Figure 1. Meridional diffraction pattern of a chicken tendon collagen under different mechanical tensions.

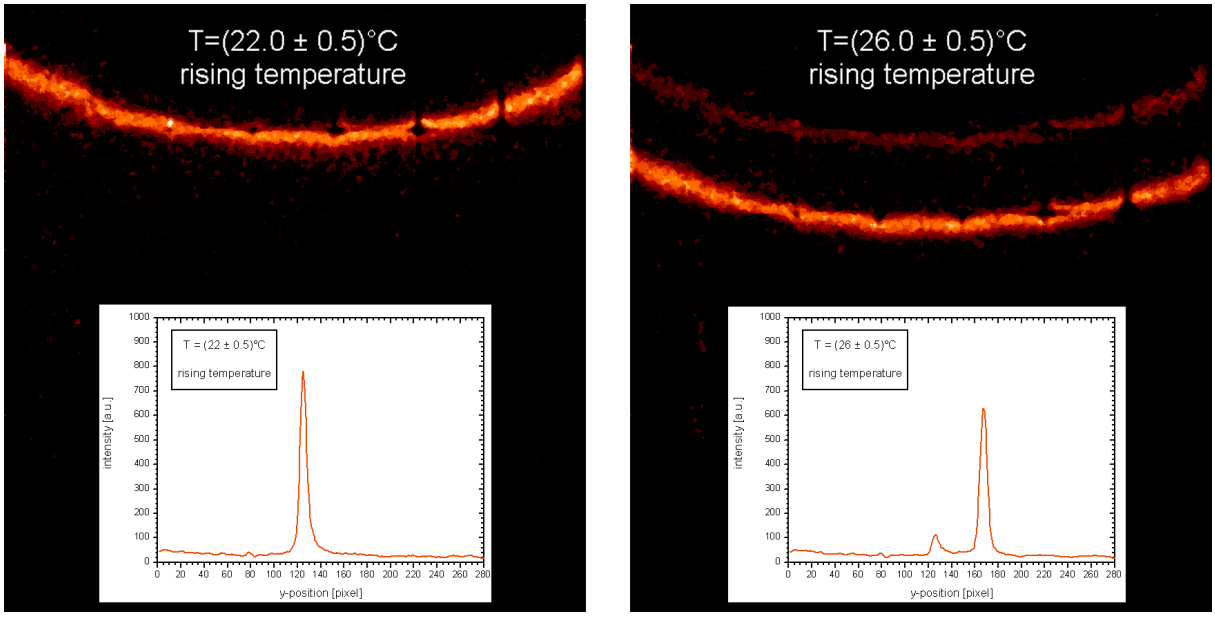

Figure 2. Diffraction pattern and corresponding intensity profile of POPE at two different temperatures recorded during heating.

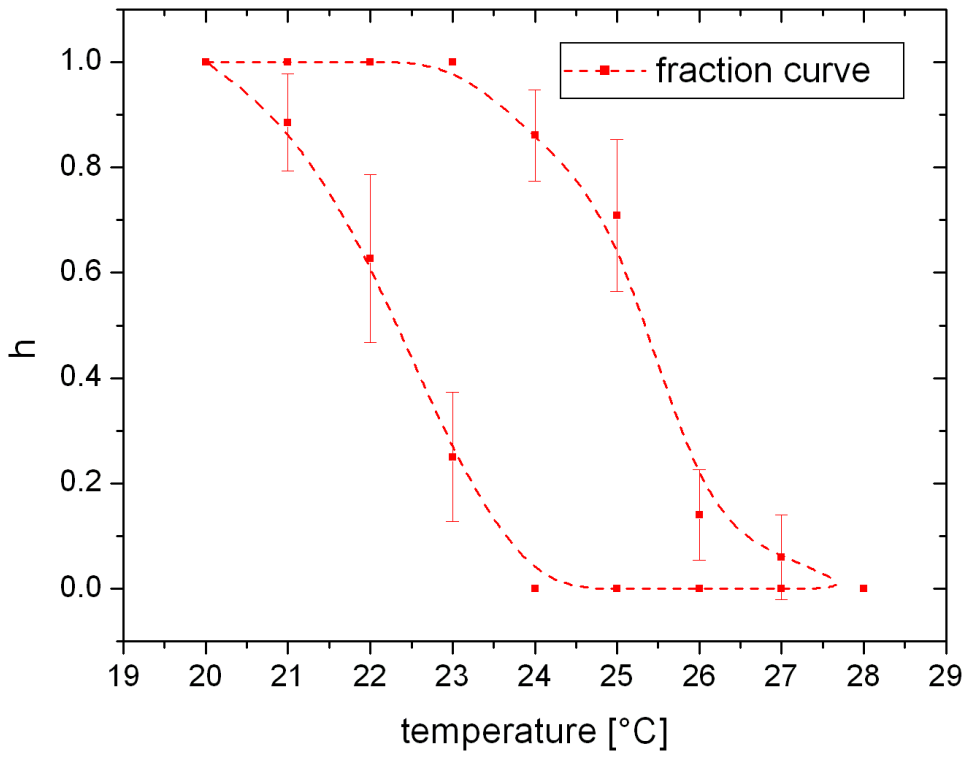

Figure 3. The fraction of the gel phase *h* shows the characteristic hysteresis of the main transition.

References:

[1] H.J. Besch, M. Junk, W. Meißner, A. Sarvestani, R. Stiehler, A.H. Walenta; *An interpolating 2D pixel readout structure for synchrotron X-ray diffraction in protein crystallography*; Nucl. Instr. and Meth. A **392**, 244-248 (1997)

[2] A. Sarvestani, H.J. Besch, M. Junk, W. Meißner, R.H. Menk, N. Pavel, N. Sauer, R. Stiehler, A.H. Walenta; *Gas amplifying hole structures with resistive position encoding: a new concept for a high rate imaging pixel detector*; Nucl. Instr. and Meth. A **419**, 444-451 (1998)

[3] H. Wagner, H.J. Besch, R.H. Menk, A. Orthen, A. Sarvestani, A.H. Walenta, H. Walliser; *On the dynamic two-dimensional charge diffusion of the interpolating readout structure employed in the MicroCAT detector*; accepted for publication in Nucl. Instr. and Meth. A (2001)

[4] A. Orthen, H. Wagner, H.J. Besch, R.H. Menk, A. Sarvestani, A.H. Walenta*; Charge transfer considerations of MicroCAT-based detector systems*; accepted for publication in Nucl. Instr. and Meth. A (2002)

[5] A. Sarvestani, N. Sauer, C. Strietzel, H.J. Besch, A. Orthen, N. Pavel, A.H. Walenta, R.H. Menk; *Microsecond time-resolved 2D X-ray imaging*; Nucl. Instr. and Meth. A **465**, 354-364 (2001)

Publications

Publications in 2001

H Amenitsch, M Kriechbaum, M Rappolt, M Steinhart, S Bernstorff, and P Laggner
New trends in surface diffraction on highly aligned phospholipids at the ELETTRAs small angle X-ray scattering beamline
Biophys. J. 80, pp. 61-. (2001)

M.A. Bagni, G. Cecchi, B. Colombini, P.J. Griffiths, C.C. Ashley, H. Amenitsch and S. Bernstorff
Effects of temperature on the intensity changes of the meridional 14.5nm X-ray reflection from activated skeletal muscle during sinusoidal oscillations
Journal of Physiology 533, pp. 135-136 (2001)

M.A. Bagni, B. Colombini, H. Amenitsch, S. Bernstorff, C.C. Ashley, G. Rapp and P.J. Griffiths
Frequency-Dependent Distortion of Meridional Intensity Changes during Sinusoidal Length Oscillations of Activated Skeletal Muscle
Biophys. J. 80, pp. 2809-2822 (2001)

J. Bonarski, M.J. Zehetbauer, Z. Swiàtek, E. Schafler, S.Bernstorff
Structural Investigation of Silicon Platelets for Solar Cells by Advanced methods of X-Ray Diffraction
Proc. from the Review Seminar „Physics and Materials Science“, Polish Academy of Sciences, Scientific Centre in Vienna, Austria, May 27-30, 2001, Ed. M.Herman, PAN, pp.171-177 (2001)

Cecchi, G., M.A. Bagni, B. Colombini, H. Amenitsch, S. Bernstorff, C.C. Ashley and P.J. Griffiths
Temperature effects on the equilibrium tilt of the myosin heads during sinusoidal length oscillations
Biophysical Journal 80 (1), A273, pp. 1100- (2001)

P. Dubcek, B. Pivac, O. Milat, S. Bernstorff and I. Zulim
X-ray reflectivity and GISAXS study of derelaxation in Kr implanted Si
Materials Research Society Symp. Proc. Vol. 678, p. EE 6.4.1 - 6.4.6 (2001)

H.Grigoriew, S.Bernstorff, A.Wolinska-Grabczyk, J.Domagala, A.G.Chmielewski;
Depth-influenced structure through permeating polymer membrane using SAXS synchrotron method
Journal of Membrane Science 186 (2001) 1-8

H.Grigoriew, A.G.Chmielewski, H.Amenitsch
Structural temperature transformation of the cellulose-water system using time-resolved SAXS
Polymer 42, pp. 103-108 (2001)

D. Grosso, A. R. Balkenende, P.A. Albouy, A. Ayral, H. Amenitsch and F. Babonneau
Formation mechanism of 2D-hexagonal mesoporous silica thin films prepared from block copolymers
Chemistry of Materials 13, 1848 (2001)

T. Hebesberger, E. Schafler, M. Zehetbauer, R. Pippan, T. Ungar, H. Amenitsch, S. Bernstorff
Electron Back Scatter Diffraction (EBSD) and Synchrotron X-Ray Profile Analysis (SXPA) as Tools for Microstructural Characterisation of Large Strain Work Hardened Metals
Z.Metallkde 92, pp. 410-416 (2001)

M. Pisani, S. Bernstorff, C. Ferrero and P. Mariani
Pressure induced cubic-to-cubic phase transition on the monoolein hydrated system
J. Phys. Chem. B105, 3109-3119 (2001)

B. Pivac, P. Dubcek, O. Milat, and I. Zulim
Structural changes in amorphous silicon annealed at low temperatures
Mater. Res. Soc. Symp. Proc. Vol. 664, p. A 19.9.1. – 19.9.6 (2001)

M. Rappolt, G. Pabst, H. Amenitsch and P. Laggner
Salt-Induced Phase Separation in the Liquid Crystalline Phase of Phosphatidylcholines
Colloids and Surfaces A 183-185 (2001) 171-181

Sarvestani, N. Sauer, C. Strietzel, H.J. Besch, A. Orthen, N. Pavel, A.H. Walenta, R.H. Menk
Microsecond time-resolved 2D X-ray imaging
Nucl. Instr. and Meth. A 465, 354-364 (2001)

M. Steinhart, M. Kriechbaum, M. Horky, J. Baldrian, H. Amenitsch, P. Laggner and S. Bernstorff
Time-Resolved SWAXS Measurements of Effects Induced by Variation of Pressure
In: „Advances in Structure Analysis“, Ed. R. Kuzel and J. Hasek, publ. by the Czech and Slovak Crystallograpghic Association (CSCA), Praha, Czech Republic (2001)

A.Turkovic**,** Z.Crnjak-Orel and and P.Dubcek
Grazing-incidence small-angle X-ray scattering on nanosized vanadium oxide and V/Ce oxide films
Materials Science & Engineering B79/1, 11-15 (2001)

Satish Vitta
Ni50Nb50/C amorphous multilayers for Water Window soft x-rays - structure and stability
Vacuum 60, 391 (2001)

I. Winter, G. Pabst, M. Rappolt and K. Lohner
Refined structure of 1,2-diacyl-P-O-ethylphosphatidylcholine bilayer membranes
Chem. Phys. Lipids 112/2, 137 – 150 (2001)

Publications in January – May 2002

P. Dubcek, N. Radic, O. Milat and S. Bernstorff
Grazing Incidence Small Angle X-Ray Scattering Investigation of Tungsten-Carbon Films Produced by Reactive Magnetron Sputtering
Surface and Coatings Technology 151-152, pp. 218-221 (2002)

R. Gianni, F. Delben, G. Liut, R. Rizzo, H. Amenitsch and S. Bernstorff
Synthesis and conformational properties of cyanoethylscleroglucan
Carbohydrate Polymers 47 (2002) 387-391

P.J. Griffiths, M.A. Bagni, B. Colombini, H. Amenitsch, S. Bernstorff, C.C. Ashley and G. Cecchi
Changes in myosin S1 orientation and force induced by a temperature increase
PNAS 99, p. 5384-5389 (2002)

H. Grigoriew, A. Wolinska-Grabczyk, S. Bernstorff
Solvent Influenced Mesostructures in Polyurethane-based Membranes of Different Transport Parameters using SAXS
Journal of Materials Science Letters **21**, 113-116 (2002)

D. Grosso, F. Babonneau, P.A. Albouy, H. Amenitsch, A.R. Balkenende, A. Brunet-Bruneau,J. Rivory
An in-situ study of mesostructured CTAB-silica film formation during dip-coating,using time-resolved SAXS and interferometry measurements
Chem. Mater. 14-2, pp. 931-940 (2002)

D. Grosso, G.A.A. Soler-Illia, F. Babonneau, H. Amenitsch, P.A. Albouy
Phase transformation during cubic mesostructured silica film formation
Chemical communications, pp. 20145-20147 (2002)

T. A. Harroun, M. J. M. Darkes, S. M. A. Davies & J. P. Bradshaw
The effect of fusion inhibitors on the phase behaviour of DOPE-Me, and their role in Fusion
Biophysical Journal 82, 542A (2002)

A. Lind, J. Andersson, S. Karlsson, P. Ågren, P. Bussian, H. Amenitsch, M. Lindén
Controlled oil solubilization by silicate-catanionic surfactant mesophases as studied by in situ and ex situ XRD
Langmuir 18 (2002) 1380

L. Pidol,D. Grosso, G.A.A. Soler-Illia, E. Crepaldi, P.A. Albouy, H. Amenitsch, P. Euzin, C. Sanchez
Hexagonally organised mesoporous alumina thin films prepared by the template approach. In-situ study of the structural evolution
Journal of Material Chemistry 12, pp. 557-564 (2002)

D. Posedel, A. Turkovic, P. Dubcek and Z. Crnjak-Orel
Grazing-incidence X-ray reflectivity on nanosized vanadium oxide and V/Ce oxide films
Materials Science & Engineering B90, 154-162 (2002)

N. Prasanth Kumar, S. Major, Satish Vitta, S.S. Talwar, P. Dubcek, H. Amenitsch, S. Bernstorff, V. Ganesan, A. Gupta and B.A. Dasannacharya
Molecular packing in cadmium and zinc arachidate LB multilayers
Colloids and Surfaces A 198-200 (2002) 75-81

N. Prasanth Kumar, S.N. Narang, S. Major, Satish Vitta, S.S. Talwar, P. Dubcek, H. Amenitsch and S. Bernstorff
Structure of CdS-arachidic acid composite LB multilayers
Colloids and Surfaces A 198-200 (2002) 59-66

R. Puxkandl, I. Zizak, O. Paris, J. Keckes, W. Tesch, S. Bernstorff, P. Purslow and P. Fratzl
Viscoelastic properties of collagen - synchrotron radiation investigations and structural model
Phil. Trans. Roy. Soc. London B 357, 191-197 (2002)

A Triolo, F Lo Celso, C Di Giovanni, H Amenitsch, R Triolo
Morphology of solid polymer electrolytes: a TR-WAXS investigation
Physica A 304, pp. 129-134 (2002)

F. Triolo, A. Triolo, F. Lo Celso, D.I. Donato and R. Triolo
Dilute and Semi dilute Solutions of Block Copolymers in water, Near-critical and Super-Critical CO_2: a Small Angle Scattering Study of the Monomer-Aggregate Transition.
Physica A, 304, 135–144 (2002)

V. Vidya, N. Prasanth Kumar, S. Major, Satish Vitta, S.S. Talwar, P. Dubcek, H. Amenitsch and S. Bernstorff
Molecular packing in CdS containing conducting polymer composite LB multilayers
Colloids and Surfaces A 198-200 (2002) 67-74

M. Zehetbauer, E. Schafler, T. Ungar, I.Kopacz and S. Bernstorff
Investigation of the Microstructural Evolution During Large Strain Cold Working of Metals by Means of Synchrotron Radiation - A Comparative Overview
J. Eng. Mater.-Technol. ASME, 124-, pp. 41-7 (2002)

Publications in print (May 2002)

J. Baldrian, M. Horky, M. Steinhart, P. Laggner, P. Vleek., H. Amenitsch, S. Bernstorff
Time-resolved SAXS/WAXS study of phase behaviour and crystallization in polymer blends
J.Macromol.Sci.Phys.

J. Baldrian, M. Horky, M. Steinhart, A. Sikora, M. Mihailova H. Amenitsch, S. Bernstorff, G.Todorova
SAXS and DSC study of cocrystallization of low-molecular PEO fractions in polymer blends
SPIE Proceedings

M. J. M. Darkes, T. A. Harroun, S. M. A. Davies & J. P. Bradshaw
The effect of fusion inhibitors on the phase behaviour of N-methylated dioleoylphosphatidyl-ethanolamine
Biochim. Biophys. Acta

Dubcek P., Bernstorff S., Desnica U.V., Desnica-Frankovic I.D. , Salamon K.
GISAXS Study of Cadmium Sulfide Quantum Dots
Surface Review Letters

H. Grigoriew, A. Wolinska-Grabczyk, S. Bernstorff, A. Jankowski
Temperature Effected Structural Transitions in Polyurethanes Saturated with Solvent Studied by SAXS Synchrotron Method
Journal of Macromolecules

H. Grigoriew, A. Wolinska-Grabczyk, S. Bernstorff
Kinetics of the Structural Changes in Polyurethanes Saturated with Benzene During Desorption Process
Journal of Materials Science Letters

D. Grosso, P.A. Albouy, H. Amenitsch, A.R. Balkenende and F. Babonneau
Time-resolved in-situ X-ray diffraction study of the formation of 3D-hexagonal mesoporous silica films
Mater. Res. Soc. Symp. Proc. Vol 628

D. Grosso, F. Babonneau, C. Sanchez, G. A. A. Soler Illia, E. Crepaldi,, P. A. Albouy, H. Amenitsch, A.R. Balkenende, A.Brunet-Bruneau
First insight of the mechanisms involved in the self assembly of templated SiO_2 and TiO_2 mesoorganised films during dip-coating
Journal of Sol-Gel Science and Technology

F. Lo Celso, A. Triolo, F. Triolo, J. McClain, J.M. Desimone, R.K. Heenan, H. Amenitsch, R. Triolo
Industrial Applications of Aggregation of Block Copolymers in Supercritical CO_2: a SANS Study
Applied Physics A

M. Lucic-Lavcevic and A.Turkovic
The morphological parameter of nanostructured TiO_2 films
Acta materialia

M.Pisani, T.Narayanan, G.M. Di Gregorio, C. Ferrero, H. Amenitsch and P. Mariani
Compressing inverse lyotropic phases: effects on dioleoyl phosphatidyl ethanolamine at low hydration
Phys. Rev. E

J.B. Rosenholm, M. Lindén
Controlled synthesis and processing of ceramic oxides – A molecular approach
Handbook of Surface and Colloid Science, 2nd edition, CRC Press

A. Triolo, F. Lo Celso, F. Triolo, H. Amenitsch, M. Steinhart, P. Thiyagarajan, S. Wells, J. M. DeSimone and R. Triolo
Kinetics of block copolymers aggregation in super critical CO_2
J. of Non Cryst. Sol

H. Wagner, H.J. Besch, R.H. Menk, A. Orthen, A. Sarvestani, A.H. Walenta, H. Walliser
On the dynamic two-dimensional charge diffusion of the interpolating readout structure employed in the MicroCAT detector
Nucl. Instr. and Meth. A

International Conferences and Workshops in 2001

H. Amenitsch, S. Bernstorff, P. Dubcek, M. Rappolt , and P. Laggner
The Austrian SAXS-Beamline at ELETTRA
The 4th CEI Summit Economic Forum, Trieste, Italy, 21-24 November 2001 (poster)

H. Amenitsch, S. Bernstorff, M. Kriechbaum, M. Rappolt & P. Laggner
Time-resolved small-angle X-ray scattering in mesoscopic systems: Its applications from bulk to surfaces
ESF Exploratory Workshop on: „Time-resolved Investigations of Structural Changes in Soft and Solid Matter with Neutrons and X-rays“, Sommerfeld near Berlin, Germany. 05.-07.09.2001 (Talk)

H. Amenitsch, I. Carrera, J. Caelles and R. Pons
Formation and properties of Miniemulsions formed by Microemulsions Dilution
XV Conference European Colloid and Interface Society, Coimbra, Portugal 16-21 September 2001

H. Amenitsch, M. Kriechbaum, M. Rappolt, M. Steinhart, S. Bernstorff & P. Laggner. *New trends in surface diffraction on highly aligned phospholipids at the ELETTRA's small angle scattering beamline*
45th Annual Meeting of the Biophysical Society, February 17 - 21, 2001, Boston, Massachusetts, USA (poster)

H. Amenitsch, M. Hainbuchner, M. Villa, M. Baron, P. Ågren, M. Linden, J.B. Rosenholm, H. Rauch and P. Laggner
A time-resolved USANS study of the microstructure-formation during the synthesis of MCM-41 and MCM-50
ESF Exploratory Workshop on: „Time-resolved Investigations of Structural Changes in Soft and Solid Matter with Neutrons and X-rays“, Sommerfeld near Berlin, Germany. 05.-07.09.2001 (Poster).

H. Amenitsch, M. Kriechbaum, M. Rappolt, M. Steinhart, C. Teixeira, S. Bernstorff, P. Laggner
Surface Diffraction on Highly Aligned Phospholipids at the ELETTRA - SAXS Beamline
9th Congress of SILS (Societá Italiana Luce di Sincrotrone), Florence, Italy, July 5-7, 2001 (poster)

H. Amenitsch, M. Kriechbaum, M. Rappolt, M. Steinhart, C. Teixeira, S. Bernstorff, P. Laggner
Surface Diffraction on Highly Aligned Phospholipids at the SAXS Beamline: Status Report
9th International Users‘ Meeting, ELETTRA, Trieste, Italy, 3. - 4.12.2001 (poster)

F. Babonneau
Surfactant-templated silicates: access to materials with ordered porosity
6th International Conference on Frontiers of Polymers and Advanced Materials, Recife (Brasil), 4-9 March 2001 (invited talk)

M.A. Bagni, G. Cecchi, B. Colombini, H. Amenitsch, S. Bernstorff, C.C. Ashley, P.J. Griffiths
Temperature effects during sinusoidal oscillations on the 14.5 nm x-ray meridional reflection from activated skeletal frog muscle fibres
9th Congress of SILS (Societá Italiana Luce di Sincrotrone), Florence, Italy, July 5-7, 2001 (talk)

Bagni, M.A., G. Cecchi, B. Colombini, P.J. Griffiths, C.C. Ashley, H. Amenitsch and S. Bernstorff
Effects of temperature on the intensity changes of the meridional 14.5nm X-ray reflection from activated skeletal muscle during sinusoidal oscillations
Physiological Society Meeting, Oxford UK, 19-21 March 2001 (poster)

J.Baldrian, M.Horky, M.Steinhart, A.Sikora, M.Mihailova, H.Amenitsch,S. Bernstorff
SAXS and DSC study of cocrystallization of low-molecular PEO fractions in polymer blends
X-Ray Investigations of Polymer Sructure XIPS '2001, Satellite conference of the 20th European Crystallographic Meeting, Bielsko-Biala, Poland 5.-8. 12. 2001, invited lecture, Book of abstracts L3

J.Baldrian, M.Horky, M.Steinhart, A.Sikora, P.Laggner, H.Amenitsch, S.Bernstorff
Time-resolved SAXS/WAXS study of structure development in polymer blends
PPS'2001, The Polymer Processing Society 2001, Regional Meeting, Antalya, Turkey 22.-24.10.2001, Book of Abstracts 409-410 (poster)

J.Baldrian, M.Horky, M.Steinhart, A.Sikora, M.Mihailova, H.Amenitsch, S. Bernstorff
Cocrystallization behaviour of low-molecular-weight PEO fractions in polymer blends
Kolokvium STRUKTURA' 2001, Bedoichov, Czech Republic 18.-22.6.2001,
Mater. Struct. in Chem., Biol., Phys. and Tech. 8 (2001) 67 (poster)

J. Baldrian, A. Sikora, M. Horký, M. Steinhart, H. Amenitsch and S.Bernstorff
Cocrystallization of PEO-b-PPO-b-PEO/PEO blends: Time-resolved SAXS/WAXS and DSC Study
EPS - European Conference on Macromolecular Physics: Morphology and Properties of Crystalline Polymers, Eger, Hungary 5.-7.9.2001, Book of Abstracts pp. 172-173 (poster)

S. Bernstorff
Neutronen- und Synchrotronstrahlungsquellen
NESY Ferienschule & Universitätsübergreifende Lehrveranstaltung on: "Forschung mit Neutronen und Synchrotronstrahlung an Europäischen Großforschungsanlagen", 11. - 17.03.2001, Planneralm, Steiermark, Austria (invited lecture)

J. Bonarski, M.J. Zehetbauer, Z. Swiàtek, E. Schafler,. S.Bernstorff
Structural Investigation of Silicon Platelets for Solar Cells by Advanced Methods of X-Ray Diffraction
Review Seminar on scientific co-operation between Austria and Poland on „Physics and Materials Science“, Polish Academy of Sciences, Scientific Centre in Vienna, Austria, May 27-30, 2001 (lecture)

P. Bussian, P. Agren, J. Anderson, M. Linden, W. Schmidt, H. Amenitsch and F. Schueth
In-Situ-Ssmall Angle X-ray Scattering Investigations on Zinc Sulfide Precipitation in a Liquid Jet
9th International Users‘ Meeting, ELETTRA, Trieste, Italy, 3. - 4.12.2001 (talk)

Giovanni Cecchi
Basi strutturali della generazione di forza nel muscolo scheletrico.
Congresso 2001 dell’Associazione Nazionale Specialisti in Medicina dello Sport. Chieti, Italia, 24-27 Giugno 2001 (talk)

Giovanni Cecchi
Muscle mechanics at molecular level
Symposium at the occasion of the retirement of Dr Tugendhold Blengé, Academical Medical Center, Meibergdreef, Amsterdam, Netherland, October 18, 2001 (talk)

Cecchi, G., M.A. Bagni, B. Colombini, H. Amenitsch, S. Bernstorff, C.C. Ashley and P.J. Griffiths
Temperature effects on the equilibrium tilt of the myosin heads during sinusoidal length oscillations
45th Annual Meeting of the Biophysical Society, February 17 - 21, 2001, Boston, Massachusetts, USA (poster)

S. Cinelli, F. Spinozzi, R. Itri, S. Finet, F. Carsughi, G. Onori, P. Mariani
Structural characterisation of the pH-denatured states of ferricytochrome-C by synchrotron small angle X-ray scattering
IX Convegno SILS, Firenze, Italy, 5-7.7.2001 (talk + poster)

F. Corsi, R. Favilla, M. Goldoni, F. Spinozzi, P. Mariani
Denaturation of pepsin studied by saxs and optical techniques
INFM meeting, Roma Eur, Italy 18-22 Giugno 2001

U.V. Desnica
Formation of Quantum Dots by Ion Implantation
8th International Scientific Meeting on Vacuum Science and Technique, Brdo pri Kranju, Slovenia, May 23, 2001 (Abstract published in Book of Abstracts, p. 14), talk

U.V. Desnica, I.D. Desnica-Frankovic, O. Gamulin, M. Ivanda, C.W. White, E. Sonder, R.A. Zuhr, A. Tonejc, P. Dubcek and S. Bernstorff
Synthesis of CdS nanocrystals in amorphous SiO_2 by ion implantation
Meeting of Croatian Physical Society, Zagreb, Croatia, December 5-7, 2001 (talk)

P. Dubcek
Structural Changes in annealed, hydrogen implanted monochrystalline silicon
Elettra Seminar, Trieste, Italy, Thursday, 22.3.2001 (talk)

P. Dubcek, U.V. Desnica, I.D. Desnica-Frankovic and S. Bernstorff
GISAXS Study of Cadmium Sulfide Quantum Dots
VUV XIII, July 23-27, 2001, Trieste, Italy (poster)

P. Dubcek, U.V. Desnica, I.D. Desnica-Frankovic , K. Salamon, S. Bernstorff, C.W. White, E. Sonder and R.A. Zuhr
GISAXS study of CdS quantum dots in SiO_2
9th International Users‘ Meeting, ELETTRA, Trieste, Italy, 3. - 4.12.2001(Poster)

P. Dubcek, B. Pivac, O. Milat, S. Bernstorff and I. Zulim
X-Ray Reflectivity and GISAXS Study of Derelaxation in Kr Implanted Si
MRS spring meeting, April 16-20, 2001 San Francisco, California

P. Dubcek, B. Pivac, O. Milat, S. Bernstorff, R.Tonini, F. Corni and G. Ottaviani
Structural changes in annealed, hydrogen implanted monocrystalline silicon
VUV XIII, July 23-27, 2001, Trieste, Italy (poster)

P. Dubcek, B. Pivac, O. Milat, S. Bernstorff, R.Tonini, F. Corni and G. Ottaviani
GISAXS study of annealed, hydrogen implanted, monocrystalline silicon
9th International Users‘ Meeting, ELETTRA, Trieste, Italy, 3. - 4.12.2001 (Poster)

P. Dubcek, N. Radic, O. Milat and S. Bernstorff
Grazing Incidence Small Angle X-Ray Scattering Investigation of Tungsten-Carbon Alloys Produced by Reactive Magnetron Sputtering
Proceedings of Spring Meeting of the European Materials Science Conference, Strasbourg, France, June 5-8, 2001 (poster)

P. Fratzl
Collagen structure and elasticity
Royal Society Discussion Meeting on elastomeric proteins, London, England, 16.-19.05.2001

P. Fratzl
Hierarchical structure of collagen and bone studied by X-ray scattering
CCP13, Keynote Lecture, Stirling, Schottland, 13.-15.06.2001

P. Fratzl
Ortsaufgelöste Streuung mit Synchrotronstrahlung
Nesy-Ferienschule, Planneralm, Austria, 11.-17.03.2001 (invited lecture)

P. Fratzl, R. Puxhandl, I. Zizak, H. S. Gupta, P. Roschger, O. Paris, H. Amenitsch, S. Bernstoff, K. Klaushofer
Importance of intermolecular cross-links for the mechanical behavior of collagen under tensile stress
7th International Conference on the Chemistry and Biology of Mineralized Tissues, Sawgrass Marriott Resort, Ponte Vedra Beach, Florida, USA, 04.-09.11, 2001

P. Fratzl, R. Puxkandl, I. Zizak, O. Paris
Structure and mechanical properties of collagen studied by time-resolved x-ray diffraction
ESF Exploratory Workshop on TINX, Sommerfeld, Berlin, Germany, 05.-07.09.2001

H. Grigoriew, S. Pikula, H. Amenitsch, M. Plusa
SAXS Synchrotron Measurements of Some Proteins
International Symposium on Synchrotron Crystallography (SYNCRYS 2001), Cracov, Poland, 31 August – 4 September 2001 (Poster)

H. Grigoriew, A. Wolinska-Grabczyk
SAXS Synchrotron Study of Temperature Transition in the System: Polyurethane-Solvent
International Symposium on Synchrotron Crystallography (SYNCRYS 2001), Cracov, Poland, 31 August – 4 September 2001 (Poster)

D. Grosso, F. Babonneau, P.-A. Albouy, R. Balkenende, H. Amenitsch
Mesoporous silica thin films with various structures: in-situ time-resolved XRD experiments
ACS National Meeting, San Diego (USA), 1-5 April 2001 (talk)

Lind, J.Andersson, S. Karlsson, M. Lindén
Catanionic surfactant assisted synthesis of mesoporous silica with tunable pore size and mesoscopic order
Silica 2001 conference, Mulhouse, France, 3-6.9.2001

F. Lo Celso
TR SAXS Investigation on Aggregation Phenomena in Supercritical carbon dioxide
Workshop: "Chimica e luce di sincrotrone: programmi attuali e prospettive future ad Elettra", Sincrotrone Trieste, Italy, 28-29 May 2001

M. Lucic-Lavcevic and A. Turkovic
The morphological parameter of nanostructured TiO_2 films
9th International Users‘ Meeting, ELETTRA, Trieste, Italy, 3. - 4.12.2001 (Poster)
Book of Abstracts p. 27

M. Ollivon, D. Kalnin, C. Lopez, P. Lesieur, C. Bourgaux, F. Artzner, H. Amenitsch and G. Keller
Combined DSC and time-resolved synchrotron X-ray diffraction for fat crystallization monitoring with reference to palm oil
International Palm Oil Congress (PIPOC 2001), Kuala-Lumpur (Malaysia), C25 pp 1-20 (2001) talk

A. Orthen, H.Wagner
Recent progress in the microcat gaseous imaging detector
Wire chamber conference, Vienna, Austria, 19-23 Feb 2001 (talk)

G.Pabst, H. Amenitsch, J. Katsaras, D. Kharakoz, P. Laggner, V.A. Rhagunathan and M. Rappolt
Global Fit of X-Ray Diffraction Data Reveals Secrets of Anomalous Swelling
9th International Users‘ Meeting, ELETTRA, Trieste, Italy, 3. - 4.12.2001 (poster)

G.Pabst, M. Rappolt, H. Amenitsch, J. Katsaras and P. Laggner
Revisiting critical swelling of phospholipid bilayers.
45th Annual Meeting of the Biophysical Society, February 17 - 21, 2001, Boston, Massachusetts, USA (talk)

O. Paris
Investigation of hierarchically structured materials by scanning micro-beam X-ray scattering
Conference of Stability of Materials, Ascona, Schweiz, 04.-10.03.2001

D.Posedel, A.Turkovic, Z.Crnjak-Orel and P.Dubcek
Grazing-incidence X-ray reflectivity on nanosized vanadium oxide and V/Ce oxide films
Zbornik radova: MATH/CHEM/COMP 2001, Inter-University Centre, Dubrovnik, Croatia 25-30 June 2001, Dubrovnik, p76

D.Posedel, A.Turkovic, Z.Crnjak-Orel, M.Graberscek and P.Dubcek
Spektroskopija impedancije i rasprsenje sinhrotronskog zracenjana malim kutovima priklona i rasprsenja kao metode prepoznavanja elektricnih i morfoloskih svojstava nanostruktura, Knjiga sazetaka: Treci znanstveni sastanak hrvatskog fizikalnog drustva, Fizicki odsjek Prirodoslovno-matematickog fakulteta, Croatia, Zagreb, Dec. 5-7 2001, p. 103 (poster)

D. Posedel, A. Turkovic, P. Dubcek and Z. Crnjak-Orel
Grazing-incidence X-Ray reflectivity on nanosized vanadium oxide and V/Ce oxide films
9th International Users Meeting, ELETTRA, Trieste, Italy, 3. - 4.12.2001 (poster)
Book of Abstracts p.28

M. Rappolt, G. Pabst, H. Amenistch, S. Bernstorff and P. Laggner
Salt-Induced Phase Separation in the Liquid Crystalline Phase of Phosphatidylcholines
9th International Users Meeting, ELETTRA, Trieste, Italy, 3. - 4.12.2001 (poster)

E. Schafler, M. Zehetbauer, T. Ungar, R. Pippan, I. Kopacz and S. Bernstorff
Time and Space Resolved Scanning Synchrotron X-Ray Profile Analyses During Plastic Deformation of Cu)
51st Annual Conference of the Austrian Physical Society, Vienna, Austria, Sept. 17-21, 2001 (poster)

E. Schafler, M. Zehetbauer, T. Ungar, R. Pippan, I. Kopacz and S. Bernstorff
Time and Space Resolved Scanning Synchrotron X-Ray Profile Analyses During Plastic Deformation of Cu
9th International Users Meeting, ELETTRA, Trieste, Italy, 3. - 4.12.2001 (Poster)

M. Steinhart, M. Kriechbaum, H. Amenitsch, S. Bernstorff, P. Laggner, J. Baldrian, R. Triolo
Recent Achievements in SWAXS Measurements at High Pressures
Prague Meetings on Macromolecules (60th meeting - 20th discussion conference) on „Scattering Methods for the Investigation of Polymers“, Prague, Czech Republic, 9.–12. July 2001 (Poster)

M.Steinhart, M.Kriechbaum, H.Amenitsch, S.Bernstorff, P.Laggner, J.Baldrian, R.Triolo
SWAXS measurements on polymers and biopolymers at elevated presures
Kolokvium STRUKTURA' 2001, Bedoichov, Czech Republic 18.-22.6.2001,

Mater. Struct. in Chem., Biol., Phys. and Tech. 8 (2001) 19
M. Steinhart, M. Kriechbaum, H. Amenitsch, S. Bernstorff, P. Laggner, J. Baldrian
SWAXS measurements on polymers and biopolymers at elevated presures
20th Discussion Conference "Scattering Methods for the Investigation of Polymers", Prague, Czech.Republic 9.-12.7. 2001 (poster)

F. Sussich, H. Amenitsch, A. Cesàro
Calorimetric and Time-resolved SWAXS study of lipid structural transformations in presence of trehalose
Meeting of the ISBC XII (International Society for Biological Calorimetry), Santiago de Compostela, Spain, 7-11/09/2001 (poster)

F. Sussich, H. Amenitsch and A. Cesàro
Calorimetric and Time-Resolved SWAXS Study of DPPC Transformations in Presence of Trehalose
9th International Users‘ Meeting, ELETTRA, Trieste, Italy, 3. - 4.12.2001 (talk)

C.V. Teixeira, H. Amenitsch, M. Rappolt, M. Majerovicz and P. Laggner
Use of surface diffraction to study lipids under influence of salt
9th International Users‘ Meeting, ELETTRA, Trieste, Italy, 3. - 4.12.2001 (poster)

A. Triolo
Kinetics of block copolymers aggregation in supercritical CO_2
4th International Discussion Meeting on Relaxations in Complex Systems,
Heraklion Crete, Greece, 18-26 June 2001 (poster)

A. Triolo, F. Lo Celso, H. Amenitsch, S. Bernstorff, M. Kriechbaum, M. Steinhart, R. Trioilo
Aggregation Phenomena in Supercritical Carbon Dioxide
9th International Users‘ Meeting, ELETTRA, Trieste, Italy, 3. - 4.12.2001 (invited talk)

Roberto Triolo
Applications of scattering techniques to material science
Indiana University, Bloomington Indiana 2/2/2001 (talk)

T.Ungar
Evolution of the dislocation structure in copper single crystals during plastic deformation; in-situ experiments at the Synchrotron ELETTRA, Trieste
Seminar Lecture, Department of General Physics, Eoetvoes University Budapest, Hungary, May 2001

M. Vidal, M. Kriechbaum, C.V. Teixeira, M. Steinhart, H. Amenitsch, S. Bernstorff and P. Laggner
Non-Linear Concentration Effects of Cholesterol on Lipid Bilayers Studied by Pressure Scanning SAXS
9th International Users‘ Meeting, ELETTRA, Trieste, Italy, 3. - 4.12.2001 (poster)

ELETTRA News 2001

R.H. Menk, S. Bernstorff, H.J. Besch and H. Amenitsch,
First results of a continuos delay line MicroCAT detector
ELETTRA News 42 - October 5, 2001

W. Tesch, P. Roschger, I. Zizak, O. Paris, S. Bernstorff, H. Amenitsch, K. Klaushofer and P. Fratzl
Characterization of mineralization in bone diseases
ELETTRA News 43 – December 14, 2001

ELETTRA Highlights 2000-2001

W. Tesch, P. Roschger, I. Zizak, O. Paris, S. Bernstorff, H. Amenitsch, K. Klaushofer and P. Fratzl
Characterization of mineralization in bone diseases

D. Grosso, F. Babonneau, C. Sanchez, G. J. de A. A. Soler-Illia, E. L. Crepaldi, P.A. Albouy, H. Amenitsch, A.R. Balkenende, A. Brunet-Bruneau
Self-assembly of 2D-Hexagonal templated TiO_2 mesostructured films during dip-coating

P. Dubcek, S. Bernstorff, U.V. Desnica and I.D. Desnica-Frankovic
GISAXS study of cadmium sulfide quantum dots reveals clues for design optimization of electro-optical semiconductor devices

P. Bussian, W. Schmidt, F. Schueth, P. Agren, J. Anderson, M. Linden and H. Amenitsch
In-Situ-SAXS Investigations on Zinc Sulfide Precipitation in a Liquid Jet on a Microsecond Time Scale

Diplom Theses (Tesi di Laurea)

Gianluca Croce
Chemical and physical investigation of siliceous materials of biological origin
Universita' del Piemonte Orientale „A. Avogadro", Alessandria, Italy, Academic year 2000/2001

PhD Theses

Manfred Roessle
Time resolved small angle scattering of proteins: The structural intermediates of the chaperonin GroEL and GroES upon ATPase cycle
Technische Universität München, Germany, 2001

Patrick Bussian
In situ - Untersuchungen zur Festkoerperbildung
Fakultät für Chemie der Ruhr-Universität Bochum, Germany, 10.12.2001

Mercè Cócera
Estudi del efectes derivats de la incorporació d'alquil sulfat a bicapes lipídiques. (Study of the effects due to the incorporation of alkyl-sulphate to lipid bilayers)
Universitat de Barcelona, Facultat de Farmàcia. December 2001

Christelle Lopez
Contribution à l'étude de la cristallisation des triacylglycérols:Application aux émulsions laitières. (Contribution to the study of triacylglycerol crystallizations: application to dairy emulsions)
Université Paris VI, France, 21.9.2001

V. Vidya
Study of polyaniline and polyalkylthiophene based LB multilayers and composites containing semiconducting nanoclusters
Indian Institute of Technology, Bombay (2001)

Ingrid Winter
Liposomen als Transportvehikel für antimikrobielle Peptide (Liposomes as Delivery Vehicles for Antimicrobial Peptides)
Technische Universität Graz, Austria, 2001

Author Index